37
40

A Strategy for Modeling Hydroelectric Plants and Improving Their Performance

by

James Arthur Rule, Jr.

Dissertation submitted to the Faculty of the
Virginia Polytechnic Institute and State University
in partial fulfillment of the requirements for the degree of
Doctor of Philosophy
in
Mechanical Engineering

APPROVED:

Robert G. Leonard, Chairman

Robert H. Fries

Lee W. Johnson

Hal L. Moses

Harry H. Robertshaw

April, 1988

Blacksburg, Virginia

A Strategy for Modeling Hydroelectric Plants and

Improving Their Performance

by

James Arthur Rule, Jr.

Robert G. Leonard, Chairman

Mechanical Engineering

(ABSTRACT)

A plan for integrating modeling techniques and improving hydroelectric plant performance is presented. The plan begins with defining and establishing basic plant modeling parameters from the physical plant description. Guidelines for forming linear or nonlinear mathematical models are developed and the plan culminates in the determination of settings for P-I-D control which achieve optimum plant performance.

Mathematical models are developed for the hydroelectric plant components -- the penstock, the hydraulic turbine (specifically a Francis turbine), the generator with its connected electrical system, and the control system. A unique method for characterizing turbine performance from a hill diagram is presented.

Stability regions for linear models are determined and control settings which result in optimum plant performance are established. Settings associated with high derivative gains are indicated as giving optimum performance when a linear plant model is used. Nonlinear simulations at various operating conditions reveal that less lively gains must be used for the required gate motion to be achievable.

For the representative plant model studied, the optimum governor settings resulted in a 7 percent improvement over other recommended P-I-D settings while satisfying gate speed constraints which the other recommended settings violated. The benefit of this work is in an improved ability to develop and utilize appropriate mathematical models for a hydroelectric plant and in the determination of control settings which improve plant performance.

Acknowledgements

I would like to express my sincere appreciation to my advisory committee, Drs. Robert Leonard, Robert Fries, Lee Johnson, Hal Moses, and Harry Robertshaw for their guidance and suggestions concerning this work. Dr. Leonard has been particularly patient and helpful in our discussions of the control of hydraulic and mechanical power systems. The evolution of this work began with an interest in the modeling, simulation, and control of hydraulic transients in large pipelines. With the valuable input of Drs. Leonard and Robertshaw, the interest grew to incorporate the automatic control of both hydraulic and mechanical transients in hydroelectric plants. Dr. Leonard's guidance in integrating aspects of classical and modern control theory into hydroelectric plant modeling, simulation, and tuning has helped to greatly enhance this work.

I appreciate the opportunity provided me by Drs. J. B. Jones and Robert Comparin to serve the Mechanical Engineering Department as an Instructor. This employment experience has been the most rewarding and enjoyable one I have had.

I would like to express my appreciation to Lucy Croom for her patience and understanding through the final months of this work. Finally, I would like to express my appreciation to my parents for their unfailing support and love through all aspects of my personal and professional education. Their support, along with the help and confidence of many others, has provided the inspiration to undertake and complete this work.

Table of Contents

1. Introduction **1**

2. Review of Literature **6**

Penstock Models 6

Hydraulic Turbine Models 11

Hydroelectric Plant Governor Models 15

Generator and Electrical Connection Models 20

Overall Hydroelectric Plant Models 22

3. Formulation of Plant Components **29**

Representation of the Reservoir 31

Formulation of Penstock Models 32

Concepts of Fluid Dynamics 32

Basic Equation of Waterhammer and Determination of Pressure Wavespeed 37

Governing Equations for Transient Flow 40

Two-Port Representation and Head/Flow Transfer Function 41

Rigid Water Column Model 44

Summary of Penstock Model Formulations 45
Formulation of Hydraulic Turbine Models 46
Turbine Speed Dynamics 47
Turbine Characteristics of Theoretical Model 49
Turbine Characteristics for Linearized Model 52
Turbine Characteristics Described by Hill Diagrams 53
Analytical Representation of Constant Gate Lines on Hill Diagram 56
Analytical Representation of Constant Efficiency Lines of Hill Diagram 57
Determination of Turbine Characteristic Partial Derivatives 58
Formulation of Governor Models 67
Formulation of Generator and Electrical Connection Models 75
Overview of Candidate Plant Models 79
Theoretical Linear Model 79
Linearized Model with Isolated Load 81
Linearized Model with Equivalent System Load 81
Transcendental Model 81
Nonlinear Model 82
Model Selection Insights 82
Plant Characterizing Time Ratios 83
Estimation of Waterhammer Head and Duration 89
Steady-State Comparisons 92
Summary of Model Selection Insights 96

4. Development of Candidate Plant Models 98
Linearized Model with Isolated Load 99
Transcendental Model 109
Linearized Model with Equivalent System Load 120
Nonlinear Model 125

Turbine Dynamics 128
Control Dynamics 130
Fluid Dynamics - Method of Characteristics 130
Fluid Dynamics - Boundary Conditions 137
Quasi-steady Torque Relationship 139
Summary of Plant Model Developments 140

5. Optimum Governor Settings and Zones of Satisfactory Operation 141
Optimization Procedure 143
Pattern Search Method 148
Summary of Optimization Procedure 150

6. Application of Analysis to Hydroelectric Plants 151
Step 1 -- Gather Plant Information 154
Step 2 -- Establish Plant Characterizing Parameters 158
Step 3 -- Establish the Validity of Linear Models 160
Step 4 -- Linear System Performance 162
Step 5 -- Nonlinear System Performance 167
Step 6 -- Compare Linear and Nonlinear Simulations 172
Step 7 -- Linear Plant Model Stability Limits 178
Linearized Model 178
Theoretical Versus Linearized Model 179
Transcendental Versus Linearized Model 179
Step 8 -- Linear Model Optimization 183
Step 9 -- Nonlinear Model Optimization 185
Step 10 -- Zone of Satisfactory Operation 188
Step 11 -- Establish Best Control Settings 192
Step 12 -- Effects of Initial Load and Load Change 195

Step 13 -- Allowable Gate Speeds for Grid Connection Configuration 202
Effects of Varying the Plant Characterizing Ratios 210
"Waterhammer Penstock" Plant Model 210
"Long Penstock" Plant Model 213
"Short Penstock" Plant Model 215
Summary of Analysis 215

7. Discussion and Recommendations 219
Evaluation of Objectives 220
Provide Component Models. 220
Characterize Plant Behavior. 220
Provide Plant Models. 221
Study Linear and Nonlinear Simulations. 222
Determine Optimum Settings. 222
Determine Zones of Satisfactory Operation. 223
Establish Best Control Settings. 223
Recommendations for Future Work 224

References 226

Coefficients for Matrix Representation of Linearized Plant Model with Equivalent System Load 229

Vita 234

List of Illustrations

Figure 1. Schematic of a Hydroelectric Plant. 3

Figure 2. Representative Hill Diagram. 14

Figure 3. Illustration of Steady-State Speed Droop. 16

Figure 4. Simplified Hydroelectric Plant Governor. 17

Figure 5. Detailed Hydroelectric Plant Governor. 19

Figure 6. Generator and Electrical Connection Models. 21

Figure 7. Steady Flow in a Frictionless Penstock. 34

Figure 8. Unsteady Flow in a Frictionless Penstock as a Result of Instantaneous Wicket Gate Closure. 35

Figure 9. Sequence of Waterhammer Events Following Instantaneous Stoppage of Flow in Penstock. 36

Figure 10. Head and Flow at Penstock Discharge Upon Flow Changes in a Frictionless Penstock. 38

Figure 11. Analytical Representation of a Line of Constant Efficiency. 59

Figure 12. Turbine Operating Condition Change Holding Speed and Head Constant. 61

Figure 13. Turbine Operating Condition Change Holding Gate Position Constant. 63

Figure 14. Functional Block Diagram of Governor and Hydroelectric Plant Components. . . 69

Figure 15. Development of Simplified Governor Model. 70

Figure 16. Quality of Speed Regulation Depending on Gate Motion Times (Gordon's Curves). 74

Figure 17. Frequency-Domain Penstock Model Comparison. 87

Figure 18. Qualitative Map for Identifying Dominant Plant Dynamics. 88

Figure 19. Block Diagram of Linearized Plant Model. 101

Figure 20. Reduced Block Diagram of Linearized Plant Model. 102

Figure 21. Stability Limits for a Theoretical Linear Plant. 106

Figure 22. Example of Theoretical Linear Plant Response. 110

Figure 23. Comparison of Linearized Model Simulation with Grand Coulee Third Powerplant Response to Isolated Load Change. 111

Figure 24. Block Diagram of Transcendental Plant Model. 113

Figure 25. Stability Limits for Transcendental Plant Model. 118

Figure 26. Stability Limit Comparisons for Various Theoretical Linear Plants. 119

Figure 27. Block Diagram of Linearized Plant with Equivalent Electrical System. 121

Figure 28. Connected Electrical System Response for Thorne and Hill's Linearized Plant Model. 124

Figure 29. Functional Block Diagram of Hydroelectric Plant Model. 127

Figure 30. Computational Diagram of Nonlinear Model. 129

Figure 31. Characteristic Lines for Fluid Dynamics Representation. 134

Figure 32. Method of Characteristics Solution Grid for Fluid Dynamics Simulation. 135

Figure 33. Optimization Results for Theoretical Linear Model. 145

Figure 34. Formulation of Pattern Search Optimization. 149

Figure 35. Information Required to Establish Characteristic Plant Parameters -- Representative Plant. 155

Figure 36. Characterization of Representative Hill Diagram. 156

Figure 37. Steady-State Operating Conditions for Representative Plant at 85 MW and 76 MW. 157

Figure 38. Location of Plant Characterizing Time Ratios on Qualitative Plant Dynamics Map. 161

Figure 39. Linearized Plant Model Response to Step Change in Isolated Load -- Hovey's Settings. 164

Figure 40. Linearized Plant Model Response to Step Change in Isolated Load -- Hagihara's Settings. 165

Figure 41. Comparison of Theoretical Model Response to Linearized Model Response. . . 166

Figure 42. Nonlinear Plant Model Response to Step Change in Isolated Load. 168

Figure 43. Nonlinear Plant Response to Various Load Changes -- Hovey's Settings. 170

Figure 44. Nonlinear Plant Response to Various Load Changes -- Hagihara's Settings. . . . 171

Figure 45. Linear and Nonlinear Model Comparisons for Anticipated Load Conditions -- Hovey's Settings. 173

Figure 46. Linear and Nonlinear Model Comparisons for Anticipated Load Conditions -- Hagihara's Settings. 174

Figure 47. Plant Speed Response Comparisons for Various Load Changes. 175

Figure 48. Plant Speed Response for 30% Load Rejection, Hagihara's Settings, and Gate Speed Limit. 177

Figure 49. Linearized Model Stability Limits for Representative Plant. 180

Figure 50. Comparison of Theoretical Linear Model Stability Limits to Those of Linearized Model. 181

Figure 51. Comparison of Transcendental Model Stability Limits to Those of Linearized Model. 182

Figure 52. Results of Linear Optimization Process for Representative Plant. 184

Figure 53. Results of Nonlinear Optimization Process for Representative Plant. 186

Figure 54. Nonlinear Plant Model Response to 30% Load Rejection Using Optimum Settings. 190

Figure 55. Zone of Satisfactory Operation for Optimum Settings Corresponding to 2.0 sec Derivative Gain. 191

Figure 56. Zone of Satisfactory Operation for Optimum Proportional-Integral Control. . . . 193

Figure 57. Zone of Satisfactory Operation for Optimum Settings Corresponding to 0.5 sec Derivative Gain. 194

Figure 58. Comparison of Plant Model Response Using Hovey's, Hagihara's, and Suggested Settings. 196

Figure 59. Representative Plant Response for Selected Governor Settings at Anticipated Operation. 197

Figure 60. Hill Diagram Tracking of Representative Plant Response to 10% Load Rejection. 198

Figure 61. Representative Plant Response for Selected Governor Settings and 30% Load Rejection. 200

Figure 62. Hill Diagram Tracking of Representative Plant Response to 30% Load Rejection. 201

Figure 63. Representative Plant Response for Heavy Load and 10% Load Rejection. 203

Figure 64. Representative Plant Response for Light Load and 10% Load Rejection. 204

Figure 65. Allowable Full Gate Motion Times for Grid Connection Configuration. 206

Figure 66. Representative Plant Response for 50% Change in Desired Generation -- Grid Connection Configuration. 207

Figure 67. Location of Demonstration Plants on Dominant Plant Dynamics Map. 211
Figure 68. Response of "Waterhammer Penstock" Plant Model. 212
Figure 69. Response of "Long Penstock" Plant Model. 214
Figure 70. Response of "Short Penstock" Plant Model. 216

List of Tables

Table 1. Comparison of Turbine Characteristic Partial Derivative Values. 66

Table 2. Governing Equations for Candidate Plant Models. 80

Table 3. Steps of Hydroelectric Plant Analysis for Linear, Nonlinear, and Mixed Plant Models. 153

Table 4. Turbine Characteristics and Plant Parameters at Expected Operating Conditions. 159

Nomenclature

Hydraulic Turbine Related Variables

Variable	Description
H	static head
M	torque
N	rotational speed
P	power
Q	volumetric flow rate
Wr^2	polar moment of inertia of rotating machine
Y	wicket gate position (dimensionless)
η	turbine efficiency
ω	circular speed of rotating machine

Penstock Related Variables

Variable	Description
A	penstock cross-sectional area
D	penstock diameter
L	penstock length
Z	characteristic impedance
c	pressure wave speed
f	friction factor
Γ	propagation operator
ρ	water density

General Variables

Variable	Description
K	constant
K_p	proportional gain
K_I	integral gain
K_d	derivative gain
T	characteristic time related to a plant component
g	acceleration due to gravity
s	Laplace operator
t	time

Normalized Departure Variables

Variable	Description
h	departure of turbine head from initial operating value, $(H - H_0)/H_0$
m	departure of turbine torque from initial operating value, $(M - M_0)/M_0$
n	departure of turbine speed from initial operating value, $(N - N_0)/N_0$
p	departure of power from initial operating value, $(P - P_0)/P_0$
q	departure of turbine flow from initial operating value, $(Q - Q_0)/Q_0$
y	departure of wicket gate position from initial operating value, $(Y - Y_0)/Y_0$

Subscripts

Variable	Description
c	related to the wavespeed of the water
g	related to full gate motion
gc	related to full gate closure
go	related to full gate opening
hyd	related to hydraulic power
$load$	related to the connected electrical system
m	related to the turbine-generator machine
max	maximum value
min	minimum value
new	related to new steady operation
r	related to rated turbine value
res	related to reservoir
w	related to the water in the penstock
0	related to initial steady operation
1	unit value, related to turbine performance
$2-port$	related to two-port penstock model
RWC	related to rigid water column penstock model

Chapter 1

Introduction

Hydroelectric power plants utilize the natural downhill flow of rivers in order to produce electric power. Often, dams or reservoirs are constructed to channel the river flow through hydraulic turbines with as much head as the natural river gradient and terrain will allow. Hydroelectric power generating units currently account for about twelve percent of the United States' electric generation [1][1] and even larger percentages in some countries.

Some plants are designed to utilize the entire flow of the stream and are referred to as run-of-the-river plants. These units involve little to no water storage in reservoirs upstream of the turbines. Usually, they involve relatively small drops in head across the turbines [2].

Other hydroelectric plants utilize large storage reservoirs which supply water through closed conduits to the turbines. The turbines produce power in an amount proportional to the flow of the water and to the head drop of the water across the turbines [2]. Conduits which supply water to the turbines can be very long with huge flows. The head at the turbine inlets can be as high as 1500 feet. For example, the Bath County, Virginia units have supply conduits over 9000 feet long delivering water from the storage reservoir to the turbines and the head drop across the turbines is

[1] Numbers in brackets [ ] refer to entries in the reference list.

approximately 1000 feet. The rated flow for each of six Bath County hydraulic turbines is 2.4 million gallons per minute [3].

Pumped storage plants utilize upper and lower storage reservoirs. When producing electric power, the units operate as normal turbine/generators. During times of low power demand, the units may operate as pump/motors utilizing excess generation from other plants to transfer water from the lower reservoir back to the upper reservoir. For example, the Bath County Pumped Storage Project has been designed to generate 24 million kwhr in 13.5 hr and then refill the upper reservoir in 11.3 hr which requires 30 million kwhr [3]. This work applies to both conventional hydroelectric plants and to pumped storage plants operating in the generation mode, both of which must accomodate the rotating dynamics of the hydraulic turbine and the dynamics of the water in the supply conduit.

Consider a hydroelectric plant model which represents a typical installation. The model is shown schematically in Fig. 1 and consists of the following components:

- A reservoir or lake which serves as an unlimited, constant level source of water.
- A closed upstream conduit, referred to as a penstock, which conveys water from the upstream reservoir to a hydraulic turbine.
- A hydraulic turbine, specifically a Francis turbine, which produces power proportional to the water flow and head drop across the turbine.
- An electric generator which is mechanically coupled to the turbine.
- A controller which is designed to maintain the turbine/generator speed and in some situations to adjust the power generated by the plant. The controller regulates the flow through the turbine by adjusting the position of wicket gates which are an integral part of the Francis turbine. For the hydroelectric plant, the controlling device is referred to as a governor although its purpose is controlling the generated power in addition to regulating the speed of the turbine.
- A short discharge conduit which conveys the flow of the water from the turbine to a lower reservoir or river.

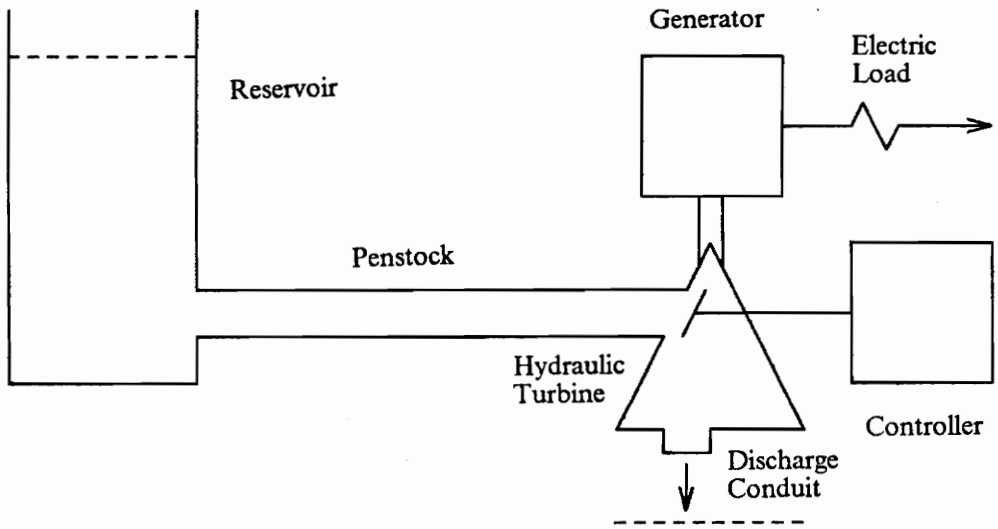

Figure 1. Schematic of a Hydroelectric Plant.

Proper governing of a hydroelectric plant is important for a number of reasons. For example, when the electric load on the generator drops, the turbine and generator speed will increase since the water is supplying more power to the turbine than is required by the generator. The governor must adjust the flow of the water so that the turbine/generator speed returns to its initial speed. If the adjustment is too slow, then a turbine overspeed condition will occur. If the adjustment is too fast, then rapid deceleration of water in the penstock may result in overpressure and unwanted fluid dynamics. The task of proper governing is to react to a load change in a manner which minimizes turbine overspeed (or underspeed), achieves a new steady operation as quickly as possible, and also avoids dangerous fluid dynamics in the penstock. Thus, a proper governing scheme with appropriate control settings is necessary in order for the generator to deliver electric power with nearly constant frequency.

The literature concerning hydroelectric plant modeling, mathematical simulation, performance, and system stability is reviewed. In addition, methods for modeling the penstock water dynamics and hydraulic turbine characteristics are investigated. Mathematical models of actual hydraulic turbine governors are reviewed. Descriptions of the dynamics of connected electrical systems are also reviewed. Investigations of system stability are summarized along with the literature concerning plant performance optimization.

Review of the pertinent literature suggests the need to investigate improving plant performance by determining optimum governor settings different from those currently suggested in the literature. In addition, there is a need to unify and improve plant modeling techniques in one work to determine the mathematical model that most simply, but adequately, describes plant performance. The appropriate mathematical models may then be utilized to select governor settings which improve plant performance.

Mathematical models for each component of the hydroelectric plant are developed. A method of analytically describing real hydraulic turbine performance characteristics is presented. Guidelines for the selection of a plant model based on characteristic plant parameters are established and candidate models for the plant are presented. The analytical relations for simulation and stability of general linear hydroelectric plant models are determined and a technique for nonlinear plant model

simulation is also developed. Based on characteristic parameters, insights concerning the dominant plant component or components are provided. Further guidelines for the selection of a linear or nonlinear plant model are based on a steady state analysis of expected operational conditions.

An index of performance is selected which quantifies the effects of settling time and turbine speed departure. The index of performance serves as the basis for selecting governor settings which result in optimum plant performance. In order to account for physical limitations, wicket gate speed limits and penstock maximum pressure are recognized as constraints to insure that recommended optimum settings are reasonable.

The outline for analysis of a general plant is presented using the developments, guidelines, and insights. A representative plant is selected and the analysis is applied to it in order to demonstrate the developments of this work. Optimum settings suggested by the analysis are compared to settings currently recommended in the literature. Particular attention is given to identifying sources of possible nonlinear plant response such as the initial operating condition, the magnitude of the load change, and the wicket gate speed limit. Satisfactory operational regions are identified based on governor settings which do not require a wicket gate speed greater than achievable. Conclusions are made concerning the improvement in plant performance, the analysis method in general, and the benefit of unified modeling methods. Recommendations are made concerning the implementation of the proposed strategy which will ultimately lead to improved hydroelectric plant performance.

The purpose of this investigation is to present a logical plan of analysis for a general hydroelectric power plant which starts with the establishment of basic plant parameters from physical plant information, provides guidelines for plant mathematical modeling, and culminates in the determination of control settings to achieve optimum plant performance. The benefit of this work will be in plant performance improved over that which is suggested as optimum in the literature.

Chapter 2

Review of Literature

Hydroelectric plant modeling, performance, stability, and governor tuning are covered in literature which addresses one, some, or all of those topics. The review is first divided into literature which addresses component modeling alone: the penstock, the hydraulic turbine, the governor, and the generator and its electrical connection. Recommendations from the literature are presented which guide the selection of a load model for governor tuning studies. Following component models, the literature which addresses aspects of performance, stability, and tuning of various hydroelectric plant models is reviewed.

Penstock Models

Mathematical models which describe fluid flow in a pipe are well established. In the case of modeling the hydro plant penstock as a part of the entire dynamic system, selection of the simplest valid model becomes the task. There are three possible types of models which arise as candidates

to describe the penstock -- the rigid water column model, elastic waterhammer models, or a quasistatic model.

Most dynamic hydroelectric plant models utilize the rigid water column model to describe the dynamics of the fluid in the penstock. The water is treated as an incompressible fluid and only the effects of momentum change are considered in the model. The net force acting on the fluid is equal to the rate of change of momentum of the rigid column of water in the penstock. For this model, penstock friction forces are neglected so that the only forces acting on the fluid are the static pressure forces at the penstock inlet and outlet. The momentum equation describes the relation between flow departure and head departure and is given by:

$$T_w \frac{dq}{dt} = -h \qquad [2.1]$$

where h=the departure of the head from its initial condition, $(H - H_0)/H_0$

q=the departure of the flow from its initial condition, $(Q - Q_0)/Q_0$

T_w=the water starting time $(LQ_0)/(AgH_0)$

This description results in the flow and head both being time dependent, but independent of location within the pipe. The water starting time is similar to the time constant of a first order ordinary differential equation. Thus, a penstock with a small water starting time (one which is short, has low flow, has high head, or has a very large diameter) will exhibit a more rapid response than its long, high flow, low head, small diameter counterpart.

If the length of the penstock is very short or if the flow is very small, then the dynamics of the water may be insignificant compared to the dynamics of the rest of the plant. The water starting time corresponding to such a situation is small, resulting in the dynamics of the water being very fast compared to the other components of the plant so that the water flow may be considered to be time independent. If this is the case, the mathematical description of the steady flow in a pipe is presented in many introductory fluid mechanics texts such as Streeter [5] or Brebbia and Ferrante [6].

Watters [7] reviews the basic mathematical formulation for the rigid water column model although there are no guidelines presented which indicate the conditions under which the model is valid. The rigid water column model is a popular one for two reasons. First, compressible effects of the water are negligible in transient hydro plant situations where the turbine gate motion is very slow. In this situation, the rigid water column model is entirely valid. Second, the rigid water column model results in a simple first order ordinary differential equation describing the penstock dynamics. This aspect fits conveniently into an overall linear plant description.

More sophisticated mathematical models of the dynamics of fluid in a pipeline include the effects of the elastic properties of water and the pipe along with the momentum change of the water during a transient. These types of models are referred to as elastic models and incorporate the phenomenon of waterhammer in the mathematical description of pipeline dynamics. The elastic models for transient flow all rely on two governing differential equations as a basis: 1) the continuity equation (conservation of mass) which includes the elastic properties of both the fluid and the pipe and 2) the momentum equation.

Because of the broad and general nature of fluid dynamics in piping, numerous works have effectively developed models for these transients. According to Wiley [8], the subject of unsteady flow of liquids has been studied since the 1850's. Chaudhry [9] has discussed the historical progress of unsteady pipe flow modeling and computational methods up to recent times.

A qualitative review of the waterhammer phenomenon (Wylie [8], for example) reveals that during a fluid transient brought on by wicket gate closure, pressure waves are propagated up and down the penstock at a speed approximately equal to the speed of sound of the water. For this reason, the round trip time T_c of a pressure wave to travel from the wicket gate to the reservoir and then to be reflected back to the wicket gate is given by:

$$T_c = \frac{2L}{c} \qquad [2.2]$$

where L= the length of the penstock

c= the speed of the pressure wave

Comparison of this time with the water starting time will be one consideration in the choice of a penstock model.

The nature of the two governing equations, momentum and continuity, gives rise to two partial differential equations which are classified as hyperbolic. The momentum equation sets the rate of change of momentum of the fluid contained in a differential control volume equal to the net force acting on the control volume. Effects of penstock friction are considered along with the static pressure forces acting on the control volume. Wylie and Streeter [8] have demonstrated that for this application, an average value of the Moody friction factor for steady flow is appropriate for pipe friction. The continuity equation is also based on a control volume approach in which the compressibility of the fluid and the elasticity of the penstock are both considered. The momentum and continuity equations are, respectively:

$$g\frac{\partial H}{\partial x}+\frac{1}{A}\frac{\partial Q}{\partial t}+\frac{f}{2DA^2}Q|Q|=0 \qquad [2.3]$$

$$\frac{\partial H}{\partial t}+\frac{c^2}{Ag}\frac{\partial Q}{\partial x}=0 \qquad [2.4]$$

in which the wavespeed c is adjusted to account for the compressible effects of the water and for the elastic effects of the pipeline. The set of partial differential equations expresses the relation of flow and head at any point in the pipe at any time. Solution of this set of equations requires that the initial conditions be specified for all points in the pipe, and that boundary relations at the pipe ends be specified for all time.

A general analytical time-domain solution to the hyperbolic partial differential equations is not available, but the equations may be transformed by the method of characteristics into particular total differential equations. These differential equations are integrated to yield finite difference equations which may be treated numerically. Wylie and Streeter [8] have developed and presented an effective method of utilizing the method of characteristics to mathematically describe the dynamics of the fluid in a pipeline. The result is a numerical finite difference scheme which computes

the flow and head at discrete positions in the pipe at discrete points in time. Similar finite difference methods are presented by Chaudhry [9] and Watters [7].

Fluid transients including elastic effects in a pipeline may also be modeled as that of a distributed parameter system. Takahashi [10] has presented the general Laplace domain transfer function which describes the dynamics of a uniform, two-port transmission line. Goodson and Leonard [11] have reviewed the analytical transfer function which applies to the hydro plant penstock model in particular. The two-port transmission line transfer function depends on two functions which are determined by the physical attributes of the line and of the fluid. These functions are the characteristic impedance and the propagation operator. The governing equations result in a transcendental transfer function which relates the flow and head at each end of the transmission line (penstock). In matrix form, the head and flow at the pipe inlet (h_1 , q_1) are releated to the outlet head and flow (h_2 , q_2) by:

$$\begin{bmatrix} h_2 \\ q_2 \end{bmatrix} = \begin{bmatrix} \cosh \Gamma(s) & -Z \sinh \Gamma(s) \\ -\frac{1}{Z} \sinh \Gamma(s) & \cosh \Gamma(s) \end{bmatrix} \begin{bmatrix} h_1 \\ q_1 \end{bmatrix} \qquad [2.5]$$

where $\Gamma(s)$=the propagation operator $\frac{L}{c} s$ or $\frac{T_c}{2} s$

Z=the characteristic impedance $\frac{c Q_0}{H_0 A g}$ or $\frac{2T_w}{T_c}$

Wozniak [12] used a truncated Maclaurin series expansion of the two-port transmission line to represent the dynamics of the fluid in the penstock. The leading three terms of the series were retained and the result was a third order linear ordinary differential equation. The purpose of that work was to refine the rigid water column model but to retain the advantages of a linear representation.

To summarize the penstock models, two types of dynamic models may be incorporated into the hydro plant model. A linear ordinary differential equation, particularly the rigid water column model as outlined by Watters [7], may be used to describe the dynamics of the fluid flow in the penstock if the elastic effects of the fluid and the pipe are negligible. When elastic effects are important, the method of characteristics is utilized for finite difference modeling of the penstock dy-

namics as outlined by Wylie and Streeter [8]. Unfortunately, assessment of when elastic effects of the fluid are or are not important is not covered in the literature. For this reason, guidelines concerning this modeling decision must be covered as a part of the present work. For plant stability considerations, the transcendental two-port transmission line transfer function model [10] may be incorporated into the system model to advantage.

Hydraulic Turbine Models

The mathematical model for hydraulic turbine speed change is presented in basic references [8, 9, 13]. The equation for the speed dynamics of a rotating device is given by Newton's second law of motion as:

$$T_{net} = I\frac{d\omega}{dt} \qquad [2.6]$$

where T_{net}=the net torque applied to the rotating device

I=the polar moment of inertia of the device

$\frac{d\omega}{dt}$=the angular acceleration

The water torque which is supplied to the hydraulic turbine depends on the hydraulic characteristics of the turbine which are based on relations of head, speed, wicket gate position, and turbine blade angle. There are two general classifications for hydraulic turbines [6] -- impulse and reaction types. The impulse turbine, also referred to as a Pelton wheel, is intended for use only in high head situations (greater than 1000 ft). Of the reaction types, Kaplan turbines and bulb turbines are both of a propeller design and are intended for low head situations (less than approximately 100 ft). These propeller-type turbines are equipped with variable pitch blades in order to operate efficiently when the turbine head changes.

The Francis turbine which is also of the reaction type may be visualized as a large centrifugal or mixed flow pump operating in reverse. These hydraulic turbines operate over a large range of heads and have been selected as the basis for this study because of their wide range of applicability and also their close relationship to hydraulic pump-turbine machines [6].

The simplest representation for hydraulic turbine characteristics was presented by Paynter and utilized by Hovey [13]. This model of a theoretical machine utilized the reasoning that the fluid torque was directly proportional to the wicket gate position and to the head at the turbine inlet. Dependence of torque on turbine efficiency or speed was neglected. This simple linear relation is given by:

$$m = y + \frac{3}{2}h \qquad [2.7]$$

in which all variables represent dimensionless departures from initial operating conditions.

Goldwag [15] showed that the theoretical representation presented by Paynter was valid for Pelton wheel turbines undergoing very small speed transients. He extended the linear representation to account for real turbine behavior around a local operating point and also included a load self-regulation factor to account for changes in fluid torque due to departure in speed. Load self-regulation introduces a damping torque in addition to the water torque and the generator load torque whenever the speed is different from the desired operational speed. The damping torque may be due to speed-dependent turbine torque variations and also due to generator torque variations when operating off the design speed. For his turbine model, Chaudhry [9] maintained the theoretical linear relation of torque on wicket gate position and head, but did adopt the use of the load self-regulation factor which empirically accounts for the dependence of the fluid torque on turbine speed as follows:

$$m = y + \frac{3}{2}h + \alpha n \qquad [2.8]$$

where α is the load self-regulation factor.

A more sophisticated model for turbine characteristics was used by Thorne and Hill [16, 17] and Phi et. al. [18]. Similar to the theoretical model, both torque and flow were assumed to be linearly related to wicket gate position, head, and speed. Six partial derivatives evaluated about the anticipated operating point describe the linear turbine characteristic model. These partial derivatives, being treated as constant, maintain the linear nature of the model while accounting for turbine behavior that deviates from the simple theoretical relationship. The flow and torque dependence on gate position, head, and speed are given by:

$$q = \frac{\partial q}{\partial h}h + \frac{\partial q}{\partial y}y + \frac{\partial q}{\partial n}n \qquad [2.9]$$

$$m = \frac{\partial m}{\partial h}h + \frac{\partial m}{\partial y}y + \frac{\partial m}{\partial n}n \qquad [2.10]$$

The authors relied on the turbine manufacturer to supply the values of the partial derivatives at various operating points that they had requested.

Turbine characteristic data are supplied by various manufacturers in different forms [8]. However, recurring reference is made [8, 9, 6, 15] to hill diagrams in which two parameters, turbine unit discharge and turbine unit speed are related graphically. Lines of constant wicket gate position relate the unit discharge to the unit speed for a fixed gate position. Lines of constant efficiency also shown on the diagram complete the graphical description of the turbine characteristics which fully describes the steady-state relation between head, flow, torque, speed, and wicket gate position. A representative example of a hill diagram is shown in Fig. 2.

According to Chaudhry [9], no useful data have been reported for turbine characteristics during transient-state conditions. Therefore, steady-state hill diagrams are assumed to be valid during the transient state as well. In his reference to Perkins et al.[19], Chaudhry confirms that this assumption is valid. Similarly in their analyses, Wylie and Streeter [8] along with the previously cited authors utilize this quasi-steady representation as valid. This assumption is considered to be valid in this work as well.

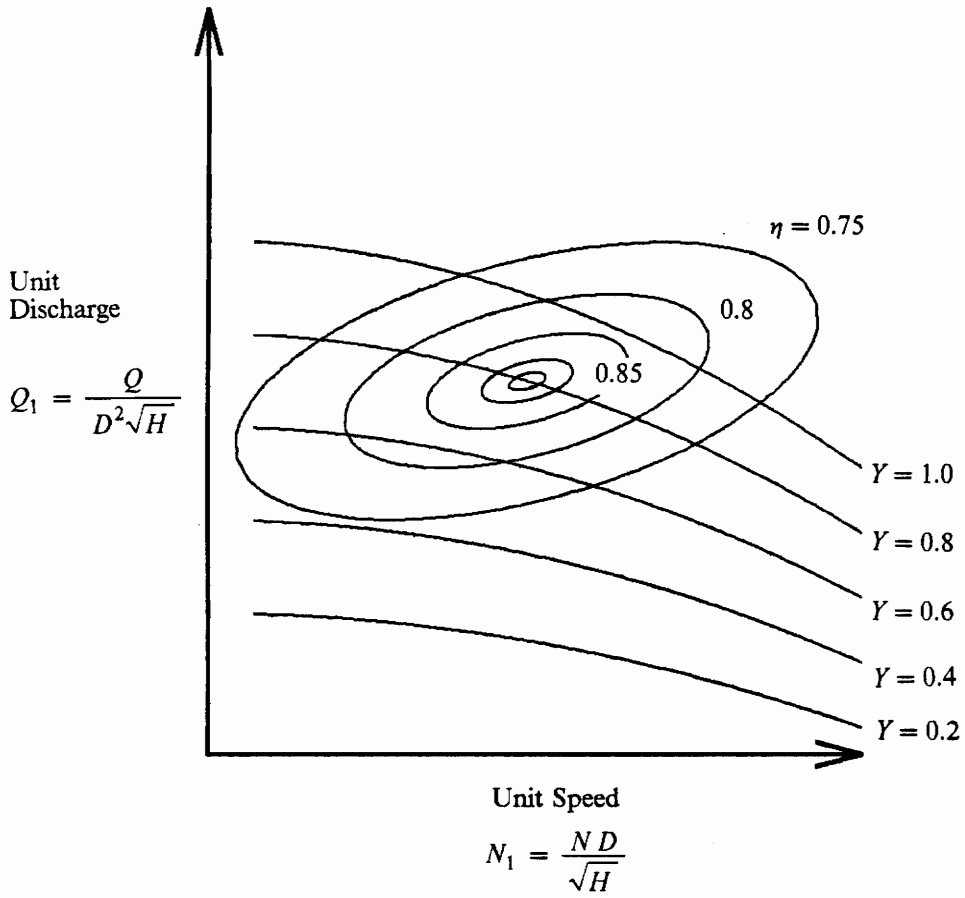

Figure 2. Representative Hill Diagram.

Hydroelectric Plant Governor Models

In its report on dynamic models for steam and hydro turbines in power system studies, the IEEE Power System Engineering Committee [20] provided a functional block diagram which outlines the hydroelectric speed governing system and its relation to the hydraulic turbine and to the complete connected electrical system. The speed governing system is used to position the turbine wicket gate which controls the hydraulic power delivered to the turbine.

There are two command signals to the speed governing system which may cause the wicket gate position command signal to change. First is the turbine speed error signal which will cause the gate to move when there is a departure of the turbine speed from the desired speed. Second is the unit generation signal which is utilized in the event that it is desired to change the generation of the unit even when there is no error in the desired speed of the turbine.

The concept of coordinated turbine speed control along with control of desired unit generation is illustrated by Gurney [21] in his paper entitled "Control and Protection Design of the Revelstoke Hydroelectric Project." The Revelstoke Project included four generating units which were placed into service in 1984. In that paper, the author provides a block diagram of the plant's electric-hydraulic speed governor. The block diagram shows that the turbine speed control is of the proportional, integral, and derivative type -- a P-I-D controller. A generation control signal is included so that unit power generation may be controlled independent of turbine speed errors. Finally, a steady-state speed regulation signal is added into the governor block diagram in order to allow for the operation of the entire electrical system in a state of permanent droop. Figure 3 illustrates the concept of permanent droop (also called steady-state speed regulation) in which the desired operational steady-state system frequency (and, therefore, turbine speed) is linearly related to the system load.

A simplified model for the electronic/hydraulic governor is shown in the block diagram of Fig. 4 based on the governor installed at the Revelstoke plant as presented by Gurney. It may be observed that in the event of a mismatch between the turbine speed and the desired speed, the gov-

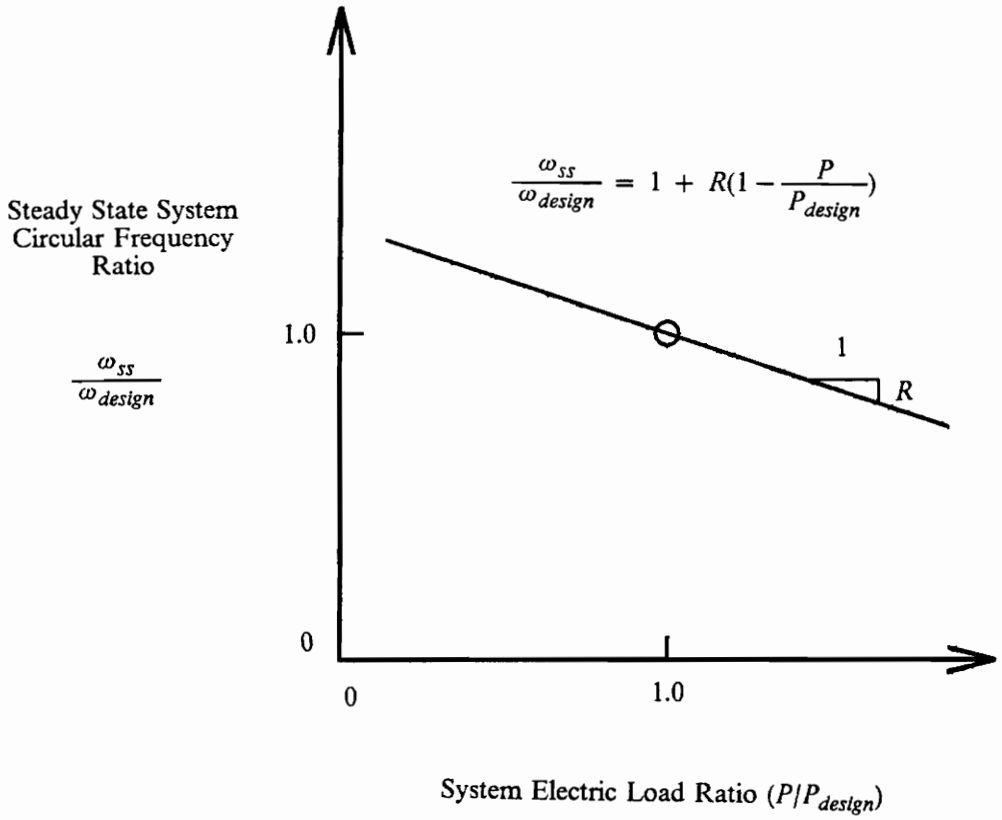

Legend

R	Steady State Speed Regulation
ω_{ss}	Steady State System Circular Frequency
ω_{design}	Design System Circular Frequency
P	System Electric Load
P_{design}	Design System Electric Load

Figure 3. Illustration of Steady-State Speed Droop.

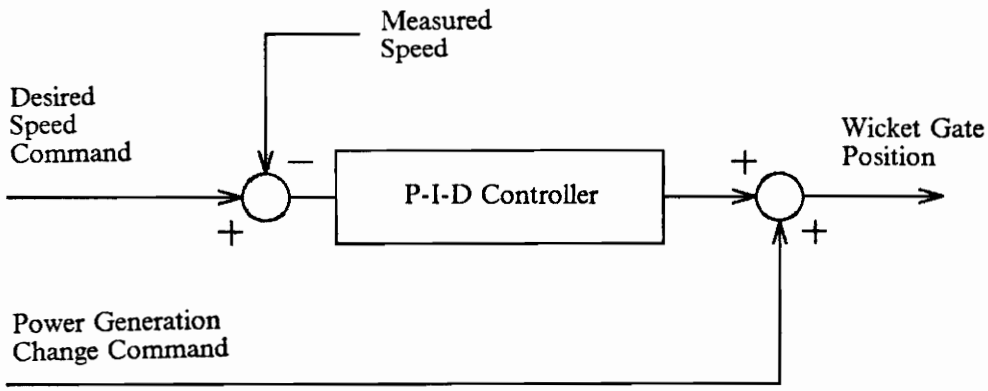

Figure 4. Simplified Hydroelectric Plant Governor.

ernor operates in the speed regulation mode. When it is desired to change the power produced by the plant, the operator (or automatic dispatcher) repositions the wicket gates in a prescribed open-loop mode independent of plant speed regulation.

For simulation purposes, Phi et al. [18] used a governor model similar to that of the block diagram presented by Gurney. The block diagram which describes that model is shown in Fig. 5. The P-I-D control scheme is utilized for turbine speed control and a power feedback signal is provided to the governor for steady-state speed regulation (permanent droop). The authors included a time lag to account for the time required to compute the derivative of speed in the electrical control circuitry. The authors included additional time lags in the governor model to account for gate positioning servo delay, for speed error feedback delay, and for delay due to a capacitor in the circuitry. They demonstrated that these lag times affect system stability in a secondary manner.

From a historical standpoint, hydromechanical governors were the first type of speed governors to be widely utilized in hydroelectric generation service. In general, the hydromechanical governor utilizes a linkage connected to a flyball mechanism to provide proportional speed error control and a hydraulic oil dashpot to reset the system when a new steady state condition had been reached following a speed transient. Two control parameters were to be specified in order to provide effective speed control. These parameters are known as temporary droop δ and the dashpot reset time T_r . In his 1960 paper, Hovey described a simple and effective method for making field adjustments to the hydromechanical governor to achieve and verify these specified settings. Three references in particular, Hovey [13] Chaudhry [9], and Wylie and Streeter [8] provide clear derivations of the dynamic governing equations which use the physical governor dimensions and governor settings in order to relate speed error to the turbine wicket gate position.

Thorne and Hill [16] demonstrated that the mechanical-hydraulic governor could be modeled as an equivalent proportional-integral control. They demonstrated how the temporary speed droop and the dashpot reset time were algebraically related to proportional gain and integral gain. This algebraic relation has been utilized by subsequent authors because of the wide familiarity with proportional-integral control and because of the modern use of electro-hydraulic and digital control.

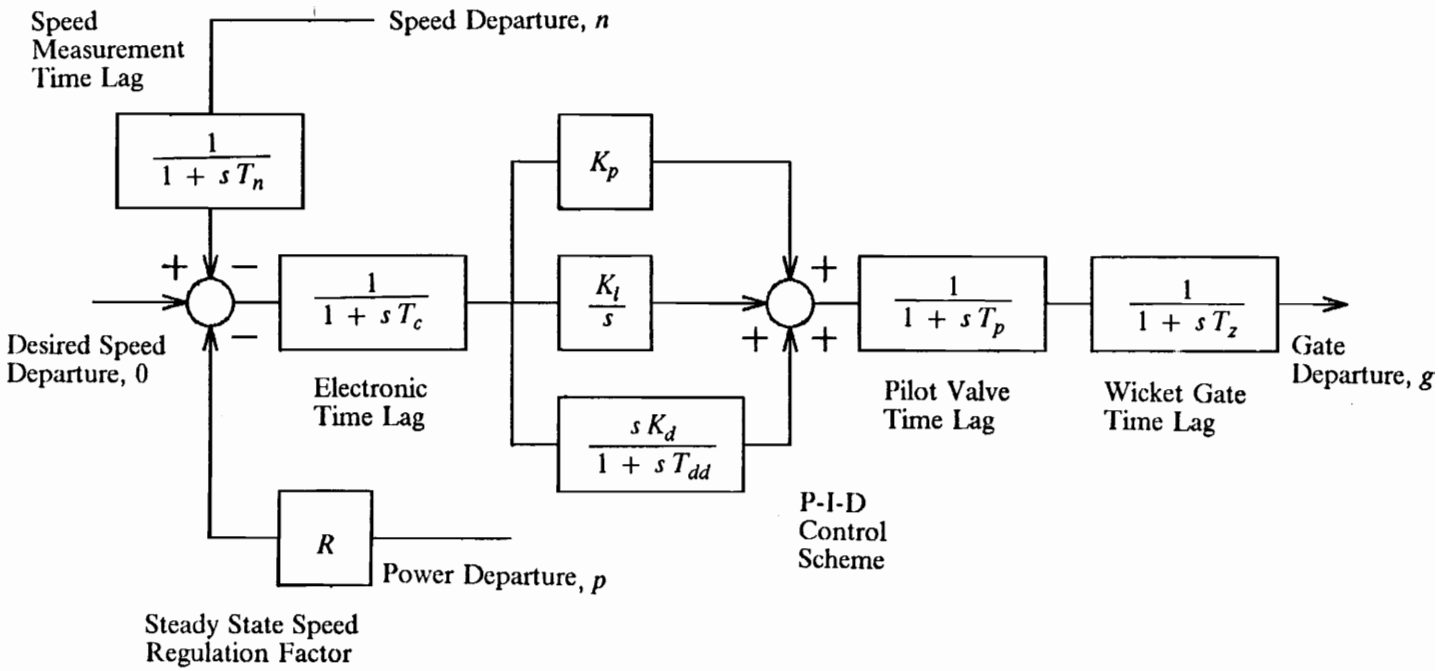

Figure 5. Detailed Hydroelectric Plant Governor.

Generator and Electrical Connection Models

As shown in the generalized sketch of Fig. 6, there is a dynamic interaction of the generator and its associated electrical connection with the hydromechanical plant. This electrical/mechanical interaction is expressed in terms of the load torque that the generator supplies to the hydraulic turbine and the speed of the hydraulic turbine.

Demello and Concordia [22] presented the concepts of a synchronous machine (generator) and its interconnection to the electrical system and the turbine. Marshall and Smolinski [23] verified that the generator system including its field controls could be represented by a single synchronizing torque coefficient K_s and a single damping torque coefficient D_s . The resulting model provides the possibility for there to be a mismatch in the equivalent frequency of the turbine/generator set versus the equivalent frequency of the connected electrical system during a system transient. The block diagram of Fig. 6 shows the relation of the hydraulic turbine to the generator and its electrical connection. Variables labeled as torque, power, or speed are normalized departures. In the block diagram, the frequency mismatch is represented by a mismatch in machine versus system speed. Using this model for the generator, the only way for there to be a change in load torque on the turbine is for there to be a mismatch in the machine speed versus system speed.

In order to model the electrical system to which the plant is connected, Thorne and Hill [16] utilized an equivalent model which was based on field measurements. It is assumed that the connected electrical system is supplied by several power plants and that the hydroelectric plant carries a fraction, $1/B$, of the entire load. In the event of a change in power demanded by the connected electrical system, all of the power plants respond dynamically to a change in that load. The equivalent system was modeled as having an equivalent inertia, equivalent damping, and an equivalent proportional control. The values of the time lags T_{s1} and T_{s2} and the damping terms D_{s1} and D_{s2} are determined by the nature of the plants connected to the system. If all the connected plants are hydroelectric, then the second time lag T_{s2} becomes zero and the second damping term D_{s2} be-

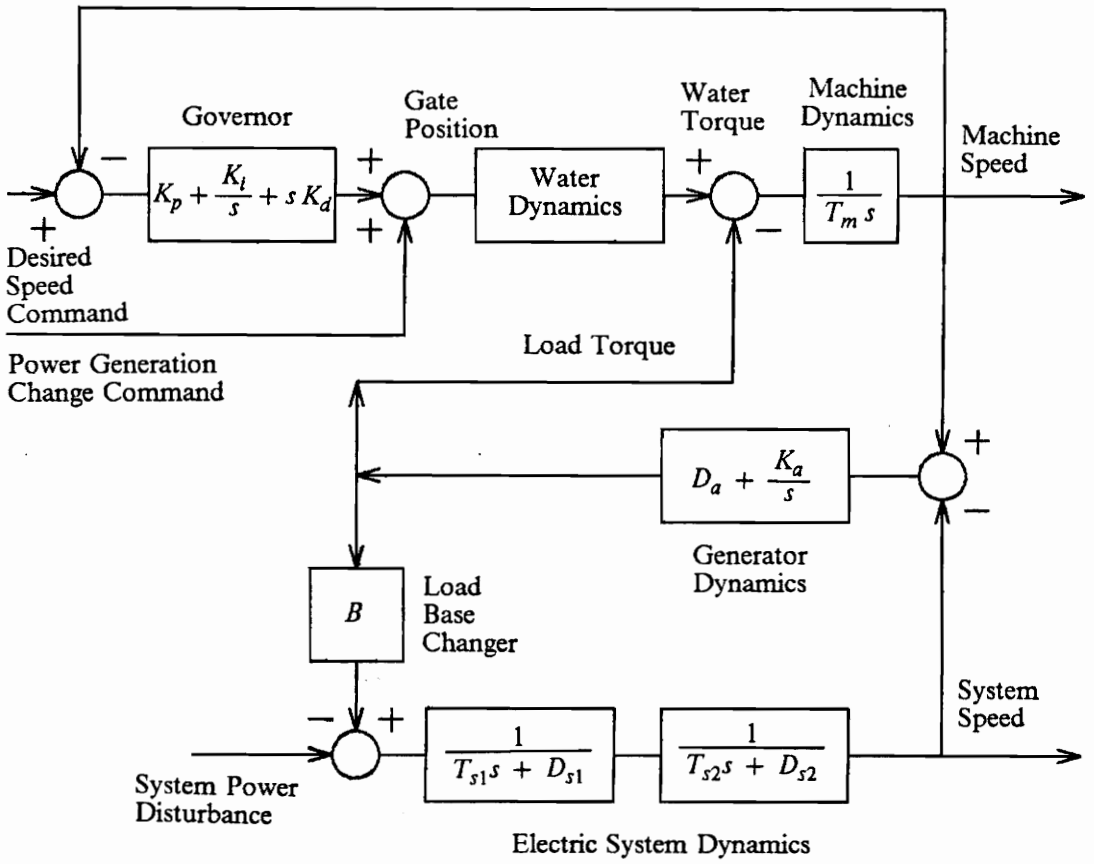

Figure 6. Generator and Electrical Connection Models.

comes unity. In other words, steam plants respond slower to load changes than hydroelectric plants.

The hydroelectric plant response to a change in load depends on the type of electrical system which the plant serves. The plant may be the only one supplying power to a small electrical system; it may be one of a few plants supplying power to a system; or it may be one of many plants connected to a large power distribution grid. The selection of an appropriate load model is an important aspect of a governor tuning study in which optimum gain settings are determined.

In the situation that the plant is the sole supplier of power to a purely resistive electrical system, then changes in plant speed translate directly into changes in system frequency. This situation is referred to that of a resistive, isolated load [13]. In the situation where numerous plants serve a large connected electrical system, changes in hydroelectric plant speed may have little to no effect on the frequency of the connected system.

Schleif and Wilbor [24] recommended that the governor of each prime mover connected to an electrical system should yield good speed regulation for purely resistive, isolated loads. The authors went on to illustrate their recommendation with field test results. In his discussion of that work, Hovey [24] stated that "... this discusser is completely in accord with the observation that it is poor practice to liven up a hydro governor in the hope that this will improve performance. We have found, to our sorrow, that this simply does not work." Effects of the generator and connected electrical system dynamics are considered in this work and the results confirm the recommendations of Schlief and Wilbor.

Overall Hydroelectric Plant Models

There are many works which utilize mathematical models to describe hydroelectric plants consisting of a hydraulic turbine, a penstock, and a speed regulator. Simulation of performance, stability of the plant, and governor tuning for optimum performance are addressed in various works.

Mathematical models for the hydraulic turbine range from a simple, theoretical resistance model to a nonlinear model in which the head/flow/torque/speed relationships are described by a manufacturer's turbine characteristic diagram. In the penstock model ususally selected, the water is considered to be incompressible and act as a rigid water column undergoing a momentum change. In a second penstock model, the water is considered to be compressible and various mathematical representations are used. For the governor, proportional, integral, and derivative control may be incorporated. Steady state speed droop, various measurement time lags, and gate response time lag may also be included. Models concerned primarily with system stability assume that the generator supplies power to an isolated load, resulting in a step change in turbine load torque due to a step electric load change. In all the works, stability limit determination depends on the mathematical model being linear, which allows use of the Routh-Hurwitz criteria or use of eigenvalue analysis techniques.

The first work which addressed the mathematical modeling, stability, and governor tuning of a hydroelectric plant is attributed to Paynter [25]. In this work, the turbine was considered to behave as a simple linear fluid resistance, the penstock was modeled as a rigid water column, the governor was modeled as a P-I controller, and the electrical load was considered to be isolated from system dynamics. Hovey [13, 14] utilized a mathematical model identical to that of Paynter, verified Paynter's stability limits, applied hydro plant modeling techniques to eight operational plants, and made recommendations for optimum gain settings for the plants. The basis for his recommendations for optimum performance was by inspection of numerous analog computer simulations. Hovey made a qualitative recommendation based on the simulation that gave the lowest speed overshoot and slightly underdamped performance.

Goldwag [15] demonstrated that real hydro turbines (Francis turbines, in particular) do not behave with the theoretical characteristics as suggested by Paynter. Goldwag showed that hydraulic turbine performance depends on the speed of the unit which can greatly affect the stability limits for the plant. His work was primarily concerned with plant stability, giving few details on the effect of turbine characteristics on the dynamic performance of the plant.

Chaudhry [9] extended the work of Hovey and Paynter by incorporating permanent speed droop and load self-regulation, an aspect of Goldwag's work, into the mathematical hydro plant model. Similar to previous authors, Chaudhry chose the rigid water column model for the penstock and was dealing with a third order linear differential equation which described the dynamics of the model. He used the Routh-Hurwitz criteria to determine the analytical stability boundary for the third order linear system. He went on to describe the speed dynamics of the plant undergoing a change in load. By qualitative inspection of numerous simulations, Chaudhry recommended those governor settings as optimum which give the "shortest settling time, but slightly underdamped response [9]."

Thorne and Hill [16, 17] developed a linear hydroelectric plant model which incorporated a dynamic model for the electrical system. The plant model utilized the rigid water column representation for the penstock, a turbine model with characteristics linearized about a particular operating point, permanent speed droop, P-I control, and a model for the load torque based on field measurements. Their work included simulation of plant dynamics and comparison with field measurements. The primary interest of the work was in the area of predicting plant stability boundaries and not in governor tuning for optimum performance.

Thorne and Hill's work was extended by Phi et. al. [18]. The plant model was extended to a fourteenth order linear model. The high order of this model was a result of the incorporation of dynamic models for the generator and its electrical connection, the incorporation of three first order time lags related to the governor circuitry, and the incorporation of a gate position servo time lag. The plant model retained the rigid water column model for the penstock and the partial derivative representation for the turbine characteristics. The authors demonstrated that the effects of circuitry time lags had a secondary effect on the stability limits of the plant model and that the hydraulic turbine performance at various load conditions had a major impact on plant stability.

Dhaliwal and Wichert [26] investigated the effects of derivative gain on the stability of a system which consisted of two hydroelectric plants supplying power to an isolated load. The authors used the root-locus method to conclude that there is a limit to the derivative gain for stable plant oper-

ation. The models for both hydro plants neglected the dynamics of the penstock and used a theoretical model for turbine performance.

Hagihara et. al. [27] presented an analytical relation for the stability limits of a plant model similar to that of Chaudhry. Unlike Chaudhry, the P-I-D control law was utilized and the effect of derivative gain was shown to extend the model's stability limits beyond that of simple P-I control. A root-locus analysis was presented and led to a set of governor settings which was suggested to be an optimum set. The authors chose the rigid water column model for the penstock and a theoretical head/flow relation for the hydraulic turbine characteristics. The system model was fourth order, but was reduced to third order by assigning a value of zero permanent speed droop. Two open loop poles were located at the origin and the third was located in the left half-plane. An open loop zero was located in the left half-plane by nature of the integral part of the control scheme. The rigid water column model resulted in an open loop zero being located in the right half-plane. For P-I control, the position of the positive zero caused the complex roots of the locus to move into the right half-plane, bringing on unstable plant response as the gain was increased. By introducing derivative gain, an additional zero was added in the left half-plane and tended to keep the complex roots in the stable region. In performing the root-locus analysis, the derivative gain was increased, forcing the imaginary roots of the locus to remain in the left-half plane. This improvement was made at the expense of allowing the real root to move further to the left and, ultimately, to move into the right half-plane from $-\infty$. The optimum derivative gain was selected as the one which resulted in the root-locus pattern which insured stable complex roots while also avoiding real root movement into the right-half plane. With the derivative gain selected, the authors performed numerous simulations in order to qualitatively select appropriate proportional and integral gains which replicated waveforms presented as optimum by previous authors. Similar to previously recommended optimum settings, no method of quantitatively assessing plant performance was used. No other settings involving derivative gain were considered, nor was the possibility of gate speed limitation considered.

Ramamurthi et. al. [28] essentially repeated the stability work of Chaudhry and included gate servomotor time lag. The analytical expression of the stability limits for P-I control were once

again presented. The authors examined the sensitivity of the stability limits to changes in plant model parameters at different loads. As in most of the previous works, interest was primarily in system stability rather than governor tuning.

All of the work previously discussed uses the rigid water column model for the dynamics of the water in the penstock. Two papers have incorporated a more sophisticated penstock model which takes the compressible nature of water into account. The classical two-port transmission line transcendental transfer function replaces the first order ordinary differential equation which described the rigid water column model.

Xiao and Dong [29] presented the analytical relation which specifies the stability limits for a hydro plant model similar to that of Paynter and Hovey except that the penstock model utilized the two-port transmission line model. The resulting characteristic equation for the plant model is trancendental and, therefore, the Routh-Hurwitz criteria for stability cannot be applied. A complex identity was utilized and roots of the characteristic equation which have zero-valued real parts were determined. In this manner, the settings which result in marginal plant stability were analytically determined. The authors demonstrated that the stability limit for the model with the two-port penstock representation was always more restrictive than the model with the rigid water column penstock representation. Their work centered around consideration of plant stability, and did not address simulation or governor tuning.

Murty and Hariharan [30] incorporated the two-port transmission line model into a plant model which included P-I-D control, permanent speed droop, and load self-regulation. Using the same mathematical approach as Xiao and Dong, the authors demonstrated that the stability limits are decreased as the penstock length increases.

Nonlinear hydro plant models have been presented which are intended for simulation only and are not amenable to the determination of stability limits. The nonlinear models have arisen because of the need to simulate factors that become important when the plant undergoes a large change that causes the small operating point departure assumption required by the linear model to be invalid. Aspects that may cause the linear model to be invalid are: turbine characteristic changes during a

transient, waterhammer phenomena in the penstock due to rapid gate motion, gate saturation in the open or closed position, and gate speed limited by hydraulic actuator saturation.

Swiecicki [31] developed a computational procedure to simulate the speed and pressure transients of a hydro plant during a large load change. Nonlinear turbine characteristics, penstock dynamics, and governor response lag and speed limit were included his computational scheme. Swiecicki's numerical method of simulation was carried out by hand with turbine characteristics and penstock dynamics being evaluated graphically at each time step.

Wylie and Streeter [8] extended and sophisticated the procedure of Swiecicki to be amenable to simulation on a digital computer. In their simulation, the dynamics of the penstock were described with the method of characteristics and a full description of the turbine characteristics as given on the manufacturer's hill diagram were stored and utilized in matrix form.

Chaudhry [9] presented a computational procedure which incorporated the nonlinear characteristics of a Francis hydraulic turbine into an overall plant model. The computational procedure matched the characteristics of the turbine with the dynamics of the water in the penstock. Gate speed limitations and hydraulic gate servo time lag were included. The simulation compared favorably with measured transient data for a plant undergoing load rejection in isolated load operation.

Wozniak and Fett [32] also presented a nonlinear simulation in which the penstock dynamics were represented by a damped two-port transmission line model. The penstock model was a truncated series representation of the two-port transcendental transfer function. In a subsequent paper, Wozniak [12] utilized the nonlinear simulation and optimization techniques to determine an optimal gate closure schedule (open loop control) for a hydroelectric plant undergoing full loss of load.

The numerous works briefly reviewed have addressed one, some, or all of the topics of hydroelectric plant modeling, performance, stability, and governor tuning. In the area of component and plant modeling, mathematical models for the components are available, but specific guidelines concerning the conditions under which a particular component model is valid appears to be lacking. Insight into model selection is further clouded when assembling all components without guidelines

concerning which component or components may dominate the performance of the plant. Once a plant model is defined, however, simulation and plant stability are covered in various existing works. Governor tuning by way of mathematical modeling, simulation, and quantitative evaluation of performance appears to be the area most overlooked. Several works have suggested optimum governor settings without quantitatively justifying their recommendations. Finally, no single work adequately addresses hydroelectric plant modeling, performance, stability, and governor tuning from start to finish. This work addresses these areas for improvement.

Chapter 3

Formulation of Plant Components

There is a need to unify the modeling of hydroelectric plant components in order to assemble an appropriate plant model. By developing models of all components in one work, effective integration of the components into one plant model becomes a simpler task. There may be several ways to describe a component, although one model may be more appropriate than another depending on the dynamics of other components which comprise the plant. Plant modeling precedes the need to investigate plant performance improvement. Therefore, the first step is to identify appropriate basic equations which govern the dynamics of each component.

The sketch shown in Fig. 1 (repeated on the following page for convenience) represents a general hydroelectric plant installation. The plant components which must be mathematically modeled are:

- The reservoir or lake.
- The penstock.
- The hydraulic turbine.
- The controller.
- The electric generator and its associated electrical load.

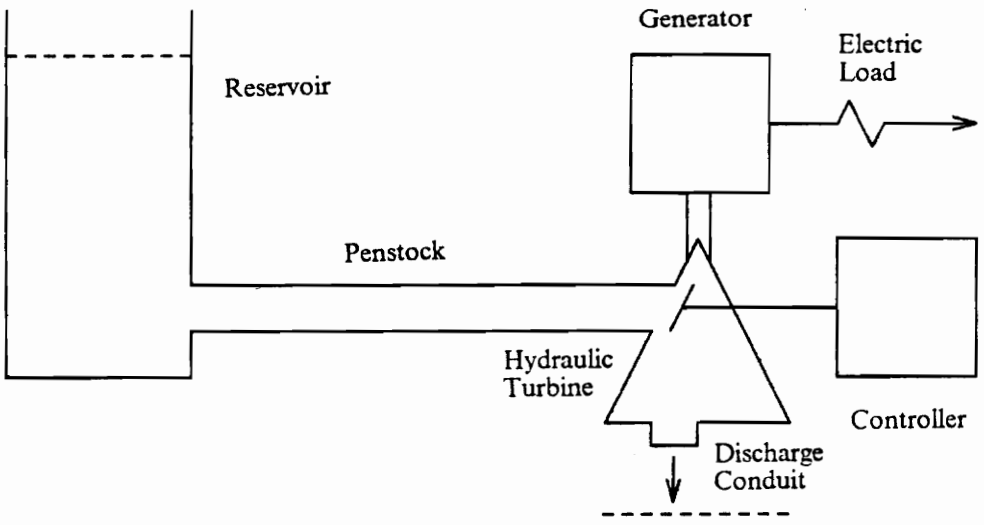

Figure 1. Schematic of a Hydroelectric Plant.

The formulations of mathematical models for each of the plant components are presented in this chapter. Three components -- the penstock, turbine, and electric load involve two or more model developments so the length of this chapter is necessarily long. Parameters which lead to the selection of appropriate plant model candidates are defined. Component selection guidelines based on the plant parameters are developed and integrated in this chapter.

Representation of the Reservoir

The reservoir shown in Fig. 1 represents an unlimited source of water which is supplied to the plant by way of the penstock and is given by:

$$H_{res} = constant \qquad [3.1]$$

Some hydroelectric plants with very long water supply conduits are equipped with a large surge tank between the reservoir and the hydraulic turbine. The design of the surge tank is intended to provide the penstock feeding the turbine with a supply of water whose head is relatively constant. The surge tank mitigates the dynamics of the water in the conduit between the supply reservoir and the surge tank. This work does not consider the dynamics of the water in the conduit between the reservoir and the surge tank and the dynamics of the surge tank level. However, the component models which will be developed in this work could be added to the basic plant model to address this case.

Formulation of Penstock Models

Concepts of Fluid Dynamics

The penstock conveys water from the upstream reservoir to the hydraulic turbine. The outflow from the turbine is handled by a draft tube and discharge conduit system. If the downstream conduit system is composed of an open conduit or very short pressurized piping system, then the downstream conduit system may be neglected. In the event that the downstream conduit system cannot be neglected, Hovey [13] and Chaudhry [9] present a method by which the equivalent length of the penstock may be adjusted to take the dynamics of the draft tube into account. For most plants, the discharge conduit length is assumed to be insignificant compared to the length of the penstock.

The flow processes in the penstock are governed by the momentum and continuity equations. In a situation of steady, uniform flow, the average velocity is constant and independent of both position and time. In a situation of unsteady, uniform flow, the average velocity is independent of position but varies with time. If the fluid in the penstock can be modeled as incompressible and the penstock can be modeled as rigid, then turbine wicket gate motion will bring on a situation of unsteady, uniform flow which is referred to as rigid water column flow. If the fluid is considered to be compressible or if the penstock is considered to be elastic, then rapid turbine wicket gate motion will bring on a situation of unsteady, nonuniform flow in which the average velocity depends on both time and penstock position. This flow situation is referred to as waterhammer.

Before the general governing equations of momentum and continuity are introduced, a discussion of instantaneous stoppage of frictionless flow in the penstock is presented. The purpose of this discussion, which parallels the presentation of Wylie [8], is to give the reader insight into the dynamics of waterhammer before treating the mathematical aspects of waterhammer and rigid water column flow. This simple example is not intended to represent typical plant operation.

Consider the steady flow in the penstock with the wicket gate position at any partially or fully open position as illustrated in Fig. 7. The average velocity at all cross-sections in the penstock is V_0 . Neglecting friction in the penstock, the head at all positions in the penstock is equal to the head of the reservoir H_{res} . Assume that the wicket gates are instantaneously closed so as to prevent any flow through the hydraulic turbine as shown in Fig. 8. Upon closure, a layer of water immediately at the turbine inlet is brought to rest ($V = 0$) from V_0 by the impulse of the higher pressure developed on the face of the wicket gate. As soon as the first layer of water is brought to rest, the same action is applied to the next layer of water, bringing it to rest. In this manner, a wave of high pressure (higher than that at the reservoir) is visualized as travelling upstream at a sonic wavespeed c (yet to be determined) and at a sufficient head to apply the impulse to each layer of fluid to bring it to rest. The remaining water in the penstock continues to move with velocity V_0 until successive layers have been compressed back to the reservoir. At this point in time ($t = L/c$), all the fluid in the penstock is under the extra head $H_{res} + \Delta H$, all the momentum has been lost, and all the kinetic energy has been converted into elastic energy.

There is an unbalanced condition at the reservoir end of the penstock at the instant of arrival of the pressure wave, since the reservoir pressure stays constant. The fluid starts to flow backward toward the reservoir as shown in Fig. 9, beginning at the reservoir. This flow returns the pressure to the value which was normal before closure and the fluid has a velocity of V_0 in the reverse direction. This process of conversion travels downstream towards the turbine at the fluid wavespeed c . At the instant $2L/c$ (referred to as the round-trip travel time), the wave arrives at the wicket gate, pressures are back to normal along the penstock, and velocity is everywhere V_0 in the reverse direction.

Since the wicket gate is closed, no fluid is available to maintain flow in the reverse direction and a low pressure $H_{res} - \Delta H$ develops such that the fluid is brought to rest. This low-pressure wave travels upstream at the sonic wavespeed c and everywhere brings the fluid to rest. At the instant the negative pressure wave arrives at the upstream end of the penstock, $3L/c$ after closure, the fluid is at rest, but uniformly at a head $H_{res} - \Delta H$, less than before gate closure. This leaves an unbalanced condition at the reservoir, and fluid flows into the pipe, acquiring a velocity V_0 forward

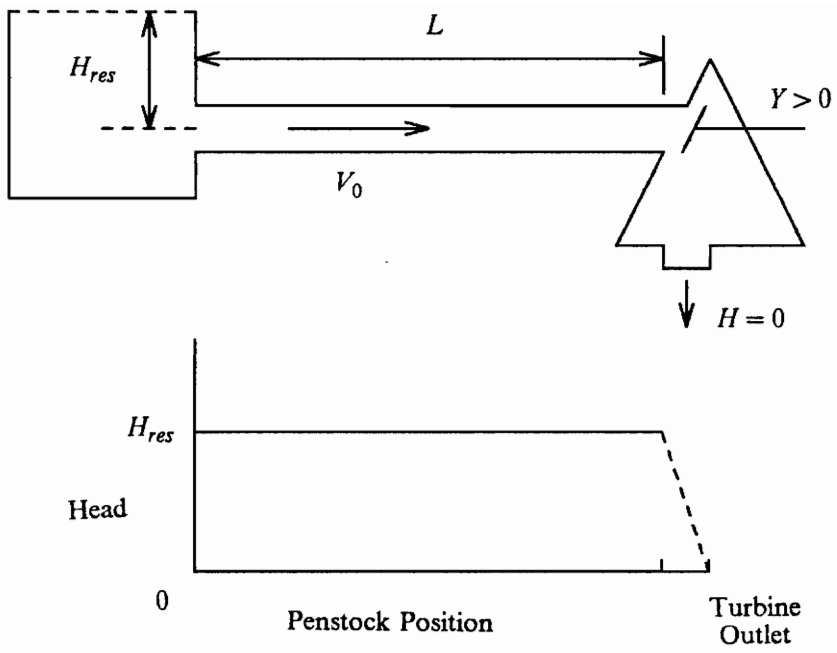

Figure 7. Steady Flow in a Frictionless Penstock.

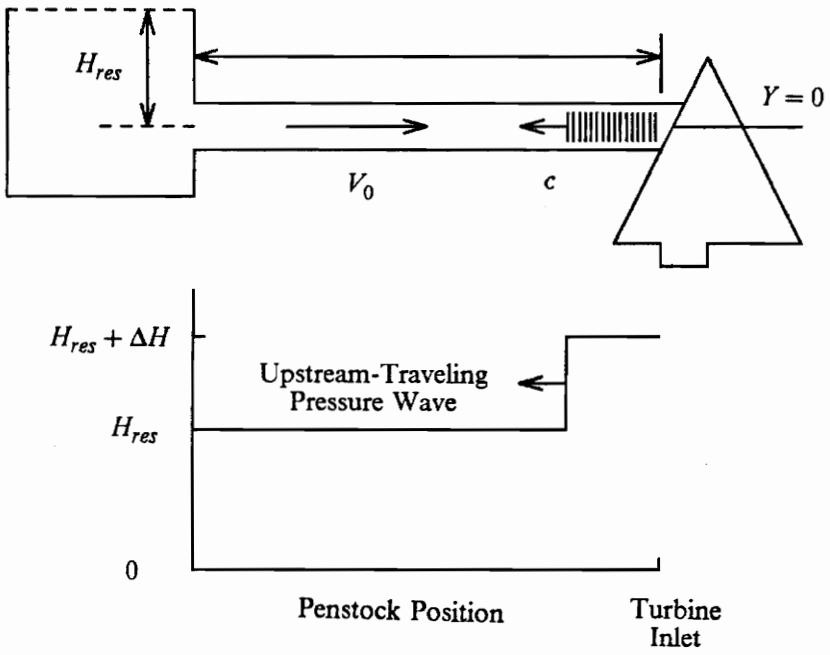

Figure 8. Unsteady Flow in a Frictionless Penstock as a Result of Instantaneous Wicket Gate Closure.

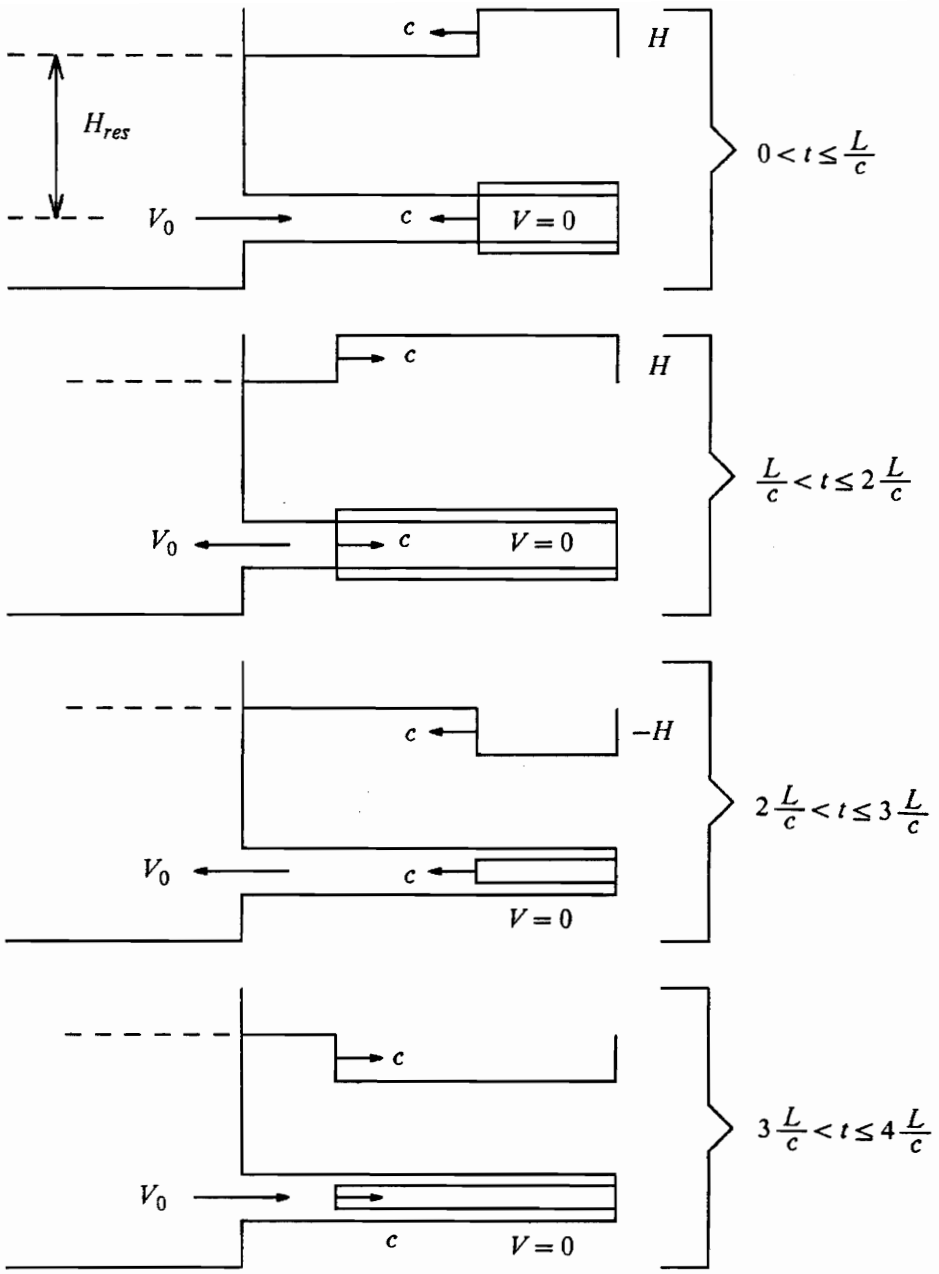

Figure 9. Sequence of Waterhammer Events Following Instantaneous Stoppage of Flow in Penstock.

and returning the fluid to normal conditions as the wave progresses downstream at speed c. At the instant this wave reaches the wicket gate, conditions are exactly the same as at the instant of closure, $4L/c$ earlier.

This cycle is repeated with a period of $4L/c$. In a real penstock, the action of fluid friction and imperfect elasticity of the water damps out the vibration and eventually the water comes permanently to rest. If the wicket gates move instantaneously but do not fully restrict flow through the turbine, the fluid vibrations will not last as long because of the dissipation of the fluid's energy when flowing through the turbine as illustrated in Fig. 10. However, the periodic phenomenon of waterhammer and the governing equations are equally valid for partial load changes.

An important result from this qualitative discussion is the demonstration of the periodic nature of waterhammer. It was shown that pressure waves move up and down the penstock at a velocity c such that a single round-trip is completed in $2L/c$. This important time parameter helps to characterize the behavior of the water dynamics compared to other time parameters yet to be developed. For this reason, the pressure wave round-trip travel time is assigned a characteristic time variable T_c as defined in Eq. 2.2 by:

$$T_c = \frac{2L}{c} \qquad [2.2]$$

Basic Equation of Waterhammer and Determination of Pressure Wavespeed

As demonstrated in the previous discussion, a change in wicket gate position results in a corresponding change in head at the hydraulic turbine and brings on a pressure pulse moving at a sonic speed back toward the reservoir. The basic equation of waterhammer is well-established and is clearly derived by Wylie [8]. In the derivation, the momentum equation is applied to a control volume and the equation of waterhammer at the turbine inlet is derived as:

$$\Delta H = -\frac{c\,\Delta Q}{A\,g} \qquad [3.2]$$

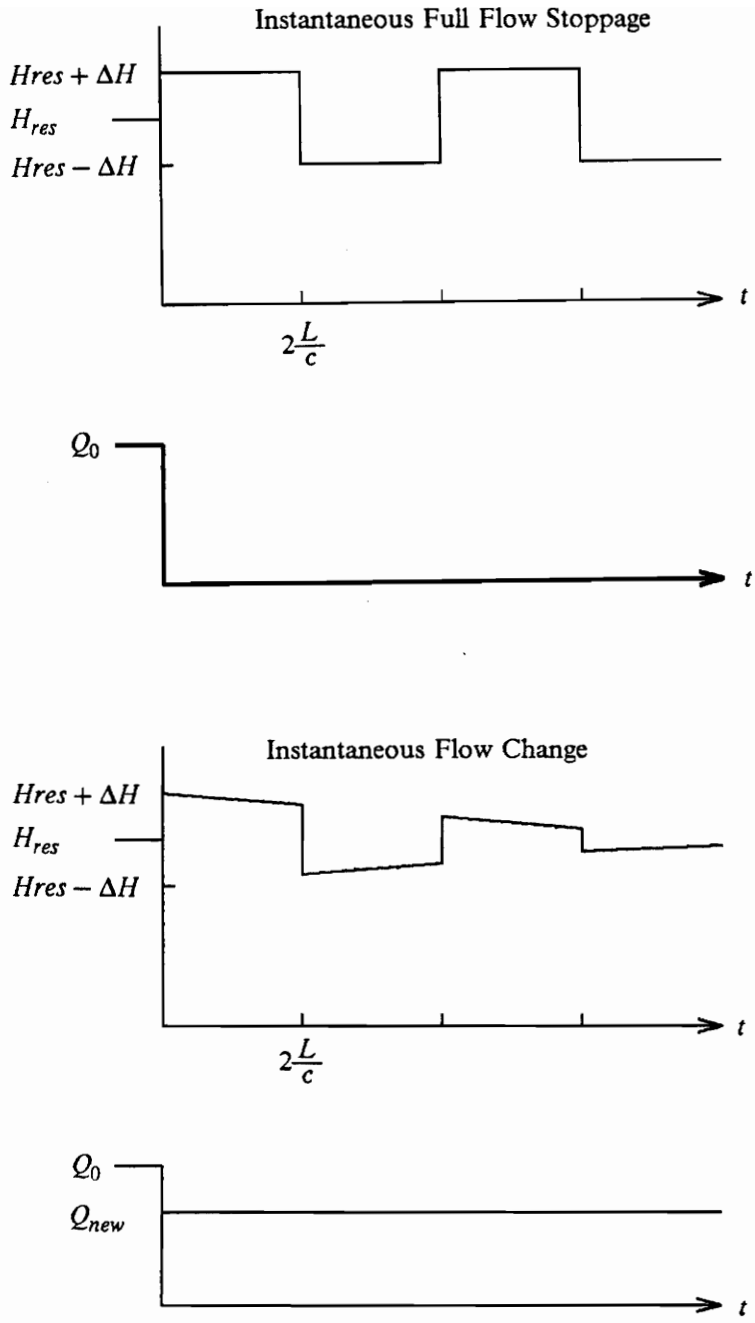

Figure 10. Head and Flow at Penstock Discharge Upon Flow Changes in a Frictionless Penstock.

where g=acceleration due to gravity

A=cross-sectional area of the penstock

c=unknown wavespeed

ΔH=change in head at the turbine wicket gate due to a change in flow

ΔQ=change in flow at the turbine wicket gate

This basic equation is valid for any movements of the turbine wicket gates as long as the pressure pulse wave has not completed one round trip ($2L/c$) of the penstock. The relation is used for the estimation of head rise (or drop) due to waterhammer when the wicket gates are moved suddenly.

Expressions for the pressure wavespeed have also been derived in many texts such as Wiley [8]. The continuity equation for the flow in the penstock is the basis for the derivation. For a rigid or very thick wall penstock, the wavespeed is simply the speed of sound of the fluid as given by:

$$c = \sqrt{\frac{K}{\rho}} \qquad [3.6]$$

where ρ=the fluid density

K=$\frac{\Delta P}{\Delta \rho / \rho}$, the bulk modulus of elasticity of the fluid

For a penstock with elastic properties, the wavespeed is given by:

$$c = \frac{\sqrt{\frac{K}{\rho}}}{\sqrt{1 + [(K/E)\,(D/e)]\,(1 - \mu^2)}}$$

where E=Young's modulus of elasticity of the penstock material

μ=Poisson's ratio of the penstock material

D=penstock diameter

e=penstock thickness

For water at ordinary temperatures, the speed of sound is 4724 ft/sec (1440 m/s). Wavespeeds for large steel penstocks may be as low as 3280 ft/sec (1000 m/s), whereas speeds in high pressure

small penstocks may be 3937 ft/sec (1200 m/s) to 4593 ft/sec (1400 m/s) [8]. The presence of small amounts of gases entrained in the water serves to substantially decrease the wavespeed and this effect may be quantified as described by Wylie [8].

Governing Equations for Transient Flow

The flow of water in the penstock is governed by the momentum and continuity equations. During a fluid transient situation, the flow and head are dependent upon position in the penstock and time. This dependence is given by:

$$Q = Q(x, t)$$
$$H = H(x, t)$$

with x being measured in the horizontal direction and $x = 0$ at the penstock inlet.

Wylie [8] presents a derivation of the momentum and continuity equations for a general fluid transient situation in a constant diameter pipe. For a control volume, the sum of the forces acting on the control volume must be equal to the rate at which the net momentum of the control volume changes. The resulting expression for the momentum equation is given by:

$$g\frac{\partial H}{\partial x} + \frac{1}{A}\frac{\partial Q}{\partial t} + \frac{f}{2DA^2}Q|Q| = 0 \qquad [2.3]$$

A major assumption used in evaluation of the wall shear force is that this shear force is considered to be the same in transient flow as in steady flow at the same velocity. The friction factor f is obtained from the Darcy-Weisbach equation as given by:

$$dH = \frac{f\,dx}{D}\,\frac{V^2}{2g}$$

The momentum equation presented in Eq. 2.3 is valid for inclined or horizontal constant diameter pipes with liquid flow. Should the penstock be comprised of pipe lengths of various diameters,

Watters [7] presents a method by which the penstock is modeled as one pipe with an equivalent length and an equivalent diameter.

The continuity equation states that the net rate at which mass flows into a control volume must equal the rate at which the mass of the control volume increases. In the case of liquid flow in an elastic pipe, the control volume may increase its mass by an increase in volume (stretching lengthwise and/or breadthwise) and by an increase in fluid density due to compression. Using this concept, the continuity equation has been derived by Wylie [8] and is given by:

$$\frac{\partial H}{\partial t} + \frac{c^2}{Ag}\frac{\partial Q}{\partial x} = 0 \qquad [2.4]$$

The elastic properties of the fluid and of the penstock wall are accomodated by adjusting the wavespeed c.

The momentum and continuity equations which describe penstock flow are first order partial differential equations with head and flow dependent upon position and time. The equations are mathematically classified as a pair of quasi-linear (due to the pipe friction term) hyperbolic partial differential equations. A general time-domain solution of these equations does not exist. It is of primary interest to obtain expressions for head and flow at the hydraulic turbine inlet which must be incorporated into the overall plant model. It is only of secondary interest to obtain detailed information concerning flow and head at positions in the penstock other than at the turbine inlet. For this reason, simplified forms of the basic penstock governing equations must be explored which adequately, and more easily represent the penstock dynamics.

Two-Port Representation and Head/Flow Transfer Function

If the fluid friction in the penstock is neglected, a uniform, two-port transmission line equation set describes the penstock model. By forming departures of flow and head from initial operating conditions, a dimensionless transfer function relates the flow and head at the penstock inlet and

outlet. The transfer function at the penstock outlet (turbine inlet) is of particular interest for implementation into a description of the entire hydroelectric plant. The development of this relation begins with the two penstock equations.

Neglecting the friction term, the momentum and continuity equations become:

$$Ag\frac{\partial H}{\partial x} + \frac{\partial Q}{\partial t} = 0 \qquad [3.7]$$

$$\frac{Ag}{c^2}\frac{\partial H}{\partial t} + \frac{\partial Q}{\partial x} = 0 \qquad [3.8]$$

Head and flow variables are manipulated into normalized departures in order to prepare for algebraic compatibility with the hydraulic turbine model. The partial derivatives become:

$$\frac{\partial H}{\partial x} = H_0\frac{\partial h}{\partial x}$$

$$\frac{\partial H}{\partial t} = H_0\frac{\partial h}{\partial t}$$

$$\frac{\partial Q}{\partial x} = Q_0\frac{\partial q}{\partial x}$$

$$\frac{\partial Q}{\partial t} = Q_0\frac{\partial q}{\partial t}$$

Substituting for the normalized departures and taking the Laplace transform of Eqs. 3.7 and 3.8 gives:

$$AH_0g\frac{\partial h}{\partial x}(s) + Q_0\, s\, q(s) = 0$$

$$\frac{AH_0g}{c^2}\, s\, h(s) + Q_0\frac{\partial q}{\partial x}(s) = 0$$

Solving for $\frac{\partial h}{\partial x}$ and $\frac{\partial q}{\partial x}$ gives:

$$\frac{\partial h}{\partial x}(s) = -\frac{Q_0}{AgH_0} s\, q(s) \qquad [3.9]$$

$$\frac{\partial q}{\partial x}(s) = -\frac{AgH_0}{c^2 Q_0} s\, h(s) \qquad [3.10]$$

Eqs. 3.9 and 3.10 may be expressed in matrix form which is given by:

$$\frac{\partial}{\partial x}\begin{bmatrix} h(s) \\ q(s) \end{bmatrix} = -\begin{bmatrix} 0 & \frac{Q_0}{AgH_0} s \\ \frac{AgH_0}{c^2 Q_0} s & 0 \end{bmatrix} \begin{bmatrix} h(s) \\ q(s) \end{bmatrix}$$

This matrix is in the form of a uniform two-port transmission line [10]. Two parameters may be defined before formulation of a head/flow transfer function. Let $\Gamma(s)$, called the propagation operator, be defined as:

$$\Gamma(s) = \frac{L}{c} s$$

and let Z , called the characteristic impedance, be defined as:

$$Z = \frac{c\, Q_0}{H_0\, A\, g}$$

The resulting solution which relates unit head to unit flow at the inlet ($x = 0$) and at the discharge ($x = L$) of the penstock is derived by Takahashi [10] as:

$$\begin{bmatrix} h(s)_{x=L} \\ q(s)_{x=L} \end{bmatrix} = \begin{bmatrix} \cosh \Gamma(s) & -Z \sinh \Gamma(s) \\ -\frac{1}{Z} \sinh \Gamma(s) & \cosh \Gamma(s) \end{bmatrix} \begin{bmatrix} h(s)_{x=0} \\ q(s)_{x=0} \end{bmatrix}$$

Since the reservoir head does not vary with time,

$$h(s)_{x=0} = 0$$

Only the transfer function at the penstock outlet is needed for the plant model. The flow departure at the inlet is algebraically eliminated to obtain:

$$\frac{h(s)_{x=L}}{q(s)_{x=L}} = \frac{-Z \sinh \Gamma(s) \cosh \Gamma(s)}{1 + \sinh^2 \Gamma(s)} \qquad [3.11]$$

This Laplace-domain relation represents the waterhammer dynamics of the penstock with the only restriction that the penstock friction is negligible. It will be used in this work for studying the effects of waterhammer on the stability limits of the entire hydroelectric plant model.

Rigid Water Column Model

The purpose of this section is to demonstrate the development of the rigid water column model and to show its relation to the previous pair of governing equations (Eqs. 2.3 and 2.4). In a section to follow, insights are provided which suggest conditions under which such a model is valid.

For the development of the rigid water column model, consider the frictionless flow of incompressible water in the penstock of length L and cross-sectional area A. Assume that the turbine wicket gates are initially positioned such that the initial flow and head at all stations in the penstock are Q_0 and H_0 respectively and that the wicket gates are instantaneously closed by a small amount. This action tends to decelerate the flow, decreasing its kinetic energy by raising the head of the column of fluid in the pipe by the amount ΔH. The head at the reservoir stays constant independent of the dynamics of the water in the penstock. By considering the entire penstock as a control volume, the equation for conservation of momentum requires that the sum of the forces acting on the control volume must equal the rate at which the momentum of the rigid water column changes. Since friction was neglected, the only forces acting on the control volume are the pressure forces at the inlet and outlet. Since the flow is considered to be acting as a rigid water column, the

rate of momentum change is simply the mass of the water multiplied by the rate at which the water column velocity changes. The momentum equation is given by:

$$\rho g A H_0 - \rho g A (H_0 + \Delta H) = \rho L A \frac{d(Q/A)}{dt}$$

Using the normalized departures of head and flow and simplifying, the momentum equation is given by:

$$\left(\frac{LQ_0}{AgH_0} \right) \frac{dq}{dt} = -h$$

The water starting time $T_w = LQ_0/AgH_0$ was defined in Eq. 2.1. The relation of flow to head in the penstock for the rigid water column model is the first order ordinary differential equation given by:

$$T_w \frac{dq}{dt} = -h \qquad [2.1]$$

The water starting time provides insight into the rate at which the flow responds during a transient. A penstock with a large water starting time (caused by any combination of a long or small diameter penstock, high flow, or low head) will be slow to respond to changes in wicket gate position. A penstock with a very small water starting time will be very quick to respond. In fact, as the penstock length approaches zero, the water starting time approaches zero, suggesting that for a very small water starting time, the penstock dynamics may be neglected.

Summary of Penstock Model Formulations

To summarize the formulation of penstock models, three mathematical models have been presented. The first model presented was the most general representation which resulted in a pair of partial differential equations with both time and penstock position being independent variables.

Penstock friction forces were included in the momentum equation. The wave round-trip travel time T_c was shown to provide a comparison of the speed of the penstock pressure wave travel compared to other times which characterize the behavior of other plant components.

A transcendental transfer function relating head and flow at the turbine inlet was developed by neglecting penstock friction. This head/flow transfer function will be valuable in studying the effects of waterhammer on the stability limits of the plant model.

The third model presented, the rigid water column model, is the one usually selected for the penstock and utilizes the assumptions that the water is incompressible and that the penstock is rigid and frictionless. The resulting momentum equation is a simple first order ordinary differential equation. The water starting time T_w was defined and shown to provide insight into the speed of penstock dynamics.

Once all the component models have been established, further insights will be presented so that an appropriate penstock model may be chosen for integration into the plant model.

Formulation of Hydraulic Turbine Models

The hydraulic turbine is mechanically coupled to the generator and supplies it with rotating mechanical power. The penstock provides a supply of water to the hydraulic turbine and this water flows through the turbine, dropping its pressure head as it passes through the turbine. The amount of power that the water delivers to the turbine depends on the flow, head drop, and on the turbine efficiency. The hydraulic turbine may be considered to be a device which transforms hydraulic water power into rotating mechanical power.

The development of a mathematical model which describes the dynamic performance of a hydraulic turbine is divided into two areas:

1. The description of the speed dynamics -- When there is an imbalance in the torque supplied by the water and the torque required by the generator, a speed change of the rotating device results.
2. The description of the turbine performance characteristics -- The relationships of turbine head, flow, torque, speed and efficiency depend on the particular hydraulic turbine which is installed.

There is unanimous agreement in the literature concerning the area of mechanical speed dynamics which is governed by Newton's second law of motion. In the second area, there are several methods which are utilized to describe the performance characteristics of a hydraulic turbine. This section is divided into two parts. The first part addresses hydraulic turbine speed dynamics. The second part addresses hydraulic turbine performance characteristics. Both of these aspects will be combined when forming the mathematical model for the entire plant.

Turbine Speed Dynamics

The basic equation for the speed dynamics of a rotating device is given by Newton's second law of motion:

$$T_{net} = I \frac{d\omega}{dt} \qquad [2.6]$$

in which T_{net}=the net torque applied to the rotating device

I=the polar moment of inertia of the device

$\frac{d\omega}{dt}$=the angular acceleration

The hydraulic turbine and the electric generator are mechanically coupled so the polar moment of inertia includes the inertia of both the turbine and generator. The net torque is determined by the water torque on the turbine and the load torque on the turbine from the electric generator. In steady, constant speed operation, the water torque equals the load torque.

When there is a difference between the water torque and the load torque, the net torque imbalance gives rise to a change in speed of the rotating turbine. Consistent with Newton's second law of motion, the first order dynamic relation is given by:

$$M_{water} - M_{load} = \frac{Wr^2}{g} \frac{d\omega}{dt} \qquad [3.12]$$

where Wr^2=the combined inertia of the turbine and generator

M_{load}=the instantaneous load torque required by the generator

M_{water}=the instantaneous water torque delivered to the turbine

The combined inertia term is expressed as the device weight multiplied by its radius of gyration rather than as the device mass because the Wr^2 expression is the one usually specified by manufacturers and design contractors in this field. The relation between Wr^2 and mr^2 is simply:

$$mr^2 = \frac{Wr^2}{g}$$

The circular speed ω is related to the rotational speed N (with the units of rpm) by:

$$\omega = \frac{2\pi N}{60}$$

The usual speed measurement N (in rpm) is substituted for the circular speed ω (in radians/sec) to achieve consistency with the turbine performance characterization developed in the next section.

Eq. 3.12 is now manipulated into a dimensionless form in order to develop a parameter which characterizes the turbine response. The normalized departures of the water torque m, the load torque m_{load}, and the speed n are defined by:

$$m = \frac{M_{water} - M_0}{M_0}$$

$$m_{load} = \frac{M_{load} - M_0}{M_0}$$

$$n = \frac{N - N_0}{N_0}$$

where M_0=the torque at the initial steady operation

N_0=the rotational speed at the initial steady operation

Making the substitutions for the dimensionless departures and for the circular speed, Eq. 3.12 becomes:

$$m - m_{load} = T_m \frac{dn}{dt} \qquad [3.13]$$

where $T_m = \frac{2\pi N_0 Wr^2}{60 M_0 g}$ and is referred to as the machine starting time.

For a very large machine starting time (corresponding to a high-inertia device) the turbine will respond slowly to a torque mismatch, whereas a device whose machine starting time is small will respond more quickly to the same torque mismatch.

Turbine Characteristics of Theoretical Model

Hydraulic turbine characteristics describe the relationships between the turbine flow, head drop across the turbine (or simply, turbine head), wicket gate position, efficiency, torque, and rotational speed. The Francis turbine has been chosen for this work because of its wide use in hydroelectric plants which include a penstock [6].

Consider that the initial operating condition of the turbine is known. The turbine wicket gate position is Y_0, the turbine head (using the turbine discharge as the zero head datum) is H_0, the flow is Q_0, the initial torque is M_0, and the initial speed (in rpm) is N_0. The theoretical relation between flow, head, and gate position which is the basis for Hovey's development is given by:

$$Q = K_1 \sqrt{H}\ Y$$

with K_1 being a constant which must satisfy the initial operating condition such that:

$$K_1 = \frac{Q_0}{\sqrt{H_0}\, Y_0}$$

Differentiating the head/flow/gate expression about the initial operating condition, the differential of flow is given by:

$$dQ = \frac{1}{2} \frac{K_1 Y_0}{\sqrt{H_0}}\, dH + K_1 \sqrt{H_0}\, dY \qquad [3.15]$$

Dividing by the relation for the initial operating condition $Q_0 = K_1 \sqrt{H_0}\, Y_0$, Eq. 3.15 becomes:

$$\frac{dQ}{Q_0} = \frac{1}{2} \frac{dH}{H_0} + \frac{dY}{Y_0}$$

The quantities dQ , dH , and dY represent small changes from the initial operating point. For example, $dQ = (Q - Q_0)$. Recalling the definitions for the dimensionless departures, the relation between head, flow, and gate departure becomes:

$$q = \frac{1}{2} h + y \qquad [3.16]$$

To develop an expression for torque in terms of head, flow, and gate position, Hovey assumed that the turbine was operating at a point of maximum efficiency and that the efficiency stayed constant. He further assumed that the torque was linearly related to the product of flow and head since changes in turbine speed must be small (less than ten percent). With these assumptions, the relation of torque, flow, and head becomes:

$$M = K_2\, Q\, H$$

with K_2 being a constant which must satisfy the initial condition such that

$$K_2 = \frac{M_0}{Q_0 H_0}$$

Differentiating the torque/head/flow expression about the initial operating condition gives:

$$dM = K_2(H_0\, dQ + Q_0\, dH)$$

Dividing by the relation for the initial operating condition $M_0 = K_2 Q_0 H_0$ yields:

$$\frac{dM}{M_0} = \frac{dQ}{Q_0} + \frac{dH}{H_0}$$

The relation above is in the form of departures from the initial operating condition and simplifies to:

$$m = q + h$$

For future convenience in assembling the overall plant model, the head/flow/gate relation is substituted in order to eliminate the flow departure and introduce the gate departure such that:

$$m = \frac{3}{2} h + y \qquad [2.7]$$

The assumptions that Hovey stated were that speed departure from initial operation must be less than ten percent and that the turbine efficiency stays constant. A tacit assumption not stated is that changes in flow, head, and gate position must also be small in order to insure that the turbine efficiency stays constant.

Turbine Characteristics for Linearized Model

Goldwag [15] showed that the theoretical representation for the torque attributed to Paynter and Hovey was valid for Pelton wheel turbines undergoing very small speed transients, but that

Francis turbines (the type which Hovey's work addressed) ususally deviated considerably from this relation. In his turbine model, he accounted for real turbine behavior and included the effect of speed changes on the torque.

A more sophisticated model for turbine characteristics was used by Thorne and Hill [16, 17] and Phi et. al. [18]. The general functional relationship is considered to be:

$$q = q(y,h,n)$$
$$m = m(y,h,n)$$

The flow and torque departures are assumed to be linearly related to gate, head, and speed departures. Six partial derivatives evaluated about the initial operating condition are required to describe the linearized turbine characteristic model. These partial derivatives, if assumed to be constant, maintain the convenient linear nature of the model while accounting for real turbine behavior. The flow and torque departures are given by:

$$q = \frac{\partial q}{\partial y}y + \frac{\partial q}{\partial h}h + \frac{\partial q}{\partial n}n \qquad [2.9]$$

$$m = \frac{\partial m}{\partial y}y + \frac{\partial m}{\partial h}h + \frac{\partial m}{\partial n}n \qquad [2.10]$$

The authors who introduced this approach relied on the turbine manufacturer to supply the values of the partial derivatives at various operating points. With this information, they showed that the turbine characteristics were similar to the theoretical model for rated turbine conditions (80 percent maximum load) but drastically departed from theoretical characteristics under other load conditions.

Although the linearized model represents real turbine behavior about a certain operating condition, a limitation is that only small departures from the initial operation are allowable in order for the partial derivatives to stay constant. In the case that the turbine operating condition changes considerably, then a representation must be used that takes the changing characteristics into account.

Turbine Characteristics Described by Hill Diagrams

Turbine characteristic information is supplied by various manufacturers in different forms [8]. However, recurring reference is made to hill diagrams in which two parameters, turbine unit discharge and turbine unit speed are related graphically. A representative hill diagram is shown in Fig. 2 (repeated here for convenience). Information from this diagram serves as the basis for the non-linear representation of turbine performance. The unit discharge Q_1 is defined in terms of flow, head, and turbine runner diameter (which is analagous to pump impeller diameter) as:

$$Q_1 = \frac{Q}{D_r^2\sqrt{H}} \qquad [3.17]$$

where Q=the turbine flow

D_r=the turbine runner diameter .

H=the turbine head

The unit speed N_1 is defined in terms of speed, head, and turbine runner diameter as:

$$N_1 = \frac{N D_r}{\sqrt{H}} \qquad [3.18]$$

where N = the turbine speed (rpm)

Lines of constant wicket gate position relate the unit discharge to the unit speed. In this manner, the relation between turbine head and flow is determined for a specified turbine speed. Lines of constant efficiency also shown on the diagram complete the graphical description of the turbine characteristics. For a specified turbine flow, head, and speed, the corresponding efficiency is determined graphically. The turbine torque is determined using the relation between torque, speed, flow, head, and efficiency as given by:

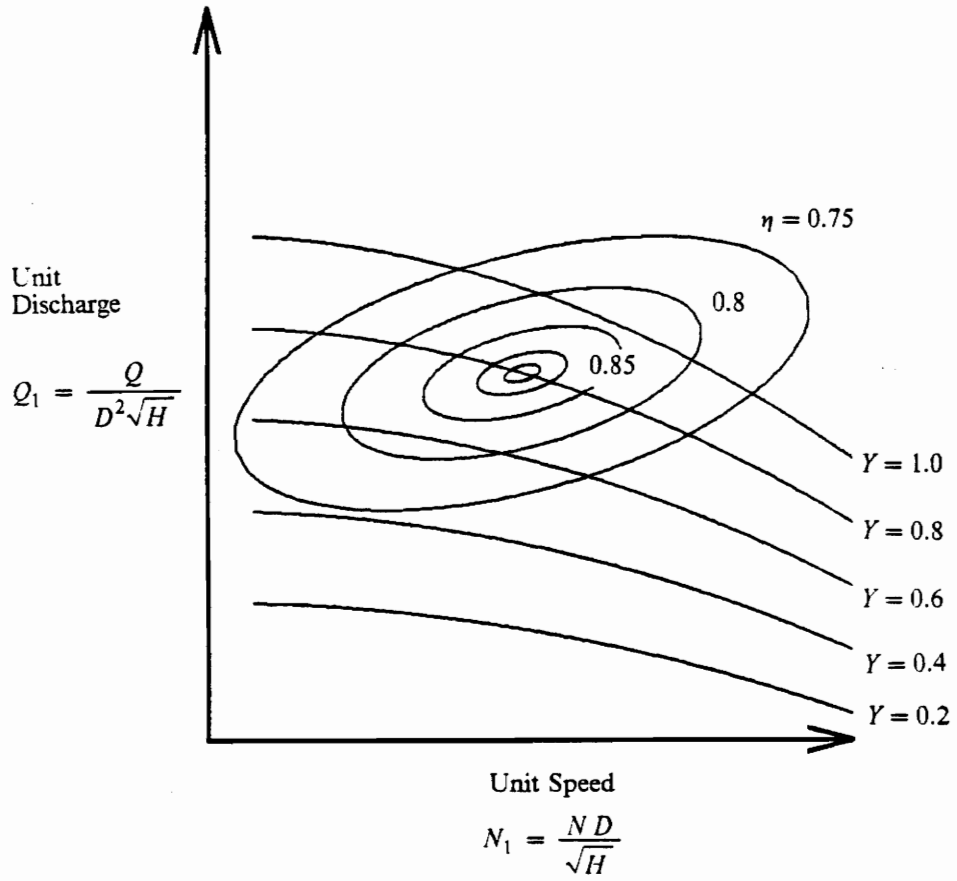

Figure 2. Representative Hill Diagram.

$$M = \frac{\eta \rho g Q H}{\left(\frac{2\pi N}{60}\right)} \qquad [3.19]$$

where M=the the water torque on the turbine

Q=the turbine flow

H=the turbine head

ρ=the water density

g=acceleration due to gravity

N=the turbine speed (rpm)

With consideration of Fig. 2, and since the runner diameter is constant for a particular machine, a unique operating condition is specified only by certain sets of three variables as follow:

Set of Specified Quantities	Remaining Quantities Which May Be Determined from the Hill Diagram
(Y, N, H)	(Q, M)
(Y, Q, H)	(N, M)
(Q, H, N)	(Y, M)

where Y= hydraulic turbine wicket gate position

(1 = gates fully open, 0 = gates closed)

Specification of any other three-set combination of (Y, Q, H, N, M) leads to the situation that two, one, or no operating conditions satisfy the specified information.

The graphical representation of turbine characteristics is inconvenient for repetitive computations. A possible improvement is to store many sets of operating conditions determined by hand from the hill diagram in a large matrix and access this information as necessary. This method was adopted by Wylie [8]. An alternative method is to analytically represent the lines of constant gate position and the lines of constant efficiency. A further benefit of this method is that the partial derivatives needed for the linearized turbine model may be determined at any operating condition.

The approach is used in this work to dispense with the need for manufacturer's input in determining the linearized turbine performance. Analytical relations which are formulated in the next sections provide the basis for evaluation of the six partial derivatives which characterize linearized turbine performance.

Analytical Representation of Constant Gate Lines on Hill Diagram

Inspection of the lines of constant gate position in Fig. 2 indicates that a polynomial expression for unit discharge versus unit speed is appropriate. For each wicket gate position, the unit discharge can be related to the unit speed by the parabolic relation:

$$Q_1 = a N_1^2 + b N_1 + c \qquad [3.20]$$

where a, b, and c are constant coefficients depending on gate position.

The method of least squares may be used to determine the coefficients which best represent the graphical data. When the Q_1 versus N_1 relation is required at a gate position between the ones specified, then a linear interpolation on gate position may be utilized to estimate the coefficients at this intermediate position.

The parabolic representation for unit discharge versus unit speed actually specifies the relation between turbine head and flow for a fixed value of turbine speed. For a particular gate position,

$$Q = \frac{a D_r^4 N^2}{\sqrt{H}} + b D_r^3 N + c D_r \sqrt{H}$$

Comparing this relation with the previously described theoretical turbine head/flow/gate relation ($Q = K_1 \sqrt{H}\ Y$) , the a, b, and c coefficient characterization of a theoretical turbine leads to the following result:

$$a=0$$

$$b=0$$

$$c=\frac{Q_0}{\sqrt{H_0}\,Y_0 D_r^2}Y$$

where Q_0= flow at the initial operating condition

H_0= head at the initial operating condition

Y_0= gate position at the initial operating condition

D_r= turbine runner diameter

Y= any arbitrary gate position between 0 and 1

In other words, the lines of constant gate position for a theoretical turbine on a hill diagram become horizontal lines linearly spaced between $Y = 0$ (closed) to $Y = 1$ (fully open).

Analytical Representation of Constant Efficiency Lines of Hill Diagram

A family of rotated, translated ellipses has been chosen to represent the lines of constant efficiency. The following set of parametric equations have been used to describe each ellipse:

$$\begin{aligned} N_1 &= x\,\cos\theta - y\,\sin\theta + N_1^0 \\ Q_1 &= x\,\sin\theta + y\,\cos\theta + Q_1^0 \end{aligned} \qquad [3.21]$$

$$\frac{x^2}{d^2}+\frac{y^2}{e^2}=1$$

where θ= the counterclockwise rotation of the ellipse from the horizontal N_1 axis

N_1^0= the unit speed coordinate of the center of the ellipse

Q_1^0= the unit discharge coordinate of the center of the ellipse

d= half the magnitude of the major axis

e= half the magnitude of the minor axis

x, y= dummy variables used for generation of the ellipses

The analytical representation is more easily understood with the review of Fig. 11.

Determination of Turbine Characteristic Partial Derivatives

The analytical representations for turbine performance serve as the basis for evaluation of the six partial derivatives required by the linearized turbine model. The development for each expression is presented in this section. In addition, the performance characterization of a theoretical turbine is compared to the description used by Hovey [13].

Consider hydraulic turbine operation which is defined by the set of values (Y_0, H_0, N_0) . The hill diagram is utilized to complete the set of operating condition values (Y_0, H_0, N_0, Q_0, M_0) . The six partial derivatives needed for the linearized turbine model are $(\partial q/\partial y)$, $(\partial q/\partial h)$, $(\partial q/\partial n)$, $(\partial m/\partial y)$, $(\partial m/\partial h)$, and $(\partial m/\partial n)$.

The first partial derivative to be evaluated is $(\partial q/\partial n)$. The flow is a function of gate position, head, and speed ($Q=f(Y,H,N)$) so the partial derivative must be evaluated while holding Y and H constant at Y_0 and H_0 . The partial derivative in terms of the operating condition variables is given by:

$$\frac{\partial q}{\partial n}=\frac{N_0}{Q_0}\frac{\partial Q}{\partial N}$$

The parabolic expression for unit discharge was given in Eq. 3.20 as:

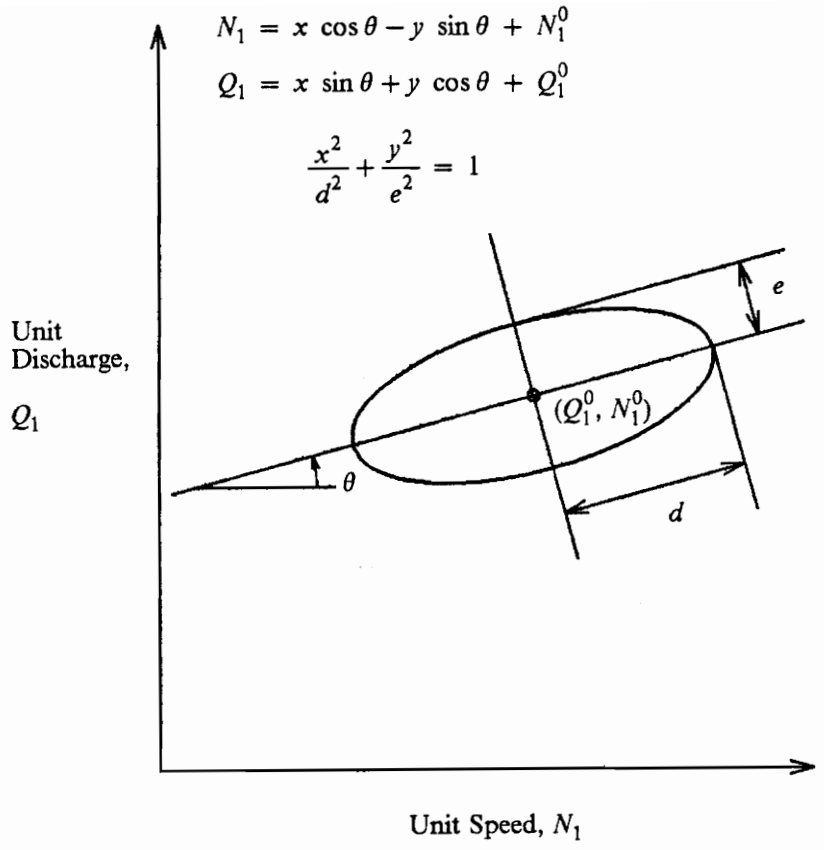

Figure 11. Analytical Representation of a Line of Constant Efficiency.

$$Q_1 = \frac{Q}{D_r^2\sqrt{H}} = a\left(\frac{ND_r}{\sqrt{H}}\right)^2 + b\left(\frac{ND_r}{\sqrt{H}}\right) + c \qquad [3.20]$$

Performing the partial derivative of Eq. 3.20, $(\partial q/\partial n)$ is determined to be:

$$\frac{\partial q}{\partial n} = \frac{N_0 D_r^3}{Q_0}\left[2a\left(\frac{N_0 D_r}{\sqrt{H_0}}\right) + b\right] \qquad [3.22]$$

The evaluation of $(\partial q/\partial h)$ follows in a similar manner and yields:

$$\frac{\partial q}{\partial h} = -\frac{N_0^2 D_r^4 a}{2Q_0\sqrt{H_0}} + \frac{c D_r\sqrt{H_0}}{2Q_0} \qquad [3.23]$$

Evaluation of $(\partial q/\partial y)$ requires a perturbation approach because there is not a continuous analytical relation between the flow and gate position. An illustration of such a change in unit flow is shown in Fig 12. By changing the gate position a small amount ΔY and holding the unit speed constant, the resulting change in unit discharge ΔQ_1 may be easily computed. The analytical relation for unit discharge leads to:

$$\Delta Q_1 = (a_* - a_0)N_1^2 + (b_* - b_0)N_1 + (c_* - c_0)$$

where the subscript 0 represents the initial operating condition and the subscript * represents the new gate condition as shown in Fig. 12. The change in flow is given by:

$$\Delta Q = D_r^2\sqrt{H_0}\ \Delta Q_1$$

For small ΔY the resulting expression for $(\partial q/\partial y)$ becomes:

$$\frac{\partial q}{\partial y} = \frac{Y_0}{Q_0}\frac{\Delta Q}{\Delta Y} \qquad [3.24]$$

All three of the partial derivatives which involve the torque require perturbation approaches because torque changes depend on efficiency changes for which there is no continuous represen-

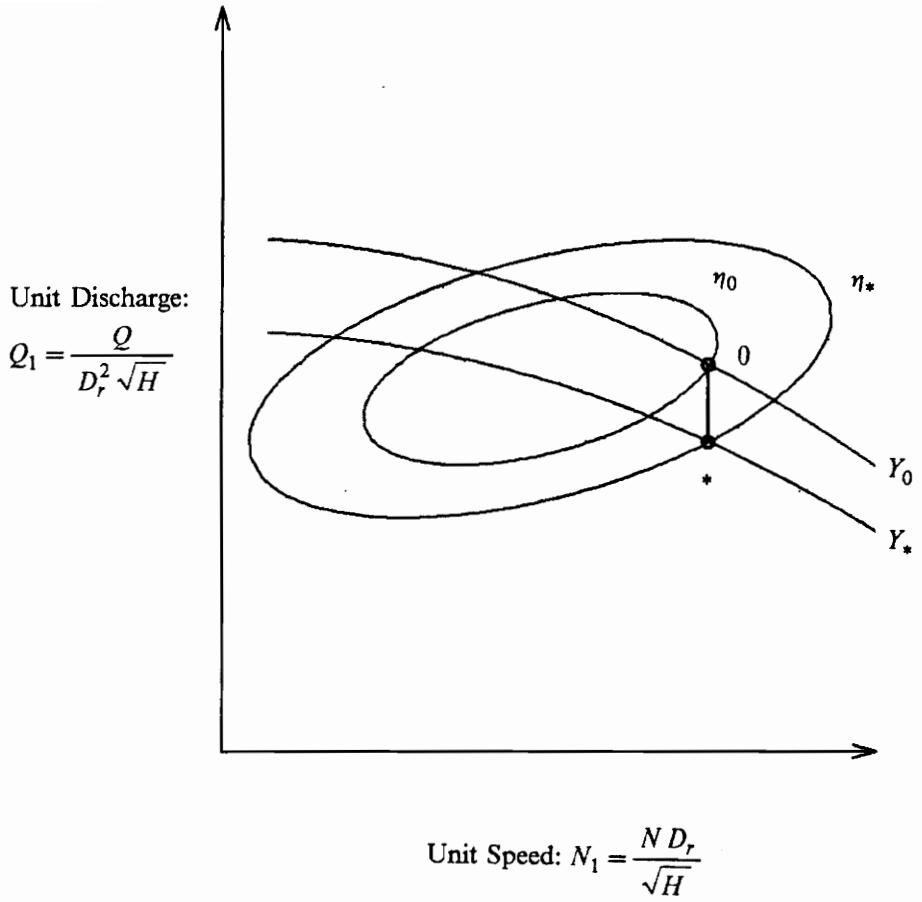

Figure 12. Turbine Operating Condition Change Holding Speed and Head Constant.

tation in the analytical expressions. The torque is a function of gate position, head, and speed ($M = f(N,H,Y) = (60\rho g\eta QH)/(2\pi N)$). The partial derivative ($\partial m/\partial n$) is evaluated while holding the head and gate position constant at H_0 and Y_0. In terms of the dimensional plant variables, ($\partial m/\partial n$) is given by:

$$\frac{\partial m}{\partial n} = \frac{N_0}{M_0}\frac{\partial M}{\partial N}$$

Substituting the expression for the torque into the partial derivative and applying the chain rule, the expression ($\partial m/\partial n$) is given by:

$$\frac{\partial m}{\partial n} = \left(\frac{60\rho g N_0 H_0}{2\pi M_0}\right)\left[\frac{Q_0}{N_0}\frac{\partial \eta}{\partial N} - \frac{\eta_0 Q_0}{N_0^2} + \frac{\eta_0}{N_0}\frac{\partial Q}{\partial N}\right]$$

The expression for ($\partial Q/\partial N$) has been evaluated previously. The value for ($\partial \eta/\partial N$) must be estimated by determining the change in efficiency due to a small change in speed while holding the head and gate position constant. A small change in speed results in a proportional change in unit speed as illustrated in Fig. 13. Using the assumption that the partial derivative is accurately represented by the change in efficiency due to the small change in speed while holding the head and gate position constant, the resulting expression for ($\partial \eta/\partial N$) becomes:

$$\frac{\partial \eta}{\partial N} = \frac{\eta_* - \eta_0}{N_* - N_0}$$

Thus ($\partial m/\partial n$) is given by:

$$\frac{\partial m}{\partial n} = -1 + \frac{N_0}{\eta_0}\frac{\partial \eta}{\partial N} + \frac{N_0}{Q_0}\frac{\partial Q}{\partial N} \qquad [3.25]$$

where $\frac{\partial Q}{\partial N} = D_r^2\sqrt{H_0}\left[\frac{2aD_r^2 N_0}{H_0} + \frac{b\,D}{\sqrt{H_0}}\right]$

$$\frac{\partial \eta}{\partial N} = \frac{\eta_* - \eta_0}{N_* - N_0}$$

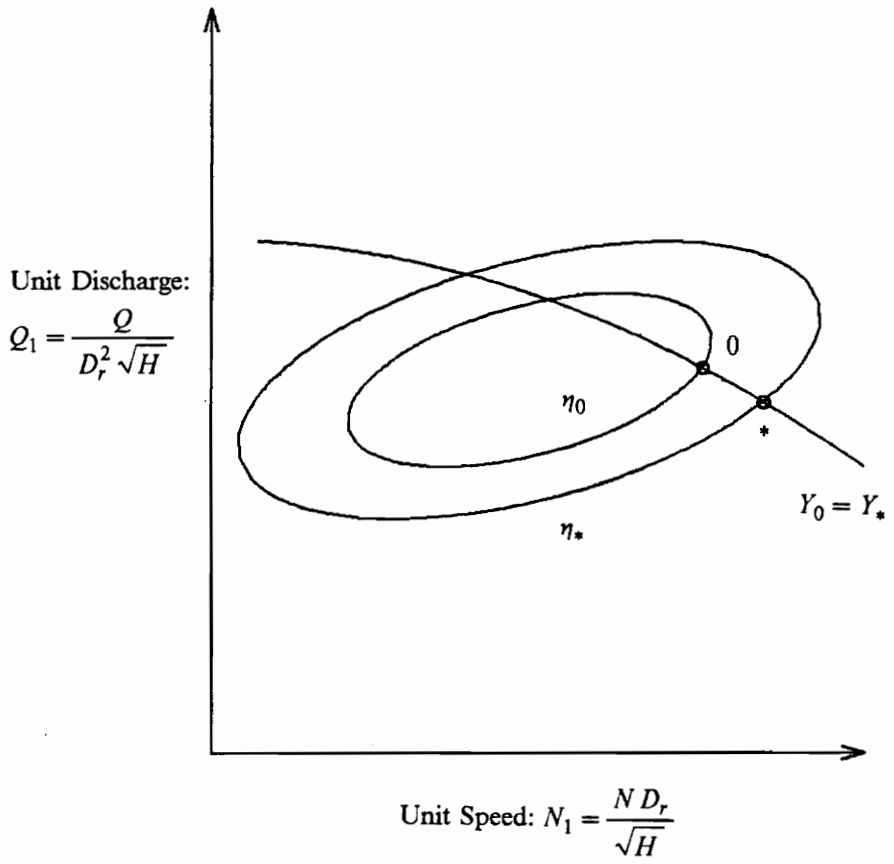

Figure 13. Turbine Operating Condition Change Holding Gate Position Constant.

The development of $(\partial m/\partial h)$ proceeds in a similar manner. The partial derivative is evaluated while holding N and Y constant. The expression for $(\partial m/\partial h)$ becomes:

$$\frac{\partial m}{\partial h} = \left(\frac{60\rho g H_0}{2\pi N_0 M_0}\right)\left[\eta_0 Q_0 + \eta_0 H_0 \frac{\partial Q}{\partial H} + Q_0 H_0 \frac{\partial \eta}{\partial H}\right]$$

The expression for $(\partial Q/\partial H)$ has been evaluated previously. The value for $(\partial \eta/\partial H)$ must be estimated by determining the change in efficiency due to a small change in head while holding the speed and gate position constant. A small change in head results in a change in unit speed as illustrated in Fig. 13. The resulting expression for $(\partial \eta/\partial H)$ becomes:

$$\frac{\partial \eta}{\partial H} = \frac{\eta_* - \eta_0}{H_* - H_0}$$

and $(\partial m/\partial h)$ is given by:

$$\frac{\partial m}{\partial h} = 1 + \frac{H_0}{\eta_0}\frac{\partial \eta}{\partial H} + \frac{H_0}{Q_0}\frac{\partial Q}{\partial H} \qquad [3.26]$$

where $\dfrac{\partial \eta}{\partial H} = \dfrac{\eta_* - \eta_0}{H_* - H_0}$

$$\frac{\partial Q}{\partial H} = -\frac{a}{2}N_0^2 D_r^2 H_0^{-3/2} + \frac{c}{2}D_r^2 H_0^{-1/2}$$

The final partial derivative to be evaluated is $(\partial m/\partial y)$. The partial derivative is evaluated while holding N and H constant. The value for $(\partial M/\partial Y)$ must be estimated by determining the change in torque due to a small change in gate position while holding the speed and head constant. A small change in gate position while holding the unit speed constant results in a change in flow as well as efficiency as illustrated in Fig. 12. The resulting expression for the partial derivative $(\partial m/\partial y)$ becomes:

$$\frac{\partial m}{\partial y} = \left(\frac{Y_0}{M_0}\right)\left(\frac{(\rho g H_0)}{\dfrac{60N_0}{2\pi}}\right)\left(\frac{\eta_* Q_* - \eta_0 Q_0}{N_* - N_0}\right) \qquad [3.27]$$

With the expressions determined for the six partial derivatives, it is now a simple task to compute the values of the derivatives at any operating condition -- providing numerical estimates for linearized turbine performance.

The turbine relations attributed to Paynter and Hovey are now compared to linearized characteristics of a theoretical turbine. The coefficients a, b, and c which describe the unit discharge versus unit speed relationship for the theoretical turbine were shown to be:

$$a=0$$

$$b=0$$

$$c=\frac{Q_0}{\sqrt{H_0}\,Y_0 D_r^2}\,Y$$

The other assumption for the theoretical turbine is that the efficiency remains constant $\eta = \eta_0$. The resulting values for the partial derivatives are tabulated in comparison to values used in Hovey's model in Table 1.

Review of Table 1 reveals that five of the partial derivatives compare exactly to Hovey's model, but the value of $(\partial m/\partial n)$ does not. This is due to Hovey's assumption that the torque was proportional to the product of flow and head where, more appropriately, the product of torque and speed is proportional to the product of flow and head. An intriguing observation is that many authors have introduced the concept of a "load self-regulation factor" in the modification of Hovey's theoretical expression for the torque departure. This modification takes the form presented in Eq. 2.8 as:

$$m = \frac{3}{2}h + y - \alpha n \qquad [2.8]$$

where α = the load self-regulation factor

Compared to Hovey's model:

$$m = \frac{3}{2}h + y \qquad [2.7]$$

Table 1. Comparison of Turbine Characteristic Partial Derivative Values.

Partial Derivative	Value Determined Analytically from Theoretical Turbine Model	Value Corresponding to Hovey's Theoretical Model
$\partial q/\partial y$	1	1
$\partial q/\partial h$	1/2	1/2
$\partial q/\partial n$	0	0
$\partial m/\partial y$	1	1
$\partial m/\partial h$	3/2	3/2
$\partial m/\partial n$	-1	0

Compared to the partial derivative representation:

$$m = \frac{\partial m}{\partial h} h + \frac{\partial m}{\partial y} y + \frac{\partial m}{\partial n} n \qquad [2.10]$$

The value for the load self-regulation factor depends on empirical information. Chaudhry [9] presented a table which guided the selection for a value of α . The selection was based on the type of turbine and on the type of electrical system connected to the plant. The resulting value for the factor is approximately unity, which approximately corresponds to the evaluation of $(\partial m/\partial n)$ as presented in this work. In order to avoid estimation of the load self-regulation factor, the linear characterization of the turbine torque departure is based on the partial derivative approach in this work.

Formulation of Governor Models

A hydroelectric plant governor controls the turbine wicket gate position in order to change the torque that the water supplies to the turbine. There are two purposes that the governor serves:

1. To regulate the rotational speed at the desired speed in the event that a mismatch in the water torque and load torque occurs.
2. To adjust the power that the hydroelectric plant delivers to the connected electrical system.

A mathematical model representative of a currently installed hydro plant governor is formulated in this section. The oldest governors are mechanical-hydraulic devices. Some governors incorporate electronic circuitry and hydraulic servo positioning of the turbine wicket gates. The most modern governors may include digital control in addition to electronic circuitry and hydraulic turbine gate positioning. Common to all the hydroelectric plant governors are proportional and in-

tegral control, hydraulic servo positioning of the turbine wicket gates, and a means of adjusting the plant power delivered to the connected electrical system.

The IEEE Power System Engineering Committee [20] provided a block diagram which outlines the function of a steam plant or hydroelectric plant governing system which is summarized in Fig. 14. As shown in Fig. 14, there are two input signals to the speed governing system which may cause the wicket gate position command signal to change. First is the turbine speed signal which will cause the gate to move when there is a deviation of the turbine speed from the desired speed. Second is the assigned power generation signal. This second signal is utilized in the event that it is desired to change the generation of the unit when there is no error in the desired speed of the turbine.

The concept of coordinated turbine speed control along with control of desired unit generation is illustrated by Gurney [21]. This information was provided as a summary of the equipment installed in the Revelstoke hydroelectric plant which went into operation in 1984. The author presents a block diagram of the plant's electronic-hydraulic speed governor system. The block diagram shows that the turbine speed control is of the proportional-integral-derivative type which includes a time lag for electronic processing to compute the speed derivative signal. A generation control signal is included. Finally, a steady-state speed regulation signal is added into the governor block diagram in order to allow for the operation of the entire electrical system in a state of permanent droop, also known as steady-state speed regulation. The block diagram presented by Gurney is used as a basis to represent a typical modern hydroelectric governing system.

Using the block diagram of the Revelstoke plant as a guide, a simplified model for the electronic/hydraulic governor is shown in the block diagram of Fig. 15. This model neglects aspects of hydraulic actuator time lags, electronic circuitry time lags, and steady state speed regulation. In the event of a mismatch between the turbine speed and the desired speed, the governor operates in the speed regulation mode. When it is desired to change the power produced by the plant, the operator (or automatic dispatcher) repositions the wicket gates in a prescribed open-loop mode independent of plant speed regulation.

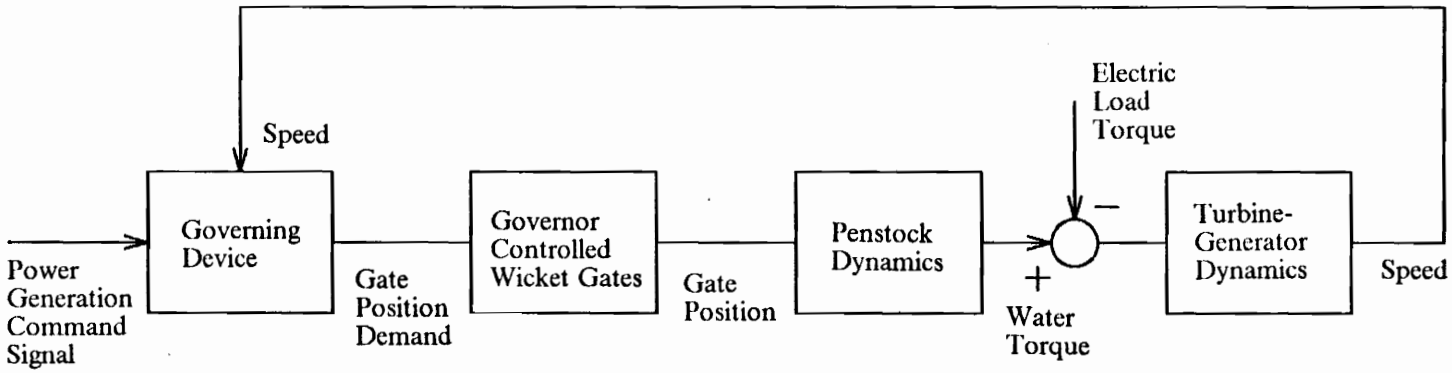

Figure 14. Functional Block Diagram of Governor and Hydroelectric Plant Components.

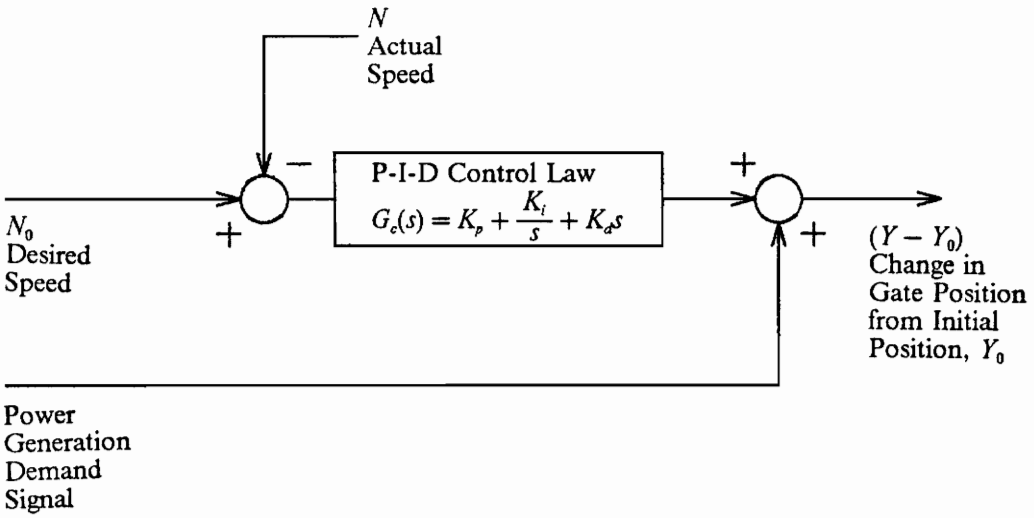

Figure 15. Development of Simplified Governor Model.

In order to formulate the control law for the speed control portion of the governor, consider that the initial gate position is Y_0 when the turbine is operating steadily at the desired speed N_0. When there is an error in the turbine speed, a change in gate position $(Y - Y_0)$ must be implemented to correct the speed error. A control law $G_c(s)$, is expressed in the Laplace domain as:

$$(Y - Y_0) = G_c(s)\,(N_0 - N)$$

where $G_c(s) =$ the control law to be defined.

The transfer function which relates gate departure to speed departure may be expressed as:

$$\frac{y(s)}{n(s)} = -\frac{N_0}{Y_0}\,\frac{(Y - Y_0)}{(N - N_0)}\,G_c(s)$$

Incorporating the constant (N_0/Y_0) into $G_c(s)$, let the control law incorporate aspects of proportional, integral, and derivative control as given by:

$$\frac{y(s)}{n(s)} = -K_p - \frac{K_i}{s} - K_d\,s \qquad [3.28]$$

where K_p= the proportional gain

K_i= the integral gain

K_d= the derivative gain

This work is limited to the proportional-integral-derivative control law for two reasons. First, the P-I-D control law is the one which is utilized in current operational plants. Older plants operate on the P-I control law which is a simplification of P-I-D control. Second, the hydroelectric plant will be shown to operate as a nonlinear dynamic system under certain conditions and P-I-D control does not require a linear system model.

Hydromechanical governors were the first type of governor to be widely utilized in hydroelectric generation service. Two field-adjustable settings known as temporary droop (δ) and the dashpot reset time (T_r) are used to adjust the response of the governor as it positions the wicket

gates due to a departure in the turbine speed. Thorne and Hill [16] demonstrated that the hydromechanical governor could be expressed as an equivalent P-I control device. They demonstrated how the temporary speed droop and the dashpot reset time were algebraically related to proportional gain and integral gain. This algebraic relation has been utilized by subsequent authors because of the wide familiarity with concepts of proportional and integral gains and because of the modern use of electronic-hydraulic and digital control. The relation between temporary speed droop, dashpot reset time, and proportional and integral control settings are given by:

$$K_p = \frac{1}{\delta}$$

$$K_i = \frac{1}{\delta T_r}$$

where δ= the temporary speed droop

T_r= the dashpot reset time

The speed with which the governor system can position the turbine wicket gates is an important part of hydro plant governor operation. Since the gates can be massive and since the torque imparted on the gates by the water during a transient can be large, there is a physical limitation on how fast the gates can be moved. As presented by Chaudhry [9], Gordon has provided information concerning the relation of gate motion times compared to the water starting time and to the machine starting time. Gordon has made a graphical presentation of the quality of control of a plant depending on the full-gate-closure and full-gate-opening times. The quality of control is divided into areas of good, fair, and poor quality as shown in Fig. 16. His presentation is based on experience with 40 different installations. The dividing line between poor and fair quality is given by:

$$\frac{T_w}{T_{gc}} = 1.7\frac{T_m}{T_{go}} - 0.96$$

where T_w= the water starting time

T_m= the machine starting time

T_{gc}= the gate closure time from fully open to fully closed

T_{go}= the gate opening time from fully closed to fully open

Generally, the full gate closure time is about 1 1/2 sec longer than the full gate opening time. The dividing line between fair and good control quality is given by:

$$\frac{T_w}{T_{gc}} = 1.25\frac{T_m}{T_{go}} - 1.04$$

For estimation purposes, if the gate closure and gate opening times are equal, then the full gate motion time (opening or closing) which falls between good and fair control quality is given by:

$$T_g = \frac{1.25T_m - T_w}{1.04} \qquad [3.29]$$

where T_g = the full gate motion time for opening or closing.

This gate motion time estimate should be conservative since it represents the gate speed that will barely give good plant control. According to Gordon's curves, better plant control is achieved for faster available gate speeds (corresponding to smaller gate motion times). The estimate for available gate speed will be used when various control settings are explored while determining settings which result in optimum plant performance. Control settings that require a faster gate motion than available will have to be rejected.

Now that the model for the governor has been formulated, the last component model to be developed is for the electric generator and connected electrical system. This model will form the basis for the load torque and will complete the component descriptions for the plant.

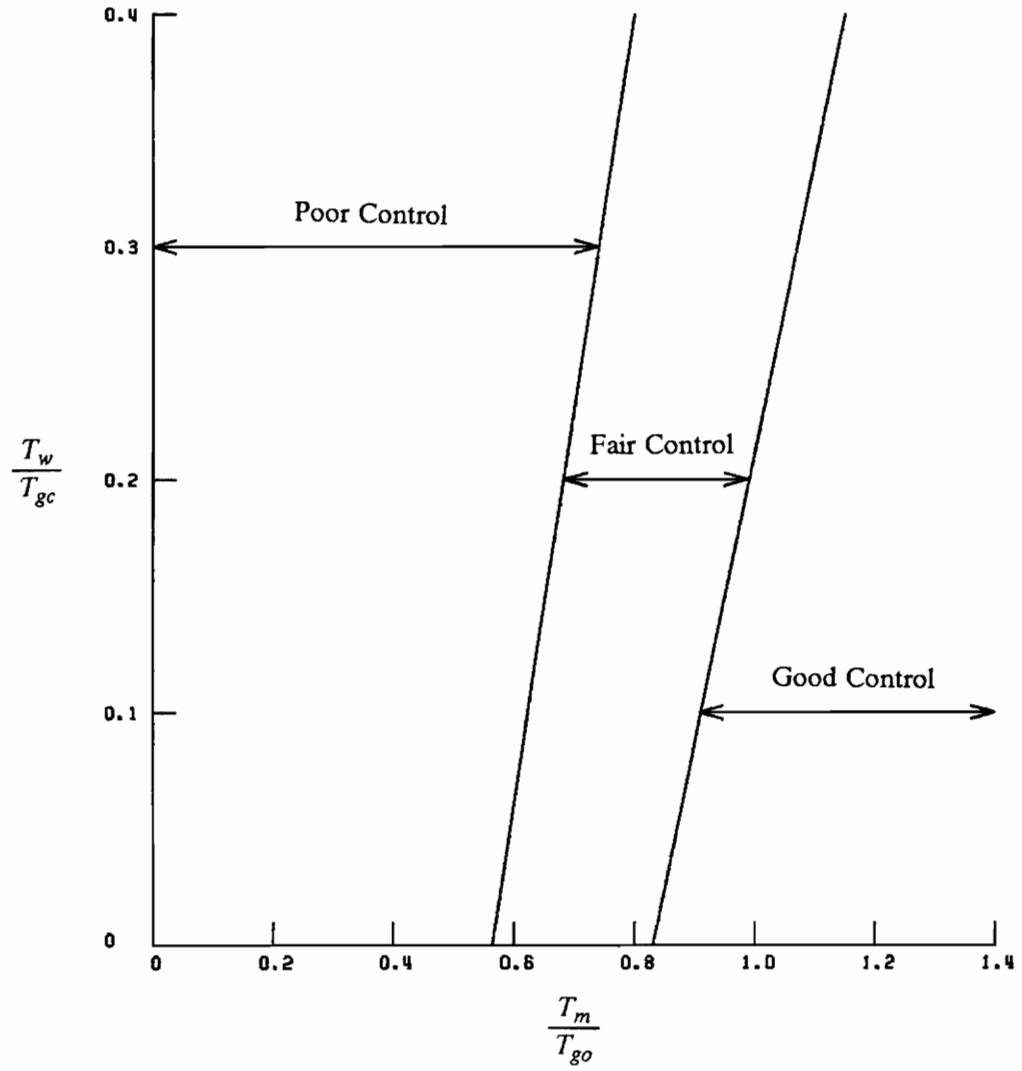

Definitions:

Poor Control	Units in this range cannot provide any frequency regulation unless fitted with relief valves operating on both load-on and load-off operation.
Fair Control	Units in this range will provide frequency regulation on large connected electrical systems only.
Good Control	Units in this range will provide good regulation in isolated operation or system operation.

Figure 16. Quality of Speed Regulation Depending on Gate Motion Times (Gordon's Curves).

Formulation of Generator and Electrical Connection Models

Since the hydraulic turbine has been characterized as a device which transforms hydraulic power supplied by the water into rotating mechanical power to be supplied to the generator, it remains to formulate a mathematical model for the load torque that the generator demands from the turbine. The complexity of the mathematical model depends on the type of electrical load that is connected to the generator.

Figure 6 (which is presented on the following page for convenience) is based on the block diagram presented by Thorne and Hill [16] and shows the dynamic interaction of the generator, the connected electrical system, and the hydromechanical plant. The electrical/mechanical interaction is expressed in terms of the load torque that the generator supplies to the hydraulic turbine and the speed of the hydraulic turbine. For the purpose of this work, it is desired to obtain models for the load torque as a function of the turbine speed. In the block diagram, the frequency mismatch of the generator is represented by a mismatch in machine versus system speed departures. The dynamic model for the generator provides the possibility for there to be a mismatch in the equivalent frequency of the turbine/generator set versus the equivalent frequency of the connected electrical system during a system transient. Using this model for the generator, the only way for there to be a change in load torque on the turbine is for there to be a mismatch in the machine speed versus system speed.

The block diagram of Fig. 6 includes the dynamic model of a connected electrical system as presented by Thorne and Hill [16]. It is assumed that the connected electical system is supplied by several power plants and that the hydroelectric plant carries a fraction $1/B$ of the entire load. In the event of a change in power demanded by the connected electrical system, all of the power plants respond dynamically to a change in that load. The equivalent system is modeled as having an equivalent inertia, equivalent damping, and an equivalent proportional control. The values of the

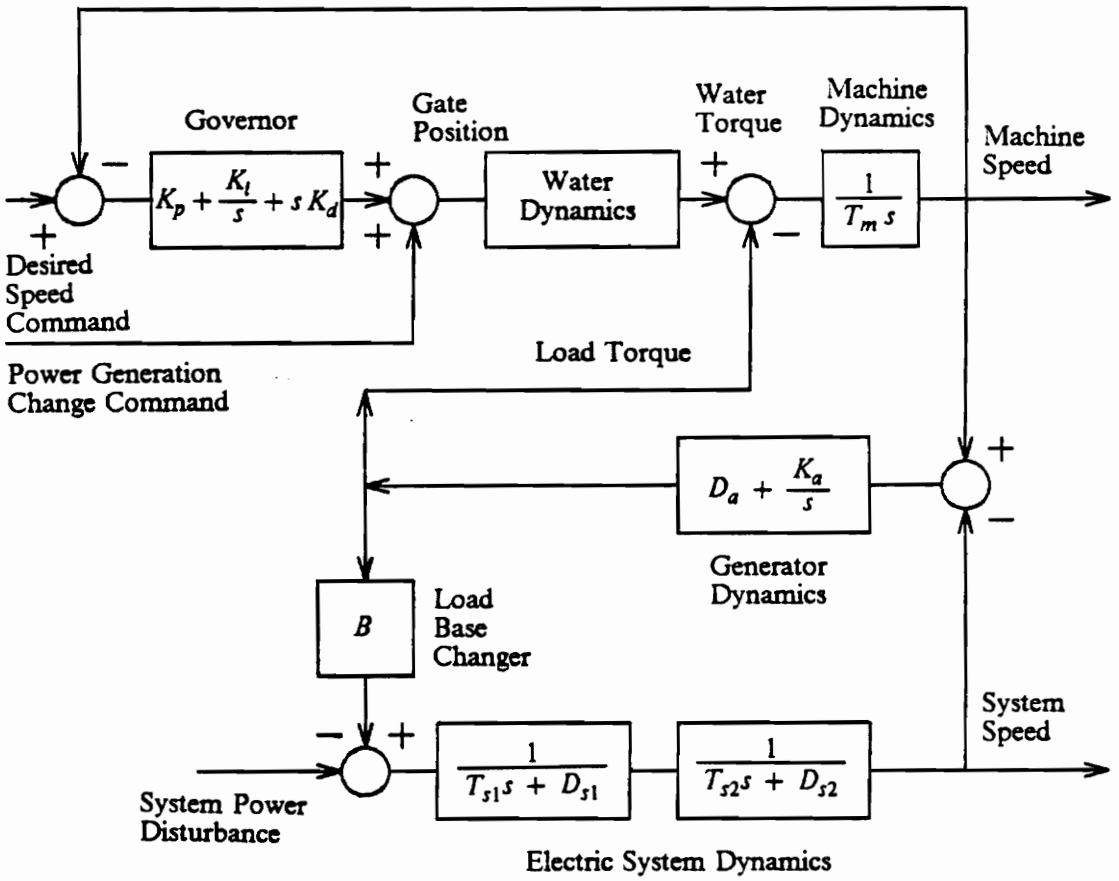

Figure 6. Generator and Electrical Connection Models.

time lags T_{s1} and T_{s2} and the damping terms D_{s1} and D_{s2} are determined by field information concerning the nature and dynamics of the connected plants and electrical system itself. If all the connected plants are hydroelectric, then the second time lag T_{s2} becomes zero and the second damping term D_{s2} becomes unity.

As illustrated by the block diagram of Fig. 6, the hydroelectric plant response to a change in system load or to a change in the desired plant load depends on the type of electrical system which the plant serves. The plant may be the only one supplying power to a small electrical system; it may be one of a few plants supplying power to a system; or it may be one of many plants connected to a large power distribution grid. The following three load configurations are presented for the purpose of representing a range of possible plant operating situations.

Configuration 1) Isolated Load - Change in Load Torque: The plant is the sole supplier of power to the connected system. Changes in plant speed translate directly into changes in system frequency. This situation is equivalent to the generator supplying power to a purely resistive load [13]. For a change in system load, the mismatch in water versus system load gives rise to a speed change of the turbine. The governor responds in the speed regulation mode to maintain the desired turbine speed. For the initial load torque M_0 , a step change to a new load torque M_{load} corresponds to a load torque departure given by:

$$m_{load} = \frac{M_{load} - M_0}{M_0} = constant \qquad [3.30]$$

According to the recommendation of Schleif and Wilbor [24], the isolated load model is the one which will be used for the purpose of governor tuning studies for improving plant performance.

Configuration 2) Plant Supplies a Fraction of Load to a Connected System - Change in System Demand. A decrease in system load gives rise to an increase in the system speed by way of a first (or second) order lag according to the model of the connected system as shown in Fig 6. The mismatch between system speed and machine speed gives rise to a decrease in the generator

load torque by way of the generator model dynamics. The mismatch between load torque and water torque gives rise to an increase in machine speed. The governor responds in the speed regulation mode to maintain the desired turbine speed.

Manipulation of the transfer functions as shown in the block diagram of Fig. 6, leads to the Laplace domain relation of the load torque departure to the connected electrical system load departure and turbine speed departure. The load torque relation for this operating configuration is given by:

$$m_{load}(s) = \frac{n(s)}{\frac{1}{D_a + \frac{K_a}{s}} + \frac{B}{(T_{s1}s + D_{s1})(T_{s2}s + D_{s2})}} + \frac{p_{sys}(s)}{B + \frac{(T_{s1}s + D_{s1})(T_{s2}s + D_{s2})}{(D_a + \frac{K_a}{s})}}$$

Configuration 3) Plant Speed Constant - Operator Adjusts Generation Reference Signal: If the plant is connected to a very large system and if the generator field control is sufficient to maintain the load torque equal to the water torque, then the turbine speed will be constant. If this is the situation, then the governor is independent of the speed regulation mode and gate motion resulting from the generation reference command will affect only the water dynamics. Since the generator reference command is determined by the operator (or automatic dispatcher), care must be taken to limit the gate speed in order to avoid unwanted water dynamics during the gate travel. Problems may be avoided by enforcing a gate speed limit or by carefully scheduling the gate motion so as to avoid penstock overpressure at the turbine. The variables needed for the plant model are given by:

$$n(t)=0$$

$$m_{load}(t)=m(t)$$

Overview of Candidate Plant Models

With mathematical models formulated for each of the plant components the task of forming an appropriate plant model can begin. Several candidate plant models arise because some components have two or more mathematical models. An overview of the governing equations which comprise each candidate plant model is presented in Table 2. The models vary in complexity from the theoretical linear one originally presented by Hovey to a plant model which includes the nonlinear formulations for waterhammer in the penstock and the nonlinear characteristics of the hydraulic turbine.

All of the candidate dynamic models have several aspects in common. The height of the reservoir is considered to be constant for each of the models. The discharge conduit (draft tube) of the hydraulic turbine is considered to be very short so that the datum for hydraulic head ($H = 0$) may be assigned at the turbine discharge. The dynamic equation for the turbine speed is the same for all models. The mathematical model for the governor follows the P-I-D control law for all of the candidate models.

Theoretical Linear Model

The simplest dynamic model that may be assembled from the plant component formulations is the linear model similar to that of Hovey. The only difference in this model from Hovey's original model is the P-I-D control law. Hovey's model can therefore be duplicated by simply assigning a value of zero to the derivative gain.

Table 2. Governing Equations for Candidate Plant Models.

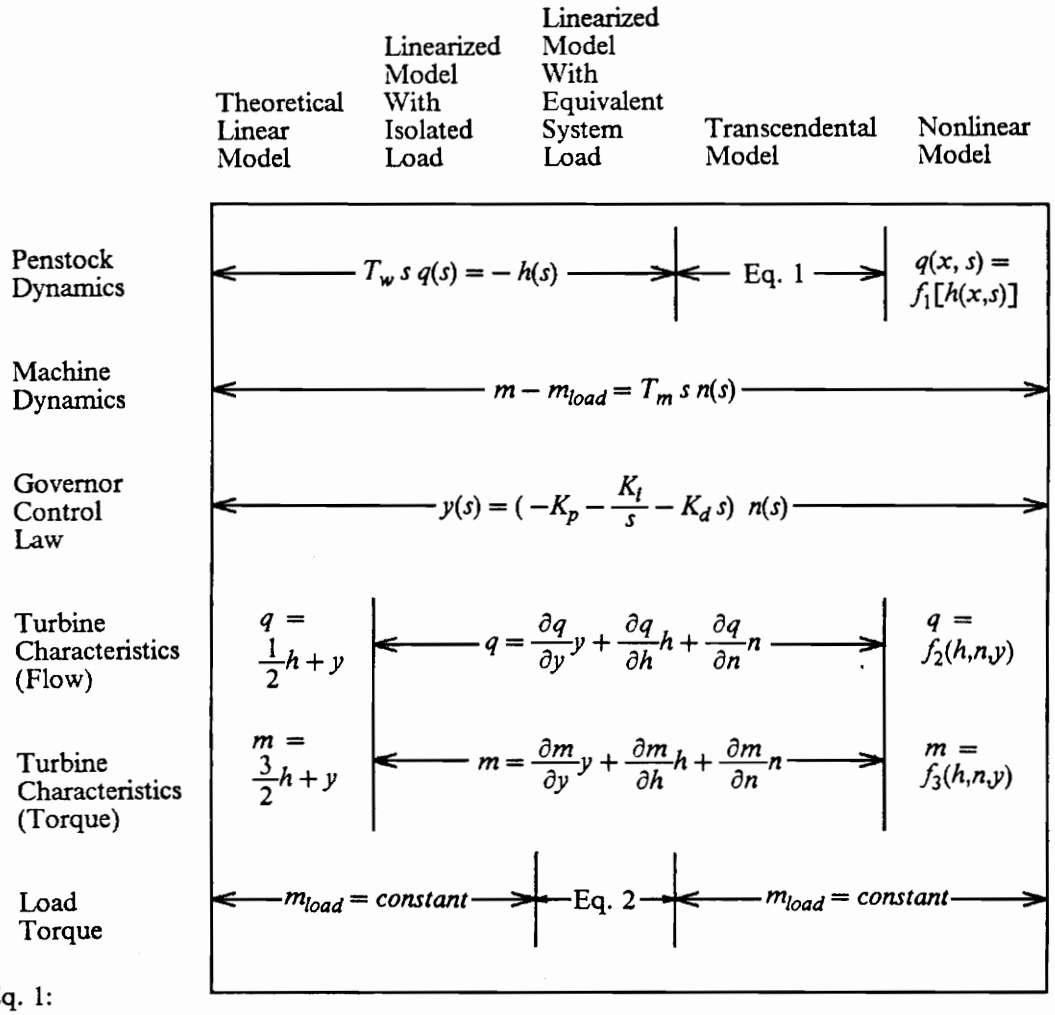

Eq. 1:

$$m_{load}(s) = \frac{n(s)}{\frac{1}{D_a + \frac{K_a}{s}} + \frac{B}{(T_{s1}s + D_{s1})(T_{s2}s + D_{s2})}} + \frac{p_{sys}(s)}{B + \frac{(T_{s1}s + D_{s1})(T_{s2}s + D_{s2})}{(D_a + \frac{K_a}{s})}}$$

Eq. 2:

$$q(s) = -\frac{1 + \sinh^2\Gamma(s)}{Z \sinh\Gamma(s)\ \cosh\Gamma(s)}\, h(s)$$

$$\text{with } Z = \frac{2T_w}{T_c} \quad \text{and} \quad \Gamma(s) = \frac{T_c}{2}s$$

Linearized Model with Isolated Load

It was shown that the performance characteristics of the hydraulic turbine could be represented by partial derivatives evaluated at a specified operating condition. The benefit of this representation was that the flow and torque relations could better approximate actual turbine performance while preserving the linear nature of the relationships.

Linearized Model with Equivalent System Load

This model may be used for the situation in which it is desired to simulate plant performance including the dynamics of the equivalent connected electrical system. Similar to the previous model, the linearized turbine model is utilized, but the simple isolated load model is replaced by the more detailed generator and electrical system model.

Transcendental Model

This model includes the linearized model for the turbine characteristics and the isolated load model. Different from the previous models, the two-port transmission line representation is used for the penstock model. This plant model will serve to demonstrate the effect that waterhammer has on the system stability as compared to a plant which uses the rigid water column model for the penstock.

Nonlinear Model

There are two major factors that may cause the linear representations to become invalid. The turbine performance characteristics become nonlinear when changes in operating conditions are large. The basic equations of the water dynamics are nonlinear. Some dynamics such as rapid gate motions may cause the rigid water column model, a linear representation, to become invalid. The presence of either of these conditions will require the plant model to accomodate these nonlinearities.

Model Selection Insights

Overviews of five plant models have been presented. Logical questions arise concerning the selection of a particular model. Which model is the simplest appropriate model? Which plant model or models are inappropriate? Under what conditions must the nonlinear model be used?

Three areas of insight are developed in this section which guide the selection of an appropriate plant model. Emphasis is placed on determining which plant component or components are dominant. In the first area of insight, ratios of three plant characterizing times: machine starting time T_m, water starting time T_w, and round-trip pressure wave time T_c are utilized to provide insight into the importance of the water dynamics as compared to the turbine speed dynamics. In the second area of insight, concepts of rapid gate motion, the rigid water column model for the penstock, and the linearized turbine model are used to predict the potential magnitude of the waterhammer head and to predict the time interval during which waterhammer dynamics should dissipate. In the third area of insight, steady-state values at the start and end of an anticipated load change are utilized to predict the extent of nonlinear plant behavior.

Plant Characterizing Time Ratios

In order to determine whether the penstock, the turbine inertia, or neither component dominates the plant dynamics, the steady state water kinetic energy in the penstock is compared to that of the hydraulic turbine and generator at the operating condition described by the set (Q_0, H_0, Y_0, M_0, N_0). The kinetic energy for the water in the penstock and the rotating machine (turbine and generator) are:

$$KE_w = \frac{1}{2} m V_0^2 = \frac{1}{2} \frac{\rho L Q_0^2}{A}$$

$$KE_m = \frac{1}{2} I \omega^2 = \frac{1}{2} \frac{W r^2}{g} \omega_0^2$$

where KE_w= the kinetic energy of the water in the penstock

KE_m= the kinetic energy of the rotating machine

Using the definitions for T_m, T_w , and the turbine efficiency η_0, the ratio of the machine to the penstock kinetic energies is expressed as:

$$\frac{KE_m}{KE_w} = \frac{T_m}{T_w} \left(\frac{1}{\eta_0} \right)$$

This relationship provides insight into the dynamics of the water in the penstock versus the machine speed dynamics when a transient occurs. Consider that the turbine efficiency is nearly unity for simplicity in this discussion. For a ratio of (T_m/T_w) much greater than unity, the kinetic energy of the machine is much greater than that of the penstock so the machine speed dynamics dominate over the dynamics of the water. For the converse reasoning, a ratio of (T_m/T_w) much less than unity, the penstock dynamics dominate over the machine speed dynamics. To adopt a characterization given by Goldwag [15], a plant with large (T_m/T_w) is described as a "heavy plant" whereas a plant corresponding to small (T_m/T_w) is described as a "light plant."

The rate at which energy flows out of the penstock and is delivered to the turbine may be expressed in terms of the hydraulic power as given by:

$$P_{hyd} = \rho g H Q$$

Differentiating the relation for the hydraulic power about the specified operating point, the hydraulic power departure is expressed as:

$$p_{hyd} = q + h = q\,(1 + \frac{h}{q})$$

Recall that the Laplace domain transfer function $h(s)/q(s)$ has been developed for both the rigid water column model (from Eq. 2.1) and the two-port transmission line model (Eq. 3.11) for the penstock. With these transfer functions, the Laplace domain ratio of hydraulic power delivered to the turbine for each model with the same $q(s)$ may be formulated as:

$$\frac{p_{hyd-2-port}(s)}{p_{hyd-RWC}(s)} = \frac{\left[1 - \frac{2T_w}{T_c}\,\frac{\sinh\Gamma(s)\cosh\Gamma(s)}{1+\sinh^2\Gamma(s)}\right]}{(1 - T_w s)}$$

where $\Gamma(s) = \frac{T_c}{2}s$

A frequency-domain analysis is performed to compare the responses of the rigid water column and two-port transmission line models. Let the frequency substitution for the Laplace operator s be given by:

$$s = \frac{i\theta}{T_w}$$

where $\frac{\theta}{T_w}$ represents a dimensionless circular frequency ω.

In this manner the dimensionless frequency $f = \omega/2\pi$ represents the number of cycles that $q(s)$ experiences during the time period T_w. Making this substitution and manipulating algebraically, the

frequency domain relation for the ratio of power delivered using the two candidate penstock models becomes:

$$\frac{p_{hyd-2-port}(\gamma)}{p_{hyd-RWC}(\gamma)} = \frac{\left\{1 + \frac{2\theta T_w}{T_c}\left[\frac{\sin(\gamma)\cos(\gamma)}{1-\sin^2(\gamma)}\right]\right\}^2 + i\left\{\theta - \frac{2T_w}{T_c}\left[\frac{\sin(\gamma)\cos(\gamma)}{1-\sin^2(\gamma)}\right]\right\}^2}{1+\theta^2}$$

where $\gamma = \dfrac{\theta T_c}{2T_w}$

This frequency-domain comparison applies to pipe flow which has reached a steady-state oscillation in response to an oscillating forcing function ($q(i\,\omega)$ in this case). Although this situation does not exactly compare to a hydroelectric plant in response to a load change, the approach is intended to give insight into the relative importance of the ratio (T_c/T_w) and into the importance of the frequency at which the turbine/penstock/governor plant responds to a load change.

It may be noted that the power ratio which compares the two-port penstock model response to the rigid water column model response is a function only of the ratio (T_c/T_w) and the dimensionless frequency. By varying the dimensionless frequency, the magnitude and phase angle of the power ratio may be plotted, giving a comparison of the two candidate transfer functions in the frequency domain. The magnitude and phase angle are given by the following expressions:

$$\left|\frac{p_{\text{hyd-2-port}}}{p_{\text{hyd-RWC}}}\right| = \frac{\sqrt{\left\{1+\theta^2\, r(\gamma)\right\}^2 + \theta^2\{1-r(\gamma)\}^2}}{1+\theta^2}$$

$$\phi = \arctan\frac{\theta\{1-r(\gamma)\}}{\left\{1+\theta^2\, r(\gamma)\right\}}$$

where $r(\gamma) = \dfrac{\sin\gamma\ \cos\gamma}{\gamma\,(1-\sin^2\gamma)}$

As the dimensionless frequency approaches zero, the magnitude of the power ratio approaches unity and the phase angle approaches zero independent of the value of (T_c/T_w) . For the hydro-

electric plant, this means that for slow gate motions, the rigid water column model and the two-port transmission line model will result in the same dynamic response. Similarly, as the value of (T_c/T_w) approaches zero, the magnitude of the power ratio approaches unity and the phase angle approaches 0 independent of the frequency. For the hydroelectric plant, this means that for situations where the wave round-trip travel time T_c is very small compared to the water starting time T_w, then the rigid water column model will exhibit the same dynamics as the two-port transmission line model.

Several values for (T_c/T_w) are plotted in Fig. 17 which verify the previous observations. This plot provides insight into whether or not the rigid water column model accurately represents the dynamics of waterhammer. For very slow gate motion, the rigid water column model is valid, whereas for faster oscillatory gate motion, the rigid water column will not be valid depending on the value of (T_c/T_w).

The ratio of (T_m/T_w) has been shown to give insight into whether the turbine, the penstock, or neither component dominates the plant dynamics during a transient. (T_c/T_w) has been shown to give insight into the validity of the rigid water column model as compared to the two-port transmission line model which represents the waterhammer dynamics more completely. The qualitative map of Fig. 18 combines the ratios (T_m/T_w) and (T_c/T_w) into a single presentation and gives a qualitative picture of the relationships between plant parameters such as penstock length, area, turbine inertia, operational head and flow, and wicket gate motion. Scales are not provided on the map because without having assembled a plant model and without having performed a simulation, there is not sufficient information to pinpoint an exact location on the map which incorporates the dynamics of the control system in response to a load change.

Goldwag [15] has characterized a plant with $(T_m/T_w) = 2.5$ as a "light plant" and a plant with $(T_m/T_w) = 6.2$ as a "heavy plant." His investigation did not consider the effects of waterhammer on this characterization but this information provides insight into the order of magnitude of the (T_m/T_w) ratio which would indicate a light or heavy plant.

Figure 18 provides a qualitative directional picture of how the plant model and dynamics are affected by various changes in plant parameters. For example, it can be seen that the penstock

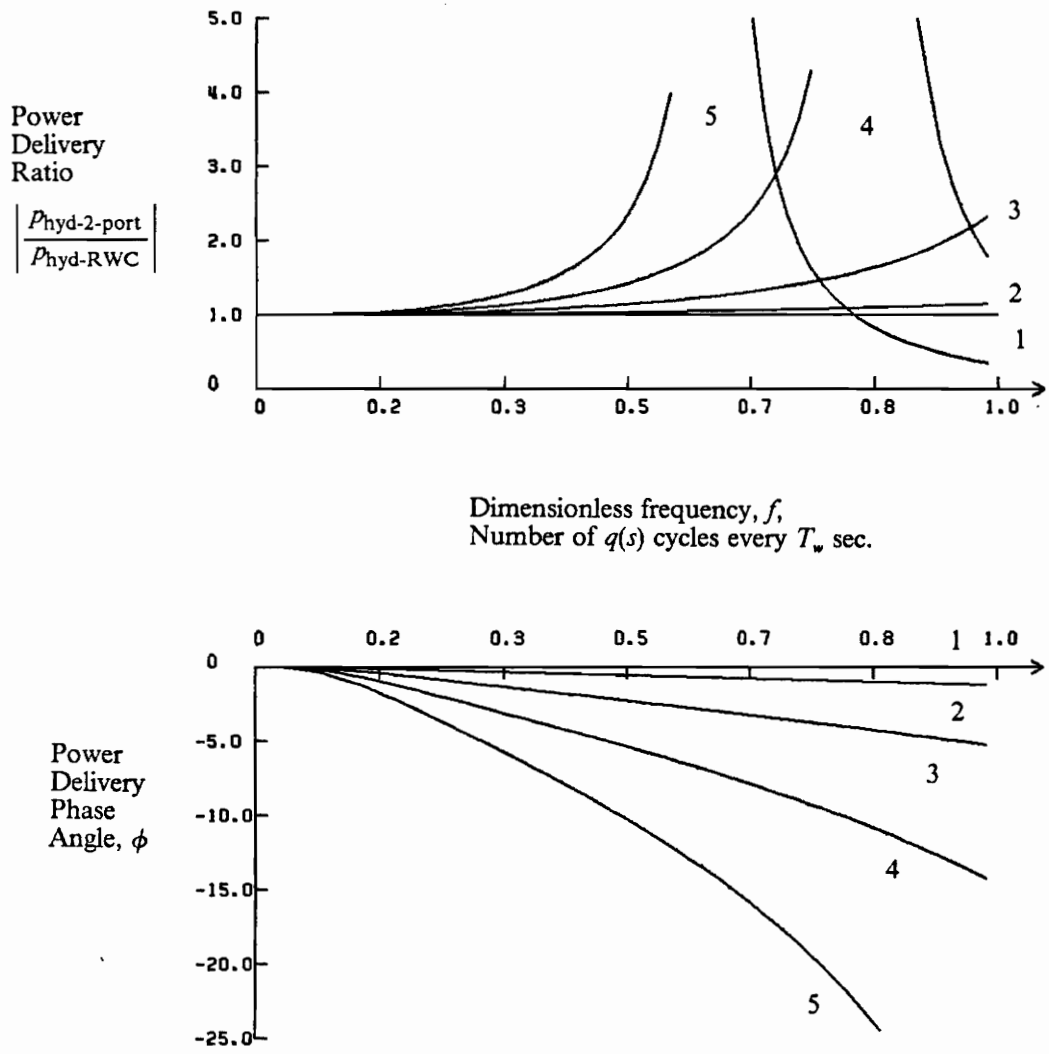

Legend

1 $T_c/T_w = 0$
2 $T_c/T_w = 0.2$
3 $T_c/T_w = 0.4$
4 $T_c/T_w = 0.6$
5 $T_c/T_w = 0.8$

Figure 17. Frequency-Domain Penstock Model Comparison.

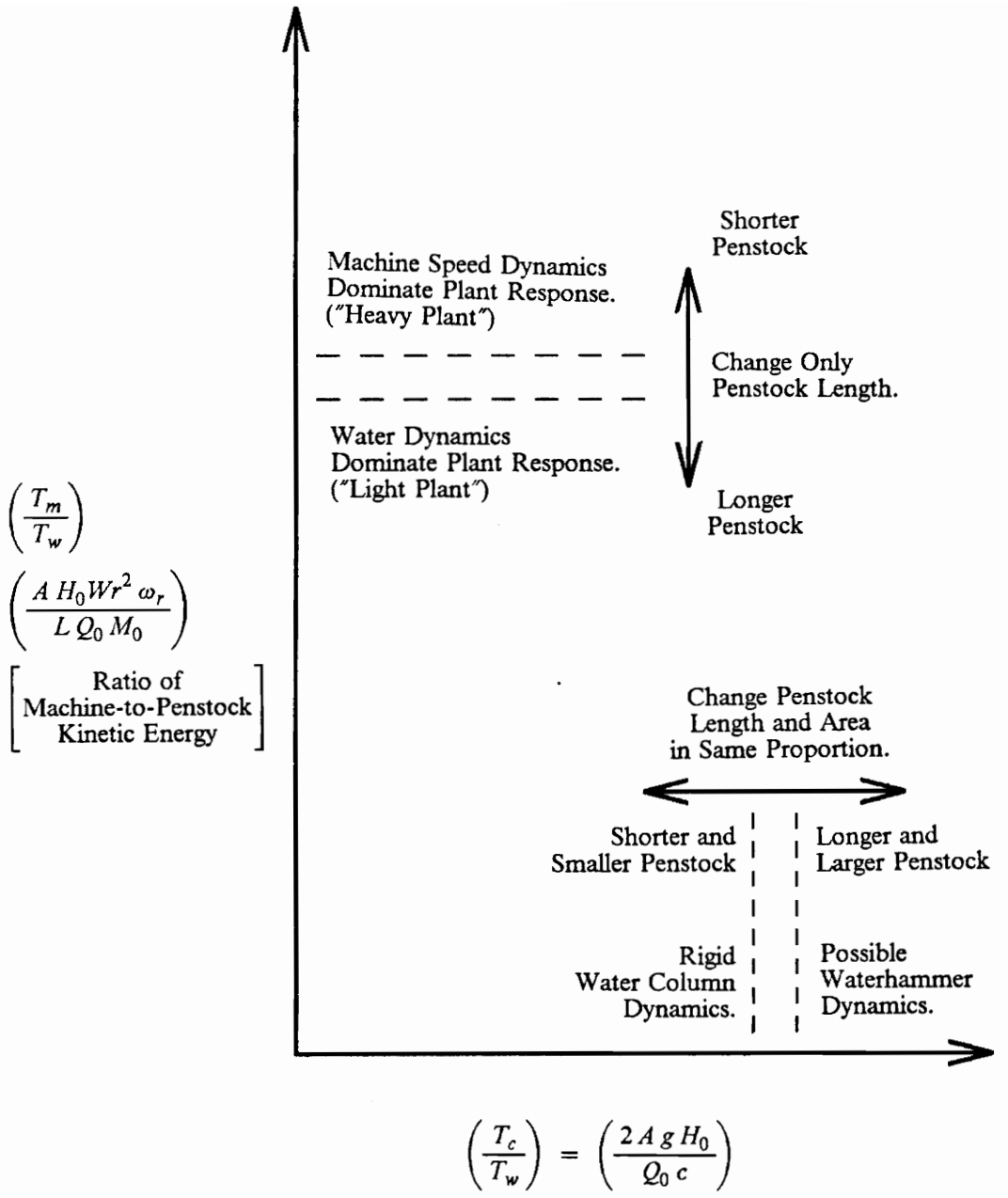

Figure 18. Qualitative Map for Identifying Dominant Plant Dynamics.

length has no effect on the value of (T_c/T_w) . An increase in penstock length will have the effect of making the water dynamics more important as compared to the machine dynamics while having a smaller effect on the validity of one penstock model over the other. A change in penstock length must be accompanied by a proportional change in area in order to maintain the relative dynamics of the water as compared to the machine. However, the change in both penstock length and area could shift the water dynamics into an area which could suggest a reevaluation of the penstock model.

Estimation of Waterhammer Head and Duration

When the initial steady operating condition of the hydroelectric plant (H_0, Q_0, Y_0, M_0, N_0) is known and the anticipated load change is known, then it is a simple task to identify the new desired steady operating condition (H_{new}, Q_{new}, Y_{new}, M_{new}, N_{new}) . With the new wicket gate position identified, the waterhammer head and its duration may be estimated assuming that the wicket gate motion takes place instantaneously. The estimate of the waterhammer head represents a worst-case estimate as long as the operational governor settings do not result in appreciable gate overshoot of the new desired position. In reality, the wicket gate motion cannot be accomplished instantaneously so the actual waterhammer head will be less than the estimate. This scenario also provides an estimate of the maximum duration of the water dynamics once wicket gate motion has ceased. The estimate of the waterhammer duration provides a comparison to the machine dynamics.

The basic equation for waterhammer and the linearized relation for hydraulic turbine performance may be utilized to determine the waterhammer head for any gate motion which occurs in a time less than the round trip pressure wave travel time T_e . Consider that the gate moves instantaneously from a position Y_0 to a new position Y . Assume that the change in turbine speed is insignificant and that the change in turbine operating condition is small so that the turbine characteristics may be represented by:

$$q = \frac{\partial q}{\partial h} h + \frac{\partial q}{\partial y} y$$

It is desired to find the values of flow and head, Q and H which result from the waterhammer brought on by the instantaneous gate motion Y_0 to Y. Transforming the turbine flow departure equation into a flow/head/gate relationship yields:

$$\frac{Q}{Q_0} - \frac{\partial q}{\partial h}\frac{H}{H_0} = \frac{\partial q}{\partial y}\frac{Y}{Y_0} + \left(1 - \frac{\partial q}{\partial y} - \frac{\partial q}{\partial h}\right) \qquad [3.31]$$

The basic equation for waterhammer (Eq. 3.2) for gate motions performed in a time less than T_c is:

$$H - H_0 = -\frac{c\,(Q - Q_0)}{A\,g} \qquad [3.32]$$

Eqs. 3.31 and 3.32 involve the two unknowns Q and H. The flow is eliminated and the waterhammer head due to the instantaneous gate motion is given by:

$$\frac{H}{H_0} = \frac{1 + \frac{\partial q}{\partial y}\left(\frac{Y}{Y_0} - 1\right) + \frac{\partial q}{\partial h}\frac{2T_w}{T_c}}{\frac{\partial q}{\partial h}\left(1 + \frac{\partial q}{\partial h}\frac{2T_w}{T_c}\right)} - \frac{\frac{\partial q}{\partial y}\frac{Y}{Y_0}}{\frac{\partial q}{\partial h}} - \frac{1 - \frac{\partial q}{\partial y} - \frac{\partial q}{\partial h}}{\frac{\partial q}{\partial h}}$$

It was shown that as $T_c \to 0$, the penstock dynamics are accurately represented by the rigid water column model. By taking the limit of the above expression as T_c approaches zero, then the waterhammer head due to instantaneous gate motion as predicted by the rigid water column model is given by:

$$\frac{H}{H_0} = 1 - \frac{\left(\frac{\partial q}{\partial y}\right)}{\left(\frac{\partial q}{\partial h}\right)}\left(\frac{Y - Y_0}{Y_0}\right) \qquad [3.33]$$

For Y less than Y_0 , the waterhammer head predicted by the rigid water column model will be greater than that predicted by the basic equation of waterhammer. Conversely, for Y greater than Y_0 , the waterhammer head predicted by the rigid water column model will be less than that predicted by the basic equation of waterhammer. This comparison provides another insight into the choice of the rigid water column model versus an elastic model which more accurately represents the waterhammer.

By considering the penstock dynamics to be adequately represented by the rigid water column model for a step motion of the wicket gates, an analytical expression may be derived which gives an insight into the duration of the water dynamics. The momentum equation of the water in the penstock was given by:

$$T_w \frac{dq}{dt} = -h \qquad [2.1]$$

Incorporating the linearized head/flow/gate expression without regard to changes in turbine speed, the dynamic penstock equation becomes:

$$\frac{dh}{dt} + \frac{1}{\frac{\partial q}{\partial h} T_w} h = -\frac{(\frac{\partial q}{\partial y})}{(\frac{\partial q}{\partial h})} (\frac{dy}{dt})$$

Considering the gate speed dy/dt to be constant, then the momentum equation becomes a simple first order ordinary differential equation. By assigning the initial condition that the head departure at $t = 0$ is h_0 , then the analytical solution for the penstock head is:

$$h(t) = \left[\frac{\partial q}{\partial y} T_w \frac{dy}{dt} + h_0\right]\left[\exp\left(\frac{-t}{T_w (\partial q/\partial h)}\right) - 1\right] \qquad [3.34]$$

Following step gate motion, the value of dy/dt is zero and the value for h_0 may be computed using the waterhammer head expression for H given in Eqn. 3.33 as:

$$h_0 = \frac{H - H_0}{H_0}$$

The time constant of the first order expression for the head departure due to step gate motion is $(\partial q/\partial h)T_w$. Following the step motion, the steady state value for the head departure $h(t)$ is zero and it will settle to within 98% of that value in $4(\partial q/\partial h)T_w$. Using this reasoning, the duration of the penstock dynamics should be about $4(\partial q/\partial h)T_w$ following the cessation of gate motion.

Steady-state errors in head, flow, and gate position introduced by a linear plant model also guide the selection of an appropriate plant model. The evaluation of these errors is developed in the next section.

Steady-State Comparisons

When simulating plant performance with a linear plant model, assumptions used in the rigid water column model and the linearized hydraulic turbine model introduce errors in the new steady-state values of head, flow, and gate position. The rigid water column model aslo utilizes the assumption that the initial head at the turbine H_0 is equivalent to the reservoir head H_{res}. The steady-state errors introduced into the model by these assumptions provide guidance into whether a nonlinear model may be required for a particular situation. For example, a large load change on a plant considered to be linear for small load changes may introduce excessive steady state errors and suggest the use of a nonlinear plant model.

When the initial steady operating condition of the hydroelectric plant (H_0, Q_0, Y_0, M_0, N_0) is known and the anticipated load change is known, then it is a simple task to identify the new desired steady operating condition (H_{new}, Q_{new}, Y_{new}, M_{new}, N_0) . It may be noted that $N_{new} = N_0$ since constant speed operation is desired. A brief description of the approach needed to determine a steady-state operating condition is presented. With this information and with the steady-state

values required to satisfy the dynamic equations for a linearized plant model, the steady state error introduced by assuming that the plant operates in a linear manner may be assessed.

The analytical expression for a line of constant gate position Y on the hill diagram provides the relation between the turbine head H, the flow Q, and the desired speed N_0 and is given by:

$$Q = \frac{a N_0^2 D_r^4}{\sqrt{H}} + b N_0 D_r^3 + c D_r^2 \sqrt{H} \qquad [3.35]$$

where Q=flow through the turbine

H=head at the turbine inlet with the outlet head being the datum $H = 0$

N_0=the desired operating speed (rpm)

D_r=the runner diameter of the hydraulic turbine

and a, b, and c are the constant coefficients for the unit discharge versus unit speed relationship

The steady flow Q through the penstock results in a head loss so that the turbine head H will be less than the reservoir head H_{res}. The head loss in the penstock is given by Darcy's equation as:

$$H_{res} - H = \frac{fL}{2gD} \left(\frac{Q}{A}\right)^2 \qquad [3.36]$$

where H_{res}=reservoir head

f=penstock friction factor

L=penstock length

D=penstock diameter

A=penstock cross-sectional area

The steady-state values of H and Q are determined by reducing Eqs. 3.35 and 3.36 into a single nonlinear equation and solving by Newton's method. With values for flow, head, and speed being determined, the unit discharge Q_1 and the unit speed N_1 are fully specified. This locates a unique point for the operating condition on the hill diagram. The turbine efficiency η may be evaluated

by sorting through the analytical lines of constant efficiency to determine which line passes through the operating condition.

With the turbine efficiency η determined, it is a simple matter to evaluate the turbine torque corresponding to the operating condition as given by:

$$M = \frac{60}{2\pi} \frac{\eta \rho g H Q}{N_0} \qquad [3.19]$$

The power delivered to the generator at the specified operating condition is computed by:

$$P = \eta \rho g H Q$$

If a linear model is selected for the penstock, then at the initial condition, there is no net head acting on the penstock ($H = H_{res}$), but for real penstock flow the initial turbine head H_0 must be less than H_{res} . With this in mind, the error in turbine head at the initial operating condition is computed by:

$$e_{H,0} = \frac{H_0 - H_{res}}{H_0} \qquad [3.37]$$

where $e_{H,0} =$ the error in turbine head at the initial operating condition

Use of the rigid water column model or the two-port transmission line model for the penstock requires that the head departure for steady-state operation must be zero, resulting in a predicted turbine head of H_{res} . For example, the equation of the water dynamics for the theoretical model and the linearized turbine/rigid water column model is:

$$T_w s\, q(s) = -h(s) \qquad [2.1]$$

so that the steady-state value of $h(t)$ must have a value of zero to insure the steady state requirement that $dq(t)/dt = 0$. The error in turbine head at the new operating condition is computed by:

$$e_{H,\,new} = \frac{H_{new} - H_{res}}{H_{new}} \qquad [3.38]$$

where $e_{H,\,new}$ = the error in turbine head at the new operating condition

Following the modeling recommendations of Hovey [13], if either of these errors are more than ten percent, then a nonlinear representation should be used for the penstock model.

Use of a linear representation for the turbine characteristics also leads to steady state errors in gate position and flow whenever the partial derivatives deviate from the initial steady operating condition values. At the new steady operation, the linearized torque/head/gate/speed relation, Eq. 2.10, is reduced to:

$$y_{new} = \frac{m_{load}}{(\partial m/\partial y)}$$

With the value of the partial derivative $(\partial m/\partial y)$ evaluated at the initial operating condition (H_0, Q_0, Y_0, M_0, N_0) and held constant, then the steady-state error in the new gate position introduced by using the linearized turbine model is expressed by:

$$e_{Y,\,new} = \frac{Y_0}{Y_{new}} \left(1 + \frac{\frac{M_{new}}{M_0} - 1}{(\partial m/\partial y)} \right) - 1 \qquad [3.39]$$

where Y_{new} and M_{new} correspond to the new steady operating condition (H_{new}, Q_{new}, Y_{new}, M_{new}, N_0) required to produce the new desired power.

Using a similar approach, the steady-state error in flow introduced by using the linearized turbine model is expressed by:

$$e_{Q,\,new} = \frac{Q_0}{Q_{new}} \left[1 + \frac{\left(\frac{\partial q}{\partial y}\right)}{\left(\frac{\partial m}{\partial y}\right)} \frac{M_{new} - M_0}{M_0} \right] - 1 \qquad [3.30]$$

If the errors in the new steady gate position and flow using the linear model deviate by more than ten percent from the values required by the hill diagram, then a nonlinear model should be used. It should be stressed that the preceeding steady state analysis does not incorporate the importance of changes in the partial derivatives during the transient state. The purpose of the steady state analysis is to provide modeling insight before a plant model is assembled and a simulation is performed. Since transient state information is not yet avaliable, then the steady state analysis can only provide partial insight into the selection of an adequate and effective plant model.

Summary of Model Selection Insights

Mathematical models have been presented for all the plant components, five candidate plant models have been presented, and model selection insights have been provided in order to aid in the selection of an adequate appropriate model before a plant simulation is performed. The preliminary selection of a linear or nonlinear plant model is based on consideration of three general areas as summarized below:

1. Ratios of (T_m/T_w) and (T_c/T_w) : A large value of (T_m/T_w) indicates that machine dynamics will dominate the plant response whereas a small value of (T_m/T_w) indicates that water dynamics will dominate the plant response. It was shown that as (T_c/T_w) increases, the liklihood of waterhammer increases.
2. Estimation of Waterhammer Head and Duration: An expression for the maximum expected waterhammer head was developed, and it was shown that water dynamics would dissipate in approximately $4(\partial q/\partial h)T_w$ following step gate motion.
3. Steady State Comparisons: Expressions for steady-state errors of head, gate position, and flow were developed which have been suggested by Hovey [13] to be less than 10 percent for linearized model validity.

A mathematical model for the plant may now be assembled for the purpose of plant simulation, governor tuning studies, or incorporation into other larger electric system mathematical models.

Chapter 4

Development of Candidate Plant Models

Mathematical models for each of the plant components have been developed. Single models were presented for the reservoir, the hydraulic turbine speed dynamics, and the governor, and two or more models were presented for the penstock, the hydraulic turbine characteristics, and the electric load. Five candidate plant models arose from combinations of the component models. As previously illustrated in Table 2 these candidate models are:

1. Theoretical Linear Model.
2. Linearized Model with Isolated Load.
3. Linearized Model with Equivalent System Load.
4. Transcendental Model.
5. Nonlinear Model.

The mathematical developments needed for a stability analysis and for simulation of the five candidate models are presented in this chapter. Since the theoretical linear model is a subset of the linearized model serving an isolated load, the development begins with the linearized model. The block diagram of the plant leads to the development of the characteristic equation for the plant.

Analytical expressions for governor settings that insure plant stability are derived and the analytical expressions for plant response are developed. The block diagram and characteristic equation for the transcendental model are presented which lead to an analytical expression for plant stability including the full effect of waterhammer dynamics. A block diagram and the set of equations describing the response of the linearized model to a change in the load on a connected dynamic electrical system is presented. Finally, the governing relations describing the nonlinear plant model are assembled and a computational scheme is developed for the purpose of simulation and comparison of the nonlinear simulation to its linear plant counterpart.

Several general observations concerning the relative performance of the linear plant models are made in this chapter. Emphasis is placed on relative stability of the models which places a limitation on the range of allowable control settings when performing governor tuning studies. Comparison of the performance of linear and nonlinear plant models is conducted in Chapter 6 when the model for a representative plant is defined.

Linearized Model with Isolated Load

The model for a linearized plant with an isolated load is developed in this section. The development begins with the governing relations for each plant component and culminates in an analytical time-domain description of plant performance. There are three dynamic equations and three auxiliary algebraic equations which describe the components of the linearized plant model. The first dynamic equation is the relation for the rigid water column model of the penstock. This relation was previously established and is given by:

$$T_w s\, q(s) = -h(s) \qquad [2.1]$$

The second dynamic equation describes the speed change of the rotating turbine/generator inertia due to a mismatch in torque and is given by:

$$T_m \, s \, n(s) \;=\; m(s) - m_{load} \qquad [3.13]$$

The third dynamic equation describes the action of the governor as it positions the turbine wicket gates in response to a departure in desired speed as:

$$y(s) \;=\; \left(-K_p - \frac{K_i}{s} - K_d \, s\right) n(s) \qquad [3.28]$$

The expression for the step departure in isolated load torque was defined as:

$$m_{load} = constant \qquad [3.30]$$

The last two algebraic relations concern the linearized model for the hydraulic turbine characteristics and are given by:

$$q(s) \;=\; \frac{\partial q}{\partial y} y(s) + \frac{\partial q}{\partial h} h(s) + \frac{\partial q}{\partial n} n(s) \qquad [2.9]$$

$$m(s) \;=\; \frac{\partial m}{\partial y} y(s) + \frac{\partial m}{\partial h} h(s) + \frac{\partial m}{\partial n} n(s) \qquad [2.10]$$

The three dynamic equations and the algebraic equations are combined and expressed in a block diagram for the linearized plant as shown in Fig. 19. The model is third order and the load torque m_{load} represents a disturbance.

Using standard techniques [33], repeated manipulation of the block diagram of Fig. 19 leads to the single-block diagram of Fig. 20. The the third order characteristic equation for the plant is expressed in standard form as given by:

$$s^3 + a_2 s^2 + a_1 s + a_0 \;=\; 0 \qquad [4.1]$$

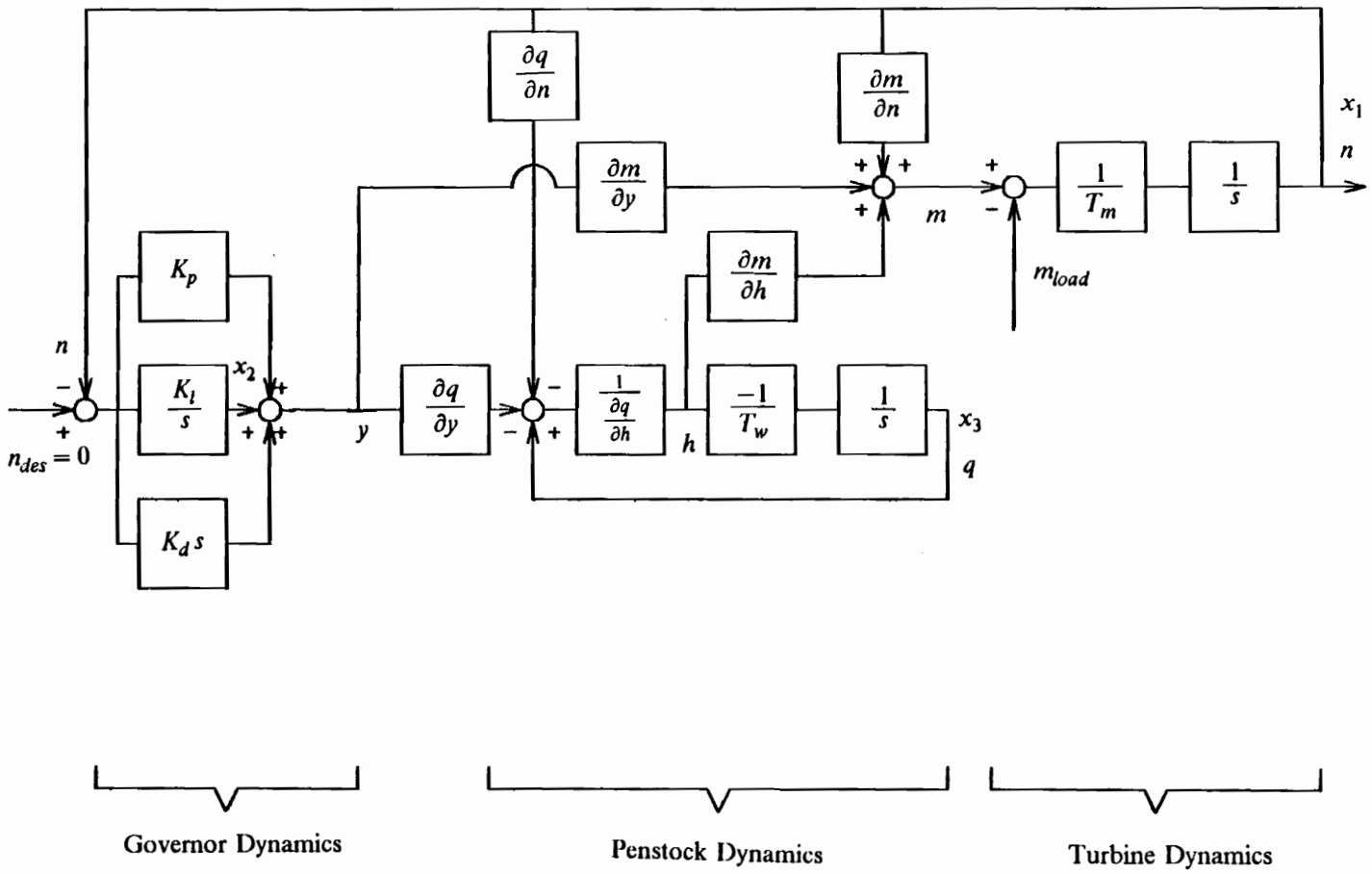

Figure 19. Block Diagram of Linearized Plant Model.

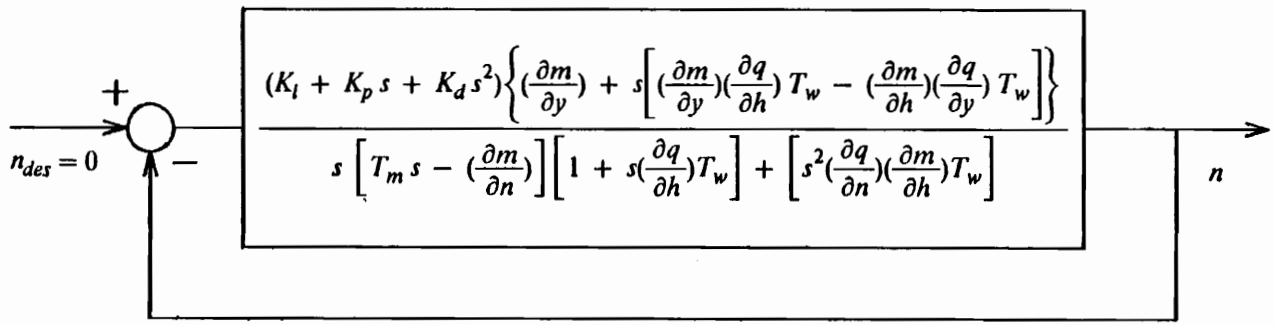

Figure 20. Reduced Block Diagram of Linearized Plant Model.

$$\text{where } a_2=\left[\frac{T_m+(\frac{\partial m}{\partial y})K_d-T_w\{(\frac{\partial q}{\partial h})(\frac{\partial m}{\partial n})-(\frac{\partial q}{\partial n})(\frac{\partial m}{\partial h})+K_p[(\frac{\partial m}{\partial h})(\frac{\partial q}{\partial y})-(\frac{\partial m}{\partial y})(\frac{\partial q}{\partial h})]\}}{d}\right]$$

$$a_1=\left[\frac{(\frac{\partial m}{\partial y})K_p-T_w K_i[(\frac{\partial m}{\partial h})(\frac{\partial q}{\partial y})-(\frac{\partial m}{\partial y})(\frac{\partial q}{\partial h})]-(\frac{\partial m}{\partial n})}{d}\right]$$

$$a_0=\left[\frac{(\frac{\partial m}{\partial y})K_i}{d}\right]$$

$$\text{and } d=T_w\left\{T_m(\frac{\partial q}{\partial h})-K_d[(\frac{\partial m}{\partial h})(\frac{\partial q}{\partial y})-(\frac{\partial m}{\partial y})(\frac{\partial q}{\partial h})]\right\}$$

The plant is stable if the real part of each eigenvalue (root of the characteristic equation) is less than zero. For the linear third order characteristic equation in the form presented above, the Routh-Hurwitz criteria [34] for plant stability are:

$$a_2>0$$

$$a_1>0$$

$$a_0>0$$

$$a_2\,a_1>a_0$$

Since the parameters K_i and $(\partial m/\partial y)$ are positive, then the third criterion $a_0>0$ can only be satisfied if the denominator of the expression is positive. This conclusion places an upper limit on the derivative gain. The derivative gain limitation becomes:

$$K_d<\frac{(\frac{\partial q}{\partial h})T_m}{(\frac{\partial m}{\partial h})(\frac{\partial q}{\partial y})-(\frac{\partial m}{\partial y})(\frac{\partial q}{\partial h})} \qquad [4.2]$$

The first criterion $a_2 > 0$ places an upper limit on the proportional gain depending on the value of K_d . Keeping in mind that the denominator of a_2 must be positive, then the limitation of the proportional gain becomes:

$$K_p < \frac{\frac{T_m + (\frac{\partial m}{\partial y})K_d}{T_w} + (\frac{\partial q}{\partial n})(\frac{\partial m}{\partial h}) - (\frac{\partial q}{\partial h})(\frac{\partial m}{\partial n})}{(\frac{\partial m}{\partial h})(\frac{\partial q}{\partial y}) - (\frac{\partial m}{\partial y})(\frac{\partial q}{\partial h})} \qquad [4.3]$$

The fourth criterion $a_2 a_1 > a_0$ is more restrictive than the second criterion and it leads to the limitation of K_i depending on the values of K_p and K_d . The limitation of the integral gain to insure plant stability is given by:

$$K_I < \frac{a_2[(\frac{\partial m}{\partial y})K_p - (\frac{\partial m}{\partial n})]}{(\frac{\partial m}{\partial y}) + a_2 T_w[(\frac{\partial m}{\partial h})(\frac{\partial q}{\partial y}) - (\frac{\partial m}{\partial y})(\frac{\partial q}{\partial h})]} \qquad [4.4]$$

where a_2 is a function of K_p, K_d, T_m, T_w, and the partial derivatives as defined in Eq. 4.1.

The theoretical linear model is a subset of the linearized model, and its description may be obtained by setting the partial derivatives equal to their theoretical counterparts as presented in Table 1. The theoretical linear model is similar to the plant described by Hovey. The only difference in this model from Hovey's original model is the P-I-D control law. Hovey's model can be duplicated by simply assigning a value of zero to the derivative gain. The theoretical linear plant model may be used as an example for the determination of stability limits. The expressions for the limiting values of K_p, K_i, and K_d become much simpler by substituting the appropriate partial derivative values corresponding to Hovey's theoretical model presented in Table 1. Making this substitution and simplifying, the stability limits for the theoretical linear model are given by:

$$K_d < T_m/2$$

$$K_p < \frac{T_m + K_d}{T_w}$$

$$K_i < \frac{\left(\frac{T_m + K_d}{T_w}\right) - K_p}{\frac{3T_m}{2K_p} - T_w}$$

Consider a theoretical plant with a machine starting time of six seconds $T_m = 6$ sec and with a water starting time of one second $T_w = 1$ sec so $(\frac{T_m}{T_w}) = 6$. Goldwag [15] classifies this situation as a "heavy machine" plant and Hovey [13] classifies this situation as a "plant with a relatively short penstock," which are equivalent classifications. The stability limits for the plant using four different derivative gain settings are shown in Fig. 21. The curve corresponding to $K_d = 0$ represents proportional-integral control and is the region of stable operation as presented by Hovey [13]. As the derivative gain is increased, the region of stable operation is also increased, up to the point of maximum derivative gain, $T_m/2$. This observation is also valid for linearized plants with partial derivatives different from those of the theoretical model.

An analytical solution for the third order plant is formulated in order to study the performance of the plant using various stable governor settings. The relation of the three states shown in Fig. 19 to the plant variables is given by:

$$x_1(s) = n(s)$$
$$x_2(s) = -K_i \frac{n(s)}{s}$$
$$x_3(s) = q(s)$$

A convenient way to represent the state equations is to express the system of equations in matrix form. The matrix equation which describes the plant is given by:

$$[\dot{X}] = [A][X] + [B]\, m_{load}$$

where $[X] = \text{col}\,(x_1, x_2, x_3)$

Algebraic manipulations of the state relationships and definition of the frequently used group c_1 as:

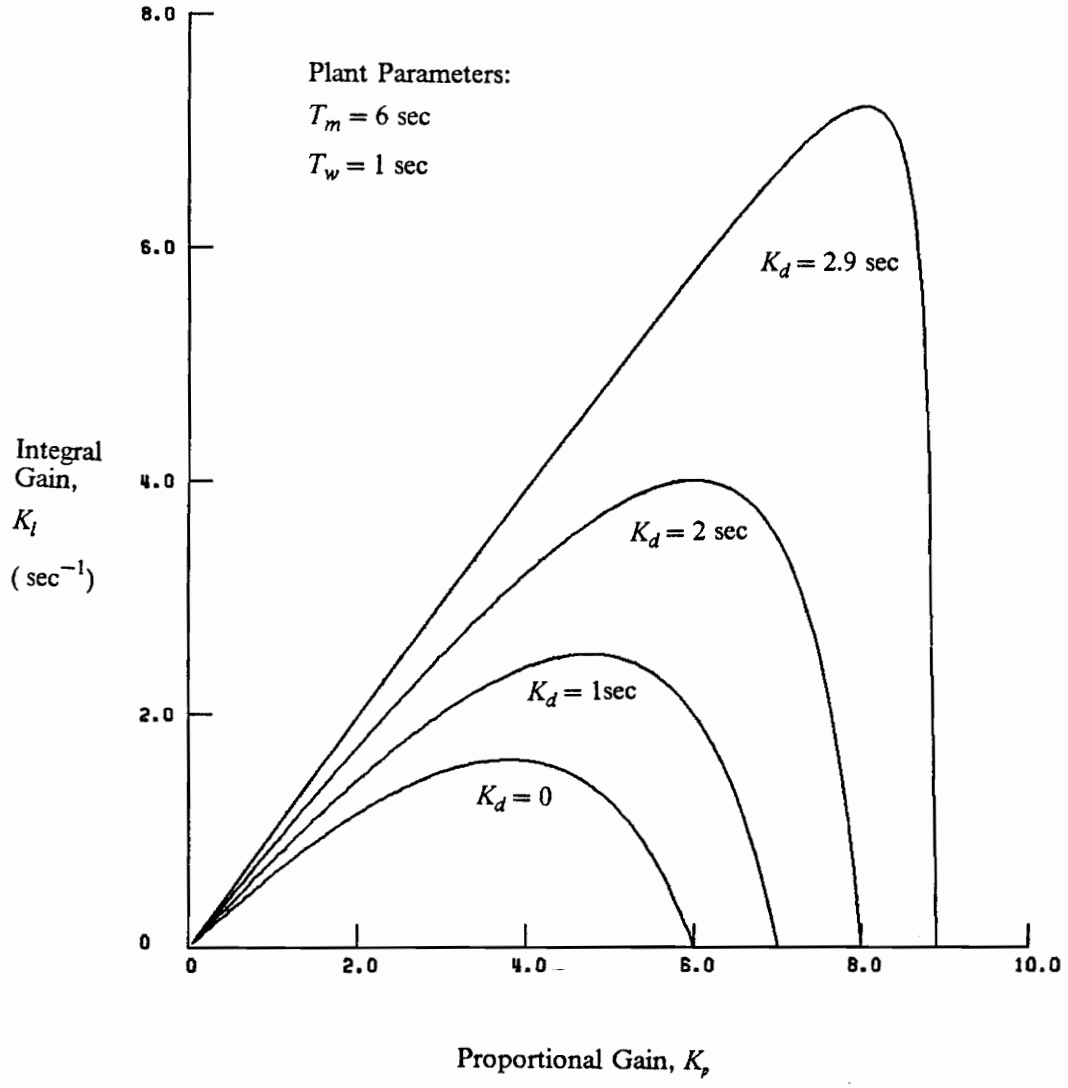

Figure 21. Stability Limits for a Theoretical Linear Plant.

$$c_1 = \frac{\left[\left(\frac{\partial m}{\partial y}\right) - \frac{\left(\frac{\partial m}{\partial h}\right)\left(\frac{\partial q}{\partial y}\right)}{\left(\frac{\partial q}{\partial h}\right)} \right]}{[T_m]}$$

leads to the evaluation of each element in the $[A]$ and $[B]$ matrices as follows:

$$a_{11} = \frac{\frac{(\partial m/\partial n)}{T_m} - c_1 K_p - (1/T_m)(\partial m/\partial h)(\partial q/\partial n)/(\partial q/\partial h)}{1 + c_1 K_d}$$

$$a_{12} = \frac{c_1}{1 + c_1 K_d}$$

$$a_{13} = -(1/T_m)\frac{1}{1 + c_1 K_d}$$

$$a_{21} = -K_i$$

$$a_{22} = 0$$

$$a_{23} = 0$$

$$a_{31} = \frac{\left[(\partial q/\partial h) - K_p(\partial q/\partial y) - a_{11} K_d(\partial q/\partial y)\right]}{T_w\,(\partial q/\partial h)}$$

$$a_{32} = \frac{\left[(\partial q/\partial y) - a_{12} K_d(\partial q/\partial y\right]}{T_w\,(\partial q/\partial h)}$$

$$a_{33} = \frac{\left[-1 - a_{13} K_d(\partial q/\partial y)\right]}{T_w\,(\partial q/\partial h)}$$

$$b_1 = \frac{(1/T_m)(\partial m/\partial h)/(\partial q/\partial h)}{1 + c_1 K_d}$$

$$b_2 = 0$$

$$b_3 = \frac{-b_1 K_d\,(\partial q/\partial y)}{T_w\,(\partial q/\partial h)}$$

The eigenvalues of the characteristic equation, Eq. 4.1, provide basic information concerning the manner in which the plant responds to a disturbance. The manner in which a state responds

concerns the speed of response, the overshoot (if any), and the oscillation (if any). The computation method for the eigenvalues is outlined by many mathematical handbooks [35].

The case of one real and two complex eigenvalues has been considered and is referred to as oscillatory response. In contrast, the simulation of situations with three real, negative eigenvalues results in sluggish plant response which is not desired. For oscillatory response, the eigenvalues for the plant are given by:

$$x_1=\alpha$$
$$x_2=\beta + i\omega$$
$$x_3=\beta - i\omega$$

The analytical solution in response to an isolated load change is given by:

$$n(t)=x_{1-ss}+A_1e^{\alpha t}+e^{\beta t}(B_1\sin\omega t+C_1\cos\omega t)$$
$$x_2(t)=x_{2-ss}+A_2e^{\alpha t}+e^{\beta t}(B_2\sin\omega t+C_2\cos\omega t)$$
$$q(t)=x_{3-ss}+A_3e^{\alpha t}+e^{\beta t}(B_3\sin\omega t+C_3\cos\omega t)$$
$$y(t)=[-K_p+x_2(t)-K_d\{a_{11}n(t)+a_{12}x_2(t)+a_{13}q(t)\}]n(t)$$
$$h(t)=[q(t)-(\frac{\partial q}{\partial y})y(t)-(\frac{\partial q}{\partial n})n(t)]/(\frac{\partial q}{\partial h})$$

The steady-state values are algebraically determined from steady-state evaluation of the state matrix equation by:

$$[\dot{X}_{ss}] = 0 = [A][X_{ss}] + [B]\,m_{load}$$

The constant coefficients A_i , B_i , and C_i are determined from the initial conditions of the plant $[X_0] =$ col (0,0,0) .

To continue the example of the theoretical plant model with $T_m = 6$ sec and $T_w = 1$ sec , consider that the plant experiences an instantaneous ten percent load rejection of its isolated load ($m_{load} = -0.1$) . Assume that the plant governor is set for proportional-integral control. At the instant of load rejection, the turbine begins to overspeed. The magnitude of the speed departure and

the time required for the speed to settle to the desired point depends on the governor settings K_p and K_i. The speed departure response of the example plant situation is shown in Fig. 22 for three different governor settings. The locations of these settings are shown with respect to the plant stability limits in Fig. 22 also. The settings corresponding to Set 1 (low K_p and K_i) result in sluggish, undesirable plant response. The settings corresponding to Set 2 are those suggested by Hovey [13] to give optimum plant response. The settings corresponding to Set 3 are close to the stability limits and result in near-marginally stable response which is also undesirable. The simulation of linear plant models illustrated by this example will be used when determining the governor settings which result in the best plant response.

Schleif and Bates [36] have presented speed transient data for the Grand Coulee Third Powerplant response to a change in isolated load. That plant is characterized by $T_m = 10.5$ sec and $T_w = 1.83$ sec. The equivalent P-I conrol governor settings are $K_p = 2.08$ and $K_i = 0.14$ sec^{-1}. The linearized model was used to simulate the response of this plant to a 10% reduction in isolated load. The result of this simulation and the transient plant response are shown in Fig. 23. Using theoretical values for the turbine partial derivatives, the simulation predicts a speed overshoot which is 25% low but with a settling time equivalent to the actual response. One reason for the discrepancy in the responses is the departure of the turbine from theoretical performance which was not addressed in the reference [36]. Various partial derivative values were tried until a linearized model simulation nearly duplicated the actual plant response. This simulation is also shown in Fig. 23. For that simulation, $(\partial m/\partial y) = 0.8$ and all other partial derivatives were equal to the theoretical values.

Transcendental Model

The purpose of the transcendental plant model is to accurately represent the effect that the dynamics of waterhammer has on the stability limits of the plant as compared to the dynamics of

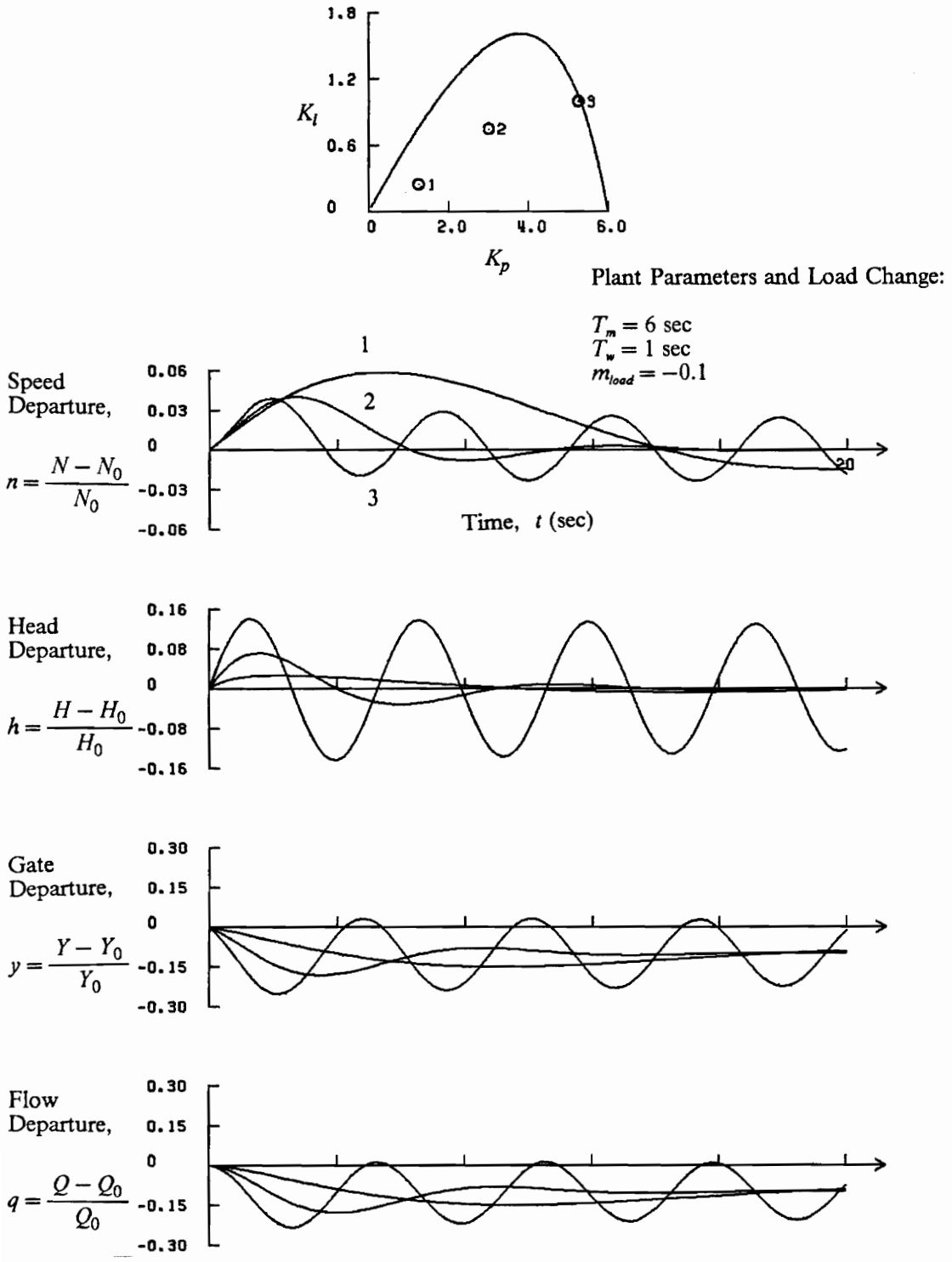

Figure 22. Example of Theoretical Linear Plant Response.

Plant Parameters and Load Change:

$T_m = 10.5$ sec
$T_w = 1.8$ sec
$K_p = 2.08$
$K_i = 0.14$ sec^{-1}
$K_d = 0$
$m_{load} = -0.1$

Legend

1 Field Data
2 Theoretical Linear Model
3 Linearized Model with
$\partial m/\partial y = 0.8$
$\partial m/\partial h = 1.5$
$\partial m/\partial n = 0$
$\partial q/\partial y = 1.0$
$\partial q/\partial h = 0.5$
$\partial q/\partial n = 0$

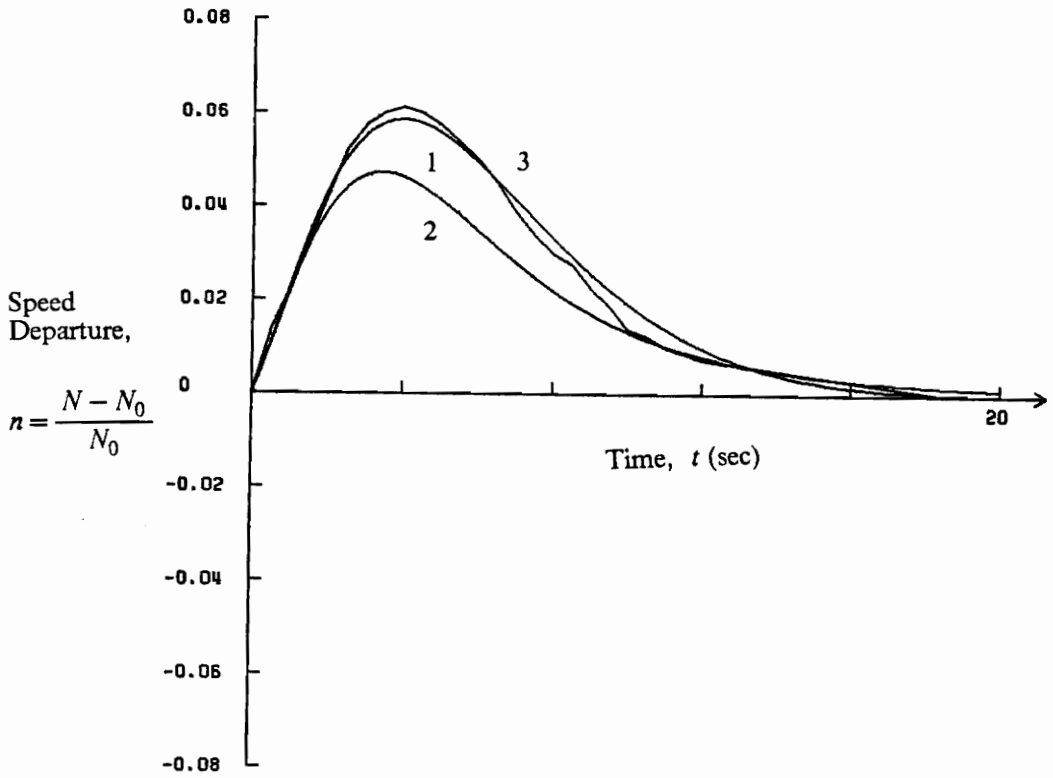

Figure 23. Comparison of Linearized Model Simulation with Grand Coulee Third Powerplant Response to Isolated Load Change.

the rigid water column penstock model. The only difference between this model and the linearized model is that the two-port transmission line $h(s)/q(s)$ transfer function replaces the rigid water column transfer function. Both models utilize the linearized turbine performance representation, P-I-D speed control, and the isolated load model. The characteristic equation of this model involves transcendental functions. A linear state matrix solution would involve a truncated series representation of the penstock and is not considered in this work.

The development for the transcendental plant model includes the overall transfer function, the characteristic equation, and the analytical representation for the limits of system stability. This development demonstrates the effect of waterhammer on stability and gives insight into the selection of a linear (rigid water column) or nonlinear model for the penstock.

The transfer function for the two-port transmission line model of the penstock was given by:

$$\frac{q(s)}{h(s)} = \frac{1 + \sinh^2\Gamma(s)}{-Z \sinh\Gamma(s) \cosh\Gamma(s)} \qquad [3.11]$$

with $Z=\frac{c\,Q_0}{A\,g\,H_0}=\frac{2\,T_w}{T_c}$

$\Gamma(s)=\frac{L\,s}{c} \quad =\frac{T_c}{2}s$

Comparison of the preceeding transfer function to that of the rigid water column model which was given by:

$$\frac{q(s)}{h(s)} = \frac{-1}{T_w\,s} \qquad [2.1]$$

leads to the substitution of the transcendental transfer function into the linearized model block diagram of Fig. 19. The substitution and resulting block diagram for the transcendental plant model is shown in Fig. 24.

The block diagram is reduced and the characteristic equation for the model is determined. The characteristic equation for the transcendental plant model is given by:

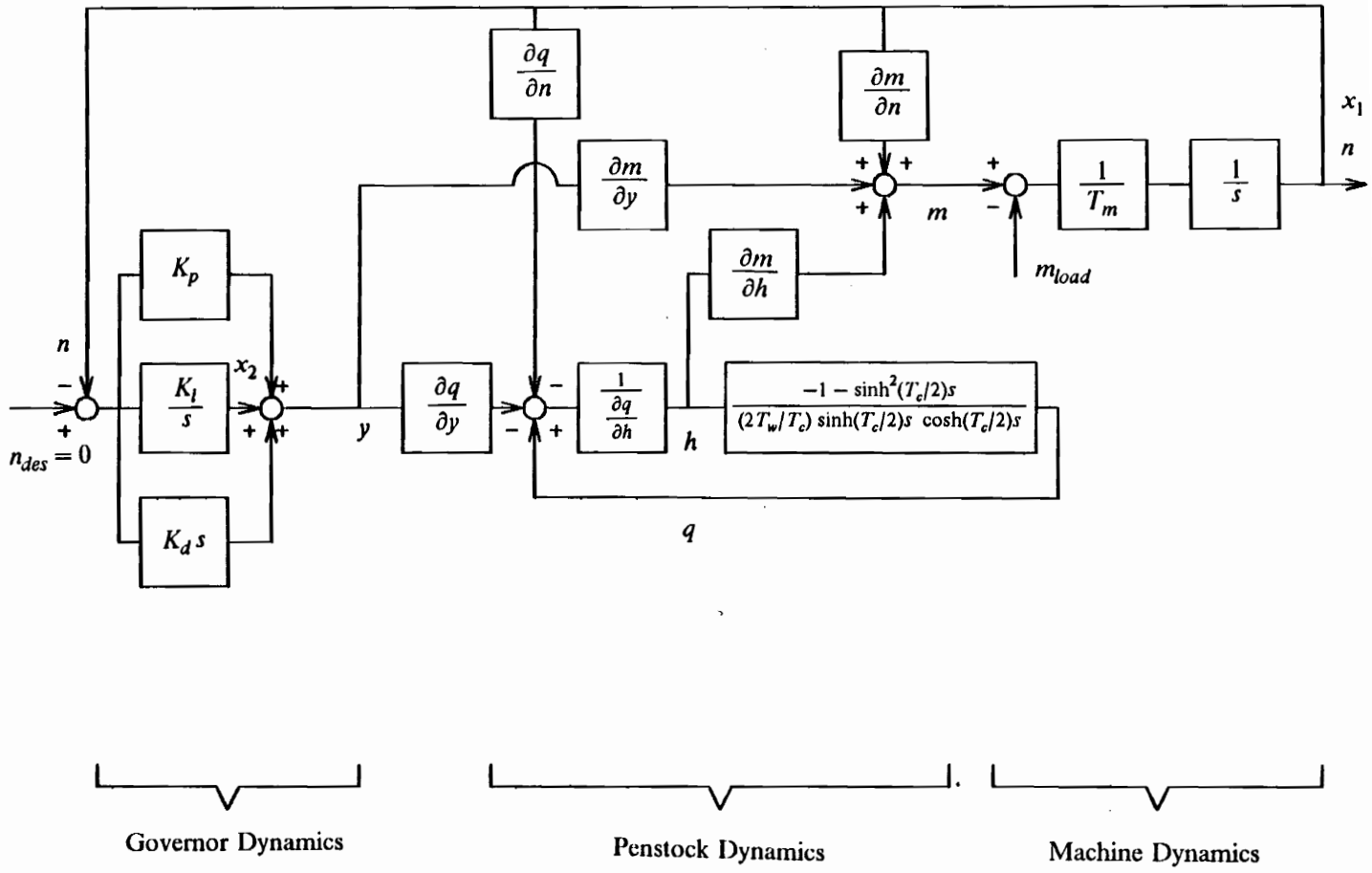

Figure 24. Block Diagram of Transcendental Plant Model.

$$s^2\{T_m + (\frac{2T_w}{T_c})[(\frac{\partial p}{\partial h})T_m + (\frac{\partial m}{\partial y})(\frac{\partial q}{\partial h})K_d - (\frac{\partial q}{\partial y})K_d] \tanh\frac{T_c}{2}s + (\frac{\partial m}{\partial y})K_d\}$$

$$+s\{(\frac{2T_w}{T_c})[(\frac{\partial m}{\partial y})(\frac{\partial q}{\partial h})K_p - (\frac{\partial q}{\partial y})K_p + (\frac{\partial m}{\partial y})(\frac{\partial q}{\partial n}) - (\frac{\partial m}{\partial n})(\frac{\partial q}{\partial n})] \tanh\frac{T_c}{2}s + (\frac{\partial m}{\partial y})K_p - (\frac{\partial m}{\partial n})\}$$

$$+\{(\frac{2T_w}{T_c})[(\frac{\partial m}{\partial y})(\frac{\partial q}{\partial h})K_i - (\frac{\partial q}{\partial y})K_i] \tanh\frac{T_c}{2}s + (\frac{\partial m}{\partial y})K_i\} \quad = \quad 0$$

Since the characteristic equation is not in the standard linear polynomial form, the Routh-Hurwitz stability criteria may not be used. A frequency-domain analysis is used in order to determine the stability limits of the plant. This approach has been presented by Xiao and Dong [29] and Murty and Hariharan [30] and applied to a hydroelectric plant with hydromechanical control and a theoretical turbine model. A similar approach is presented in this work and incorporates P-I-D control and linearized turbine performance.

The settings for marginal stability of the transcendental plant model are determined by considering complex eigenvalues whose real parts are zero. Since the characteristic equation for the plant is transcendental, there are an infinite number of eigenvalues corresponding to a particular set of K_p , K_i , and K_d. Whenever one of the eigenvalues is purely imaginary, then the plant will not operate in a stable manner. If the real part of any of the other eigenvalues is positive, then the plant will be unstable. If the real part of each of the other eigenvalues is negative, then the plant will be marginally stable. Let the one purely imaginary eigenvalue be defined as:

$$\lambda = \frac{i\omega}{T_w}$$

where ω/T_w represents a normalized frequency. The following hyperbolic trigonometric identity is utilized:

$$\tanh\frac{i\omega}{T_w} = i \tan\frac{\omega}{T_w}$$

The two substitutions presented above are incorporated into the transcendental characteristic equation which results in a complex expression given by:

$$\frac{-\omega^2}{T_w^2}\left\{T_m + (\frac{\partial m}{\partial y})K_d + [(\frac{\partial q}{\partial h})T_m + (\frac{\partial m}{\partial y})(\frac{\partial q}{\partial h})K_d - (\frac{\partial q}{\partial y})K_d](\frac{2T_w}{T_c})(i)\tan\frac{T_c\omega}{2T_w}\right\}$$

$$+\frac{i\omega}{T_w}\left\{[K_p(\frac{\partial m}{\partial y}) - (\frac{\partial m}{\partial n})] + \right.$$

$$\left.[K_p(\frac{\partial m}{\partial y})(\frac{\partial q}{\partial h}) - K_p(\frac{\partial q}{\partial y}) + (\frac{\partial m}{\partial h})(\frac{\partial q}{\partial n}) - (\frac{\partial m}{\partial n})(\frac{\partial q}{\partial h})](\frac{2T_w}{T_c})(i)\tan\frac{T_c\omega}{2T_w}\right\}$$

$$+ \quad \left\{[K_i(\frac{\partial m}{\partial y})(\frac{\partial q}{\partial h}) - K_i(\frac{\partial q}{\partial y})](\frac{2T_w}{T_c})(i)\tan\frac{T_c\omega}{2T_w} + K_i(\frac{\partial m}{\partial y})\right\} \quad = 0$$

Both the real and imaginary parts must equal zero, so two equations arise. The real part of the characteristic equation must satisfy:

$$\frac{-T_m\omega^2}{T_w^2} - \frac{(\frac{\partial m}{\partial y})K_d\,\omega^2}{T_w^2} + K_i(\frac{\partial m}{\partial y})$$
$$-(\frac{2\omega}{T_a})[K_p(\frac{\partial m}{\partial y})(\frac{\partial q}{\partial h}) - K_p(\frac{\partial m}{\partial h})(\frac{\partial q}{\partial y}) + (\frac{\partial m}{\partial h})(\frac{\partial q}{\partial n}) - (\frac{\partial m}{\partial n})(\frac{\partial q}{\partial h})]\tan\frac{T_c\omega}{2T_w} \quad = 0$$

The imaginary part of the characteristic equation must satisfy:

$$(\frac{-2\omega^2}{T_wT_c})\left[T_m(\frac{\partial q}{\partial h}) + K_d(\frac{\partial m}{\partial y})(\frac{\partial q}{\partial h}) - K_d(\frac{\partial m}{\partial h})(\frac{\partial q}{\partial y})\right]\tan\frac{T_c\omega}{2T_w}$$
$$+(\frac{\omega}{T_w})\left[K_p(\frac{\partial m}{\partial y}) - (\frac{\partial m}{\partial n})\right]\left[K_i(\frac{\partial m}{\partial y})(\frac{\partial q}{\partial h}) - K_i(\frac{\partial m}{\partial h})(\frac{\partial q}{\partial y})\right](\frac{2T_w}{T_c})\tan\frac{T_c\omega}{2T_w} \quad = 0$$

The integral gain is eliminated from the imaginary part of the characteristic equation using the K_p versus K_i relation of the real part. Solving the imaginary part of the characteristic equation for K_p yields a function of the dimensionless frequency ω , the derivative gain K_d , and the plant parameters. The real part of the characteristic equation is then solved for K_i also as a function of the fre-

quency and the derivative gain. The expressions for the maximum values of K_p and K_i which result in stable plant operation are given by:

$$K_p < \frac{r_3 - r_1 - r_4 (r_5 + r_7)}{r_2 + r_4 r_6}$$

$$K_i < r_5 + r_7 + \frac{r_6[r_3 - r_1 - r_4(r_5 + r_7)]}{r_2 + r_4 r_6}$$

where $r_1 = (\frac{-2\omega^2}{T_w T_c})[(\frac{\partial q}{\partial h})T_m + K_d\{(\frac{\partial m}{\partial y})(\frac{\partial q}{\partial h}) - (\frac{\partial q}{\partial y})(\frac{\partial m}{\partial h})\}] \tan \frac{T_c \omega}{2T_w}$

$$r_2 = \frac{\omega(\frac{\partial m}{\partial y})}{T_w}$$

$$r_3 = \frac{\omega(\frac{\partial m}{\partial h})}{T_w}$$

$$r_4 = (\frac{2T_w}{T_c})[(\frac{\partial m}{\partial y})(\frac{\partial q}{\partial h}) - (\frac{\partial q}{\partial y})(\frac{\partial m}{\partial h})] \tan \frac{T_c \omega}{2T_w}$$

$$r_5 = \frac{\omega^2}{T_w^2(\frac{\partial m}{\partial y})}[T_m + (\frac{\partial m}{\partial y})K_d]$$

$$r_6 = \frac{2\omega}{T_c(\frac{\partial m}{\partial y})}[(\frac{\partial m}{\partial y})(\frac{\partial q}{\partial h}) - (\frac{\partial q}{\partial y})(\frac{\partial m}{\partial h})] \tan \frac{T_c \omega}{2T_w}$$

$$r_7 = \frac{2\omega}{T_c(\frac{\partial m}{\partial y})}[(\frac{\partial m}{\partial h})(\frac{\partial q}{\partial n}) - (\frac{\partial m}{\partial n})(\frac{\partial q}{\partial h})] \tan \frac{T_c \omega}{2T_w}$$

The derivative gain K_d and the dimensionless frequency ω are parameters which must be specified so that the two equations may be solved explicitly. For a specified value of K_d, a curve describing the stability pairs of K_i and K_p is established by increasing the frequency ω from zero to a frequency which results in K_p or K_i being negative. Some negative values of K_p or K_i can result in stable plant operation. Depending on turbine partial derivatives, some values of ($K_p < 0$ and $K_i > 0$) or ($K_p > 0$ and $K_i < 0$) may result in stable operation. The performance of the plant with such settings is far

worse than that achievable with positive settings. For this reason, negative-valued control settings are not explored in this work.

In order to illustrate the stability limits of a transcendental plant model, the previous example is extended by defining the round-trip pressure wave travel time T_e. Let $T_e = 0.5$ sec. Recall that the partial derivatives were those of the theoretical model and that the plant parameters were $T_m = 6$ sec and $T_w = 1$ sec. The transcendental plant stability limits have been determined for three different values of derivative gain and are shown in Fig. 25. In that figure, the stability limits are compared to those of the theoretical linear plant model with comparable settings. It may be observed that the transcendental plant stability limits are more restrictive than those of the linear plant for all settings. Also, the stability limitations become more restrictive as the derivative gain is increased. The trend of transcendental model stability limitations is further illustrated in Fig. 26. In this figure, K_d, T_m, and T_e are held constant while varying T_w. In this manner, it is shown that the transcendental model stability limits are more restrictive than those of the linear model for various plants.

Xiao and Dong [29] made the bold statement that if the stability limits for the plant using the rigid water column model corresponds with the stability limits for the plant using the two-port transmission line model then the response of each plant model will be the same for any control settings. This claim does not follow simply from a comparison of the stability limits. However, by comparison of the $q(s)/h(s)$ transfer functions, a more basic requirement for linearized plant and transcendental plant duplication is that the product $T_e \omega$ be nearly zero. Either the round-trip pressure wave travel time must be nearly zero ($T_e \rightarrow 0$) or the wicket gate motion must be extremely slow ($\omega \rightarrow 0$).

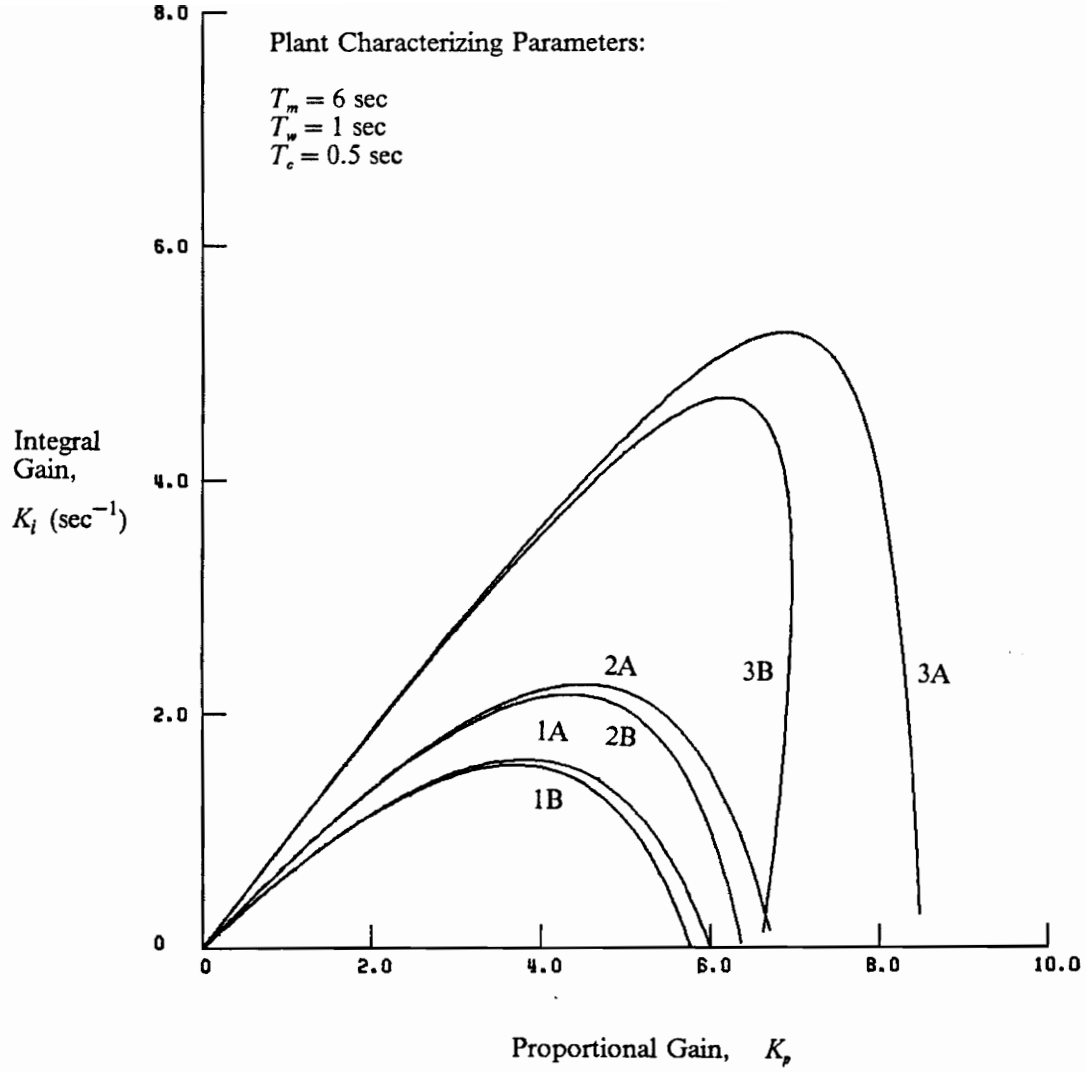

Legend:

1A Theoretical Linear Model, $K_d = 0.0$ (P-I Control)
1B Transcendental Model, $K_d = 0.0$ (P-I Control)
2A Theoretical Linear Model, $K_d = 0.75$ sec^{-1}
2B Transcendental Model, $K_d = 0.75$ sec^{-1}
3A Theoretical Linear Model, $K_d = 2.5$ sec^{-1}
3B Transcendental Model, $K_d = 2.5$ sec^{-1}

Figure 25. Stability Limits for Transcendental Plant Model.

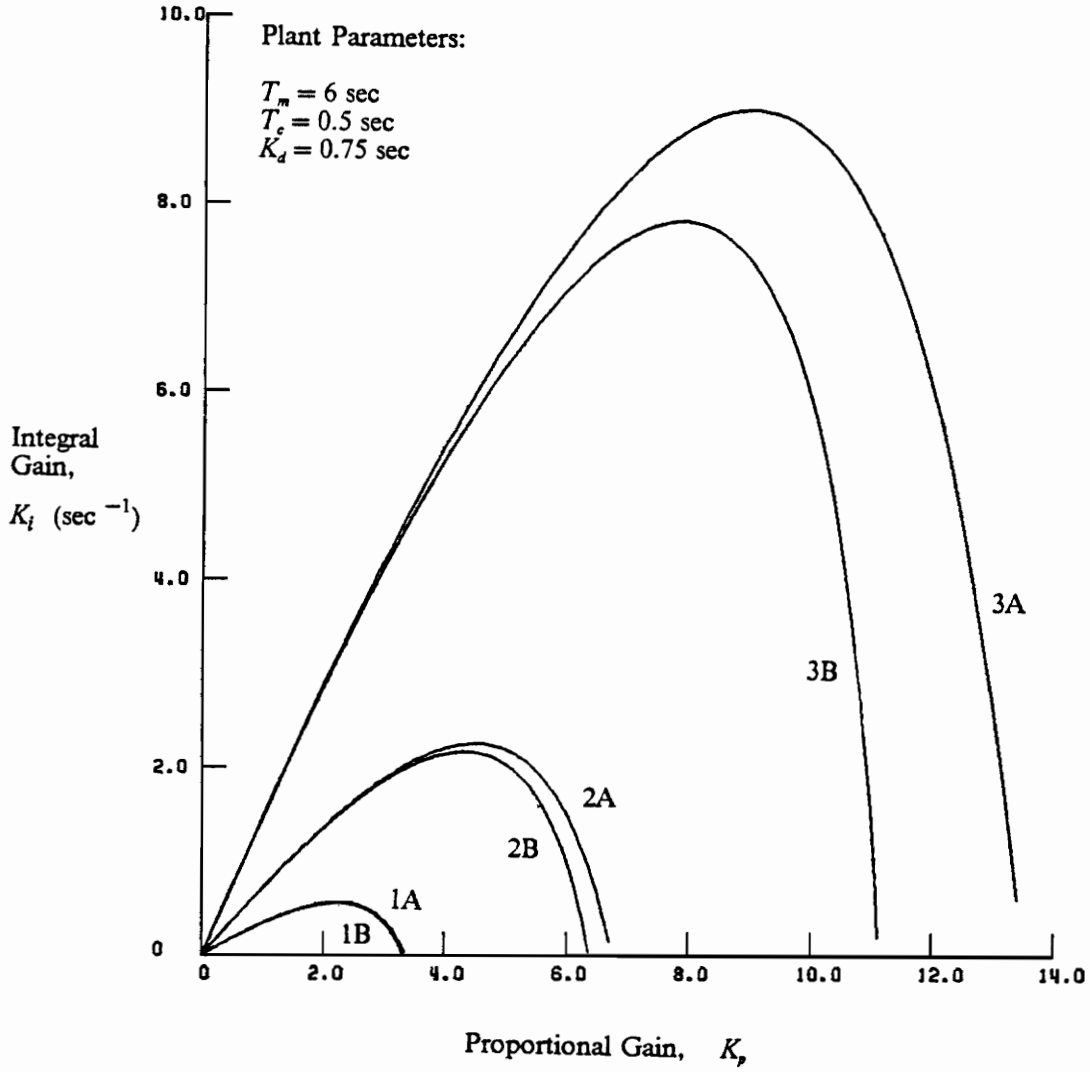

Legend:

1A Theoretical Linear Model, $T_w = 2.0$ sec
1B Transcendental Model, $T_w = 2.0$ sec
2A Theoretical Linear Model, $T_w = 1.0$ sec
2B Transcendental Model, $T_w = 1.0$ sec
3A Theoretical Linear Model, $T_w = 0.5$ sec
3B Transcendental Model, $T_w = 0.5$ sec

Figure 26. Stability Limit Comparisons for Various Theoretical Linear Plants.

Linearized Model with Equivalent System Load

The development of the candidate hydroelectric plant models continues by adding the equivalent system load model to the linearized plant model which previously used an isolated load. It was shown that the generator may be represented by a synchronizing torque coefficient and a damping torque coefficient. The connected electrical system is represented by a damped second order dynamic relation which depends on the type of plants connected to the system and on the dynamics of the electrical system itself. The generator and equivalent system models are added to the linearized plant which incorporates the rigid water column model for the penstock and the linearized representation for turbine performance. The governor model incorporates P-I-D speed control and allows for a change in the desired power generation of the hydroelectric plant.

Figure 27 is a presentation of the block diagram for the linearized plant incorporating the equivalent system load model. Comparing this block diagram to that of Fig. 19 (linearized model/isolated load), it may be observed that the new plant is sixth order which is an increase of three due to the dynamics of the generator and connected system. The system power demand disturbance p_{sys} replaces the isolated load disturbance m_{load} of Fig. 19. An additional plant disturbance, the desired generation departure p_{des} appears in this model for the purpose of adjusting the power delivered to the connected electrical system.

The system demand is defined in the usual dimensionless manner normalized at the initial operating condition as:

$$p_{sys} = \frac{P_{sys} - P_{sys,0}}{P_{sys,0}}$$

where P_{sys}= instantaneous system power demand

$P_{sys,0}$= initial system power demand

The desired generation departure is similarly defined as:

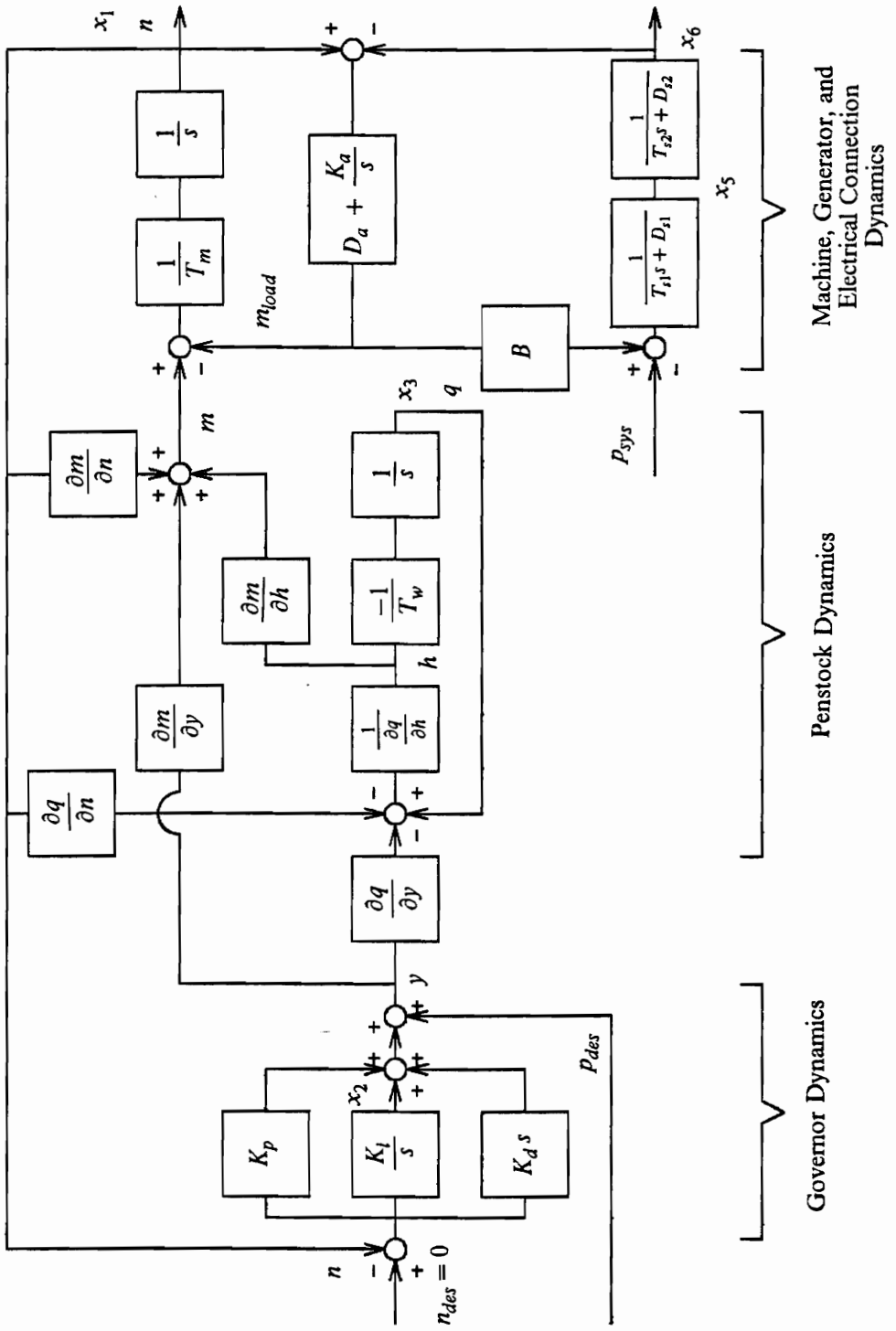

Figure 27. Block Diagram of Linearized Plant with Equivalent Electrical System.

$$p_{des} = \frac{P_{des} - P_{des,0}}{P_{des,0}}$$

where P_{des}= instantaneous desired generation

$P_{des,0}$= initial desired generation

Two sources for changing the plant load have been introduced. In the case that the electrical system load p_{sys} is increased, the hydroelectric plant is affected by that change after the dynamics of the electrical system bring on a departure in the electrical system speed (proportional to the system frequency). With a decrease in system speed, the dynamics of the generator gives rise to an increase in the load torque on the turbine. With the resulting torque mismatch, the turbine speed decreases and the governor's speed control system acts to reposition the wicket gate in order to eliminate the speed departure.

The desired generation signal p_{des} feeds directly into the gate position actuator along with the P-I-D speed control signal as illustrated in Fig. 27. In the case that an operator (or automatic dispatcher) produces a step increase in the desired plant power generation, then an immediate increase in gate position follows. An immediate increase in the water torque occurs. This brings on a turbine torque mismatch so that a speed change begins. At the same instant, water dynamics of the penstock begin and affect the water torque. The fact that there is a speed departure initiates the governor's speed control system to reposition the wicket gates. An additional effect of the increased speed is to bring on dynamic response of the generator so that the load on the turbine increases and the power delivered to the connected system increases. Eventually, a new steady-state condition is achieved in which the speed departures of both the turbine and the connected system vanish.

As shown on the block diagram, six states have been chosen with x_1 , x_2 , and x_3 being the same as in the linearized model supplying the isolated load. A matrix equation of state is used to describe the system dynamics and is given by:

$$[\dot{X}] = [A][X] + [B][U]$$

where $[X]$= the 6 x 1 column of states

$[A]$= the 6 x 6 system matrix

$[U]$= the 2 x 1 disturbance column, col (p_{sys}, p_{des})

$[B]$= the 6 x 2 disturbance coefficient matrix

The coefficients of the system matrix $[A]$ and the disturbance coefficient matrix $[B]$ has been determined algebraically from the block diagram. The expressions for all coefficients are presented in Appendix A due to the length and number of expressions.

Thorne and Hill [16] demonstrated that the stability limits for the linearized model supplying an isolated load are more restrictive than those of the same plant supplying a connected electric system. The electrical system time lags T_{s1} (19 sec in Thorne and Hill's plant model [16] and T_{s2} (nominally 16 sec for fossil plants [36]) are much slower than the time lags associated with the plant (T_m, T_w, and $1/K_i$). The electrical system lags serve to slow the response of the entire system as compared to the isolated load situation and enlarge the range of possible control settings. Governor settings must be selected within the most conservative stability limits. The necessity for stable operation in the isolated load mode has also been stated by Schleif and Wilbor [24] and confirmed by Hovey in his discussion of that same work.

The Mactaquac plant model presented by Thorne and Hill [16, 17] may be used to compare the isolated load model to that of the generator and its connected electrical system. The plant parameters from the Mactaquac plant were implemented into the linearized plant model of this work. For the Mactaquac plant study, $B = 5$, meaning that one fifth (20%) of the load change on the connected electrical system must be carried by the plant model at the new steady state. The fossil plant lag was neglected, so the values $T_{s1} = 0$ and $D_{s1} = 1$ were assigned. The resulting fifth order linear system was simulated using a fourth order Runge-Kutta integration technique [37] in response to a step rejection in system load, $p_{sys} = -1.0$.

Figure 28 is a presentation of the transient load torque $m_{load}(t)$, the speed $n(t)$, and the head $h(t)$ departures. The simulation for a corresponding isolated load change is $m_{load} = p_{sys}/B = -0.2$ and is also shown in Fig. 28. It may be observed that early in the transient, the dynamics of the gen-

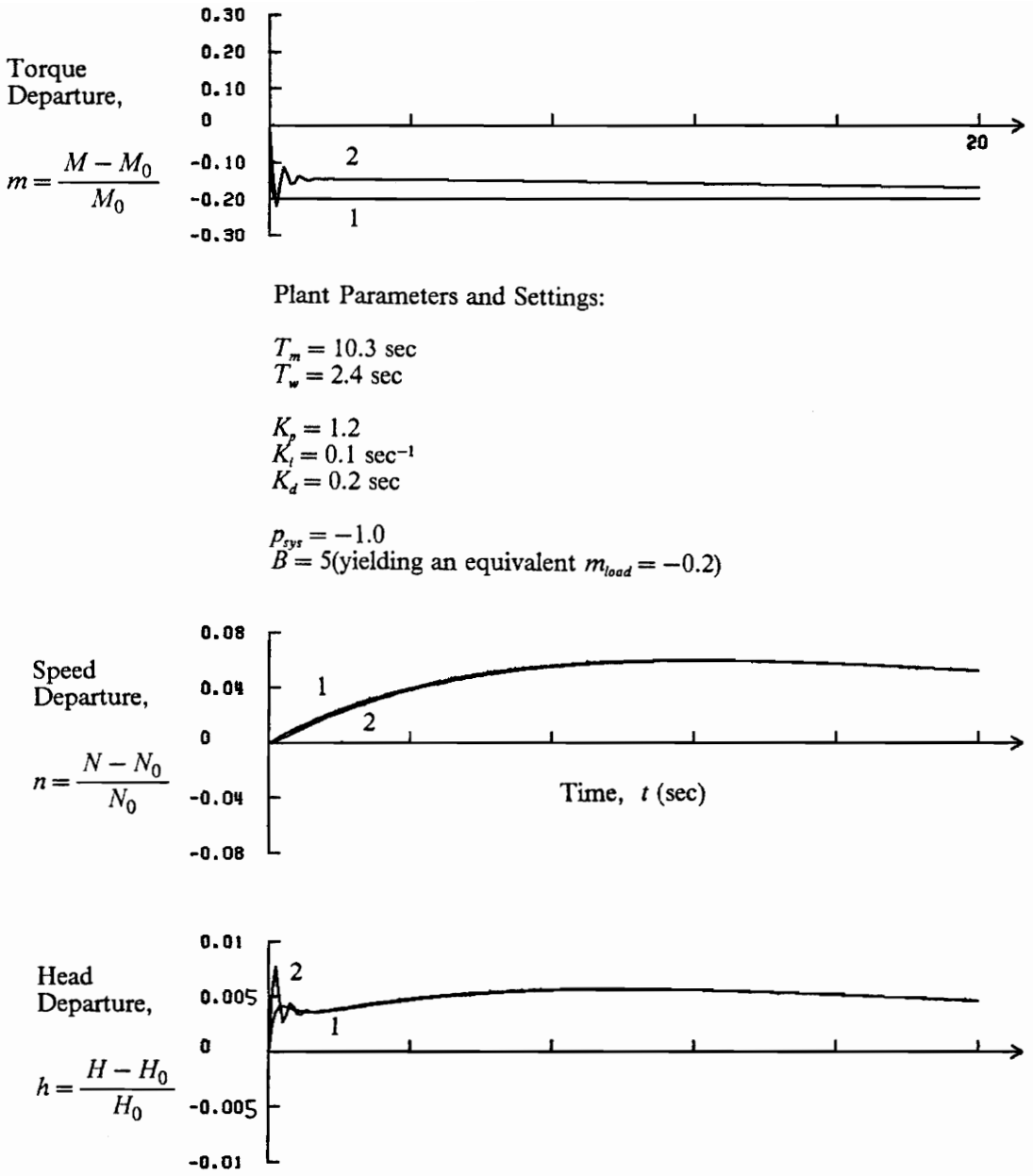

Figure 28. Connected Electrical System Response for Thorne and Hill's Linearized Plant Model.

erator model dominate the load torque response. Later, the control dynamics of the plant bring the load torque to the desired steady value $m_{load} = -0.2$. During the period in which the generator dynamics dominate the response, the load torque exceeds the corresponing isolated load by 10% for approximately 0.1 sec. For the rest of the transient, the load torque remains less than the isolated load model and takes approximately 40 sec to reach 90 percent of the isolated load rejection ($m_{load} = -0.2$) . The results of this simulation give further insight that the isolated load model will be a more demanding load configuration when selecting governor settings because of the slow dynamic interaction between the plant and the connected electrical system.

Nonlinear Model

The guidelines presented in the previous chapter may suggest a nonlinear model for the hydroelectric plant. This choice may required due to waterhammer dynamics caused by rapid wicket gate motion, or to such a large change in load that the turbine performance partial derivatives are not constant. In any case, the nonlinear plant model is formulated to accomodate the nonlinear aspects of both the penstock and the turbine performance.

So that the nonlinear plant model simulation may be compared to the linearized plant model, the isolated load model is used for the load torque. The isolated load situation also makes the nonlinear model useful in the determination of optimum governor settings as suggested by Schleif and Wilbor [24]. If it is desired to simulate a configuration in which the plant is connected to a large, constant frequency electrical electrical system, then only slight changes to the nonlinear plant model are needed.

The development of the numerical techniques required to perform a simulation of the nonlinear plant model are presented. One major difference is that the waterhammer simulation is performed by a finite difference representation of the two governing partial differential equations of the fluid. The second major difference is that the analytical representations for the hill diagram are used

to satisfy the head, flow, gate, speed, and torque relationships of the turbine. The development begins with a review of the governing equations of the plant components.

A functional block diagram of the hydroelectric plant components is shown in Fig. 29 which could represent either a linear or nonlinear model. The nonlinear model and linearized model are similar with respect to the load torque, the turbine speed dynamics, and the governor dynamics, but different in the models for the penstock and turbine performance. The turbine speed dynamics are given by:

$$T_m \, s \, n(s) = m - m_{load}$$

The governor dynamics are given by:

$$y(s) = \left(-K_p - \frac{K_i}{s} - K_d \, s \right) n(s)$$

There is a dynamic relation between the flow and head departures in the penstock which depends on both time and cross-sectional position within the penstock (referred to as the penstock station). This relation may be expressed as:

$$q(x,s) = f[h(x,s)]$$

Since this dynamic relation is based on two partial differential equations, a simple linear representation is not possible. In the development of the nonlinear simulation, the method of characteristics, which is an algebraic finite difference method, is used to represent the dynamic penstock relation.

The second nonlinear aspect of the model concerns the performance of the hydraulic turbine which is determined from the hill diagram relationships. Functionally, these relationships are:

$$q = q\,(y,h,n)$$
$$m = m\,(y,h,n)$$

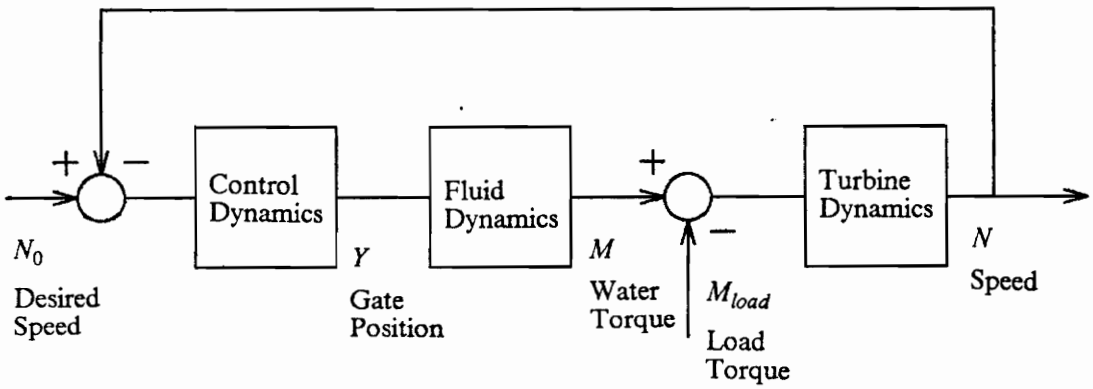

Figure 29. Functional Block Diagram of Hydroelectric Plant Model.

With the governing equation or functional relationship for each plant component established, a computational scheme for simulation of the nonlinear model was formulated and is illustrated in Fig. 30. To begin the simulation scheme, consider that all the initial steady operating values of the plant (Y_0 , N_0 , Q_0 , H_0 , M_0) are determined and that the load torque M_{load} is instantaneously changed. The torque mismatch brings on the turbine dynamics and a resulting speed N is computed. Since the new turbine speed N does not match the desired speed N_o , a new gate position Y is implemented according to the P-I-D control law. The new gate position has an effect on the flow in the penstock. The head and flow at the turbine depend on the penstock governing equations and on the turbine characteristics. The turbine characteristics serve as boundary conditions for the fluid dynamic equations at the penstock outlet. With the new flow Q determined at the turbine, the new water torque M may be determined from the hill diagram relationships. This completes the computational scheme for a single time step. The newly computed water torque results in a new torque mismatch. The computational scheme is repeated with the operating values (Y , N , Q , H , M) used as the initial conditions for the next time step as the simulation marches in time.

The numerical procedures required by the blocks in Fig. 30 labeled "turbine dynamics," "control dynamics," "fluid dynamics," and "quasi-steady torque relationship" are developed. Computational details of the fluid dynamics simulation and of the flow and torque determination are fully developed in this section.

Turbine Dynamics

Using Eq. 3.13 for the speed change of the turbine, the new speed at t_1 caused by the torque mismatch at $t = 0$ is given by:

$$N_{t_1} = N_0 + \frac{N_0}{M_0 T_m} \int_0^{t_1} (M - M_{load})\, dt$$

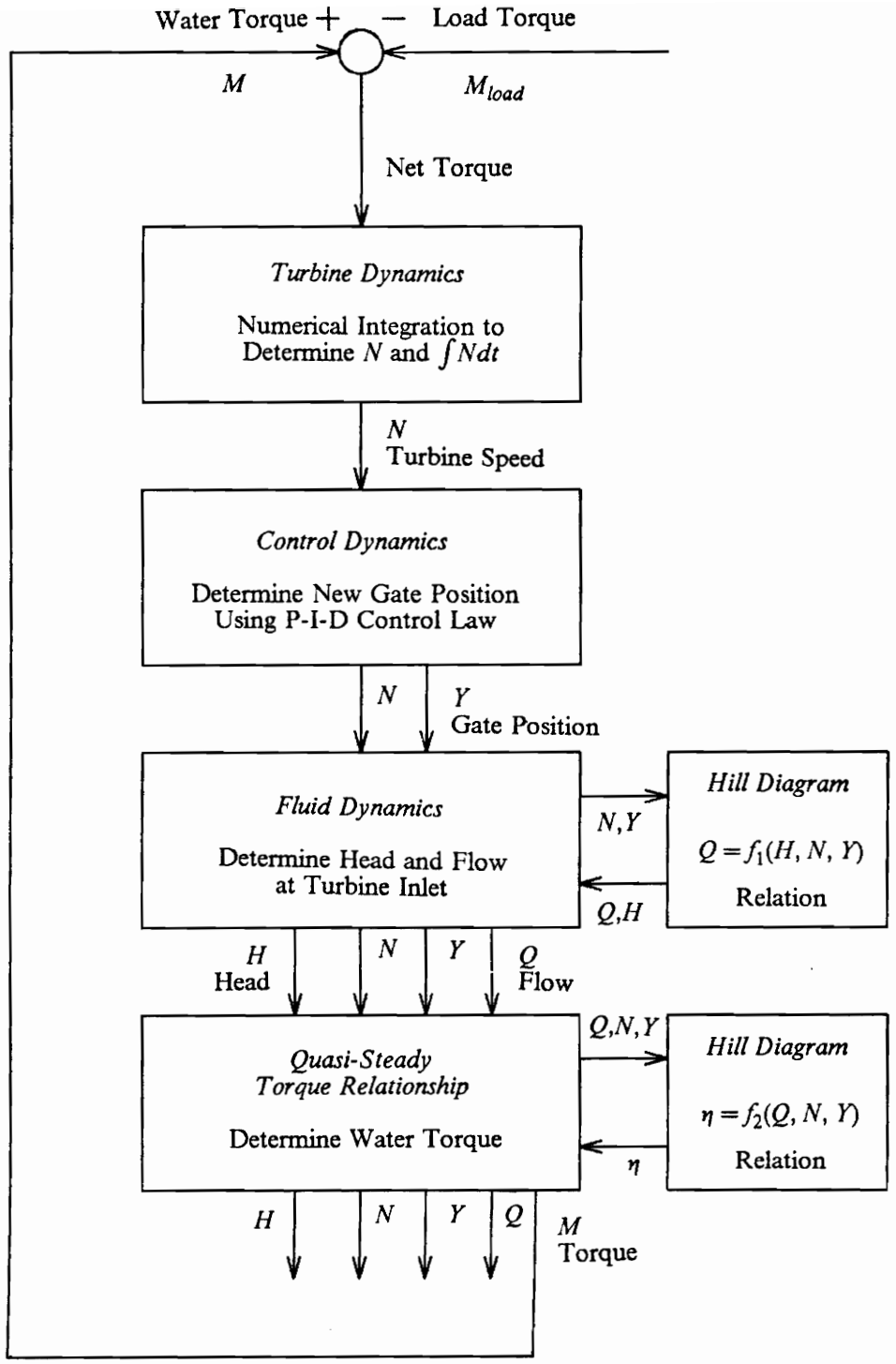

Figure 30. Computational Diagram of Nonlinear Model.

The integral may be performed by a standard technique such as the fourth order Runge-Kutta method as presented in Carnahan, Luther, and Wilkes [37].

Control Dynamics

The P-I-D control law was given in terms of the gate and speed departure by:

$$\frac{Y_{t_1} - Y_0}{Y_0} = -K_p \frac{N_{t_1} - N_0}{N_0} - \int_0^{t_1} K_i \frac{N_{t_1} - N_0}{N_0} dt - K_d \frac{dn(t)}{dt}$$

The equation for the turbine dynamics provides the expression for dn/dt so the new gate position Y_{t_1} is given by:

$$Y_{t_1} = Y_0 + Y_0 \left[K_p \left(1 - \frac{N_{t_1}}{N_0} \right) - \int_0^{t_1} K_i \, n(t) \, dt - \frac{K_d (M_{t_1} - M_{load})}{T_m M_0} \right]$$

Fluid Dynamics - Method of Characteristics

The simulation of the penstock's fluid dynamics is accomplished by the method of characteristics. The development presented herein closely follows that of Wylie and Streeter [8]. The pair of partial differential equations describing flow in the penstock were given by:

$$\frac{1}{A} \frac{\partial Q}{\partial t} + g \frac{\partial H}{\partial x} + \frac{f}{2 D A^2} Q |Q| = 0$$

$$\frac{c^2}{g A} \frac{\partial Q}{\partial x} + \frac{\partial H}{\partial t} = 0$$

Let the momentum equation be identified by $L_1 = 0$ and the continuity equation be identified by $L_2 = 0$. The two equations are combined linearly using an unknown multiplier λ to give the following relation:

$$L_1 + \lambda L_2 = \frac{1}{A}\frac{\partial Q}{\partial t} + g\frac{\partial H}{\partial x} + \frac{f}{2DA^2} Q|Q| + \lambda\left[\frac{c^2}{gA}\frac{\partial Q}{\partial x} + \frac{\partial H}{\partial t}\right] = 0$$

This relation is rearranged in order to separate the head and flow partial derivatives and is given by:

$$\lambda\left[\frac{\partial H}{\partial x}\frac{g}{\lambda} + \frac{\partial H}{\partial t}\right] + \left[\frac{\partial Q}{\partial x}\lambda\frac{c^2}{Ag} + \frac{1}{A}\frac{\partial Q}{\partial t}\right] + \frac{fQ|Q|}{2DA^2} = 0 \qquad [4.7]$$

Any two real, distinct values of λ will yield two equations in terms of the two dependent variables H and Q that are equivalent to the original partial differential equations. Appropriate selection of two particular values of λ leads to simplification of the combined equation above. In general, both variables H and Q are functions of penstock station x and time t . If the independent variable x is permitted to be a function of t , then:

$$\frac{dH}{dt} = \frac{\partial H}{\partial x}\frac{dx}{dt} + \frac{\partial H}{\partial t}$$

and $$\frac{dQ}{dt} = \frac{\partial Q}{\partial x}\frac{dx}{dt} + \frac{\partial Q}{\partial t}$$

By examination of the combined differential equation (Eq. 4.7) with the identities above in mind, it can be observed that if

$$\frac{dx}{dt} = \frac{g}{\lambda} = \frac{\lambda c^2}{g} \qquad [4.8]$$

then Eq. 4.7 becomes an ordinary differential equation given by:

$$\lambda\frac{dH}{dt} + \frac{1}{A}\frac{dQ}{dt} + \frac{fQ|Q|}{2DA^2} = 0$$

Solving Eq. 4.8 for λ yields two particular values as given by:

$$\lambda = \pm \frac{g}{c}$$

By substituting the two particular values of λ back into Eq. 4.8, the manner in which x and t are related is given by:

$$\frac{dx}{dt} = \pm c$$

This simple relation shows the change in position of a wave is related to the change in time by the wave propagation speed c. When the positive value for λ is used for the solution of dx/dt, then the positive value for λ must be used in the resultant ordinary differential equation. The same requirement holds for the negative value of λ. The substitution of both values of λ into the ordinary differential equation leads to a set of two pairs of equations which are grouped and identified as $C+$ and $C-$ equations as follows:

$$\frac{g}{c}\frac{dH}{dt} + \frac{1}{A}\frac{dQ}{dt} + \frac{fQ|Q|}{2DA^2} = 0$$

$C+$ equations

$$\frac{dx}{dt} = +c$$

$$-\frac{g}{c}\frac{dH}{dt} + \frac{1}{A}\frac{dQ}{dt} + \frac{fQ|Q|}{2DA^2} = 0$$

$C-$ equations

$$\frac{dx}{dt} = -c$$

The two real values of λ have been used to convert the original two partial differential equations to two ordinary differential equations with the restriction that each is only valid for a unique value of dx/dt. As observed by Wylie and Streeter [8], it is convenient to visualize the solution of the set of equations as it develops on the independent variable t versus x plane. The equation for each dx/dt represents a straight line on the x-t plane. These lines are referred to as the characteristic lines along which the respective ordinary differential equation is valid. The two or-

dinary differential equations are referred to as compatibility equations, each one being valid only on its appropriate characteristic line. Figure 31 is a general demonstration of the two sets of differential equations on the x-t plane. Consider that at some point in time t_1, the head and flow are known at two penstock positions A and B. By drawing the $C+$ characteristic line ($dx/dt = c$) from point A and the C- characteristic line ($dx/dt = -c$) from point B, then the flow and head are computed at position P at time t_2 by solving the two compatibility equations simultaneously. Therefore, a time-marching scheme starting at the initial steady operating condition is formulated to simulate the fluid dynamics at any desired number of discrete positions in the penstock.

Review of Fig. 31 reveals that the method of characteristics is a finite difference method whereby the flow and head are computed only at specific positions in the penstock at specific times. For the overall plant simulation, the flow and head at the penstock outlet (turbine inlet) is of primary interest. In order to determine these values in a simulation which marches in time, the penstock is divided into N equal sections, each Δx long as shown in Fig. 32. The time step is then constrained to satisfy the requirement that $dx/dt = \pm c$. The computational time step is given by:

$$\Delta t = \frac{\Delta x}{c} = \frac{L}{N c} \qquad [4.9]$$

The dependent variables Q and H are known at all positions at the initial steady operating condition $t = 0$. The $C+$ compatibility equation is valid along all points on the characteristic line AP. This ordinary differential equation is integrated between the limits A and P and thereby is expressed in terms of the unknowns Q and H at point P. By multiplying the $C+$ compatibility and characteristic equations by $c\frac{dt}{g} = \frac{dx}{g}$, a single equation is placed into the form suitable for integration along the $C+$ characteristic line as given by:

$$\int_{H_A}^{H_P} dH + \frac{c}{g A}(Q_P - Q_A)\int_{Q_A}^{Q_P} dQ + \frac{f}{2 g D A^2}\int_{x_A}^{x_P} Q\,|Q|\,dx = 0$$

where the subscript P represents values at point P and the subscript A represents values at point A. The variation of Q as a function of x in the last integral term is not known. According to

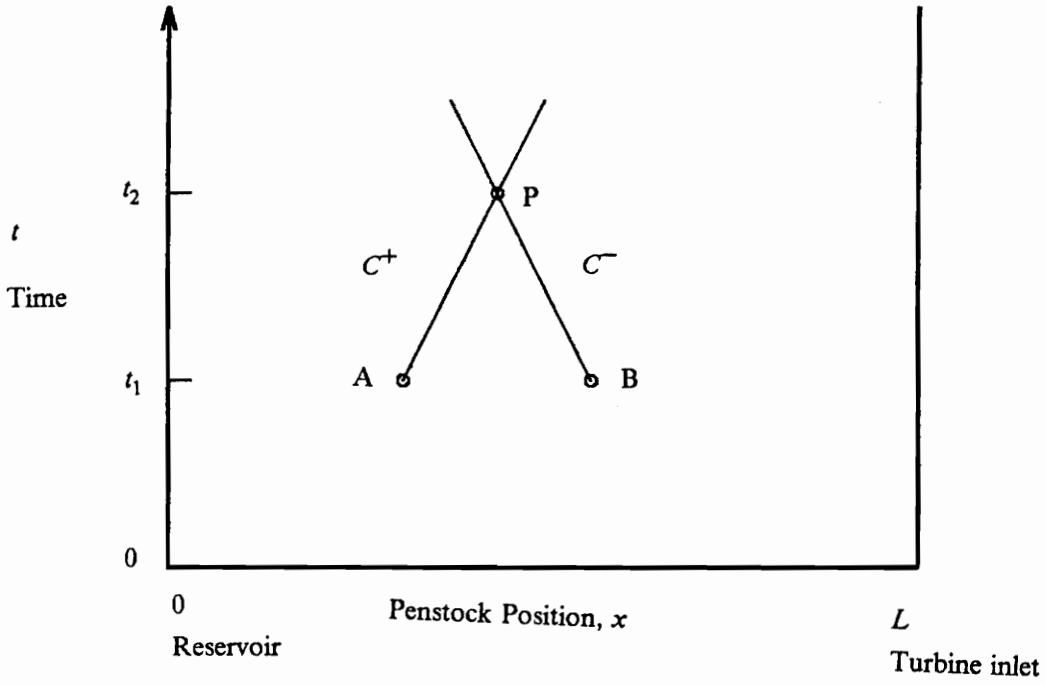

Figure 31. Characteristic Lines for Fluid Dynamics Representation.

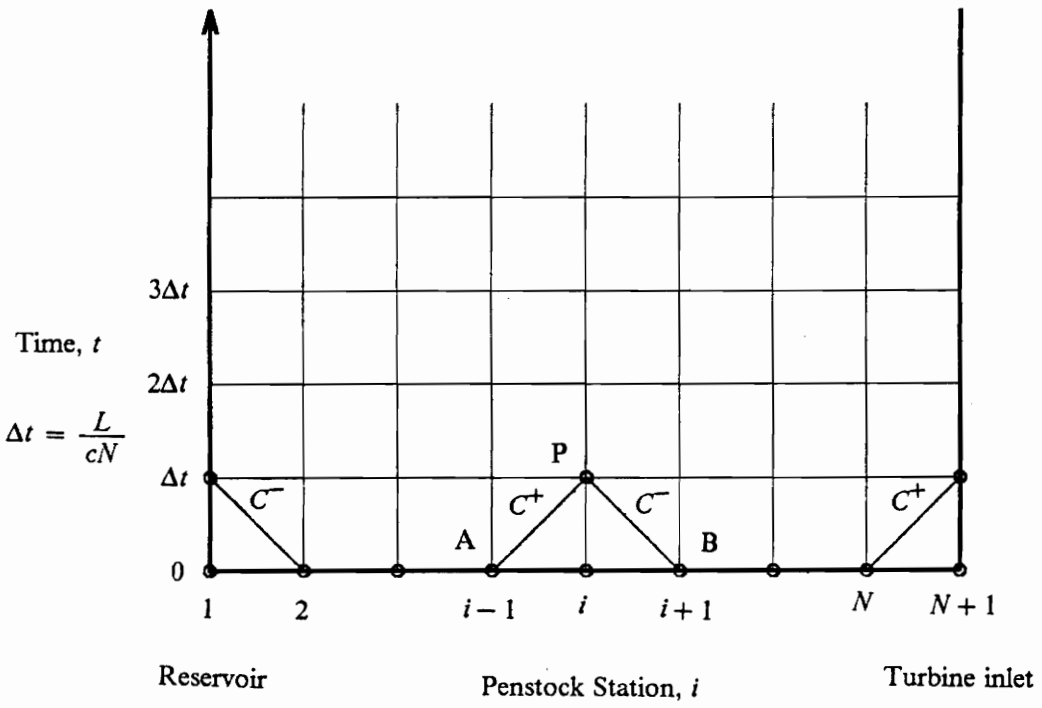

Figure 32. Method of Characteristics Solution Grid for Fluid Dynamics Simulation.

Wylie and Streeter [8], an approximation sufficient for the hydroelectric penstock situation is to consider that the flow stays relatively constant along each section during the time increment of interest. The expression for the third integral above becomes $Q\,|Q|\,\Delta x$.

A similar approach of integrating the C- compatibility equation along the C- characteristic line from B to P leads to a set of two equations with the flow and head (Q_P and H_P) at point P being unknown. Each equation is then solved for the head at point P , H_P . The resulting two expressions for H_p from the $C+$ and C- compatibility equations are respectively given by:

$$H_P = H_A - \frac{c}{g\,A}(Q_P - Q_A) - \frac{f\,\Delta x}{2\,g\,D\,A^2}\,Q_A\,|Q_A|$$

$$H_P = H_B + \frac{c}{g\,A}(Q_P - Q_B) - \frac{f\,\Delta x}{2\,g\,D\,A^2}\,Q_B\,|Q_B|$$

The time-marching solution for the penstock dynamics begins at $t = 0$ with the initial steady conditions of the penstock as a result of the initial position of the wicket gates. Steady-state analysis leads to the determination of the flow and head at each equally-spaced position in the penstock on the $t = 0$ line as shown in Fig. 32. The transient solution consists of finding each head and flow along the $t = \Delta t$ line, then proceeding to $t = 2\Delta t$, etc. until the desired plant simulation time has been completed.

At any interior grid point, represented by the general position subscript i , the two compatibility equations are written in a simple form as:

$$H_{P,i} = C_P - \frac{c}{g\,A}\,Q_{P,i} \qquad (C+ \text{ compatibility equation})$$

$$H_{P,i} = C_M + \frac{c}{g\,A}\,Q_{P,i} \qquad (C\text{- compatibility equation})$$

where the subscript P,i represents the value at penstock position i at the time corresponding to point P . The constants C_P and C_M depend only on values which have been evaluated at the previous time (denoted by $P - 1$) and are expressed by:

$$C_P = H_{P-1,i-1} + \frac{c}{gA} Q_{P-1,i-1} - \frac{f\Delta x}{2gDA^2} Q_{P-1,i-1} |Q_{P-1,i-1}| \qquad [4.10]$$

$$C_M = H_{P-1,i+1} + \frac{c}{gA} Q_{P-1,i+1} - \frac{f\Delta x}{2gDA^2} Q_{P-1,i+1} |Q_{P-1,i+1}| \qquad [4.11]$$

By eliminating the flow at point P , the head at point P is explicitly obtained by:

$$H_{P,i} = \frac{C_P + C_M}{2}$$

The value for $Q_{P,i}$ is solved algebraically by using either compatibility equation. In order to proceed with the time-marching solution, the boundary conditions of the reservoir and of the turbine performance characteristics must be introduced into the computational scheme.

Fluid Dynamics - Boundary Conditions

The boundary condition of the inlet to the penstock is easily expressed since the reservoir head is constant for the hydroelectric plant model. The head at penstock station 1 as shown in Fig. 32 is given by:

$$H_{P,1} = H_{res}$$

where the subscript $P,1$ represents the penstock inlet for all time. The flow at the penstock inlet may then be determined from the C- compatibility equation as given by:

$$Q_{P,1} = (H_{res} - C_M)\frac{gA}{c}$$

where C_M was defined in Eq. 4.11.

The boundary condition at the penstock outlet is more involved. The relation between head and flow based on the turbine performance is needed. This relation is solved in conjuction with the $C+$ characteristic equation written from the N-th station at the previous time to determine the pair of Q and H which satisfy requirements of both the turbine performance and the fluid dynamics. For a specified value of wicket gate position Y, the relation between head and flow at the penstock outlet is given by:

$$Q = \frac{a N^2 D_r^4}{\sqrt{H}} + b N D_r^3 + c D_r^2 \sqrt{H} \qquad [4.12]$$

The $C+$ compatibility equation is written along the line connecting the N-th penstock station at the previous time step to the penstock outlet ($N+1$-th station) at the time step of interest. Expressing the flow and head at the penstock outlet and at the time step of interest as Q and H, the compatibility equation is given by:

$$H = C_P - \frac{c}{g A} Q$$

where C_P was defined in Eq. 4.10.

The two equations relating the flow and head may be combined in order to eliminate the flow Q and solve for the head H. The resulting expression for the head at the penstock outlet is given by:

$$H + B\left[\frac{a N^2 D_r^4}{\sqrt{H}} + b N D_r^3 + c D_r^2 \sqrt{H}\right] - C_P = 0$$

where $B = \frac{c}{g A}$ in which c in this term is the fluid wavespeed.

The analytical expression cannot be solved explicitly for the head, but Newton's method may be used to determine the value for H. A good first guess for the head is the reservoir head. Consid-

ering that the penstock outlet head may be determined in a few iterations, the flow Q is then determined from the turbine head/flow relation presented in Eq. 4.10.

This completes the development of the fluid transient simulation of the penstock. At this point, the flow, head, and speed of the turbine are all known which specifies a unique operating point on the hill diagram. Therefore, the turbine efficiency may be determined and the resulting water torque may be computed.

Quasi-steady Torque Relationship

The set of flow, head, and speed (Q, H, N) describe a unique operating point on the hill diagram in terms of the unit discharge and the unit speed (Q_1, N_1) . As outlined in the formulation of the turbine characteristics model in Chapter 3, a search may be made for the efficiency ellipse which passes through the operating point. Once the efficiency has been determined, the torque M may be determined by way of the relation between hydraulic and mechanical power as given by:

$$M = \frac{\eta \rho g Q H}{\left(\frac{2 \pi N}{60}\right)}$$

At this point, all plant operating values have been determined and a single time step has elapsed. The torque M just computed results in a new mismatch in water versus load torque so that the nonlinear simulation scheme is repeated for another time step. The simulation continues and ultimately (assuming that the plant operates in a stable manner) a new steady operation is achieved.

Summary of Plant Model Developments

Five plant models have been developed in this chapter. Linear models have been used to illustrate that certain governor settings insure stable performance and some settings result in better performance than others. It was shown that waterhammer dynamics in the penstock tend to limit the region of stable plant operation, with this problem being more severe with large values of K_d. A nonlinear simulation technique was developed so that linear and nonlinear models may be compared when studying the optimum performance of a representative plant. This comparison will be made when a representative plant model is established in Chapter 6.

Chapter 5

Optimum Governor Settings and Zones of Satisfactory Operation

The governor settings which result in the best plant performance are referred to as optimum settings. The definition of "best plant performance" must incorporate a method for penalizing too much departure in the desired turbine speed (excessive overshoot) and for penalizing too long a time required to achieve a new steady operation (excessive settling time). The aspect of best plant performance is addressed in terms of a performance index. Takahashi [10] presents four typical forms of possible performance indexes. The integrated absolute value of error IAE is defined by:

$$IAE = \int_0^\infty |e(t)|\, dt$$

A plant variable such as speed, flow, head, or torque could serve as the error $e(t)$. The hydroelectric plant product is the electric power and it is important to maintain the power at a nearly constant frequency. The longer the plant frequency departs from the desired frequency, the poorer the quality of the power delivered to consumers. Since the frequency is proportional to the turbine

speed, then the error of importance is the departure of the turbine speed from the desired speed. Therefore, the *IAE* performance index for hydroelectric plant response is expressed as:

$$IAE = \int_0^T |n(t)|\, dt$$

where the plant has reached a new steady operating condition before the time T.

Three other forms for the performance index are common. The integral of squared error *ISE* is defined by:

$$ISE = \int_0^T n^2(t)\, dt$$

The integral of time multiplied by the absolute value of error *ITAE* is given by:

$$ITAE = \int_0^T t\, |n(t)|\, dt$$

The *ITAE* penalizes speed errors occurring late in a transient more severely than those occurring early in a transient. In fact, very early speed departures may occur with little penalty. The integral of time multiplied by the squared error *ITSE* is given by:

$$ITSE = \int_0^T t\, n^2(t)\, dt$$

The same observations apply to the *ITSE* as the *ITAE*.

The *IAE* performance index has been selected for the determination of optimum gain settings for the hydroelectric plant. It was chosen over the *ITAE* in order to penalize early and late speed departures equally. Furthermore, after an optimization technique has been determined, it will be demonstrated that the selection of either the *IAE*, *ISE*, or *ITAE* indexes result in similar optimum settings.

Optimization Procedure

In order to determine the governor settings which result in optimum plant performance, a procedure is devised which begins with the determination of the basic plant parameters, estimates and then refines optimum governor settings, and finally considers those settings for a range of plant operating conditions. The procedure for this task is presented in the following steps:

1. Assemble plant information in order to define the linearized, transcendental, and nonlinear plant models previously developed.
2. Determine the anticipated initial steady operating load condition in order to characterize the turbine performance partial derivatives.
3. For a range of derivative gains starting with zero (P-I control) and ending with the maximum, plot the stability limits for the linearized and transcendental models. This provides a boundary within which the optimum settings must lie.
4. Begin the optimization process with P-I control of the linearized plant model. Use governor settings suggested by Hovey [13] as a starting guess for the optimum settings. Hovey suggested the following settings for P-I control of a theoretical linear plant model:

$$K_p = \frac{T_m}{2\,T_w}$$

$$K_i = \frac{T_m}{8\,T_w^{\,2}}$$

5. Using a simple grid search method, starting with the first guess for a K_i , K_p pair, perform linearized plant model simulations repetitively until a minimum value for the IAE performance index has been found. The performance index for a linear model simulation is proportional to the load torque change, so the magnitude of the load change is not important.

6. Increase the derivative gain K_d and use the values for K_p and K_i determined in the previous step as a starting guess for the K_p , K_i , K_d set. Again, perform linearized plant simulations over a K_p , K_i grid until a minimum IAE value has been determined.
7. Continue to increase the derivative gain and repeat the previous step until the derivative gain has reached the maximum allowable value which insures stability of the linear plant.
8. At this point, a table of optimum gains starting with $K_d = 0$ (P-I control) and with K_d increasing is assembled. The value of IAE for each K_p , K_i , K_d set is also tabulated. The tabulated settings may be compared to those suggested by Hovey [13] and also those suggested by Hagihara [27] which are given by:

$$K_p = 0.8\frac{T_m}{T_w}$$

$$K_i = 0.24\frac{T_m}{T_w^2}$$

$$K_d = 0.267T_m$$

9. The previous five steps may be repeated using different performance indices.

The previous nine steps utilize a linear plant model. That linear optimization process was performed using a theoretical linear model with $T_m = 6$ sec and $T_w = 1$ sec, The results of that process are presented in Fig. 33. The figure shows that for each value of K_d, the use of IAE, ISE, and $ITAE$ indexes result in similar optimum settings. Using the IAE index as a basis of comparison, the linear optimization process leads to suggested settings which result in an 18 percent improvement in performance over Hovey's suggested settings. For $K_d = 1.6$ sec, the optimum settings result in an 8.5 percent improvement over Hagihara's suggested settings. For a high derivative gain ($K_d = 2.5$ sec), there is an 80 percent improvement over Hovey's settings. Although a significant improvement in performance is indicated by this set of values, gate speed limits or waterhammer will be shown to preclude the implementation of such lively settings.

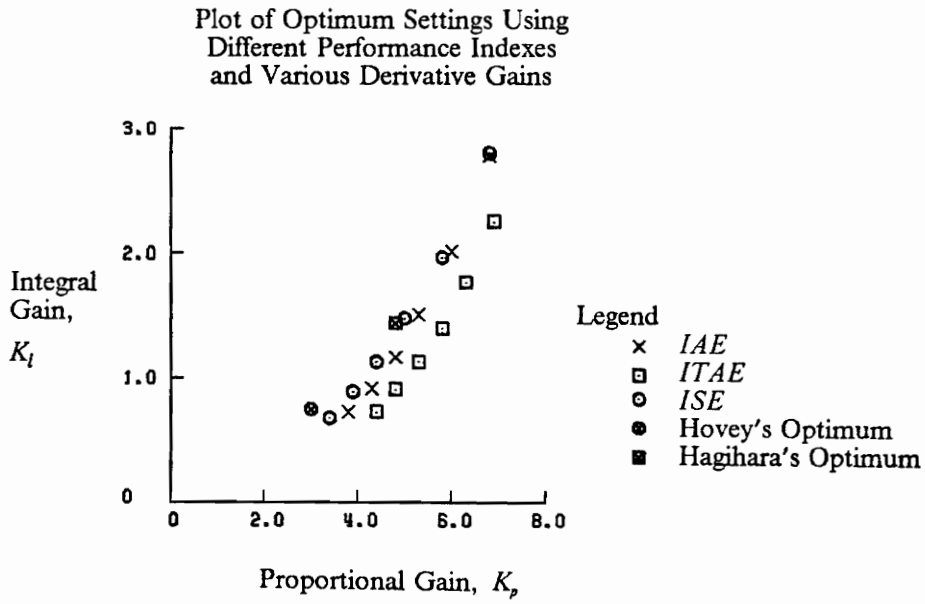

Optimum Settings Using the *IAE* Performance Index and m_{load} = -0.1.

K_p	K_i	K_d	*IAE*
3.8	0.73	0.0	0.147
4.3	0.92	0.5	0.114
4.8	1.17	1.0	0.089
5.3	1.51	1.5	0.068
6.0	2.02	2.0	0.051
6.8	2.79	2.5	0.036
3.0	0.75	0.0	0.180 (Hovey's Optimum)
4.8	1.44	1.6	0.071 (Hagihara's Optimum)

Figure 33. Optimization Results for Theoretical Linear Model.

The information gained from the linear plant model optimization provides a starting point to begin an optimization process for the nonlinear model. The nonlinear model optimization process is outlined by the following steps:

1. Determine the magnitude of the anticipated load change. This information is necessary in order to utilize the nonlinear plant model for determination of the optimum gain settings. In the most part, the magnitude of the load change places a more severe limitation on the maximum allowable derivative gain than that of the linearized model stability limit. For example, the maximum possible gate speed is not considered in the nonlinear plant model simulation. Rapid gate speed requirements are associated with high derivative gains. Also, the wicket gate position must be within $0 \leq Y \leq 1$. The conditions of $Y = 1$ and $Y = 0$ are known as gate saturation. These aspects are implemented in the nonlinear plant model simulation.
2. Begin the optimization process with proportional-integral control ($K_d = 0$) of the nonlinear plant model. For a starting estimate of settings, use those suggested by the linear model optimization process (or settings suggested by Hovey if the linear optimization process was not performed).
3. Using the same grid search method as before and starting with the first guess for a K_i , K_p pair, perform nonlinear plant model simulations repetitively until a minimum value for the IAE performance index has been found.
4. Increase the derivative gain K_d slightly in order to achieve P-I-D control and use the values for K_p and K_i suggested by the linearized model optimization as a starting guess for the K_p , K_i , K_d set. Once again, perform nonlinear plant simulations over a K_p , K_i grid until a minimum IAE value has been determined.
5. Continue to increase the derivative gain and repeat the previous step until the derivative gain has reached the maximum allowable value determined from the linearized model. Depending on the anticipated load change, gate position saturation followed by "integral control windup" may bring on instability and preclude increases in the derivative gain.

6. As in the linear plant optimization, a table of optimum gains starting with $K_d = 0$ (P-I control) and with K_d increasing is assembled. The value of the IAE for each K_p , K_i , K_d set is also tabulated in order to study the effect of derivative gain on the magnitude of the IAE . In addition, the required wicket gate speed corresponding to each K_p , K_i , K_d set is tabulated. Since nonlinear simulations depend on specific plant information, an example of this tabulation must be delayed until the next chapter when a representative plant model is established.
7. Determine the wicket gate speed limit. If this information is not available from the manufacturer, the gate speed limit is estimated from Gordon's curves [9]. This constraint will limit the selection of K_p , K_i , K_d settings to those with low values of derivative gain in order to stay within the gate speed limit.
8. For each set of optimum K_p , K_i , and K_d , investigate the regions where these settings result in satisfactory operation. An operational region map is assembled by considering various values of initial load and magnitude of load change. Operation is considered satisfactory if constraints such as maximum/minimum head, maximum gate speed, gate position saturation, speed overshoot, and settling time are not violated.
9. Finally, the K_p , K_i , K_d set which provides a sufficiently large region of satisfactory operation around the expected operating condition is recommended.

The previous nine steps utilize the nonlinear plant model. In the next chapter, a representative plant which incorporates a nonlinear plant model is formulated. The nonlinear optimization process is performed on the representative plant model and the results are compared to those of the linearized plant model optimization.

Pattern Search Method

By considering specific values of derivative gain, the task of determining the gain settings which result in the minimum IAE becomes a problem of optimization in two variables. For each value of K_d , the IAE is a function of the plant response which is controlled by values of K_p and K_i. This is expressed mathematically as:

$$IAE = f(K_p, K_i)$$

For this work, a simple pattern search method has been devised in order to determine the values for K_p and K_i which result in the minimum IAE for a specified value of K_d . As shown in Fig. 34 a four-point diamond with a centered point was chosen as the pattern. To begin the search, the point labeled 1A is positioned according to the first-guess K_p , K_i pair as suggested in the procedure above. Points 2A through 5A are positioned corresponding to a specified K_p and K_i grid size. The IAE performance index is then computed at each of the five points.

The point (2A through 5A) which has the lowest value of IAE is then assigned to point 1B and the five-point pattern is moved accordingly. In the example of Fig. 34, The IAE at point 2A is assigned to point 1B and the IAE at point 1A is assigned to point 4B. New computations for IAE must be performed for the three new points 2B, 3B, and 5B. The example illustrates three more movements of the five-point pattern to the points 1E through 5E. The procedure is repeated until point 1 contains the minimum IAE . Either the grid size is halved and the pattern search procedure is continued or the procedure is terminated. The decision simply depends on the current size of the K_p and K_i grids and the desired precision of the governor settings.

This pattern search is effective for the hydroelectric plant models for several reasons. First, the region of possible K_p , K_i pairs is defined by the stability limits of the linearized plant. Second, a method for determining the starting guess for a pair of K_p and K_i has been presented in the optimization procedure. Third, the IAE surface resulting from the plant dynamics is sufficiently smooth so that a single set of gains represents a minimum point without relative minimum points appear-

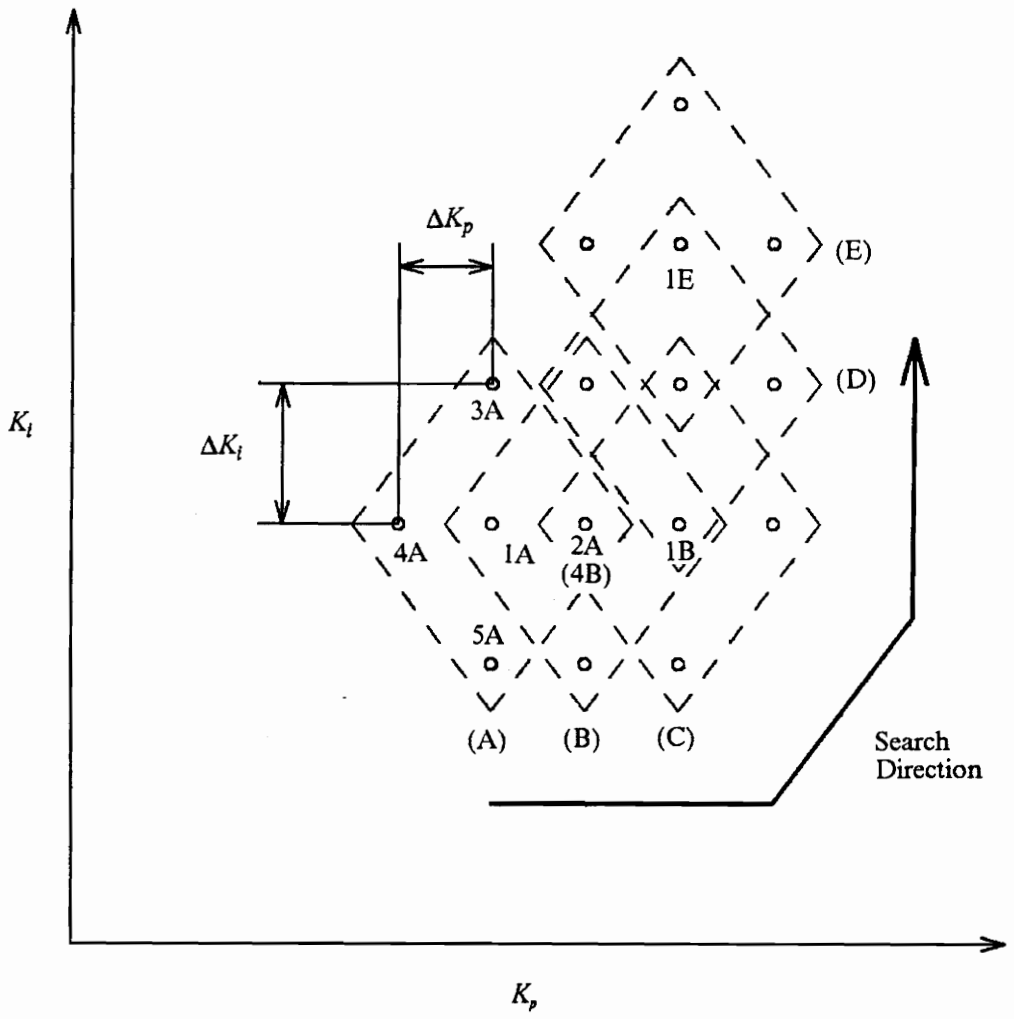

Figure 34. Formulation of Pattern Search Optimization.

ing. A more sophisticated approach which proceeds only in the direction of improving performance index (method of steepest descent) can replace the pattern seacrh method presented. In this work, optimum settings were determined quickly enough using the pattern search so as not to require more sophisticated optimization methods.

Summary of Optimization Procedure

A plan of analysis has been presented which leads to the determination of optimum governor settings for the hydroelectric plant. The plan incorporates the determination of optimum settings for linear and nonlinear models. The description of a zone of satisfactory operation was presented in order to determine the best set of gains for plant operation different from the anticipated operation. This analysis, along with the methods outlined for hydroelectric plant modeling, will be applied to a representative plant in order to demonstrate the value of this integrated approach.

Chapter 6

Application of Analysis to Hydroelectric Plants

The purpose of this work is to present a unified plan of analysis for hydroelectric plants which begins with the mathematical modeling of a plant and culminates in the determination of control settings to achieve optimum plant performance. The components of the plan have been developed in the preceding chapters. In this chapter, the plan is applied to a representative plant to demonstrate how this integrated modeling, simulation, and optimization approach leads to the improvement of plant performance. The representative plant chosen for this work will be shown to exhibit linear plant behavior around the anticipated plant operating condition and nonlinear plant behavior when operation departs from the anticipated conditions. The extent of nonlinear behavior will be shown to depend on the governor settings, the initial operating condition, the magnitude of the load change, and the wicket gate speed limit.

The steps of the plan of analysis are outlined in the form of a checklist. For a plant which exhibits both linear and nonlinear characteristics, the steps are executed in a serial manner. For plants which are fully linear or fully nonlinear, some steps (which will be identified) are omitted. The steps of the analysis to be applied to the representative plant are given in the following checklist:

1. Gather plant information required to define the mathematical models for the components.
2. Establish characteristic parameters which describe the performance of the plant components.
3. Establish the validity of linear models for simulating anticipated plant operation.
4. Use analytical solutions to study linear system performance for low order models.
5. Use nonlinear simulation techniques to study nonlinear system performance.
6. Compare linear and nonlinear simulations.
7. Determine stability limits for linear plant models.
8. Perform governor setting optimization procedure using linear model.
9. Perform governor setting optimization procedure using nonlinear model.
10. Establish zones of satisfactory operation for various governor settings.
11. Establish best settings depending on anticipated operational condition and zone of satisfactory operation.
12. Examine effects of initial operating conditions and load change magnitude using selected settings.
13. Determine allowable gate speeds for load changes when the plant is connected to a large electrical system.

After the first three steps of the analysis are completed, the plant under study may fall into the category of a fully linear plant, a fully nonlinear plant, or a plant exhibiting both linear and nonlinear characteristics. If the plant is either fully linear or fully nonlinear, some of the remaining ten steps may be omitted from the analysis. Table 3 is a presentation of the steps that must be performed depending on the type of plant under consideration.

A representative hydroelectric plant model is established in order to demonstrate the application of the integrated plan of analysis. The model is based on data which is representative of a hydroelectric plant installation although the model does not represent a particular plant. For this work, English units have been used because this system of units is the one commonly used in North American installations [9, 2]. The rated output of the hydraulic turbine is 86 MW at a speed of 200 rpm with a rated flow of 4025 cfs (1.8 million gpm). The reservoir, located 275 ft above the turbine,

Table 3. Steps of Hydroelectric Plant Analysis for Linear, Nonlinear, and Mixed Plant Models.

	Analysis Step	Fully Linear Plant	Mixed Model Plant	Fully Nonlinear Plant
1	Gather Plant Information	Yes	Yes	Yes
2	Establish Plant Characterizing Parameters	Yes	Yes	Yes
3	Establish Validity of Linear Models	Yes	Yes	Yes
4	Linear System Simulation	Yes	Yes	No
5	Nonlinear System Simulation	No	Yes	Yes
6	Compare Linear and Nonlinear Simulations	No	Yes	No
7	Linear Plant Model Stability Limits	Yes	Yes	No
8	Linear Model Optimization	Yes	Yes	No
9	Nonlinear Model Optimization	No	Yes	Yes
10	Zone of Satisfactory Operation	Yes[a]	Yes[b]	Yes[b]
11	Establish Best Control Settings	Yes	Yes	Yes
12	Effects of Initial Load and Load Change	Yes	Yes	Yes
13	Allowable Gate Speeds	Yes[c]	Yes[d]	Yes[d]

[a] Check linear simulation for speed limit, saturation, head constraint violations.

[b] Check nonlinear simulation for constraint violations.

[c] Use analytical solution for $h(t)$ to determine gate speed limits.

[d] Use nonlinear simulation to determine gate speed limits.

supplies water to the turbine by way of a 1200 ft long, 20 ft diameter penstock. In order to illustrate each step in the analysis of the representative plant, the subsections of this chapter follow the procedure outlined by the checklist.

Step 1 -- Gather Plant Information

Figure 35 shows a sketch of the arangement of the plant components and the information required to establish the characteristic parameters which describe the plant performance. The data tabulated in that figure and the graphical hill diagram should be available from the turbine manufacturer and plant information files or from a proposed design. The hill diagram for the representative hydraulic turbine is shown in Fig. 36. The coefficients which represent the analytical characteriztion of turbine performance are tabulated in the figure. The wicket gate speed constraints are estimated using Gordon's curves which depend on the values of the plant characterizing parameters.

The results of the analysis to determine steady-state flow, head, power, and efficiency for various gate positions are shown in Fig. 37. Using this figure, the initial anticipated operating point was chosen to correspond to the set of conditions for a gate position of $Y = 0.8$. At the initial anticipated operating condition, 85.1 MW power are produced, the turbine head is 271.6 ft, and the flow is 3938 ft^3/sec. The anticipated load departure was chosen to be a nominally 10% load rejection. A gate position of $Y = 0.7$ gives an output of 76.3 MW, corresponding to a load departure of $m_{load} = -0.103$ which, for this analysis, is a satisfactory representation of the nominal 10% load rejection. At the anticipated new operating condition, the turbine head is 272.3 ft, and the flow is 3525 ft^3/sec. Both the initial and new anticipated steady-state operating conditions are shown on the hill diagram of Fig. 37. The initial operating condition is nearly the same as the rated turbine condition, which typically corresponds to plant operation at design conditions. The analysis allows

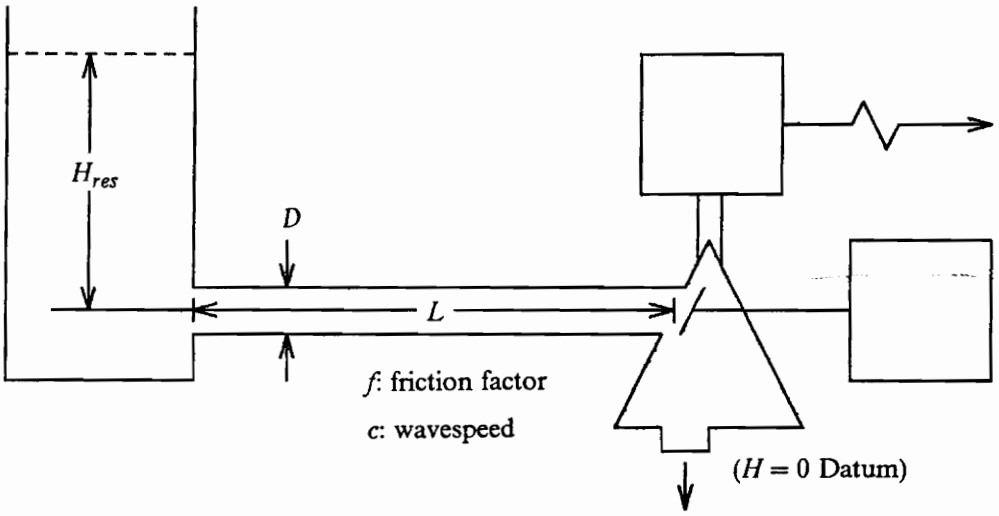

Penstock and Reservoir Information

H_{res} = 275 ft
L = 1200 ft
D = 20 ft
f = 0.018
c = 3937 fps

Turbine Information and Rated Conditions

Wr^2 = 3.55x10^7 lbf-ft^2
D_r = 15.6 ft (runner diameter)
Q_r = 4025 cfs
H_r = 269 ft
N_r = 200 rpm
M_r = 3.03x10^6 lbf-ft
η_r = 0.94

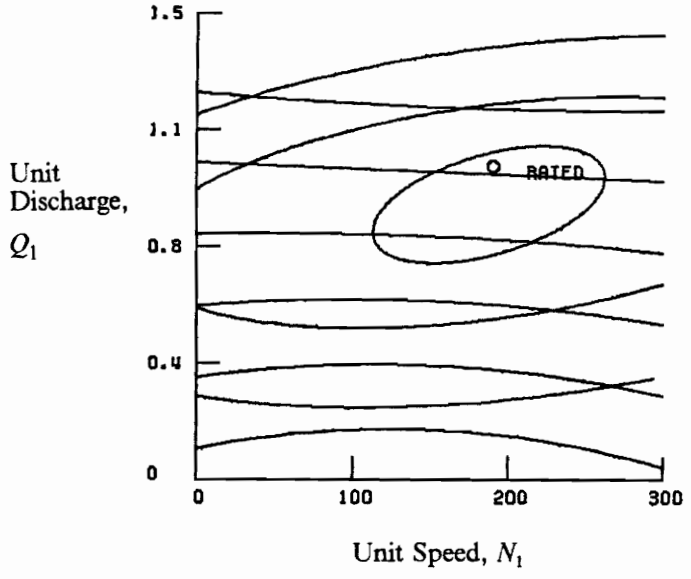

Figure 35. Information Required to Establish Characteristic Plant Parameters – Representative Plant.

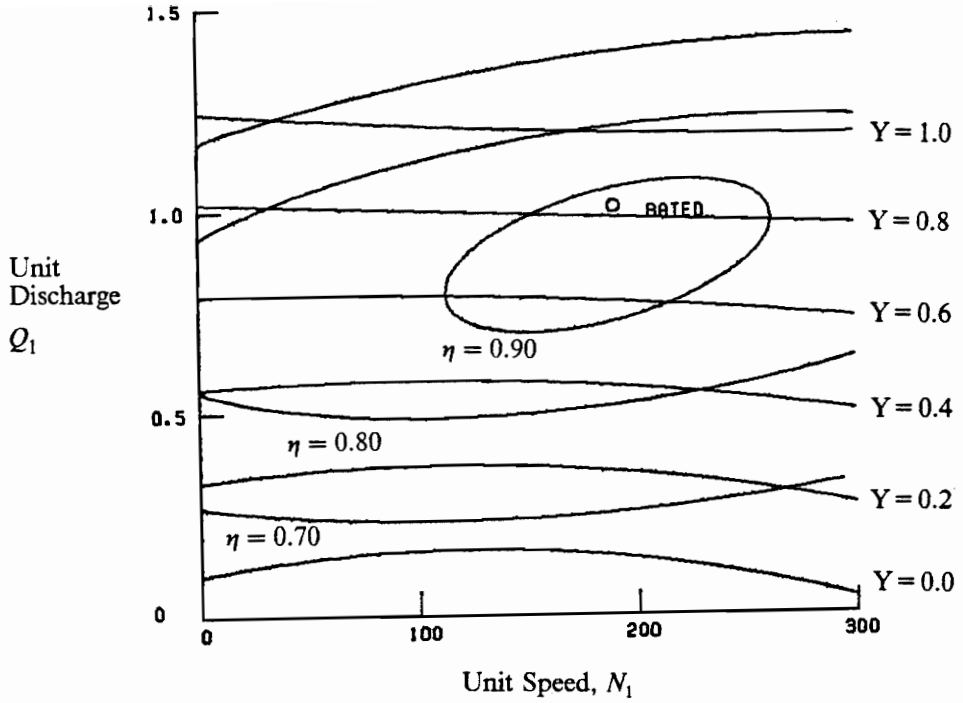

Unit Discharge Versus Unit Speed Relation Parameters
($Q_1 = a N_1^2 + b N_1 + c$)

Y	a	b	c
1.0	7.5×10^{-7}	-4.25×10^{-4}	1.25
0.8	0.0	-2.00×10^{-4}	1.02
0.6	-1.0×10^{-6}	1.00×10^{-4}	0.79
0.4	-2.0×10^{-6}	4.00×10^{-4}	0.56
0.2	-3.0×10^{-6}	7.00×10^{-4}	0.33
0.0	-4.0×10^{-6}	1.00×10^{-3}	0.10

Efficiency Ellipse Relation Parameters (Eq. 3.46)

η	Q_1^0	N_1^0	θ (degrees)	d	e
0.94	1.008	190.2	(Rated Condition)		
0.90	0.885	187.5	0.0012°	75.	0.165
0.80	0.860	187.5	0.0006°	225.	0.340
0.70	0.830	206.0	0.0005°	338.	0.340

Figure 36. Characterization of Representative Hill Diagram.

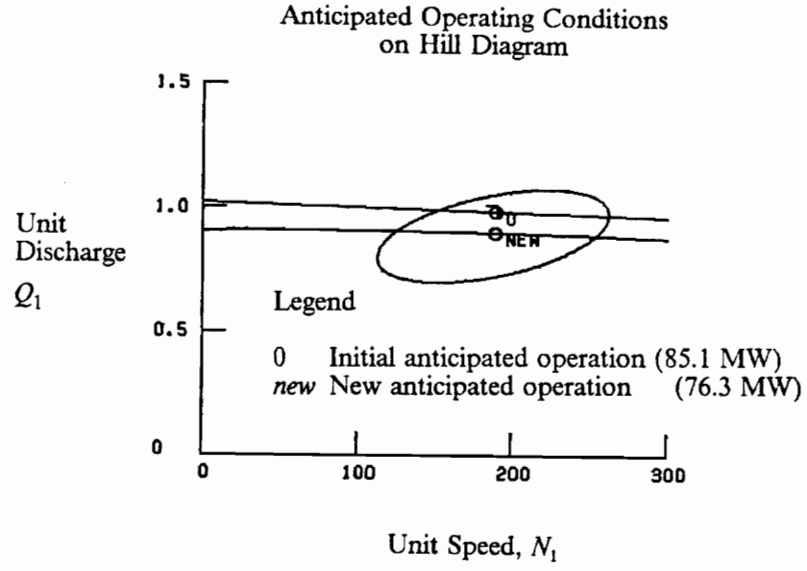

Wicket Gate Position Y	Plant Output (MW) P	Flow (cfs) Q	Turbine Efficiency η	Turbine Head (ft) H	Water Starting Time, T_w (sec)	Machine Starting Time, T_m (sec)
0.10	16.5	1013	0.70	274.8	0.4	39.8
0.20	24.6	1434	0.74	274.6	0.6	26.7
0.30	33.5	1854	0.78	274.3	0.8	19.6
0.40	43.3	2273	0.82	273.9	1.0	15.2
0.50	54.4	2692	0.87	273.4	1.2	12.1
0.60	67.5	3109	0.94	272.9	1.4	9.7
0.70 (Y_{new})	76.3	3525	0.94	272.3	1.5	8.6
0.80 (Y_0)	85.1	3938	0.94	271.6	1.7	7.7
0.90	87.5	4352	0.88	270.9	1.9	7.5
1.00	87.8	4764	0.81	270.1	2.1	7.5

Figure 37. Steady-State Operating Conditions for Representative Plant at 85 MW and 76 MW.

for initial plant operation to be at any condition, and this aspect will be studied in Step 12 of the analysis.

The linearized performance of the hydraulic turbine may be characterized at any operating condition with the analytical description of the hill diagram. Table 4 shows a comparison of the six partial derivative values at the anticipated operating conditions to corresponding values used in Hovey's theoretical linear model. The most striking difference is with the linearized value of $\partial m/\partial n = -1.04$ compared to $\partial m/\partial n = 0$ for Hovey's model. In addition, values for $\partial q/\partial y$ and $\partial m/\partial y$ are nominally 20 percent lower than Hovey's theoretical values for both partial derivatives.

Step 2 -- Establish Plant Characterizing Parameters

The parameters which characterize the performance of the plant components may be computed using the plant information and the anticipated initial operating conditions. The machine starting time, the water starting time, and the water wave round trip travel time are given by:

$$T_m = \frac{2\pi\, Wr^2\, N_r}{60\, g\, M_0} = 7.71 \text{ sec}$$

$$T_w = \frac{L\, Q_0}{A\, g\, H_0} = 1.72 \text{ sec}$$

$$T_c = \frac{2L}{c} = 0.61 \text{ sec}$$

The values for T_m and T_w depend on the operating condition as shown in Fig. 37. As the load decreases, T_m increases and T_w decreases. In other words, lowering the initial load shifts the plant toward the "heavy plant" region where machine dynamics dominate the response. In the next step, the ratios (T_m/T_w) and (T_c/T_w) are used to characterize the response of the plant model.

Table 4. Turbine Characteristics and Plant Parameters at Expected Operating Conditions.

	Initial Anticipated Operation	New Anticipated Operation	Hovey's Theoretical Linear Model
T_m (sec)	7.71	8.60	7.71
T_w (sec)	1.72	1.54	1.72
$\frac{\partial q}{\partial y}$	0.873	0.808	1.0
$\frac{\partial q}{\partial h}$	0.519	0.526	0.5
$\frac{\partial q}{\partial n}$	-0.039	-0.052	0.0
$\frac{\partial m}{\partial y}$	0.873	0.808	1.0
$\frac{\partial m}{\partial h}$	1.52	1.53	1.5
$\frac{\partial m}{\partial n}$	-1.04	-1.04	0.0

Step 3 -- Establish the Validity of Linear Models

The plant characterizing ratios at the initial operating condition are $(T_m/T_w) = 4.5$ and $(T_e/T_w) = 0.35$. These ratios and the ratios at the new operating condition are shown on Fig. 38 which is similar to the qualitative characterizing map of Fig. 18. In addition, the values cited by Goldwag [15] for light and heavy plants are shown on Fig. 38. Although Goldwag's values do not include the waterhammer effect of increasing (T_e/T_w), the expected operation of the representative plant falls between the light plant and heavy plant designations. As the load is rejected, the plant moves toward the heavy plant region and further toward the region in which waterhammer dynamics may be important. Qualitatively, the water dynamics and machine dynamics will both be important in the plant response and neither will clearly dominate plant response. For $(T_e/T_w) = 0.35$, the plant may experience waterhammer dynamics depending on the gate motion.

Waterhammer head and duration estimates and steady-state comparisons provide further insight into whether linear models are valid for the anticipated operational conditions or whether a nonlinear model must be used. The waterhammer head experienced at the turbine inlet due to a step change in gate position from the initial to the new steady-state position may be estimated from Eq. 3.55 or Eq. 3.56. Using Eq. 3.56, which represents the highest estimate due to the rigid water column model assumption, the waterhammer head estimate is 329 ft. This value represents a 21 percent overpressure compared to the initial turbine head. The estimate for the duration of penstock water dynamics is $4(\partial q/\partial h)T_w$. For the representative plant, step gate motion from $Y = 0.8$ to $Y = 0.7$ will bring on water dynamics lasting approximately 4 seconds. This information is sufficient to eliminate the possibility of using a quasi-steady penstock model in the description of the plant. Selection of the nonlinear penstock model instead of the rigid water column model cannot be based solely on the estimate of the waterhammer head and duration. Information concerning gate speed and oscillation are also needed from simulations to eliminate the use of the rigid water column penstock model.

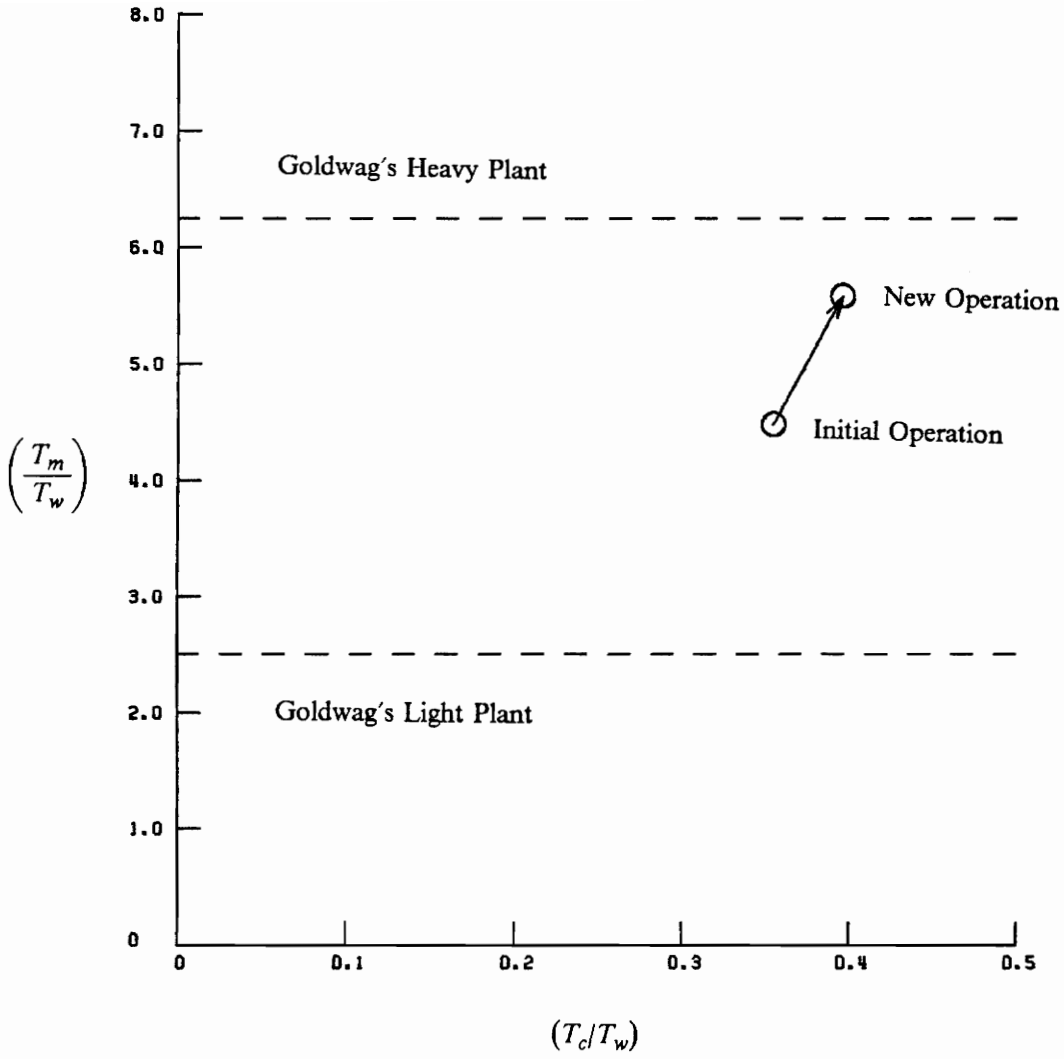

Figure 38. Location of Plant Characterizing Time Ratios on Qualitative Plant Dynamics Map.

Steady-state comparisons give further insight into whether use of the nonlinear model may be required rather than use of linear models. Four expressions have been developed which evaluate errors in steady-state values due to the use of the linearized plant model. Using Eq. 3.57, the initial error in the turbine head is $e_{H,0} = -0.01$. Using Eq. 3.58, the error in the turbine head at the new steady operating condition is $e_{H,new} = -0.013$. According to Eq. 3.59, the steady-state error in the new gate position is $e_{Y,new} = -0.007$. The error in the new steady flow is computed by Eq. 3.60 to be $e_{Q,new} = -0.002$. All four of the steady-state errors are much less than two percent. In terms of the steady operating conditions, the linear model for the anticipated gate motion from $Y = 0.8$ to $Y = 0.7$ is valid. The steady-state error analysis does not consider operating condition departures during the transient. Comparison of linear and nonlinear model simulations in Step 6 will provide a more conclusive test of linear model validty.

Step 4 -- Linear System Performance

The response of system model simulations is studied before performing the steps to determine optimum plant performance. The optimization process is based on an isolated load change so system simulations are performed with this load configuration. For the representative plant, it is necessary to study the response of both linear and nonlinear system model simulations in order to gain insight into conditions that require the use of the nonlinear model. Also, the linearized model is compared to the theoretical linear model to evaluate the validity of the theoretical linear model.

Governor settings have been suggested by Hovey [13] for P-I control and by Hagihara [27] for P-I-D control. Both authors used the theoretical linear plant model and based their suggested settings on qualitative observations of numerous simulations. Hovey's suggested settings for the representative plant are given by:

$$K_p = T_m/(2T_w) = 2.2$$
$$K_i = T_m/(8T_w^2) = 0.32 \text{ sec}^{-1}$$
$$K_d = 0$$

Hagihara's suggested settings for the representative plant are given by:

$$K_p = 0.8T_m/T_w = 3.54$$
$$K_i = 0.24T_m/T_w^2 = 0.62 \text{ sec}^{-1}$$
$$K_d = 0.267T_m = 2.03 \text{ sec}$$

Using the anticipated load departure of $m_{load} = -0.103$ (approximately 10 percent load off), the response of the linearized plant model using Hovey's settings was determined and these results are presented in Fig. 39. The response of the plant model using Hagihara's settings are presented in Fig. 40. The dimensionsless departures of speed, head, flow, and gate position are presented in each figure. Two important conclusions concerning the plant response to P-I-D control may be made by comparison of Figs. 39 and 40. The speed response of Hovey's P-I control settings is characterized by a maximum speed departure of $n_{max} = 0.040$ (a 4 percent error in speed) and 12 sec required to settle to 1 percent error. The speed response using Hagihara's P-I-D settings is characterized by a maximum speed departure of $n_{max} = 0.031$ and 7 sec required to settle to 1 percent speed departure. In terms of speed response, incorporating derivative control improves the plant response. However, comparison of the head response shows that the improved speed response results in significantly increased head departure due to rapid wicket gate motion. The maximum departure of head using Hovey's P-I control settings is $h_{max} = 0.048$ whereas the maximum head departure using Hagihara's P-I-D control settings is $h_{max} = 0.095$.

The six partial derivatives used in the linearized plant model were assigned the values corresponding to those of Hovey's theoretical linear model presented in Table 2. The resulting theoretical linear model simulation in response to the step load off were compared to that of the linearized model. This comparison is shown in Fig. 41 using both Hovey's and Hagihara's control settings. The theoretical linear model simulation is in error by at least 40 percent in predicting speed over-

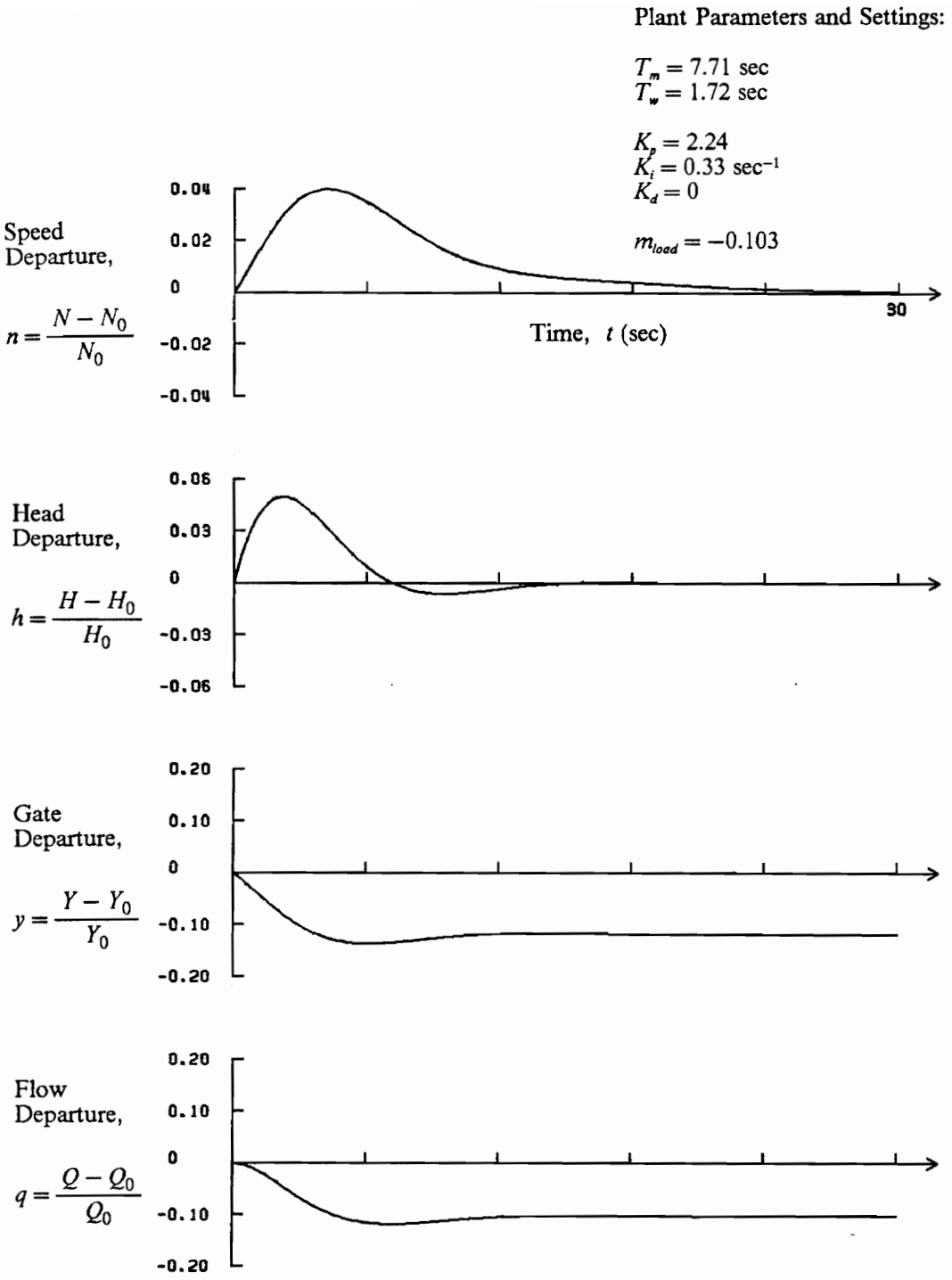

Figure 39. Linearized Plant Model Response to Step Change in Isolated Load – Hovey's Settings.

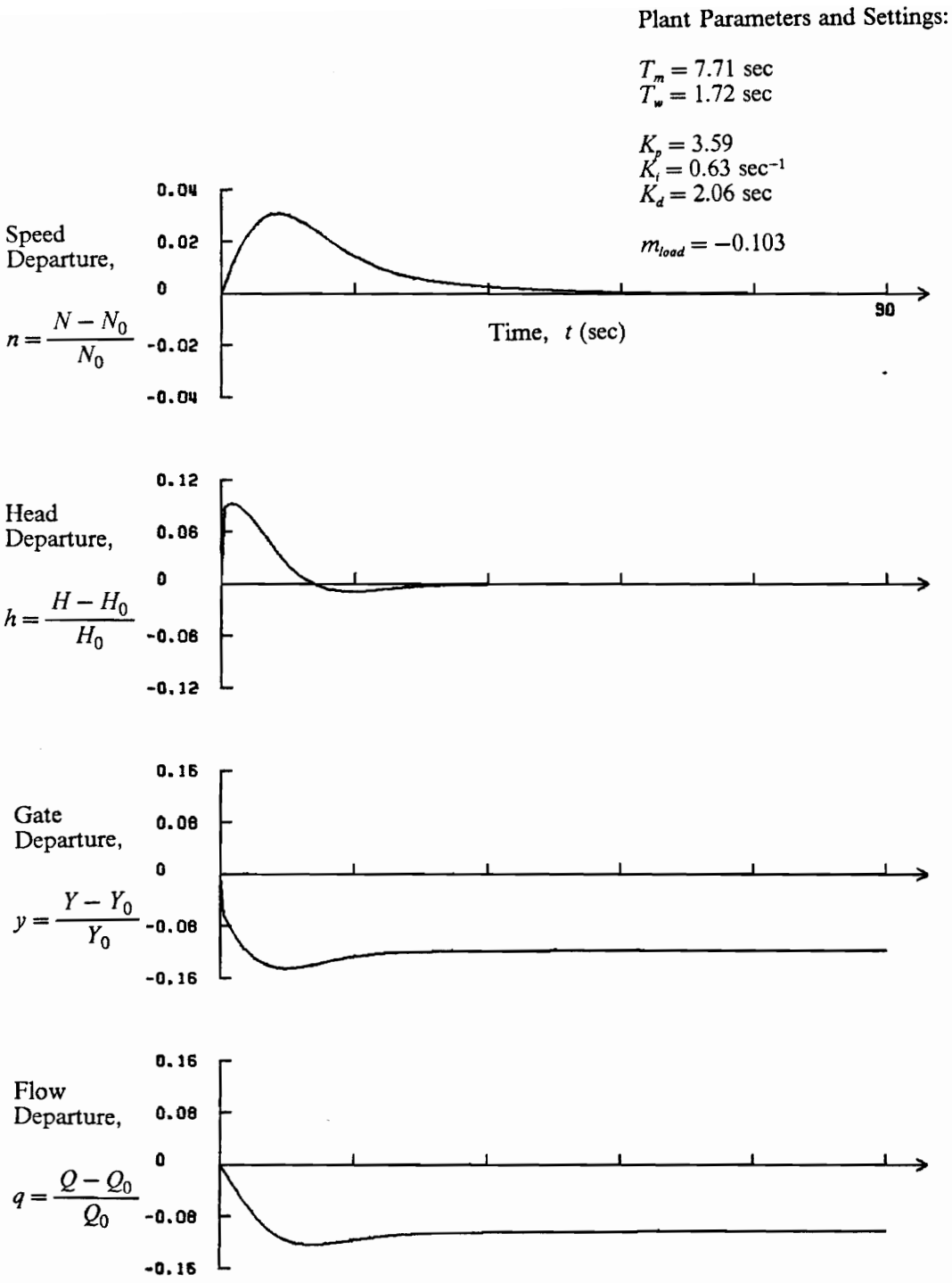

Figure 40. Linearized Plant Model Response to Step Change in Isolated Load -- Hagihara's Settings.

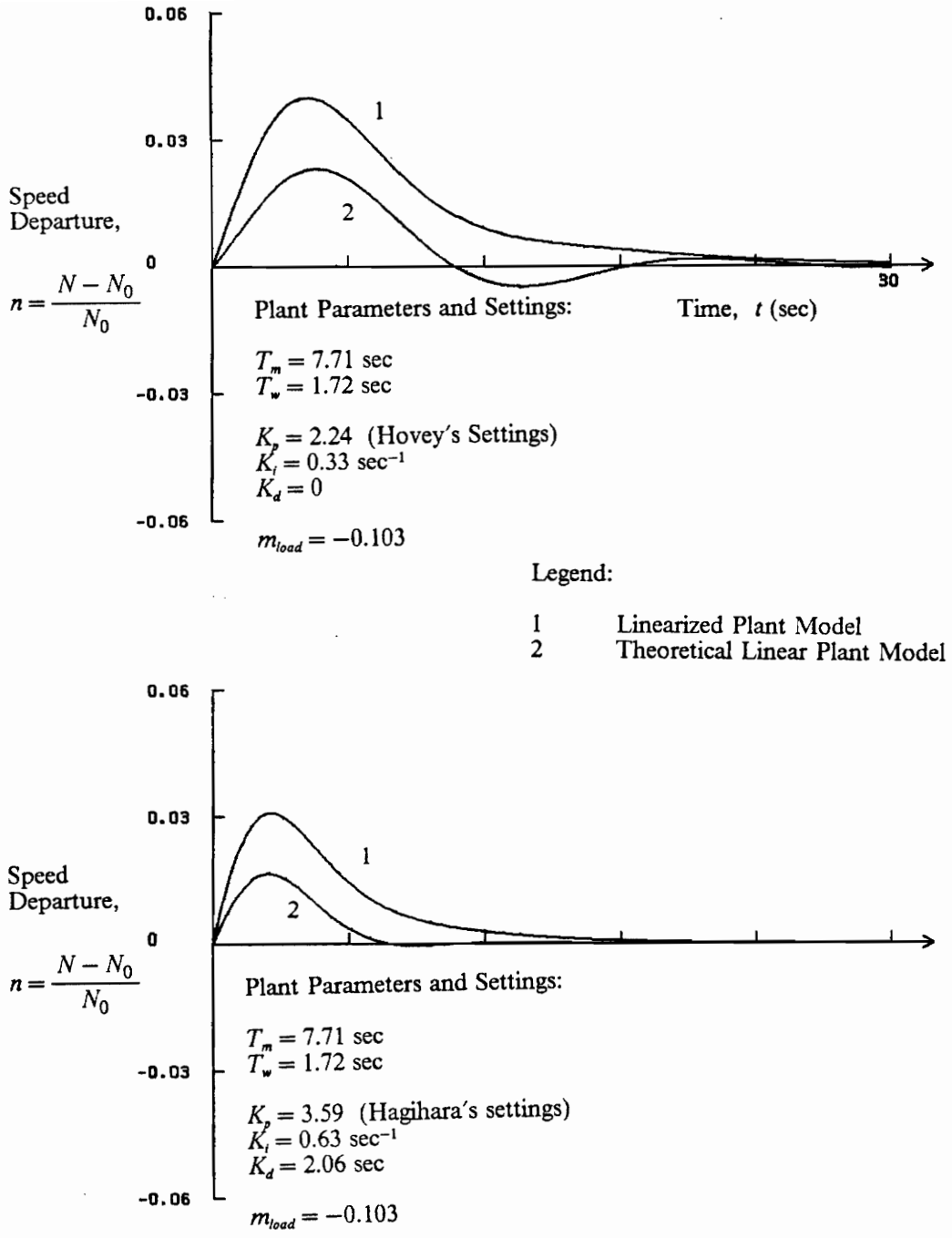

Figure 41. Comparison of Theoretical Model Response to Linearized Model Response.

shoot and by at least 25 percent in predicting the 1 percent settling time as compared to the linearized model. The theoretical linear model is an inadequate model for the representative plant even though some references use the theoretical linear model without verification [9, 12, 13, 14, 26, 27, 28, 30]. It has been a common practice to assume that if the turbine operation is near the rated operation, that the theoretical linear model would be valid.

The result of this step in the analysis of the representative plant is to confirm the linearized plant model is preferred over the theoretical linear model. The response of the linearized plant model using other governor settings and other load conditions will be investigated after nonlinear model simulations are studied and after the process of determining optimum governor settings is completed.

Step 5 -- Nonlinear System Performance

The nonlinear simulation was compared to that of the linearized model by using governor settings and the load rejection previously defined. The response of the nonlinear plant model to the anticipated load departure of $m_{load} = -0.103$ was determined by the computational procedure described in Chapter 4.

In the nonlinear simulation procedure, the mathematical model involves dividing the penstock into discrete sections. Two sections were chosen for this simulation, resulting in a computational time step (Eq. 4.9) of $\Delta t = L/(2\,c) = 0.152$ sec which is an order of magnitude smaller than the water starting time ($T_w = 1.72$ sec) and the machine starting time ($T_m = 7.61$ sec). The penstock was divided into three and four sections, which made the computational time step smaller. There was no difference in the simulation results, so the choice of two penstock sections was considered to be sufficient for this particular plant simulation. The results of the nonlinear simulation are presented in Fig. 42. As previously plotted for the linearized model, dimensionsless departures of speed, head, flow, and gate position from their initial values are presented in this figure.

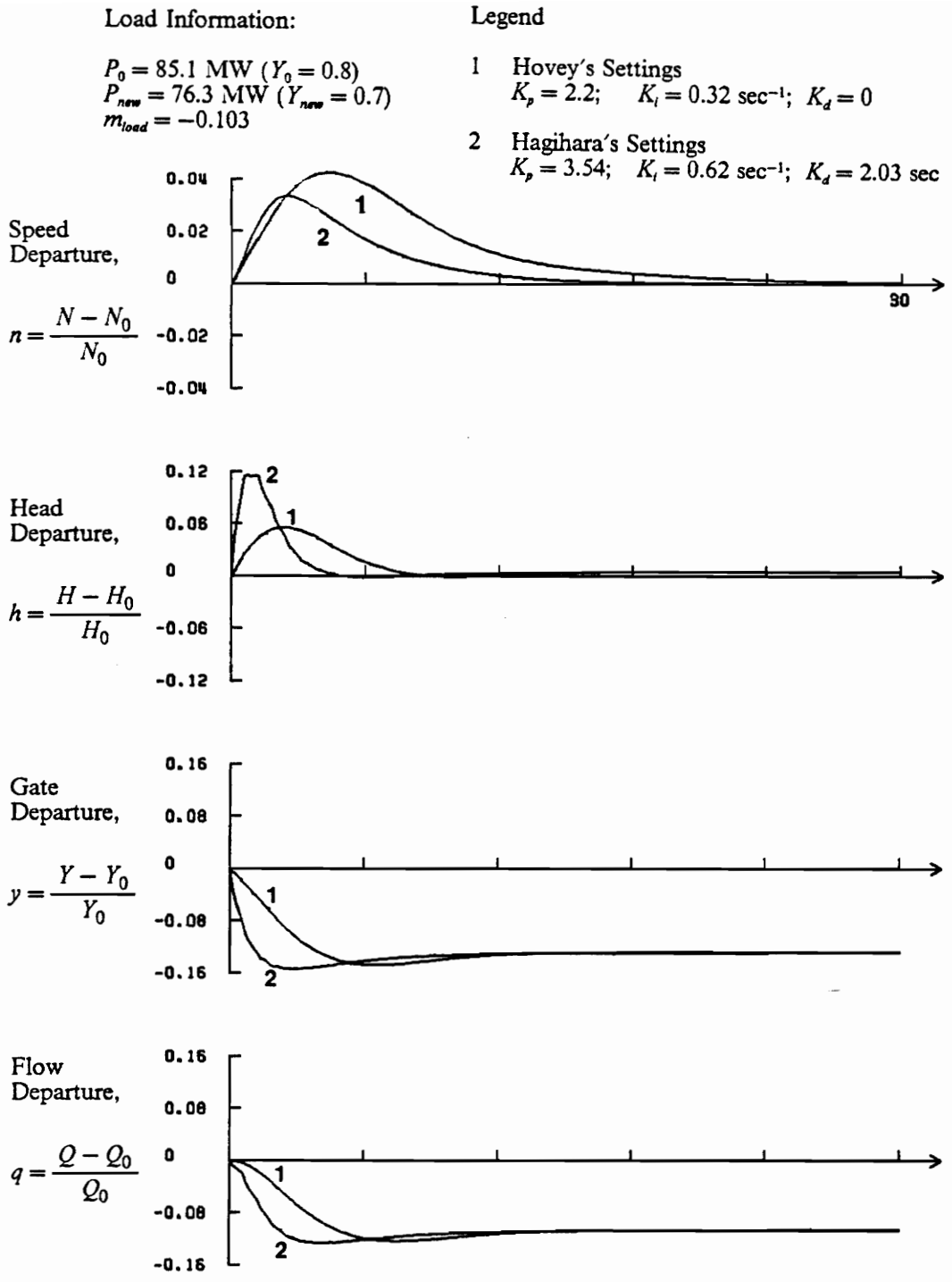

Figure 42. Nonlinear Plant Model Response to Step Change in Isolated Load.

Nonlinear plant simulations were performed using three different load changes with Hovey's and Hagihara's suggested governor settings. For all these simulations, the initial operating condition (described by $Y = 0.8$) was held constant. Plant responses to load rejections of nominally 5, 10, and 30 percent were simulated. The results of the simulations using Hovey's settings are shown in Fig. 43 and the results of the simulations using Hagihara's settings are shown in Fig. 44.

Comparison of simulations using Hovey's settings (Fig. 43) with simulations using Hagihara's settings (Fig. 44) reveals that P-I-D control can lead to improved plant speed response. For ten percent load off, Hagihara's settings resulted in a 23 percent lower speed departure overshoot and 33 percent faster settling time (to 1 percent speed error) than Hovey's settings. The penalty for this improved performance lies in the faster required gate speeds and higher head departures. The nonlinear behavior of the plant is illustrated in Fig. 44 in which Hagihara's P-I-D control settings are utilized for response to 30 percent load rejection. The rapid gate speed required to respond to this load change brings on waterhammer dynamics early in the plant transient as illustrated by the head departure response.

Two important conclusions arise from this step in the representative plant analysis. First, the magnitude of the load change has an effect on the way in which the plant responds to that disturbance -- particularly with respect to the head departure. Second, P-I-D control may be used to improve the performance of the plant, although there is a penalty in terms of increasing the required gate speed and increasing the possibility of waterhammer.

Historically, assumptions of rigid water column validity and linear plant behavior have been used without verification. These assumptions have proven to be satisfactory for situations of P-I control because the plant response to a load change has been slow enough to avoid waterhammer dynamics. A conclusion that a linear plant model is always valid could be misleading, especially with the implementation of P-I-D control. In the next step of the analysis, linear and nonlinear simulations are compared in order to investigate the relation of increased gate speeds to linear model behavior.

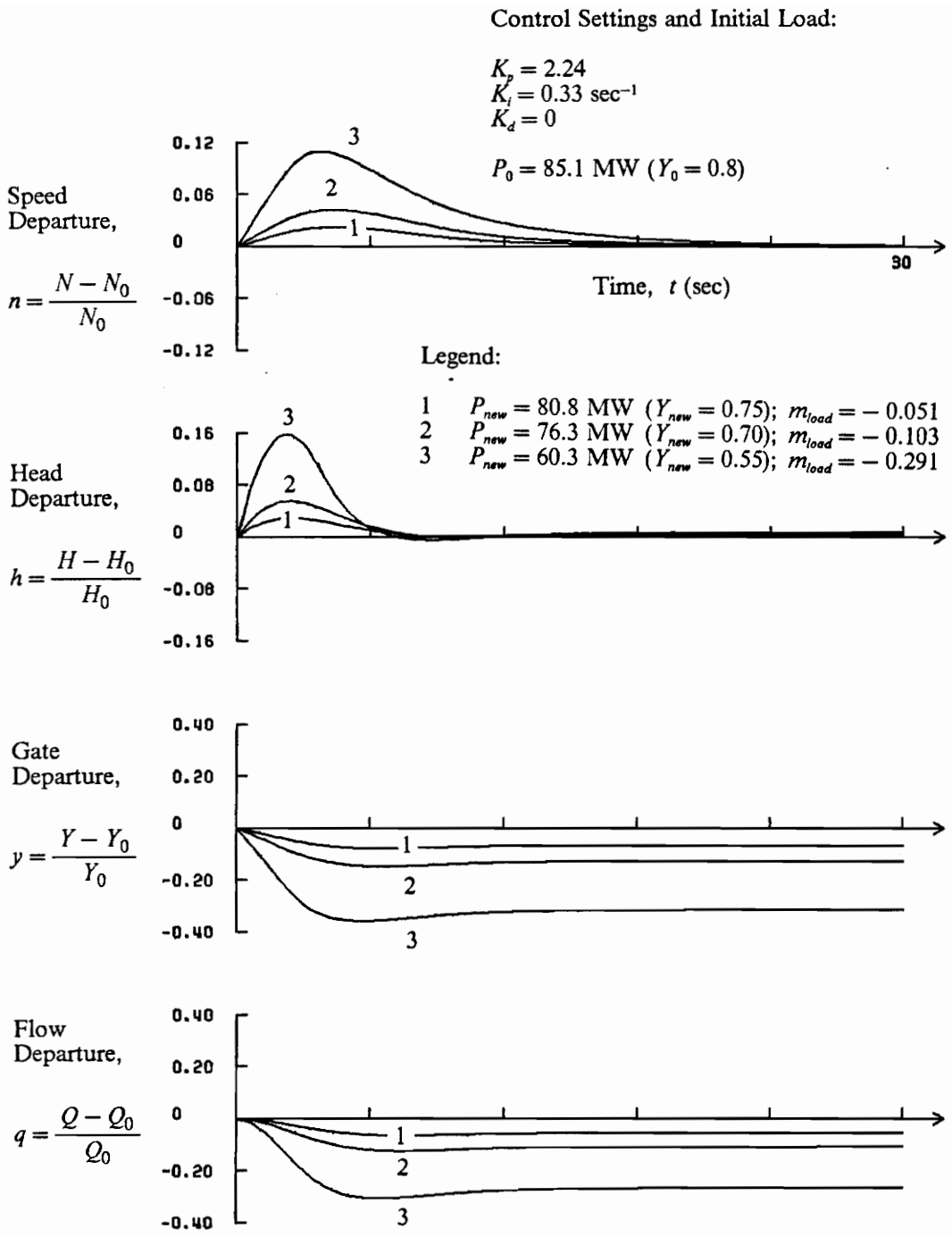

Figure 43. Nonlinear Plant Response to Various Load Changes – Hovey's Settings.

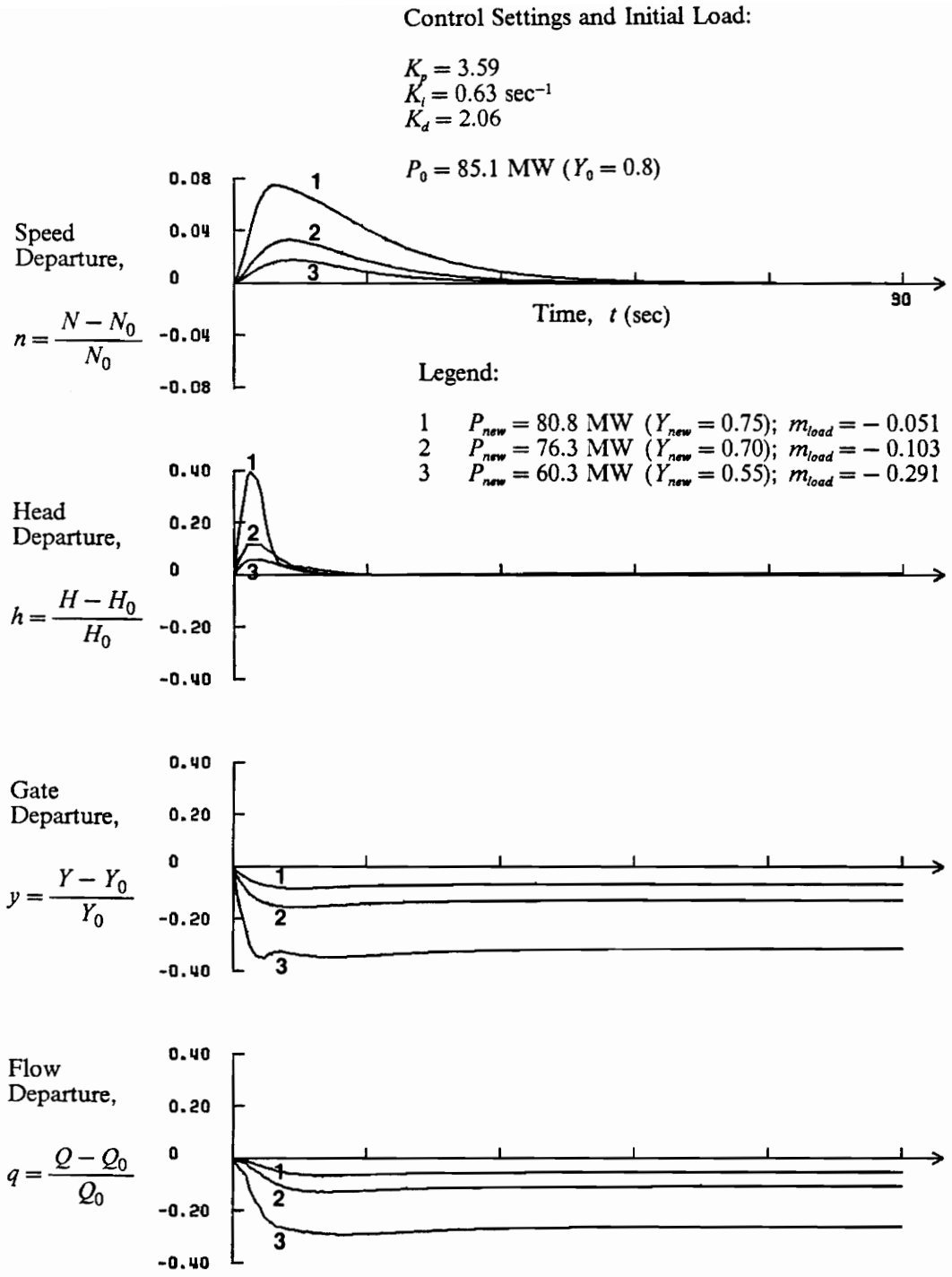

Figure 44. Nonlinear Plant Response to Various Load Changes – Hagihara's Settings.

Step 6 -- Compare Linear and Nonlinear Simulations

The linearized plant model simulations are compared to those of the nonlinear plant model because of the effects of load change and P-I-D control on the plant response. The comparison is first made for the anticipated operating situation in which nominally ten percent of the load is rejected. Departures of speed, head, flow and gate position are shown for both the linearized and nonlinear plant models using Hovey's P-I settings in Fig. 45. The plant departure comparisons using Hagihara's P-I-D settings are shown in Fig. 46. As previously determined, steady state values of all departures are in excellent agreement. For the anticipated load situation and Hovey's suggested governor settings (Fig. 45), the linear simulation and nonlinear simulation are in good agreement. Similarly, using Hagihara's settings (Fig. 46), the simulations are in good agreement, although it may be observed that the response of the head departure deviates more than in the simulations using Hovey's settings.

The speed departures of the two models are also compared for two additional load rejection situations. Load rejections of nominally 5, 10, and 30 percent were considered. The comparisons using both Hovey's and Hagihara's settings are presented in Fig. 47. As the load rejection increases, the linear model's speed response departs from the nonlinear model's response, particularly with Hagihara's P-I-D settings and 30 percent load off.

It has been shown that P-I-D control may be used to improve the speed of response of the plant model at the expense of requiring faster wicket gate speeds. A realistic limit on possible gate speed is fixed by the full gate motion time, T_g. The full gate motion time represents the time that it would take for the wicket gate to move from fully open to fully closed at the fastest possible gate speed. This speed limit may be implemented into the control law of the nonlinear model and its simulation compared to that of the linear model which does not recognize gate speed limitations. The minimum full gate motion time available for the representative plant may be computed by use of Gordon's curves. The relation for the required full gate motion time for good plant controllability was given in Eq. 3.29 as:

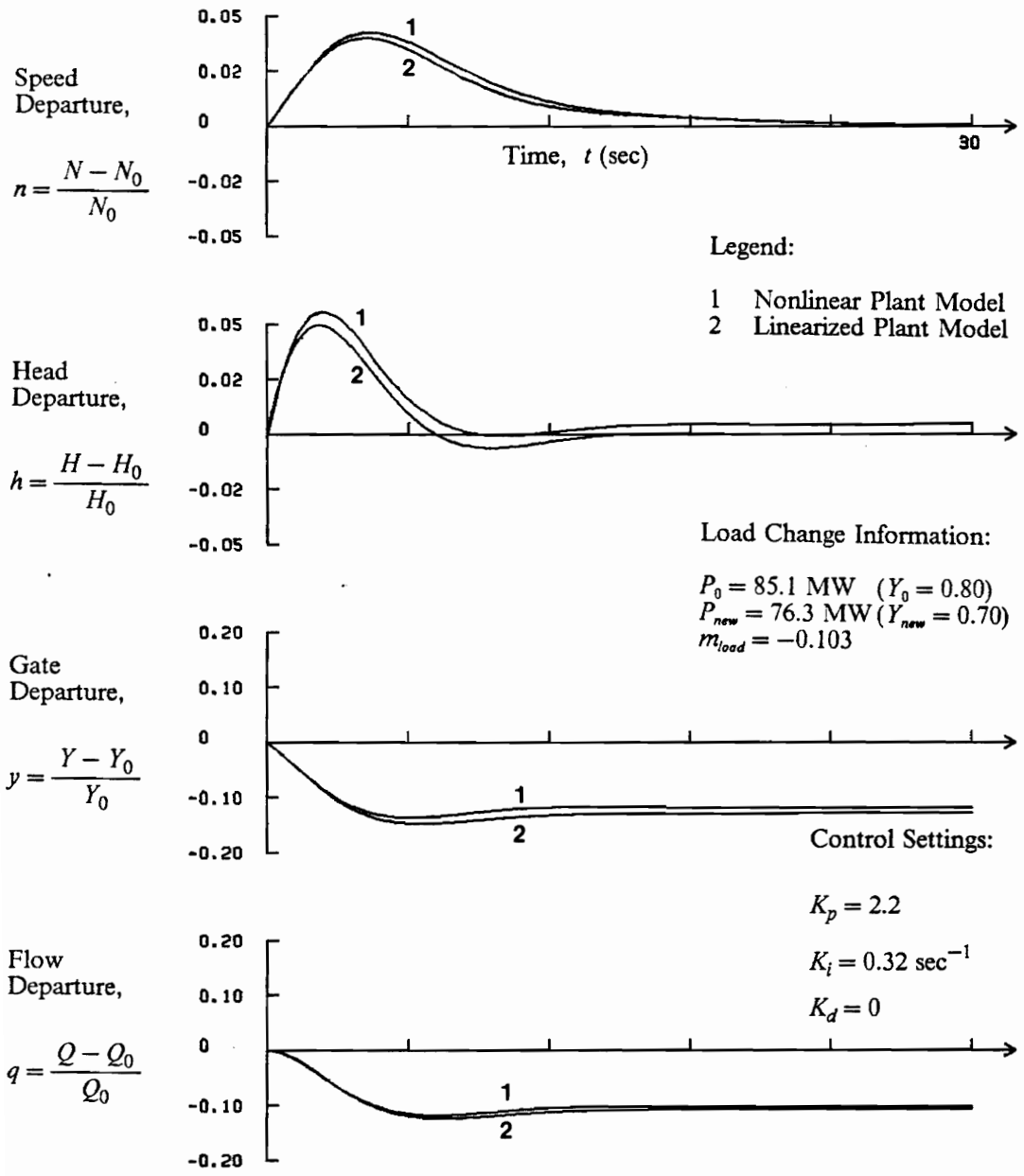

Figure 45. Linear and Nonlinear Model Comparisons for Anticipated Load Conditions – Hovey's Settings.

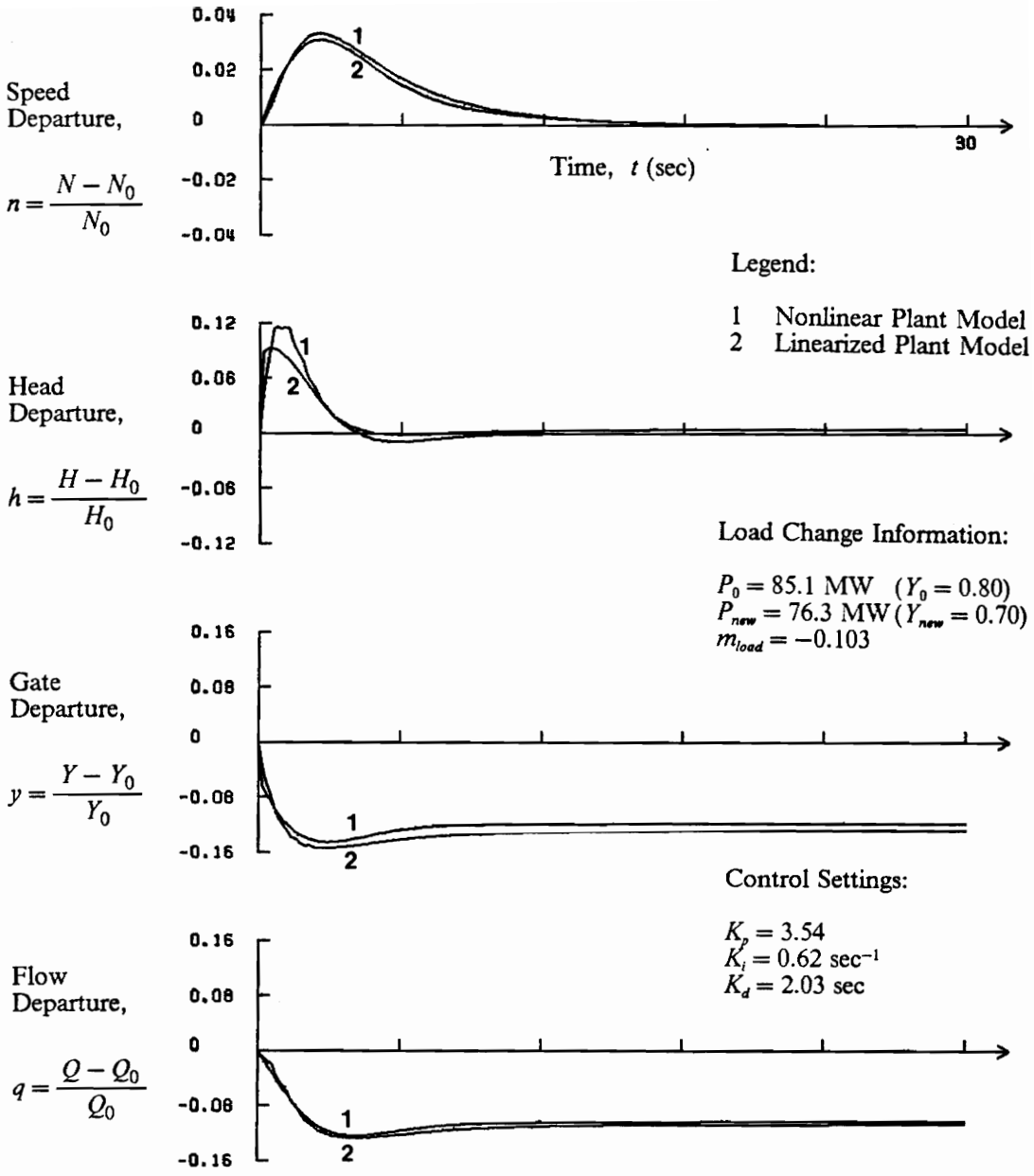

Figure 46. Linear and Nonlinear Model Comparisons for Anticipated Load Conditions – Hagihara's Settings.

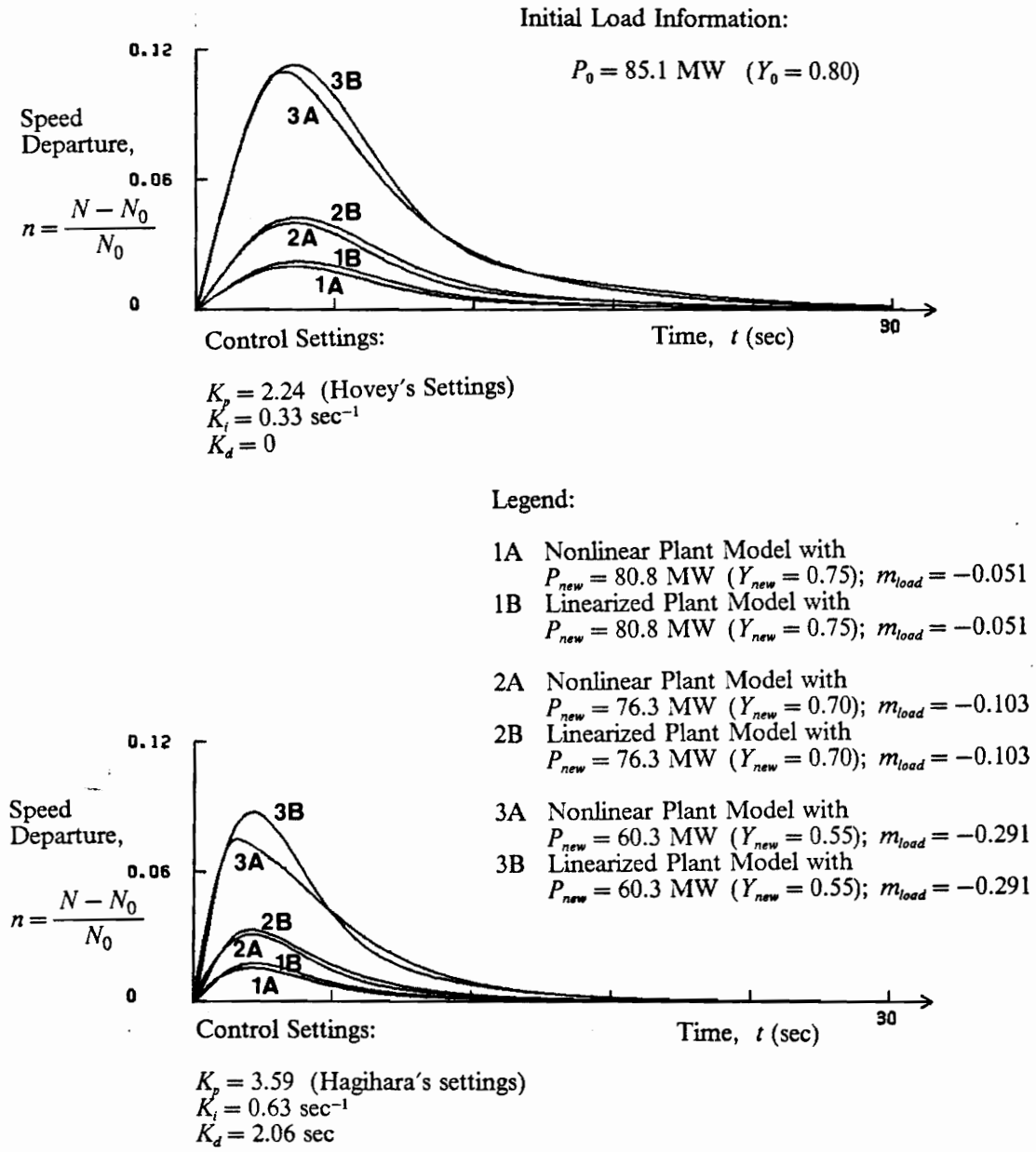

Figure 47. Plant Speed Response Comparisons for Various Load Changes.

$$T_g = \frac{1.25\,T_m - T_w}{1.04} \qquad [3.29]$$

For the representative plant, the required full gate motion time is $T_g = 7.5$ sec. Allowing for a gate speed somewhat faster than the required speed, let the minimum possible full gate motion time be given by:

$$T_{g-\min} = 5 \text{ sec}$$

Using the constraint of $T_{g-\min} = 5$ sec and Hagihara's P-I-D control settings, the nonlinear model was used to simulate the response to a 30 percent load rejection. The results of this simulation and the corresponding linearized model simulation are shown in Fig. 48. The gate of the nonlinear model closes at its maximum speed, whereas the gate of the linearized model closes without regard to a speed limit. Even though the nonlinear model gate closes more slowly, the overshoot in head response is 43 percent higher in the nonlinear model than in the linearized model. For this simulation, the speed response of both models are comparable in overshoot and settling time.

A preliminary study has been completed with the linear and nonlinear plant models using governor settings currently suggested in the literature. Comparisons of linear and nolinear simulations show that for the representative plant, the linearized model appears to be satisfactory for Hovey's P-I control settings with load rejections up to 30 percent. Hagihara's P-I-D control settings require more rapid gate speeds which bring on nonlinear water dynamics even at the anticipated 10 percent load rejection. In addition, the P-I-D settings were shown to require wicket gate speeds exceeding the capability of the wicket gates when responding to a 30 percent load rejection. With these observations in mind, the linearized model is satisfactory for the representative plant with P-I control, but as the derivative gain is increased, the nonlinear model would be more appropriate in order to accurately represent the water dynamics and to limit the wicket gate speed.

It remains to determine settings which improve the plant response over the settings currently suggested. Since analytical stability limit relationships for linear models have been developed, a

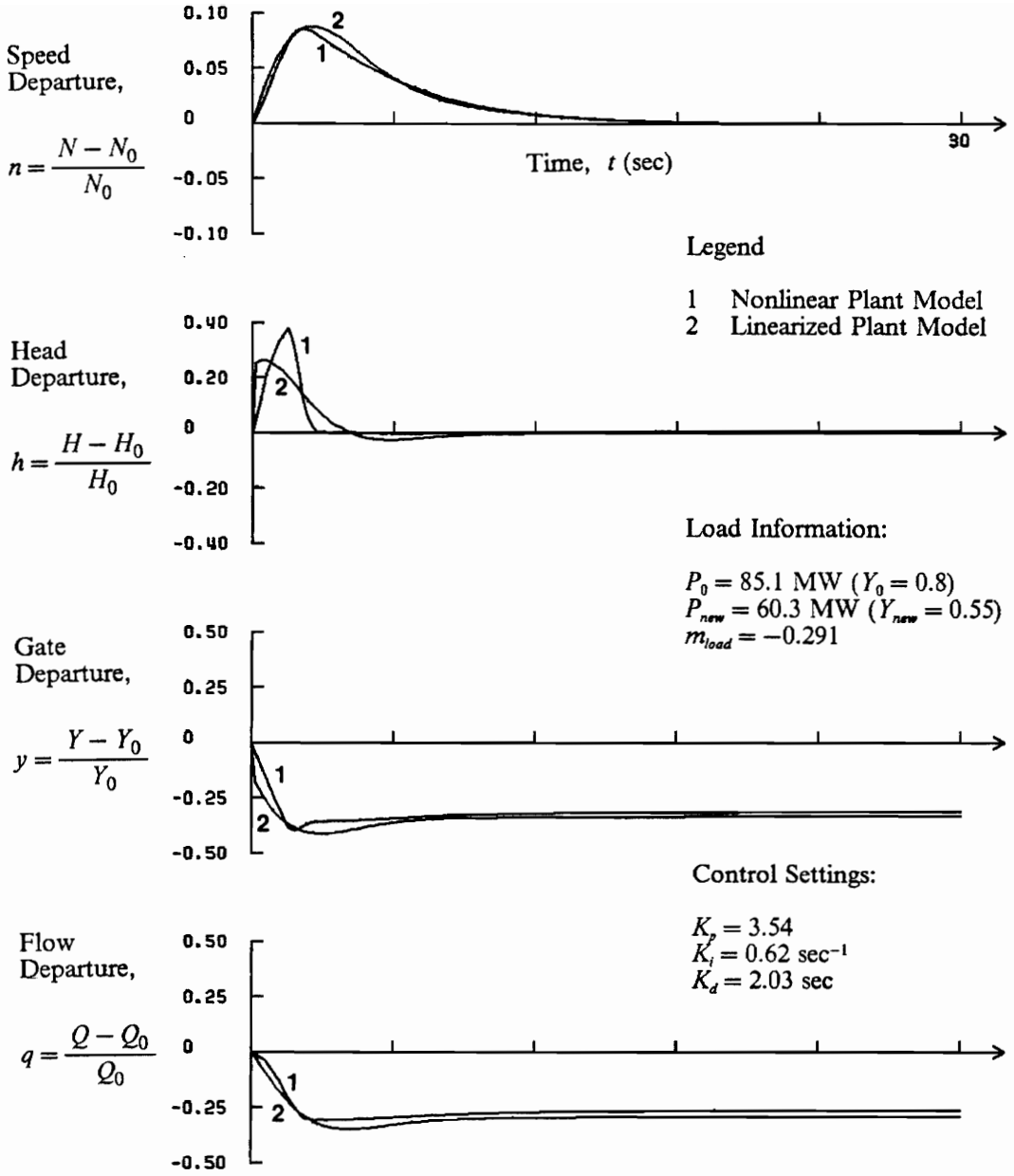

Figure 48. Plant Speed Response for 30% Load Rejection, Hagihara's Settings, and Gate Speed Limit.

map describing the region of stable governor settings provides a boundary within which the search for optimum settings may begin.

Step 7 -- Linear Plant Model Stability Limits

Analytical relationships have been developed which express the stability limits for the linearized plant model and the transcendental plant model. Since the theoretical linear model is a subset of the linearized model, comparisons of the various stability limits are made. Conclusions are made concerning the applicability of the theoretical linear model and concerning the extent to which waterhammer may dominate the plant response. The stability limits provide a region within which governor settings are selected during the optimization process for improving plant performance.

Linearized Model

The stability limits for the linearized plant model responding to a change in isolated load were established in the development of the candidate plant models. The analytical relations place limitations on the values for K_p , K_i , and K_d which result in stable plant response. The limiting value of the derivative gain K_d is computed by Eq. 4.2 for the representative plant as:

$$K_d < \frac{(\frac{\partial q}{\partial h})T_m}{(\frac{\partial m}{\partial h})(\frac{\partial q}{\partial y}) - (\frac{\partial m}{\partial y})(\frac{\partial q}{\partial h})} < 4.52 \text{ sec}$$

By varying the derivative gain from 0 (P-I control) to its maximum value, a family of stability limit curves are developed from Eqs. 4.3 and 4.4. This family of curves is shown in Fig. 49. As the derivative gain is increased, the region of stable operation also increases.

Theoretical Versus Linearized Model

By setting the six partial derivatives equal to those corresponding to Hovey's theoretical model, the stability limits of the theoretical linear model may be compared to the linearized model. The results of this comparison are shown in Fig. 50. The stability limits for corresponding values of K_d are in poor agreement. The maximum value for K_p in each theoretical model stability curve shown is in error by at least 15 percent compared to the linearized model. The maximum value for K_i in each theoretical model stability curve is in error by at least 13%. These errors increase for lower values of K_d. This observation reinforces the previous conclusion that the theoretical linear model is not satisfactory for the representative plant model.

Transcendental Versus Linearized Model

The ratio of (T_c/T_w) indicated that waterhammer dynamics may be important depending on the wicket gate motion. The stability limit of the transcendental model may be used to shed further insight into situations where waterhammer may be important. By incrementing values for the derivative gain K_d and using Eqs. 4.5 and 4.6, transcendental model stability limits are compared to linearized model stability limits. The results of this comparison are shown in Fig. 51. It may be observed that the transcendental model restricts the linearized model region of stable operation. As the derivative gain is increased, the region of stable operation becomes much more restricted. This observation may be explained by the fact that increased values of derivative gain require in-

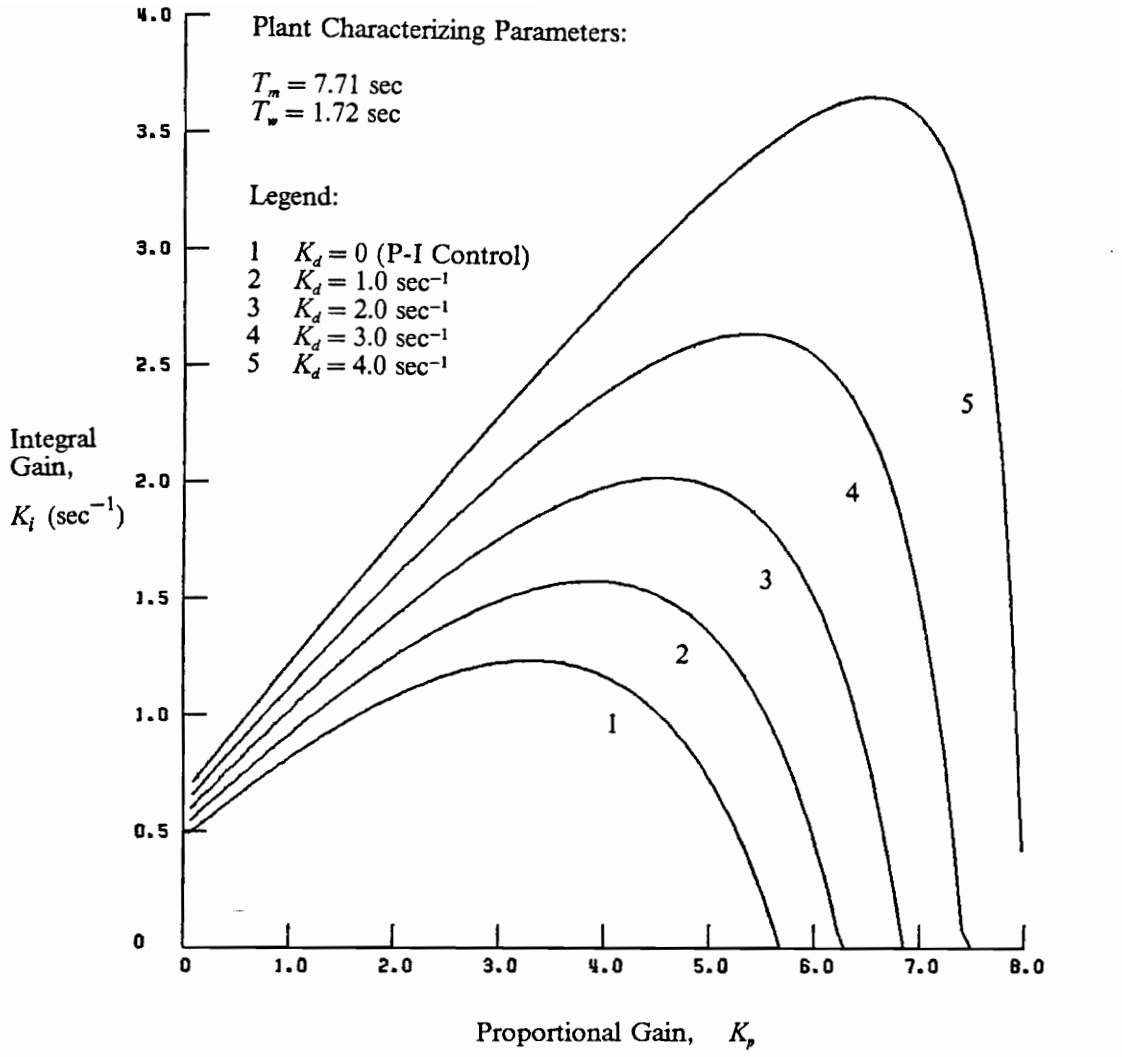

Figure 49. Linearized Model Stability Limits for Representative Plant.

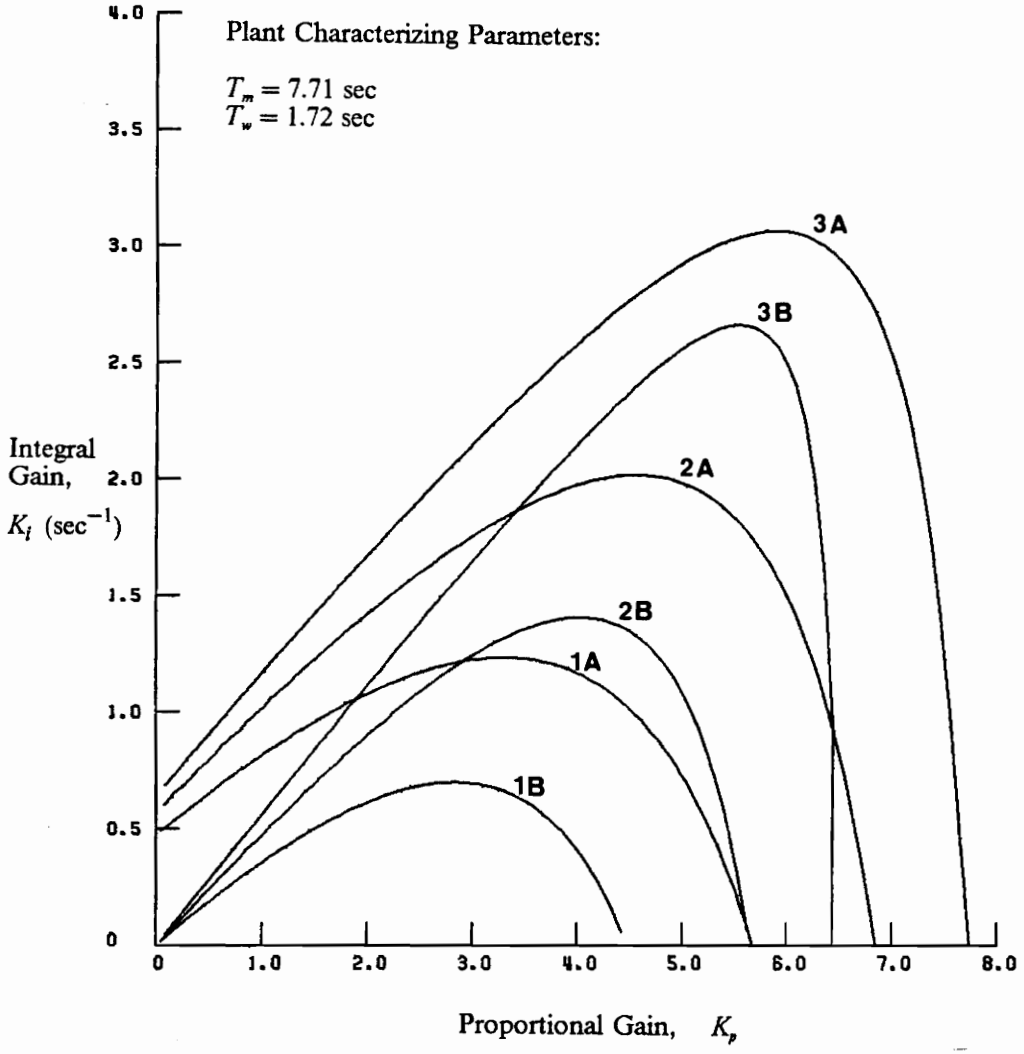

Legend:

1A	Linearized Model,	$K_d = 0.0$ (P-I Control)
1B	Theoretical Linear Model,	$K_d = 0.0$ (P-I Control)
2A	Linearized Model,	$K_d = 2.0$ sec^{-1}
2B	Theoretical Linear Model,	$K_d = 2.0$ sec^{-1}
3A	Linearized Model,	$K_d = 3.5$ sec^{-1}
3B	Theoretical Linear Model,	$K_d = 3.5$ sec^{-1}

Figure 50. Comparison of Theoretical Linear Model Stability Limits to Those of Linearized Model.

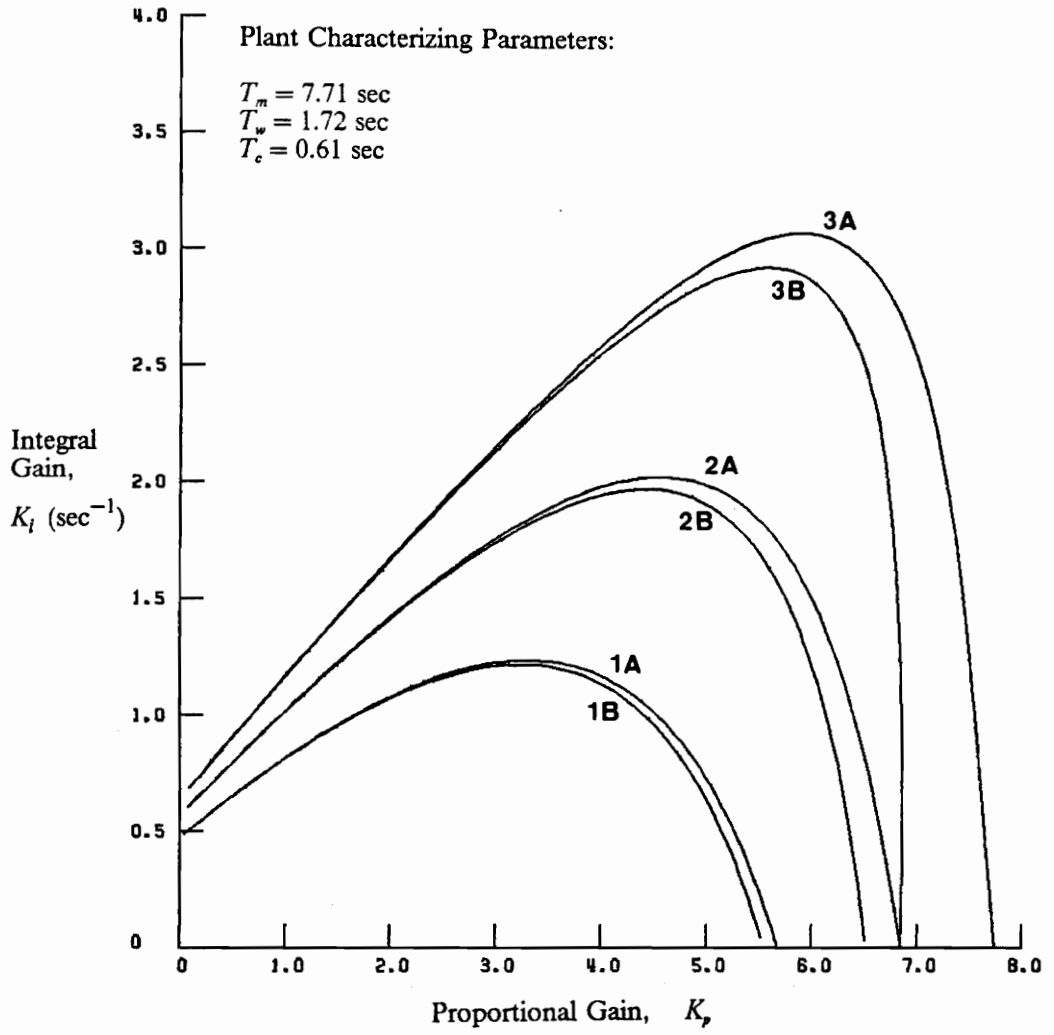

Legend:

1A	Linearized Model,	$K_d = 0.0$ (P-I Control)
1B	Transcendental Model,	$K_d = 0.0$ (P-I Control)
2A	Linearized Model,	$K_d = 2.0$ sec^{-1}
2B	Transcendental Model,	$K_d = 2.0$ sec^{-1}
3A	Linearized Model,	$K_d = 3.5$ sec^{-1}
3B	Transcendental Model,	$K_d = 3.5$ sec^{-1}

Figure 51. Comparison of Transcendental Model Stability Limits to Those of Linearized Model.

creased wicket gate speeds. The more rapid the wicket gate motion, the more likely waterhammer dynamics will adversely affect plant response.

A conclusion from this comparison is that during the process of governor tuning for improving plant performance, care must be taken when increasing the derivative gain. The linear optimization process which utilizes the rigid water column penstock model does not fully consider the aspect of waterhammer. The linear optimization process will suggest a high value of derivative gain, but the nonlinear optimization process may suggest a lower value because of adverse waterhammer dynamics.

Step 8 -- Linear Model Optimization

The stability limits for the linear plant models define the region of stable operation. The response of the plant within those regions depends on the governor settings. Using the linearized plant optimization procedure previously described, governor settings will be determined which result in plant performance improved over performance corresponding to settings currently suggested in the literature.

The linear optimization process was performed on the linearized model for the representative plant using the IAE as the index of performance. The settings suggested by Hovey were used as a first estimate to begin the optimization procedure. For each value of derivative gain, the optimization process was performed until a value of minimum IAE was located within a K_p-K_i grid as shown in Fig. 34 described by $\Delta K_p = 0.05$ and $\Delta K_i = 0.01$ sec^{-1} .

The results of the linear optimization process are plotted and tabulated in Fig. 52. The settings recommended by Hovey [13] and Hagihara [27] are also presented in that figure. Each set of K_p, K_i, and K_d represents the governor settings that result in the minimum IAE for a specified value of K_d. For corresponding values of K_d, the performance resulting from the settings determined by the linear optimization process is superior to the performance resulting from settings recommended in

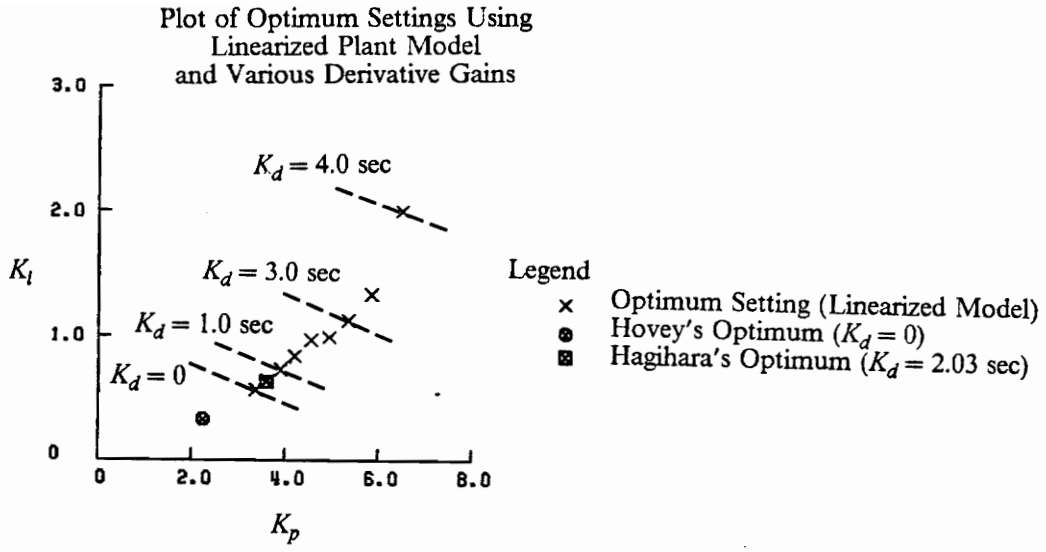

Optimum Settings Using the Linearized Plant Model and m_{load} = -0.103.

K_p	K_i (sec^{-1})	K_d (sec)	*IAE*	T_s (sec)
3.36	0.57	0.0	0.221	19.1
3.61	0.64	0.5	0.192	10.9
3.90	0.73	1.0	0.168	6.7
4.20	0.84	1.5	0.145	4.3
4.55	0.97	2.0	0.125	2.9
4.60	0.99	2.06	0.123	2.8
4.95	1.13	2.5	0.107	2.0
5.35	1.34	3.0	0.090	1.3
5.85	1.61	3.5	0.075	0.8
6.50	2.01	4.0	0.059	0.5
Hovey's Optimum:				
2.24	0.33	0.0	0.352	33.2
Hagihara's Optimum:				
3.59	0.63	2.06	0.187	3.1

Figure 52. Results of Linear Optimization Process for Representative Plant.

the literature. The performance index continuously decreases as the derivative gain increases. If the selection of governor settings resulting in minimum IAE were based solely on the linear optimization procss, then the recommended K_p, K_i, K_d set would correspond to the maximum derivative gain.

The full gate motion time T_g which is a measure of wicket gate speed has also been tabulated in Fig. 52 for each set of control settings. As the derivative gain is increased, the required full gate motion time decreases. Using the previously established gate speed limit of $T_{g-min} = 5$ sec as a constraint, then settings shown in Fig. 52 with a derivative gain greater than $K_d = 1.5$ sec must be eliminated from consideration.

Step 9 -- Nonlinear Model Optimization

As shown in the nonlinear model simulations, rapid wicket gate speeds resulting from increased derivative gains were shown to bring on the nonlinear aspects of waterhammer. Also, the response of the plant differs from the linearized model because of the nonlinear characteristics of the hydraulic turbine. For these reasons, the optimization process is repeated using the nonlinear plant model. The optimization was performed according to the process described in the previous chapter. At first, the wicket gate speed limit was not enforced during this step of the optimization process in order to study the gate speeds that would be required as the derivative gain is increased. For each value of derivative gain, the nonlinear optimization process was performed until a minimum IAE was located within a K_p-K_i grid as shown in Fig. 34 described by $\Delta K_p = 0.05$ and $\Delta K_i = 0.01$ sec^{-1}. Then, the nonlinear optimization process was repeated with the inclusion of the gate speed limit constraint.

The results of the nonlinear optimization process are plotted and tabulated in Fig. 53. Nonlinear simulation results utilizing the settings recommended by Hovey [13] and Hagihara [27] are also presented in that figure. As in the linear simulation process, each set of K_p, K_i, and K_d re-

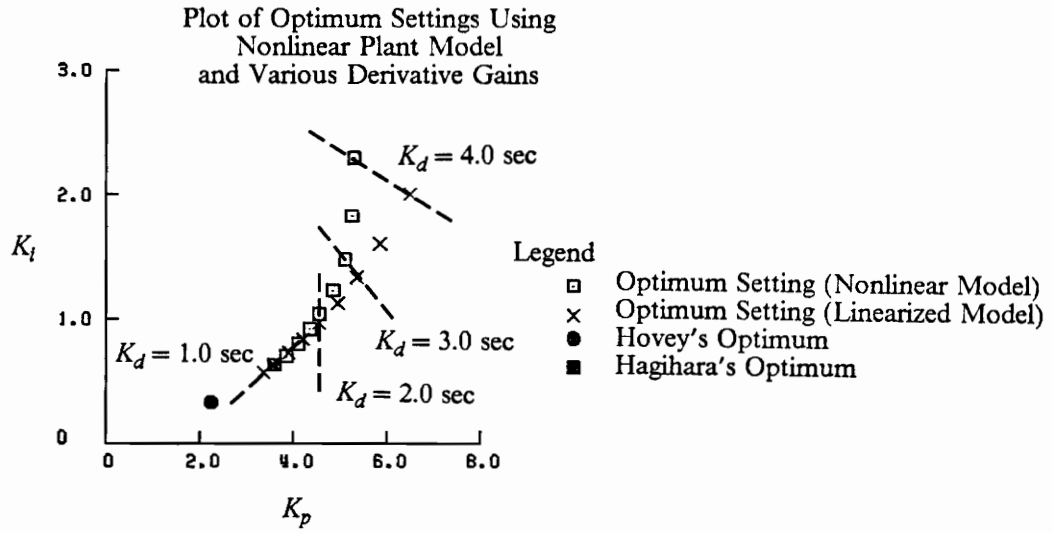

Optimum Settings Using the Nonlinear Plant Model and m_{load} = -0.103.

K_p	K_i (sec^{-1})	K_d (sec)	IAE	T_s (sec)
3.65	0.61	0.0	0.221	16.7
3.85	0.70	0.5	0.193	13.1
4.10	0.80	1.0	0.169	8.8
4.55	1.04	2.0	0.126	5.3
5.10	1.48	3.0	0.088	3.8
5.30	2.30	4.0	0.080	2.5
Hovey's Optimum:				
2.21	0.32	0.0	0.396	32.6
Hagihara's Optimum:				
3.54	0.62	2.03	0.207	5.6

Optimum Settings Using the Nonlinear Plant Model, $m_{load} = -0.103$, and $T_{g-\min} = 5$ sec

K_p	K_i (sec^{-1})	K_d (sec)	IAE	T_s (sec)	H_{max} (ft)
3.65	0.61	0.0	0.221	16.7	300
3.85	0.70	0.5	0.193	13.1	302
4.10	0.80	1.0	0.169	8.8	305
4.55	1.04	2.0	0.126	5.3	318
5.05	1.46	3.0	0.089	5.0	347
5.55	2.13	4.0	0.097	5.0	370

Figure 53. Results of Nonlinear Optimization Process for Representative Plant.

presents the governor settings that result in the minimum IAE for a specified value of K_d. The nonlinear optima are compared to those suggested in the literature by way of the plot and table of Fig. 53. As in the linear optima, for corresponding values of K_d, the performance resulting from the settings determined by the nonlinear optimization process is superior to the performance resulting from settings recommended in the literature. The optimum settings corresponding to $K_d = 0$ represent a 44 percent improvement in IAE over Hovey's suggested settings. The optimum settings corresponding to $K_d = 2.06$ sec represent a 40 percent improvement over Hagihara's suggested settings.

Figure 53 is used to compare optimum settings suggested by the linear and nonlinear optimization processes. For each set of gains with K_d being the same, values for K_i using the nonlinear optimization are nominally 10 percent greater than the corresponding K_i using the liner simulation across the range of K_d For $K_d < 2.0$ sec, the trend is also that the optimum K_p using the nonlinear model is greater than the optimum K_p using the linear model (8 percent greater for the $K_d = 0$ set). For $K_d > 2.0$ sec the trend reverses and the optimum K_p using the nonlinear model becomes less than the optimum K_p using the linear model (18 percent less for $K_d = 4$ sec). In fact, for $K_d > 2$ sec, K_p appears to reach a maximum value of nominally 5. Past this point, improvements in plant performance are due to increases in K_i and K_d, with the performance being maximized for the $K_d = 3.5$ sec settings when the gate speed limit is not enforced. The trend of diminishing improvements in IAE is also shown in the optimum settings when the gate speed limit is enforced. The gate speed limit results in diminished plant performance for the same control settings.

Step 10 -- Zone of Satisfactory Operation

A family of governor settings resulted from the nonlinear plant optimization process and was presented in Fig. 53. Sets with $K_d > 2.0$ sec required a gate speed faster than that available from the representative plant and resulted in gate motions at the maximum possible speed. The sets of gains

presented in Fig. 53 have been tailored for the anticipated operation corresponding to 85.1 MW initial load and a nominally 10 percent rejection of isolated load. Recall that increasing the load change increases the required gate speed. During a plant transient, gate speed saturation, gate position saturation, or adverse waterhammer dynamics could result depending on the selected control settings and the load change. The saturation of gate speed or position might diminish or improve the plant performance, but would increase the wear and tear on the turbine components. Waterhammer could result in overpressure -- rupturing the penstock (or in the less catastrophic case, lifting a pressure relief valve), or underpressure -- causing cavitation in the penstock, turbine, or discharge draft tube.

It is reasonable to expect that the plant will operate at loads and respond to load changes different from the anticipated ones. The optimum sets of gains must be studied at various load conditions to determine settings which do not violate the pressure constraints and which avoid gate speed limitations and gate saturation. For the representative plant, the gate speed constraint is defined by:

$$T_g \leq 5 \text{ sec}$$

The gate position constraints are:

$$0 \leq Y \leq 1$$

Since the nominal steady-state head for the representative plant's turbine is 272 ft, then the penstock pressure constraints may be defined in terms of allowable over- and underpressure from nominal operation. This constraint could also be defined by the maximum allowable and minimum required penstock pressures. For this analysis, let the penstock pressure constraints be given by:

$$200 \text{ ft} \leq H \leq 380 \text{ ft}$$

Two sets of optimum control settings have been selected to demonstrate how the combination of increased load change and a set of "too-lively" control settings may result in unacceptable plant response. Figure 54 is a presentation of the nonlinear plant model response to a 30% load re-

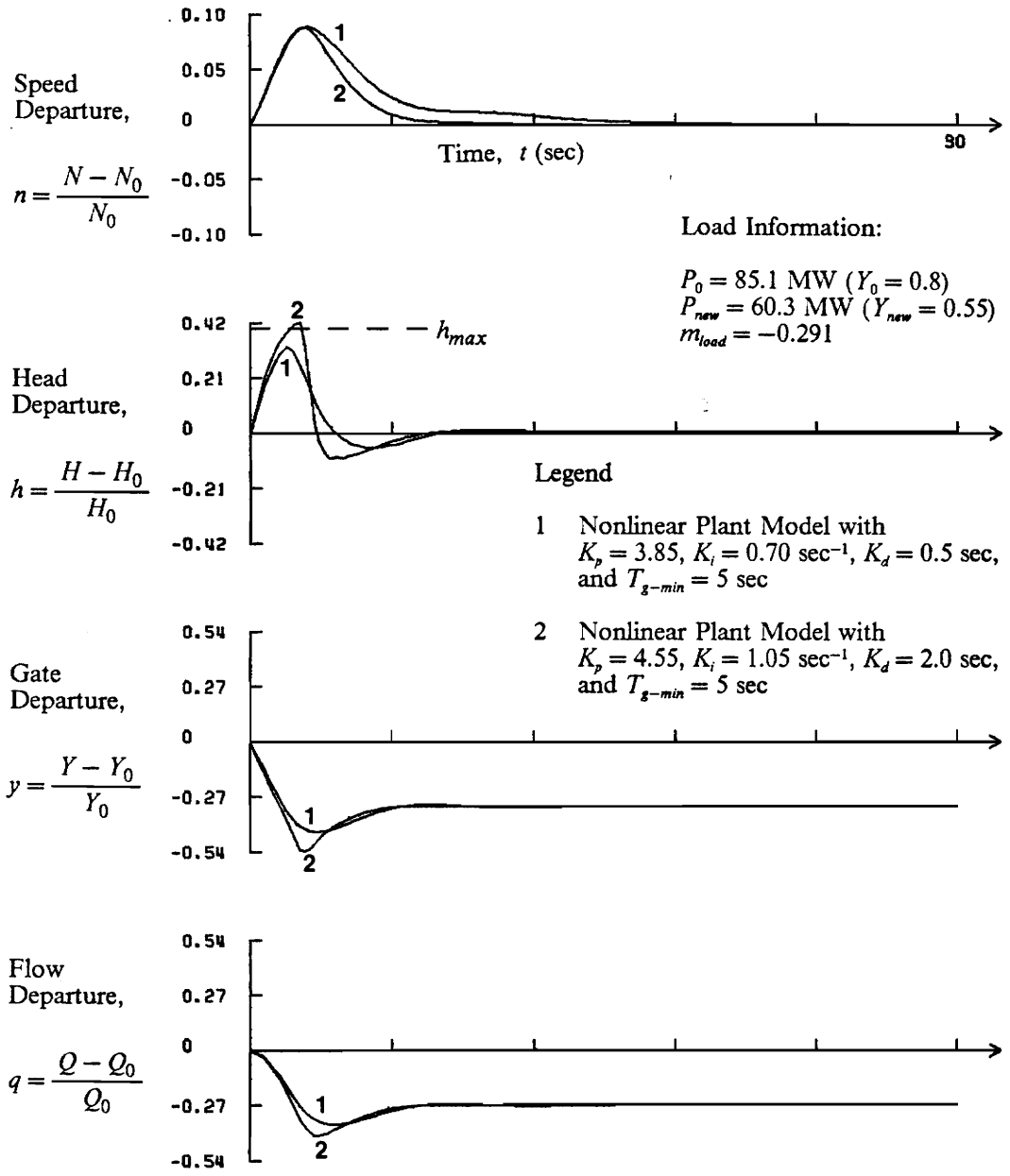

Figure 54. Nonlinear Plant Model Response to 30% Load Rejection Using Optimum Settings.

jection. The settings corresponding to $K_d = 0.5$ sec result in satisfactory plant response. The wicket gate speed limit is not reached, gate position saturation is not encountered, and the head constraints are not violated. The settings corresponding to $K_d = 2.0$ sec result in unsatisfactory plant response. The maximum gate speed is required, which is undesirable, but the head constraint $H \leq 380$ ft is violated, and this is unacceptable. This example demonstrates that various sets of control settings should be studied for a range of operational conditions.

Using governor settings of $K_p = 4.55$, $K_i = 1.04$ sec^{-1}, and $K_d = 2.0$ sec, nonlinear simulations have been performed for a variety of initial load and load change situations. Each situation was checked for violation of the constraints defined above. The results of these simulations are presented in Fig. 55. The region of satisfactory operation is severely limited if it is desired to avoid the gate speed limit. In fact, when operating at the anticipated load (85.1 MW), load rejections greater than nominally 12 percent result in the gate moving at its maximum speed. Although this situation does not result in unstable operation or violate the head constraints, it is considered to be unsatisfactory operation. For this reason, settings suggested by the optimization process with lower derivative gains must also be investigated in order to enlarge the zone of satisfactory operation.

Step 11 -- Establish Best Control Settings

Let three sets of control settings which were determined by the nonlinear optimization process be defined as follow:

- Set 0: $K_p = 3.65$, $K_i = 0.61$ sec^{-1}, $K_d = 0$. (This set corresponds to P-I control.)
- Set 1: $K_p = 3.85$, $K_i = 0.70$ sec^{-1}, $K_d = 0.5$ sec.
- Set 2: $K_p = 4.55$, $K_i = 1.04$ sec^{-1}, $K_d = 2.0$ sec.

Legend

A Anticipated Operating Condition
O Region of Satisfactory Operation
S Violates $T_{g-min} = 5$ sec Gate Speed Constraint
H Violates 200ft $\leq H \leq$ 380 ft Head Constraint
Y Results in Gate Saturation $Y = 0$ or $Y = 1$

Control Settings:
$K_p = 4.55$, $K_i = 1.04$ sec^{-1}, $K_d = 2.0$ sec

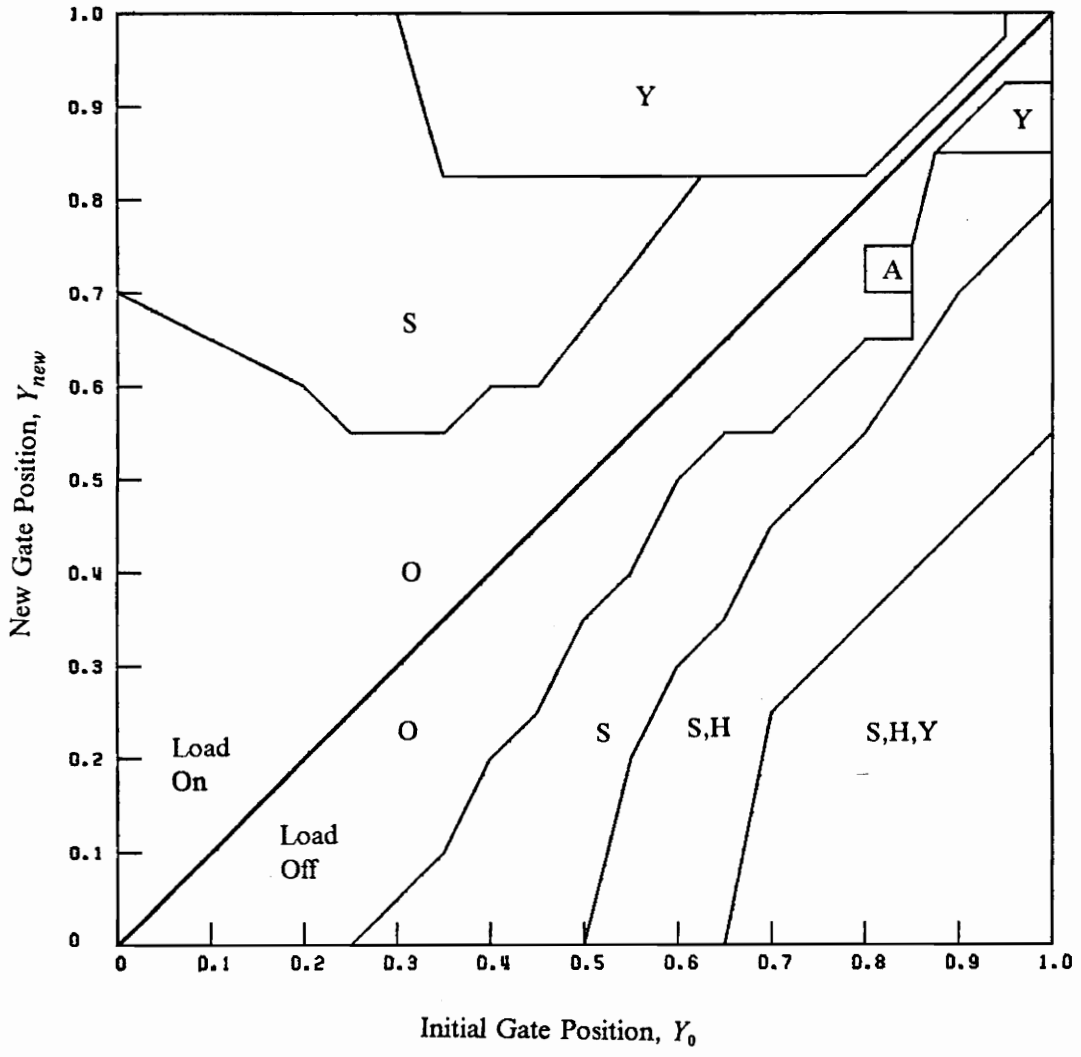

Figure 55. Zone of Satisfactory Operation for Optimum Settings Corresponding to 2.0 sec Derivative Gain.

The zone of satisfactory operation for Set 2 has been presented in Fig. 55. Zones of satisfactory operation for gain Sets 0 and 1 are presented in Figs. 56 and 57 respectively. The largest zone of satisfactory operation corresponds to Set 0 (P-I control) and the zone corresponding to Set 1 falls between Sets 0 and 2. The selection of a set of operational gains is left to qualitative judgment. Review of Figs. 55, 56, and 57 reveals the tradeoff between lively control settings for improved performance for anticipated operation and the limitation of the zone of satisfactory operation. For the representative plant, let the suggested operational gains be those of Set 1 as given by:

$$K_p = 3.85$$

$$K_i = 0.70 \text{ sec}^{-1}$$

$$K_d = 0.5 \text{ sec}$$

Step 12 -- Effects of Initial Load and Load Change

Now that a single set of gains has been suggested, the response of the plant is investigated at the anticipated operating condition and at conditions different from those anticipated. In addition, the response of the nonlinear plant model will be compared to that of the linearized plant model to evaluate the linear behavior of the plant.

The nonlinear model response is compared for the suggested settings, Hovey's settings, and Hagihara's settings. The speed, head, flow, and gate departures in response to the anticipated 10 percent load rejection are presented in Fig. 58. This figure provides visual insight into how the suggested settings result in improved performance. Using the speed response as the comparison, the response using the suggested settings is superior to that of Hovey's settings in both peak overshoot and settling time. This resulted in the *IAE* being decreased by a factor of two compared to that of Hovey. Although the peak overshoot using Hagihara's settings is 15 percent lower, the improved settling time using the suggested settings results in a 7 percent improvement in *IAE* over

Legend

A Anticipated Operating Condition
O Region of Satisfactory Operation
S Violates $T_{g-min} = 5$ sec Gate Speed Constraint
H Violates 200ft $\leq H \leq$ 380 ft Head Constraint
Y Results in Gate Saturation $Y = 0$ or $Y = 1$

Control Settings:
$K_p = 3.65$, $K_i = 0.61$ sec^{-1}, $K_d = 0$

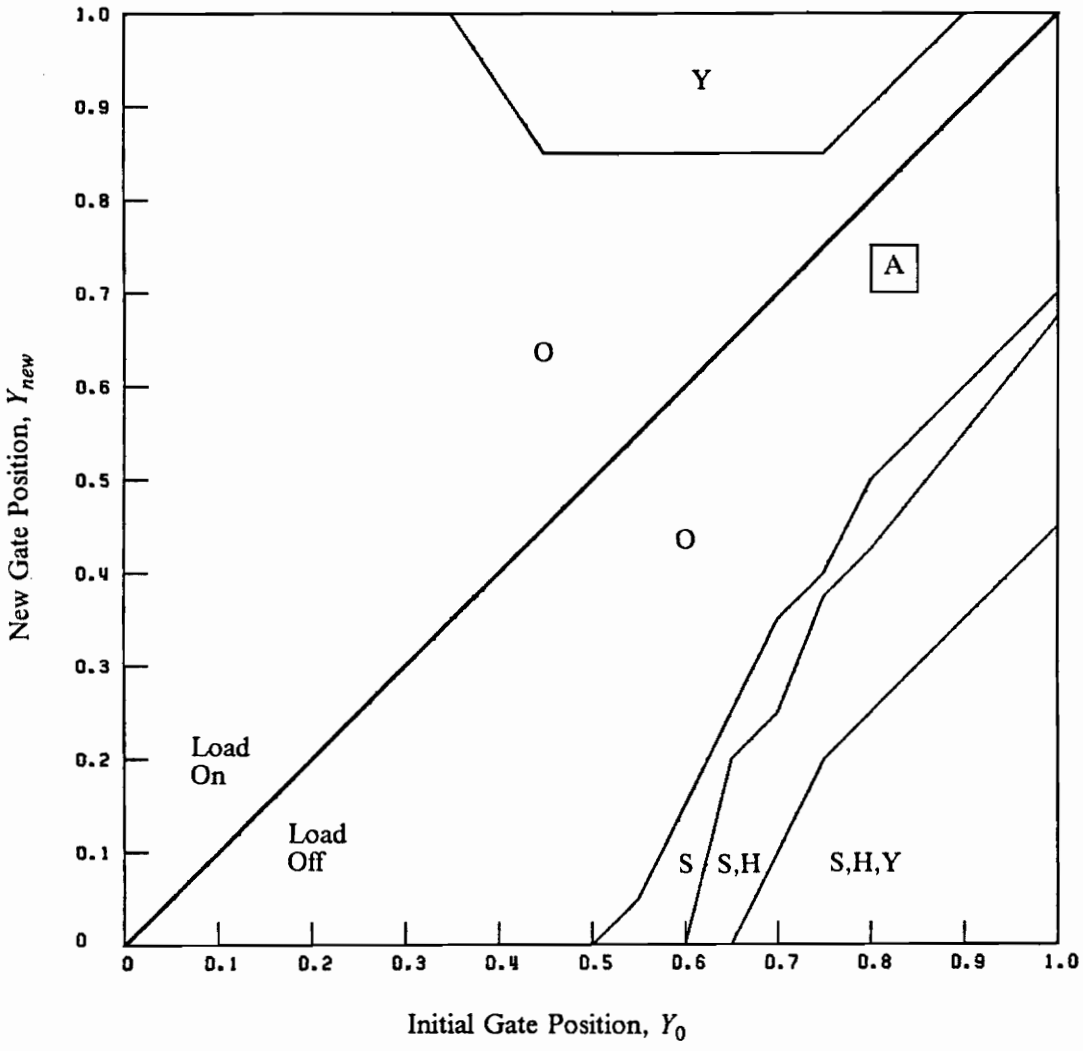

Figure 56. Zone of Satisfactory Operation for Optimum Proportional-Integral Control.

Legend

A Anticipated Operating Condition
O Region of Satisfactory Operation
S Violates $T_{g-min} = 5$ sec Gate Speed Constraint
H Violates 200ft $\leq H \leq$ 380 ft Head Constraint
Y Results in Gate Saturation $Y = 0$ or $Y = 1$

Control Settings:
$K_p = 3.85$, $K_I = 0.70$ sec^{-1}, $K_d = 0.5$ sec

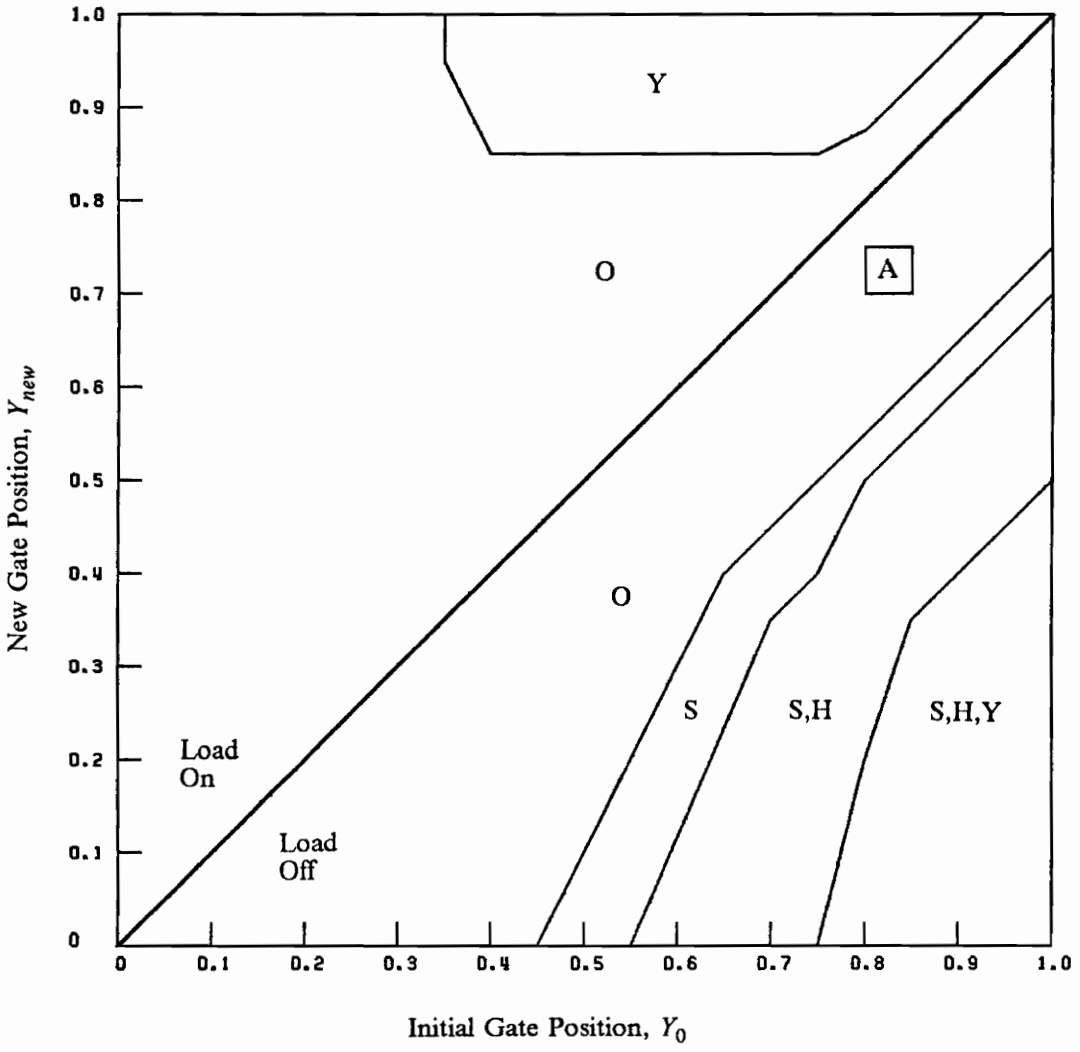

Figure 57. Zone of Satisfactory Operation for Optimum Settings Corresponding to 0.5 sec Derivative Gain.

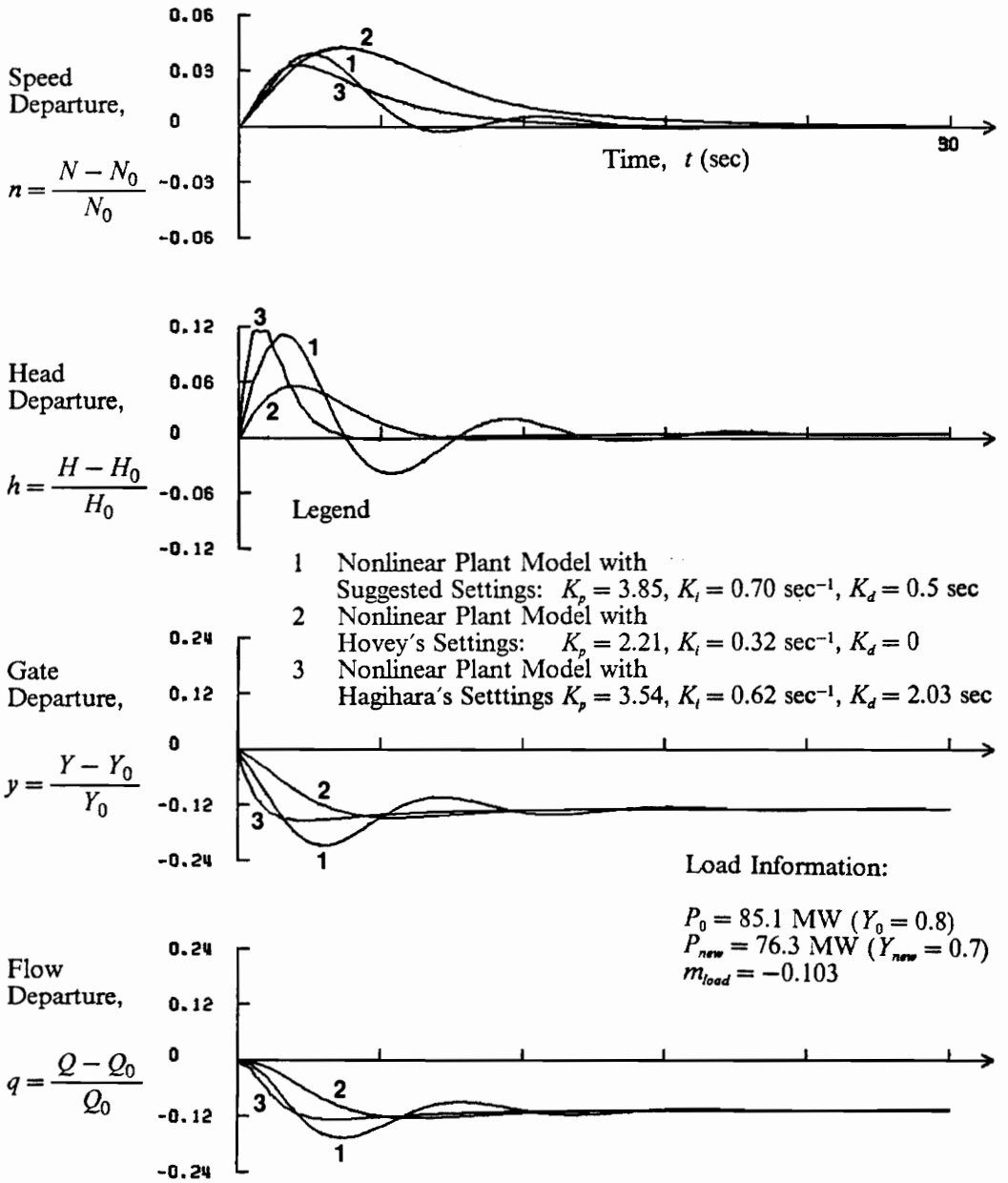

Figure 58. Comparison of Plant Model Response Using Hovey's, Hagihara's, and Suggested Settings.

that of Hagihara. An additional advantage of the suggested settings over Hagihara's settings is that the required gate speed is $T_g = 13.1$ sec compared to $T_g = 5.6$ sec for Hagihara's settings.

The responses to a 10 percent load rejection for the linearized and nonlinear plant models using the suggested settings are shown in Fig. 59. For the anticipated operation, there is good agreement between the linearized model and nonlinear model simulations for all four plant variables. The worst discrepancy between the two models in any of the variables is approximately 10 percent. One reason that the linearized model and the nonlinear model simulations do not exactly coincide is that the characteristics of the turbine are nonlinear. It was shown that the initial and final steady-state characteristics were nearly the same, but the manner in which the transient occurs affects the characteristics in the transient state. One way to study the performance of the turbine is to track the response on a hill diagram during the transient. The tracking was performed for the anticipated load situation and the results are presented in Fig. 60. There is an 11 percent decrease in unit discharge from the initial to the new steady operation, but during the transient, a nominally 18 percent decrease occurs. For simulations which exhibit more nonlinear behavior than the one of Fig. 57, the hill diagram tracking could help explain the nonlinear response.

For the next simulation, the anticipated initial operating condition is held the same, but the load rejection is increased to nominally 30 percent. The results of this simulation using both the linearized and nonlinear plant models are presented in Fig. 61. The responses of two plant models do not coincide as well as for the situation of 10 pecent load off. In particular, the speed response using the linearized model simulation is more oscillatory and indicates a 25 percent higher peak speed departure than the corresponding nonlinear model. The linearized model's response indicates an 18 percent lower peak head departure and approximately twice the settling time than that of the nonlinear model. The more oscillatory response of the linearized model is also apparent in the gate and flow responses. The hill diagram tracking of this situation, which is shown in Fig. 62, gives an insight into the poorer agreement of the two plant models responses. The change in steady-state turbine efficiency is only 4 percent ($\eta_0 = 0.94$ to $\eta_{new} = 0.90$) whereas the turbine efficiency drops to approximately 0.85 during the transient. In addition, there is a 27 percent decrease in unit discharge from the initial to the new steady operation, but during the transient, there is a 39 percent decrease.

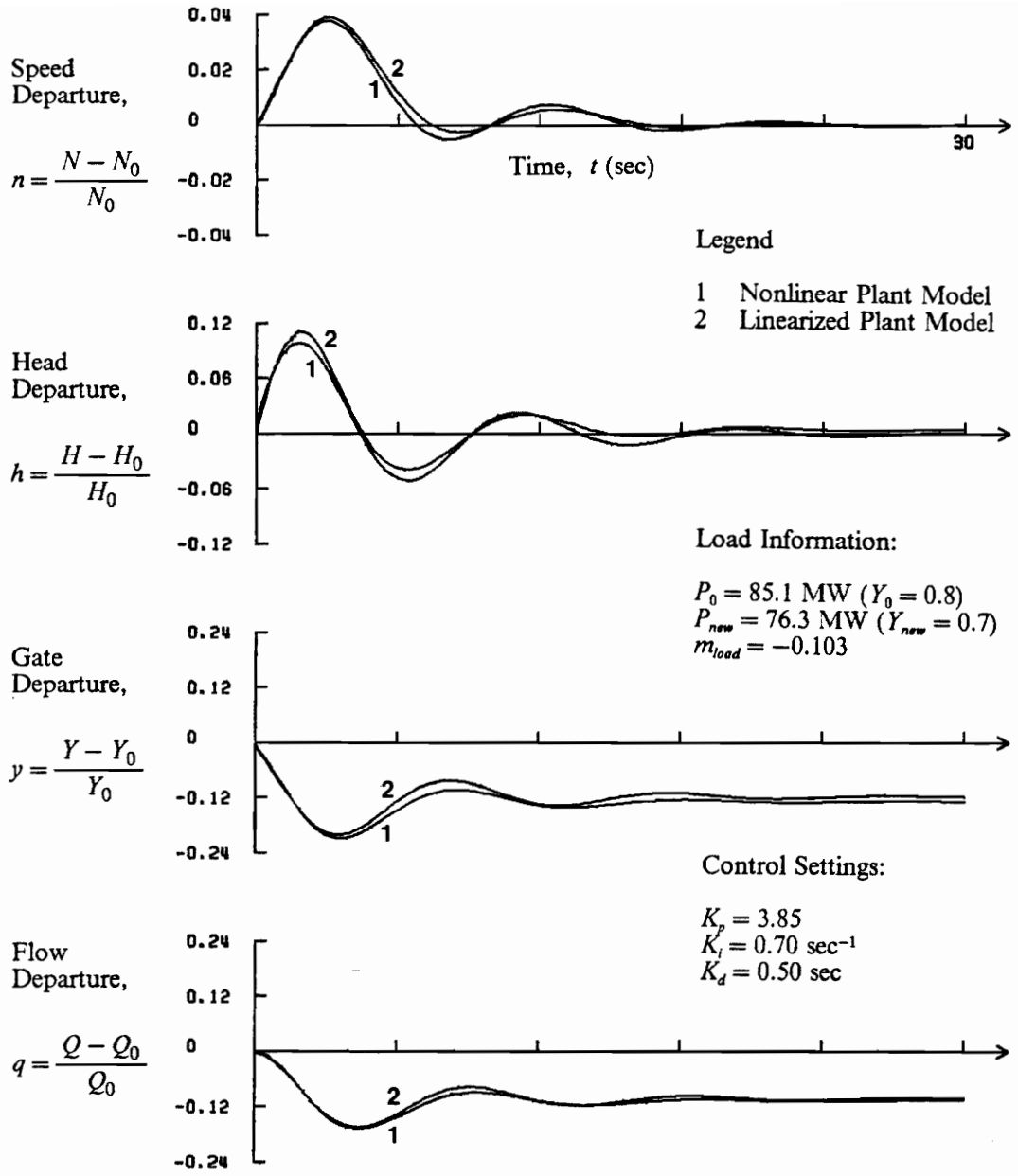

Figure 59. Representative Plant Response for Selected Governor Settings at Anticipated Operation.

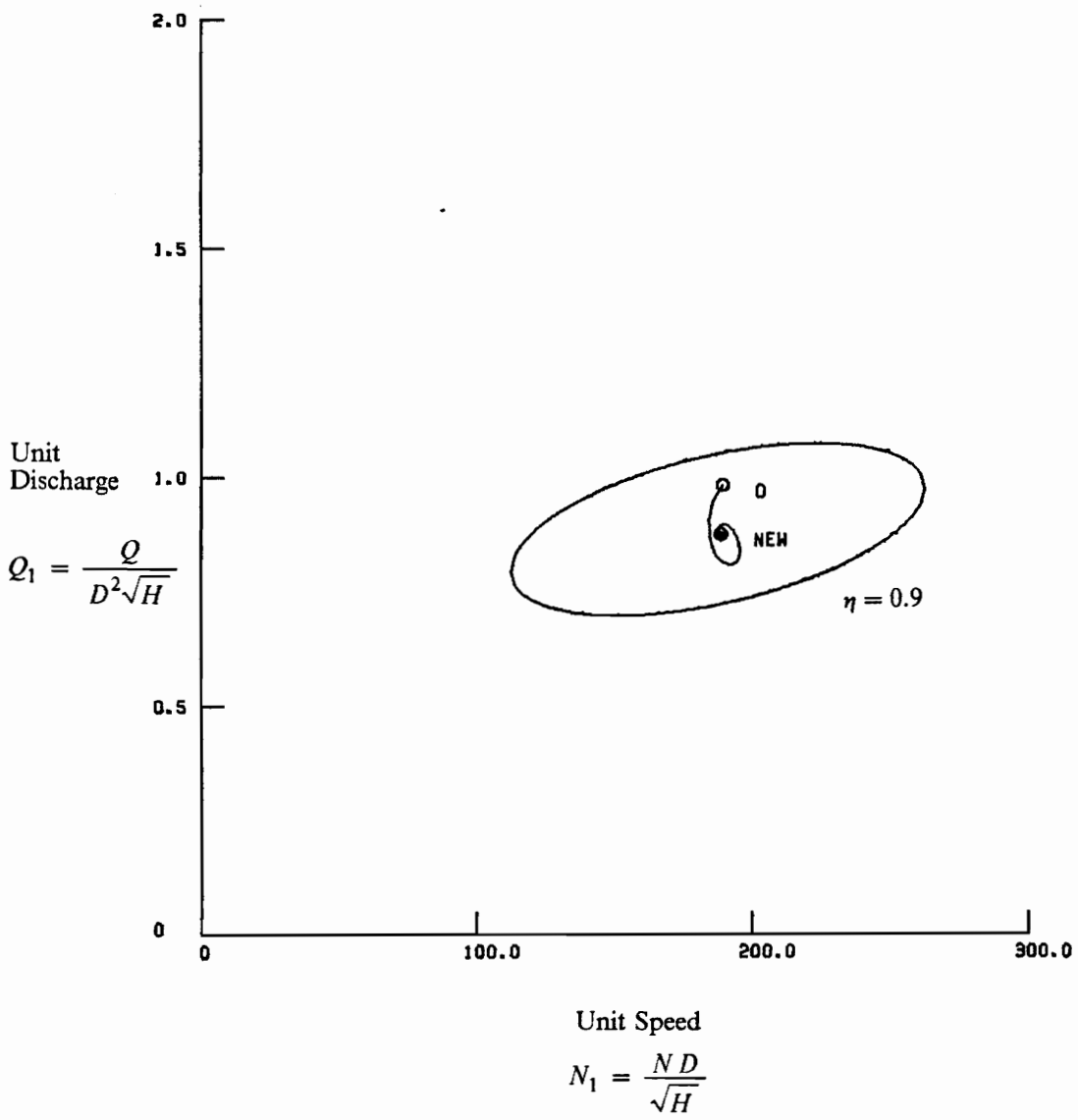

Figure 60. Hill Diagram Tracking of Representative Plant Response to 10% Load Rejection.

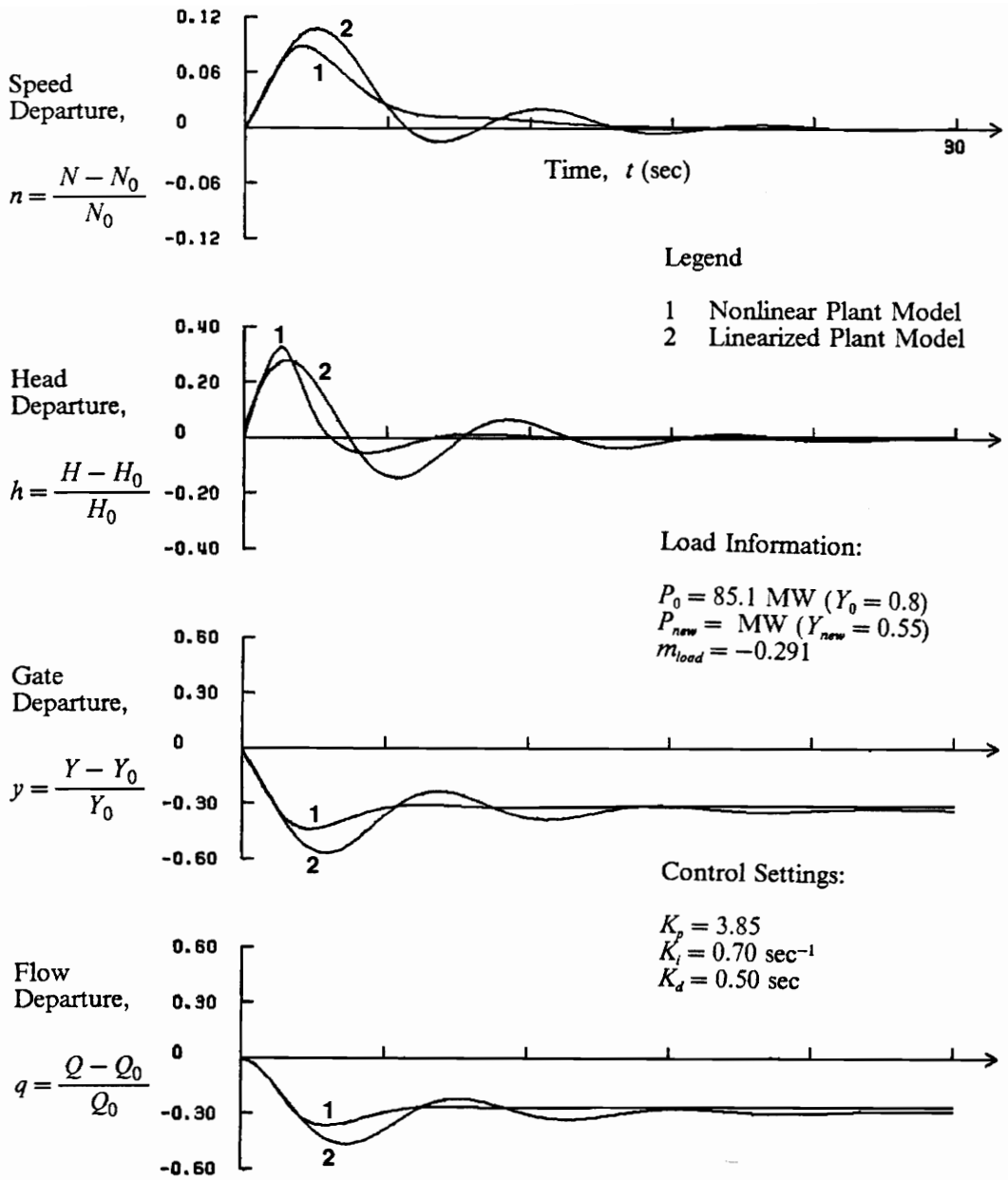

Figure 61. Representative Plant Response for Selected Governor Settings and 30% Load Rejection.

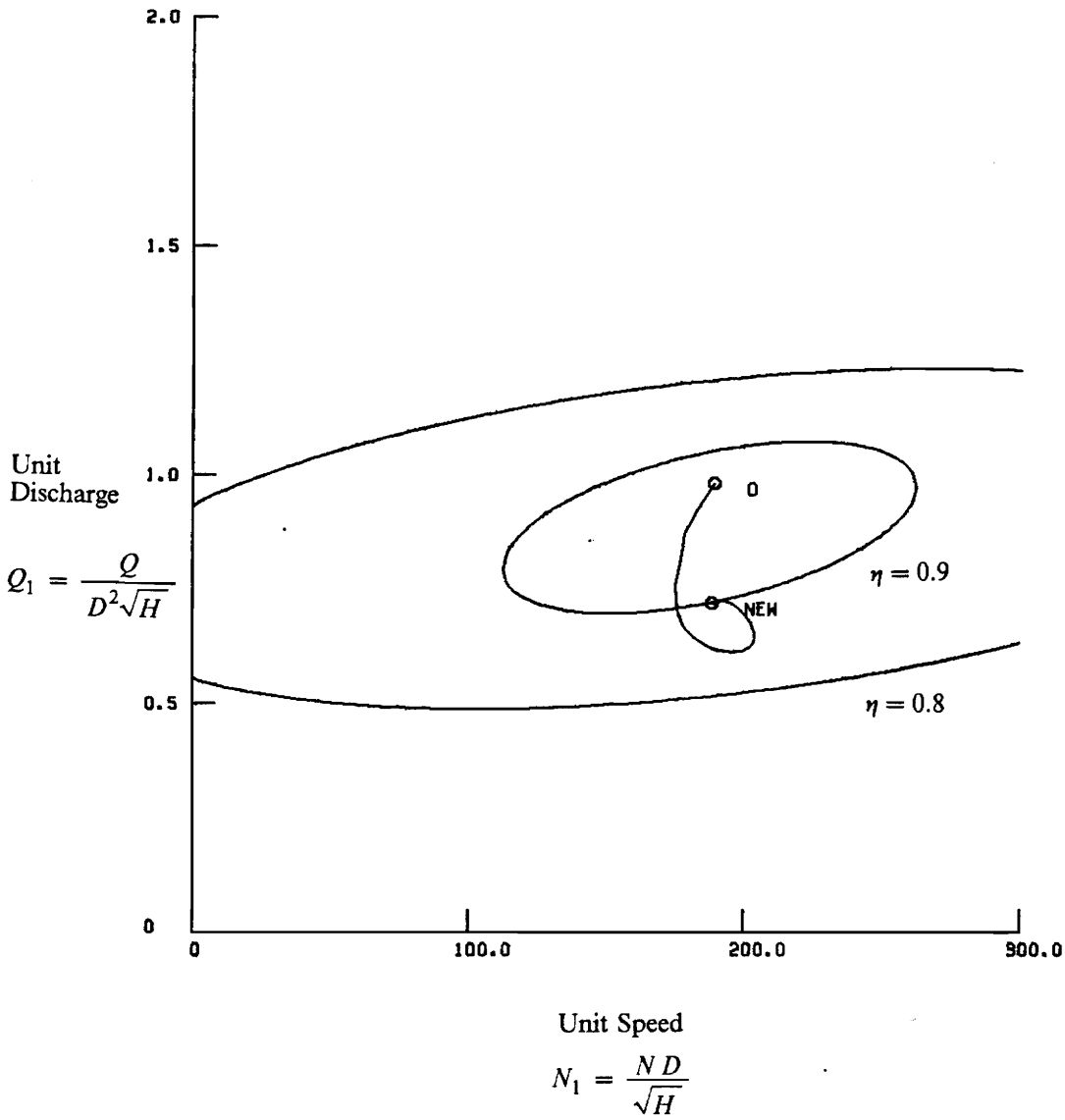

Figure 62. Hill Diagram Tracking of Representative Plant Response to 30% Load Rejection.

These facts help to explain why the initial turbine partial derivatives were a poorer linear representation of the turbine characteristics during the 30 percent load rejection transient than the 10 percent load rejection transient.

Up to this point in the study of plant response, the initial operating condition was considered to be that of the anticipated operation. Two additional situations are considered in which 1) the representative plant is loaded nearly to its maximum capacity and 2) the plant is lightly loaded. For both situations, the response to a nominal 10 percent load rejection is simulated. Since the initial load is different from the anticipated condition, it is necessary to evaluate T_m, T_w, and the turbine partial derivatives at the new initial condition.

The situation chosen to demonstrate heavy load conditions is at 87.8 MW output which corresponds to a wicket gate position of $Y = 0.95$ and is 18 percent further open than the turbine rating. For this operating situation, $T_m = 7.5$ sec and $T_w = 2.0$ sec. The results of the linear and nonlinear simulations are shown in Fig. 63. There is poor agreement between the nonlinear and linear model simulations, particularly with respect to peak overshoot of all plant variables. The linearized model simulation is in 43 percent error for the peak speed overshoot and in 57 percent error for the peak head overshoot. Settling times for all plant variables are similar.

The situation chosen to demonstrate light load conditions is at 54.4 MW output which corresponds to a wicket gate position of $Y = 0.5$ and is 32.5 percent further closed than the turbine rating. For the light load situation, $T_m = 12$ sec and $T_w = 1.2$ sec. The results of the linear and nonlinear simulations are shown in Fig. 64. Unlike the heavy load situation, there is very good agreement between the linear and nonlinear model simulations. The worst error occurs in the peak head overshoot in which the linear is in 11 percent error.

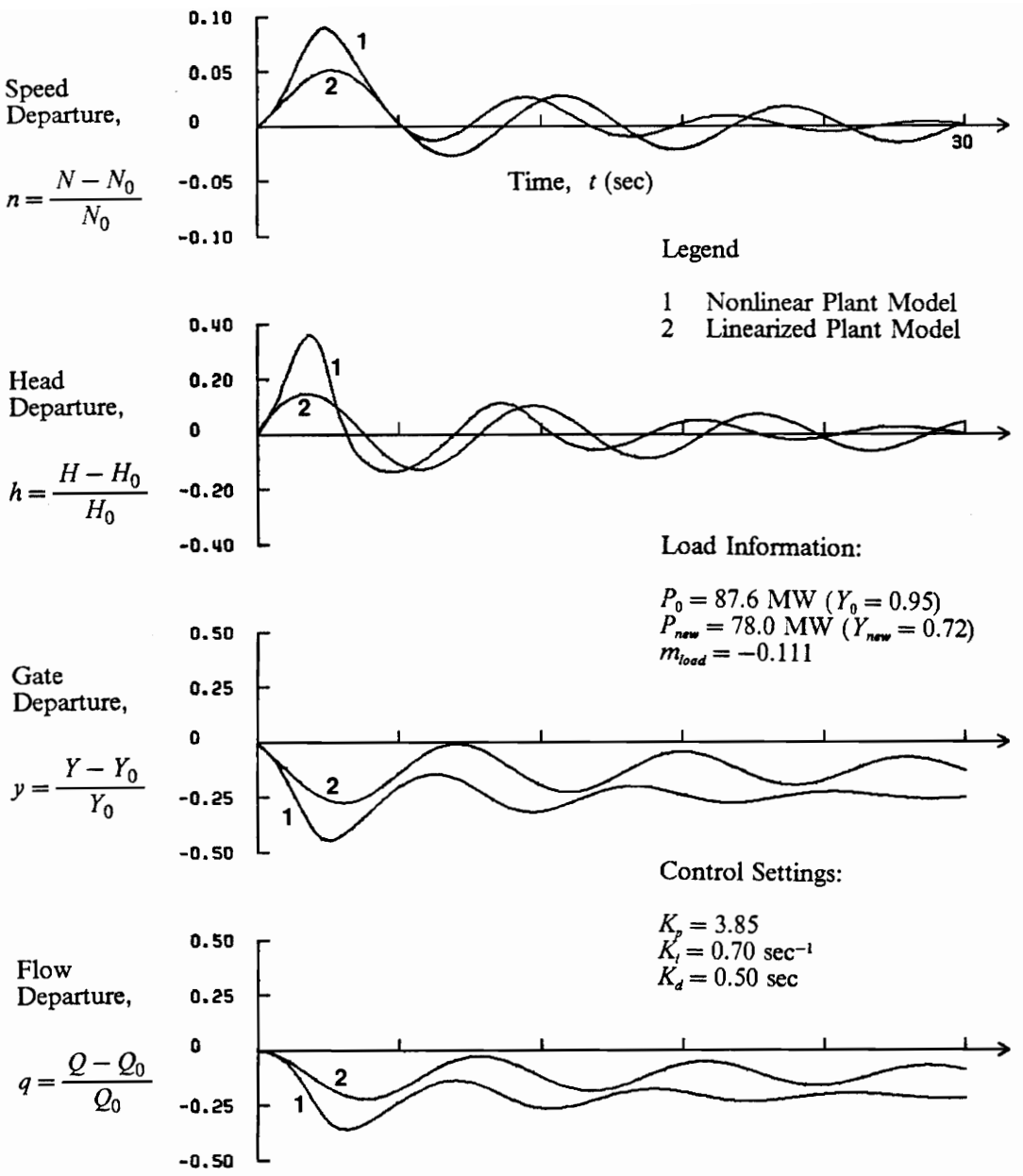

Figure 63. Representative Plant Response for Heavy Load and 10% Load Rejection.

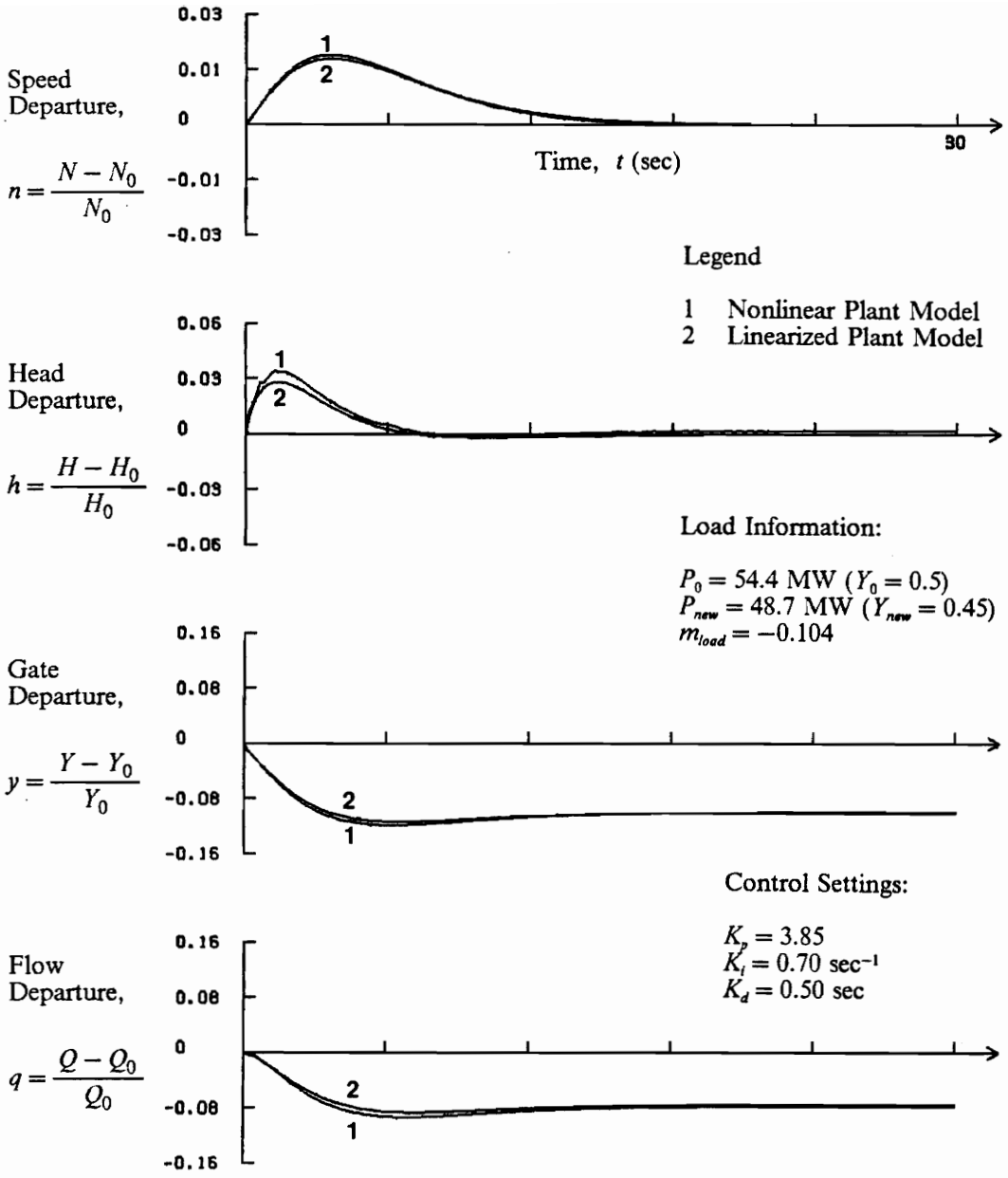

Figure 64. Representative Plant Response for Light Load and 10% Load Rejection.

Step 13 -- Allowable Gate Speeds for Grid Connection Configuration

The last step in the analysis concerns the third electrical connection configuration described in the formulation of plant components. In this configuration, the plant is connected to such a large electrical system that the turbine speed remains constant, independent of load changes. The non-linear plant model is modified to simulate hydroelectric plant response to changes in the desired power command as shown in Fig. 15. Turbine speed regulation is not a concern for this load configuration, but rapid gate motion in response to a change in desired load may violate penstock pressure constraints. The purpose of this step is to determine the maximum allowable wicket gate speed for a full range of initial operating conditions and load changes.

This step is the only part of the analysis process which involves open-loop control. The desired generation command is determined by the operator or by an automatic dispatcher. At present, the wicket gate position is made to change at a constant rate in response to a change in the desired generation command [21]. The constant rate must be set at a conservative value in order to accomodate all load situations. It would be a simple task to adjust that rate to a value which depends on the present generation and on the desired generation. The result of this step is a map of recommended gate motion rates.

The P-I-D control law for gate positioning is replaced by a relation for constant speed gate motion until the gate stops at its new desired position. Removing the turbine speed change dynamics from the model insures the constant speed configuration.

The maximum possible gate speed has previously been defined in terms of the full gate motion time as given by:

$$T_g \leq 5 \text{ sec}$$

For the purpose of illustration, let the maximum head be decreased to 350 ft such that the penstock pressure constraints are given by:

$$200 \text{ ft} \leq H \leq 350 \text{ ft}$$

After selecting an initial load and a new desired load, repeated nonlinear simulations are conducted starting with the maximum possible gate speed. If neither of the penstock pressure constraints are violated, then the desired load change is conducted at the maximum possible gate speed. If one of the pressure constraints is violated, then the gate speed is decreased and the nonlinear simulation is repeated until neither of the pressure constraints is violated.

The results of the allowable gate speed search are shown in the plant loading map of Fig. 65. As expected, small load changes may be accomodated by rapid gate speeds since the penstock head rise or drop will be small. Large load changes must be accomodated by slower gate speeds due to the dynamics of the water in the penstock. As an example of the representative plant response, Fig. 66 is a presentation of the situation of a 50 percent rejection of load from the initial operating condition of 83.1 MW. The wicket gate is closed from $Y = 0.8$ to $Y = 0.4$ in 2.9 sec. During this time, the head rises to nearly 350 ft, the maximum turbine head. The gate motion ceases and the head quickly settles to the new steady-state value in approximately 2 sec (1.2 T_w based on the initial steady operation and 2 T_w based on the new steady operation.

If the linearized model is used to represent the plant, then an analytical relation is used to determine the allowable full gate motion times for the electrical system connection configuration. Since the system speed is constant ($n = 0$), the set of equations describing the plant is given by:

$$T_w \frac{\partial q}{\partial t} = -h \qquad [2.1]$$

$$m = \frac{\partial m}{\partial y} y + \frac{\partial m}{\partial h} h \qquad [6.1]$$

$$q = \frac{\partial q}{\partial y} y + \frac{\partial q}{\partial h} h \qquad [6.2]$$

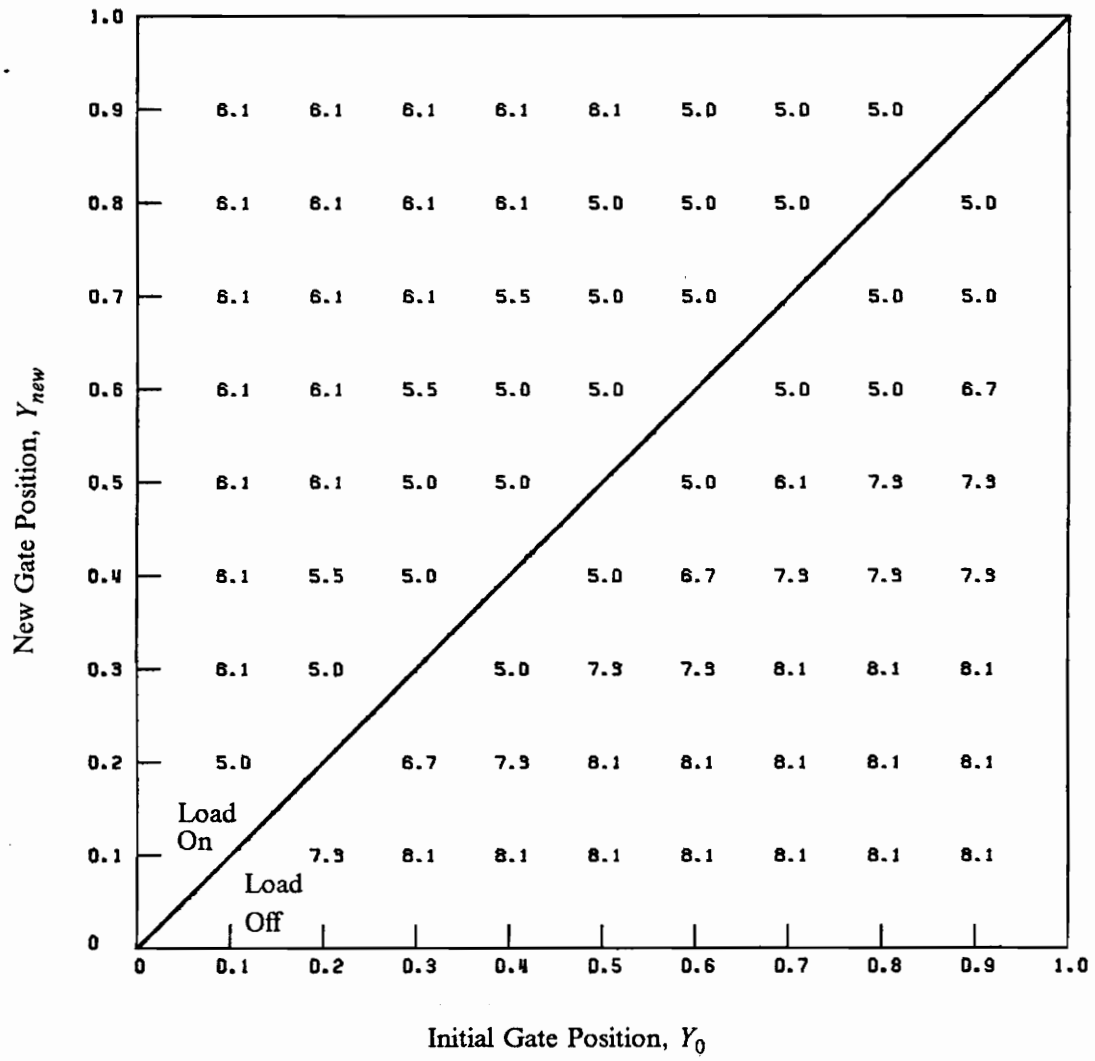

Figure 65. Allowable Full Gate Motion Times for Grid Connection Configuration.

System Load Configuration:
Large Electrical System Connection,
Constant Hydraulic Turbine Speed

Load and Gate Motion Information:
$P_0 = 85.1$ MW $(Y_0 = 0.8)$
$P_{new} = 43.3$ MW $(Y_{new} = 0.4)$
$m_{load} = -0.491$

$t_c = 2.92$ sec (gate motion time)
$T_g = 7.3$ sec (full gate closure time)

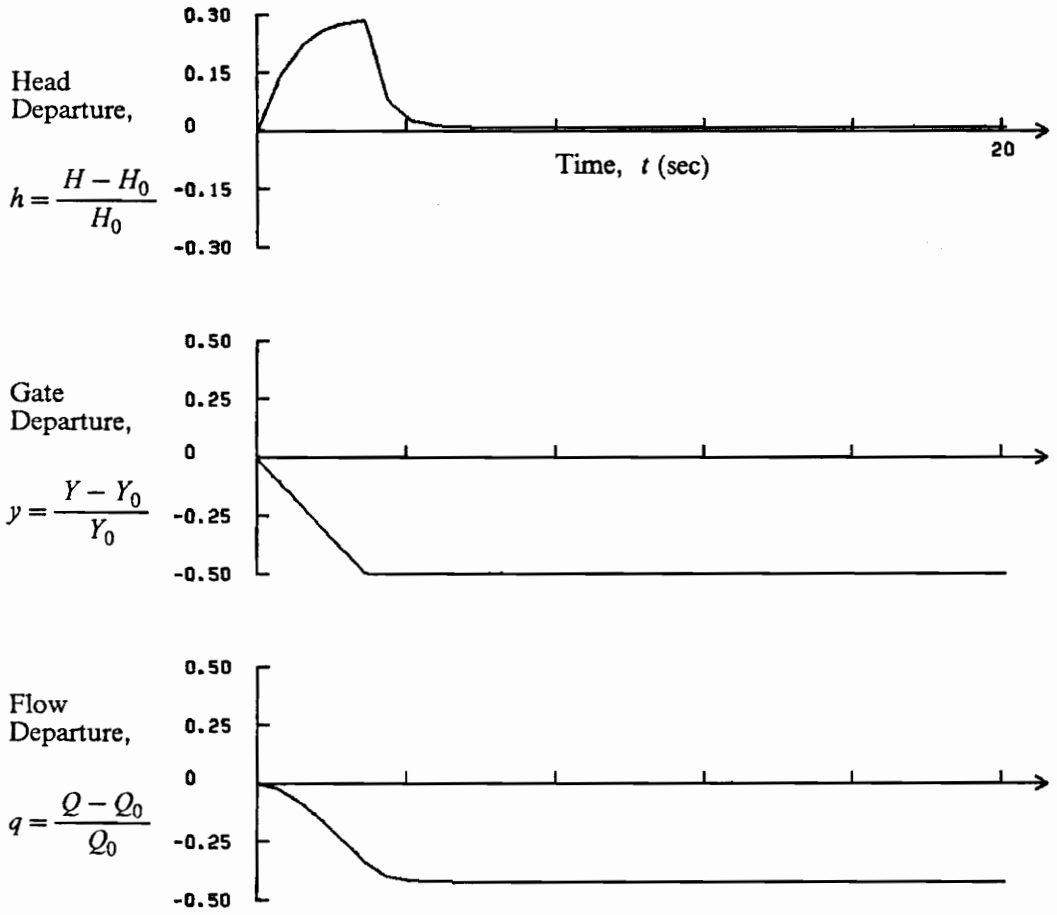

Figure 66. Representative Plant Response for 50% Change in Desired Generation – Grid Connection Configuration.

The gate departure at the new steady-state operation must satisfy Eq. 6.1 and is given by:

$$y = \frac{m_{load}}{\left(\frac{\partial m}{\partial y}\right)} \qquad [6.3]$$

For linear gate motion from Y_0 to Y_{new}, in a time t_g the gate speed is given by:

$$\dot{y} = \frac{m_{load}}{\frac{\partial m}{\partial y} t_g} \qquad [6.4]$$

Substituting Eq. 6.2 into the dynamic penstock equation, Eq. 2.1, and incorporating the gate speed expression, Eq. 6.4, leads to:

$$\frac{dh}{dt} + \frac{1}{\frac{\partial q}{\partial h} T_w} = -\frac{\left(\frac{\partial q}{\partial y}\right)}{\left(\frac{\partial q}{\partial h}\right)} \left[\frac{m_{load}}{\frac{\partial m}{\partial y} t_g}\right]$$

The initial head departure is $h_0 = 0$ so the analytical solution for the head departure for linear gate motion in time t_g is given by:

$$h(t) = T_w m_{load} \left(\frac{\partial q}{\partial y}\right)\left(\frac{\partial m}{\partial y}\right) \left[\frac{\exp\left(\frac{-t}{T_w \frac{\partial q}{\partial h}}\right) - 1}{t_g}\right] \qquad [6.5]$$

For load off (gate closure), the maximum head departure is defined in terms of the maximum head constraint by:

$$h_{max} = \frac{H_{max} - H_0}{H_0}$$

The maximum head occurs at the end of the linear gate motion $t = t_g$. Eq. 6.5 is evaluated with $h = h_{max}$ to determine the minimum time of gate motion which results in the head constraint being reached. This equation is given by:

$$T_w m_{load} \left(\frac{\partial q}{\partial y}\right)\left(\frac{\partial m}{\partial y}\right) \left[\frac{\exp\left(\frac{-t_g}{T_w \frac{\partial q}{\partial h}}\right) - 1}{t_g}\right] - h_{max} = 0$$

The full gate motion time corresponding to the partial gate motion in the time t_g is given by:

$$T_g = \frac{t_g}{Y_0 - Y_{new}}$$

For the representative plant undergoing a 50 percent load rejection while operating in the constant speed configuration, the linearized plant model indicates an allowable full gate motion time of $T_g = 7$ sec. This compares favorably with the $T_g = 7.3$ sec allowable motion from the nonlinear simulation. The result of this step is to provide an operator or automatic dispatcher with the gate speed which is achievable by the turbine wicket gates, does not result in penstock pressure constraint violations, and reaches the new steady-state operating condition as quickly as possible.

Effects of Varying the Plant Characterizing Ratios

An integrated plan of analysis has been applied to the representative plant model. Except for simulations at the initial heavy load and light load situations, the plant characterizing ratios T_m , T_w , and T_e were constant. The purpose of this additional section is to study the response of the linearized and nonlinear plant models with different ratios of (T_m/T_w) and (T_e/T_w) . For this study, different ratios of the plant characterizing parameters are achieved by varying the penstock dimensions of the representative plant model. In this manner, T_m remains constant and T_w and T_e vary.

The locations of these plant models and the original representative plant model are shown on the qualitative map for identifying dominant plant dynamics in Fig. 67. Three new plant models are referred to as a "short penstock", a "long penstock", and a "waterhammer penstock" plant model. Rather than repeating the control setting optimization process, Hovey's and Hagihara's suggested settings are used for each new plant model. These settings and the penstock dimensions are shown for each plant model are shown on Fig. 67.

"Waterhammer Penstock" Plant Model

The "waterhammer penstock" model was formulated by increasing the penstock length and area in the same proportion. The speed and head transients in response to a 10 percent load rejection are shown in Fig. 68. Using Hovey's control settings, there is fair agreement between linear and nonlinear model simulations of speed response. There is also only fair agreement between the two simulations of head response, and the descrepancy is particularly evident early in the transient when the nonlinear simulation of head lags behind the linear simulation but reaches a peak overshoot which is 28 percent higher than that of the linear simulation. For Hovey's settings, the settling times of both simulations are nearly the same and are comparable to the settling time as the original representative plant, approximately 10 seconds. This observation is supported by the fact that (T_m/T_w) was the same as the original plant.

The most interesting result from this new plant model arises from comparison of simulations in which Hagihara's P-I-D control settings were used. As shown in Fig. 68, the linearized model simulation is a poor representation of plant response. The peak overshoots of the linearized model simulation are 25 percent low for the speed and 24 percent low for the head as compared to the nonlinear simulation. The early transient head response of the nonlinear model exhibits classical waterhammer behavior. In addition, the settling time of the linear model simulation is too low by a factor of over 3. The linear response is characterized as "heavily damped" whereas the nonlinear response is characterized as "oscillatory". The important conclusion for this set of simulations is

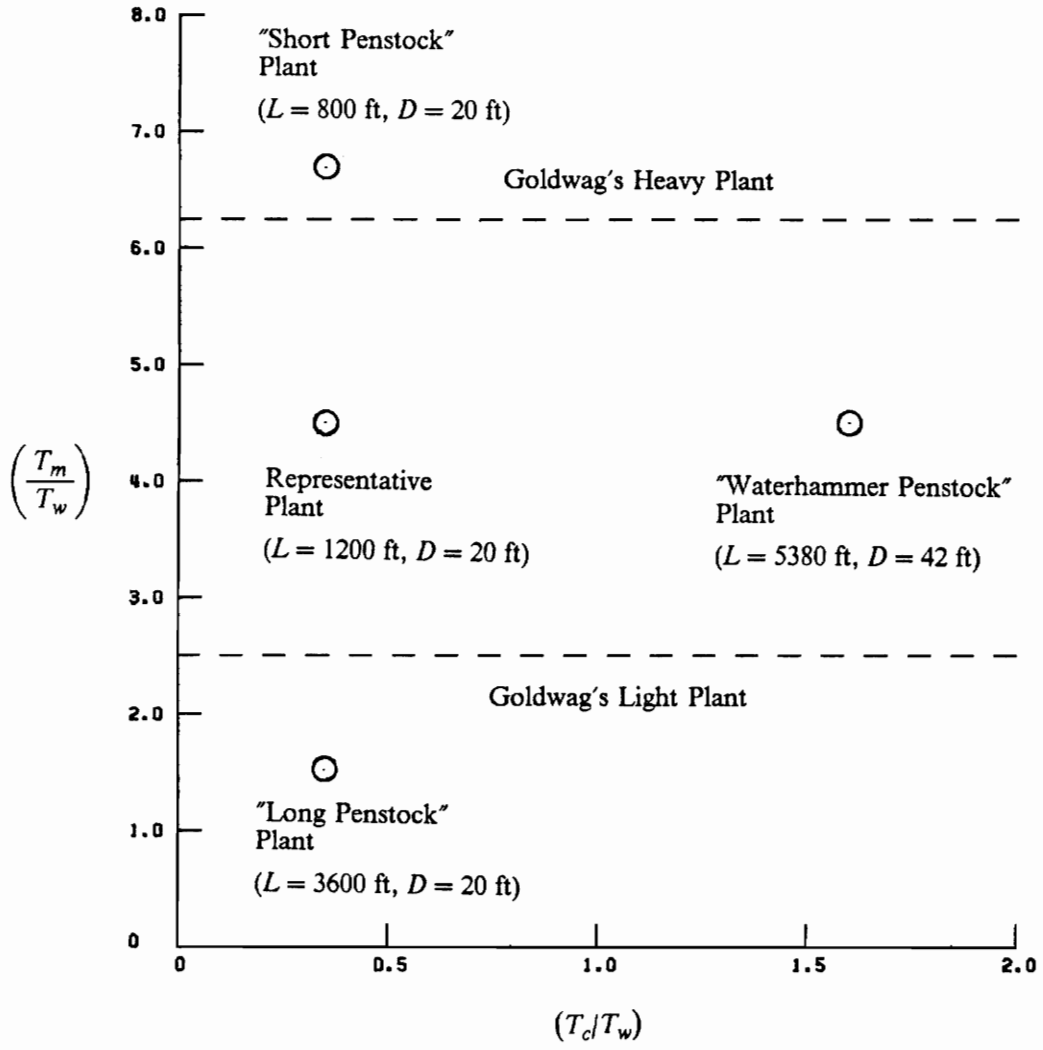

Figure 67. Location of Demonstration Plants on Dominant Plant Dynamics Map.

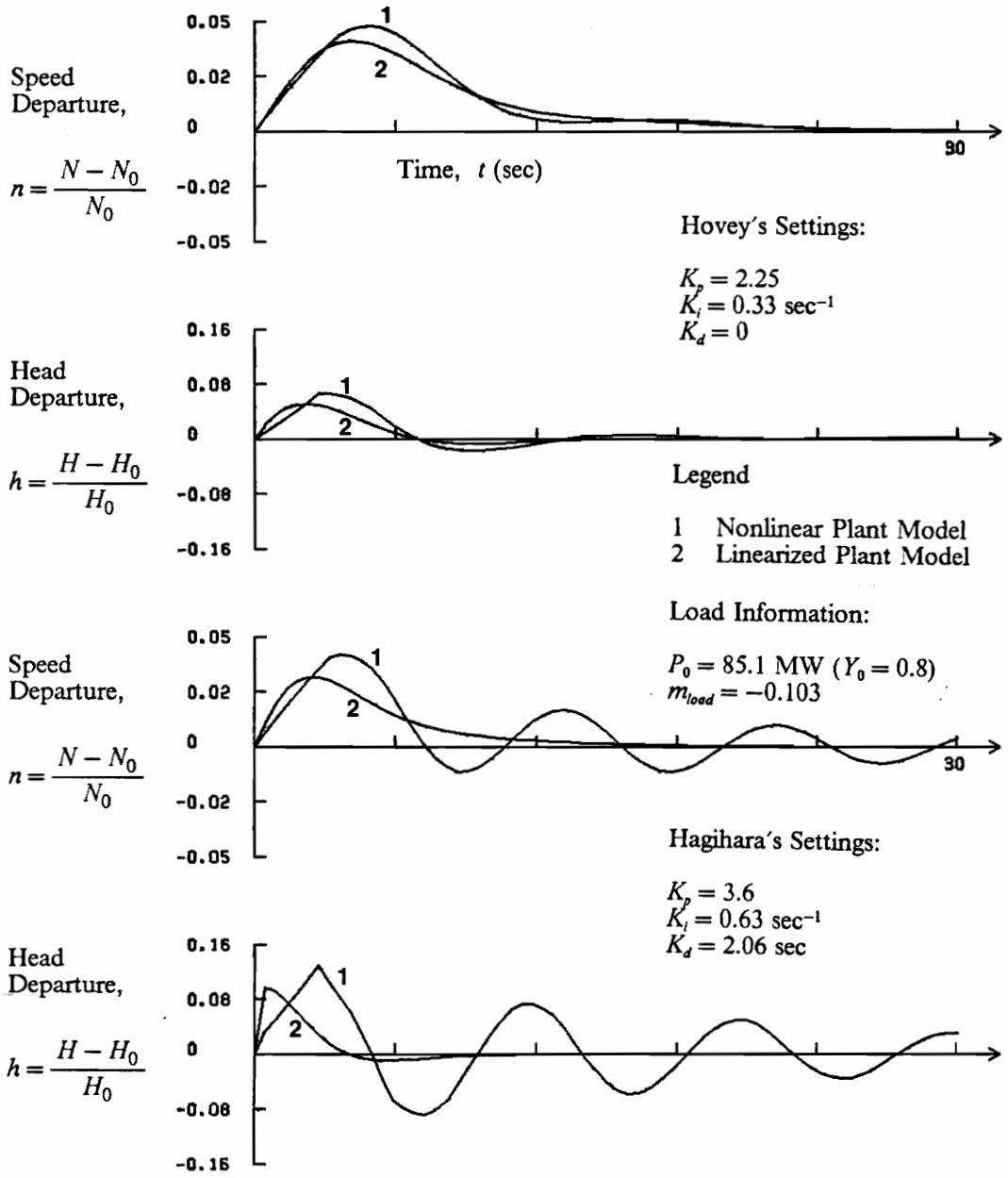

Figure 68. Response of "Waterhammer Penstock" Plant Model.

that the combination of $(T_c/T_w) = 1.6$ and Hagihara's lively control settings brought on waterhammer dynamics in the penstock. Unfortunately, the general conclusion that plants with $(T_c/T_w) = 1.6$ insure waterhammer cannot be made because the simulations using Hovey's P-I (slower) settings did not exhibit such a pronounced difference.

"Long Penstock" Plant Model

The "long penstock" model was formulated by increasing the penstock length. The ratio (T_c/T_w) was the same as the original plant model, but (T_m/T_w) was decreased by 67 percent. The speed and head transients in response to a 10 percent load rejection are shown in Fig. 69. For both Hovey's and Hagihara's settings, the major discrepancy in the linear and nonlinear simulations occurs in steady-state values, which also resulted in discrepancies in the peak overshoot values. These discrepancies support the insights provided by the steady state analysis during the model selection process. Steady state frictional losses in the long penstock account for these errors. It may also be observed that the settling time for this plant model is over twice as long as the original representative plant model. (T_m/T_w) was one third of the original value, meaning that the water inertia would tend to slow down the plant response. Control settings had to be set lower to accomodate the slower water dynamics causing the plant to respond to the load change more slowly.

"Short Penstock" Plant Model

The "short penstock" model was formulated by decreasing the penstock length of the original representative plant by one third. The ratio (T_c/T_w) was the same as the original plant model, but (T_m/T_w) was increased by one third. The speed and head transients for the "short penstock" model in response to a 10 percent load rejection are shown in Fig. 70. In general, there is good agreement in both sets of simulations using both sets of control settings. The steady state errors that were

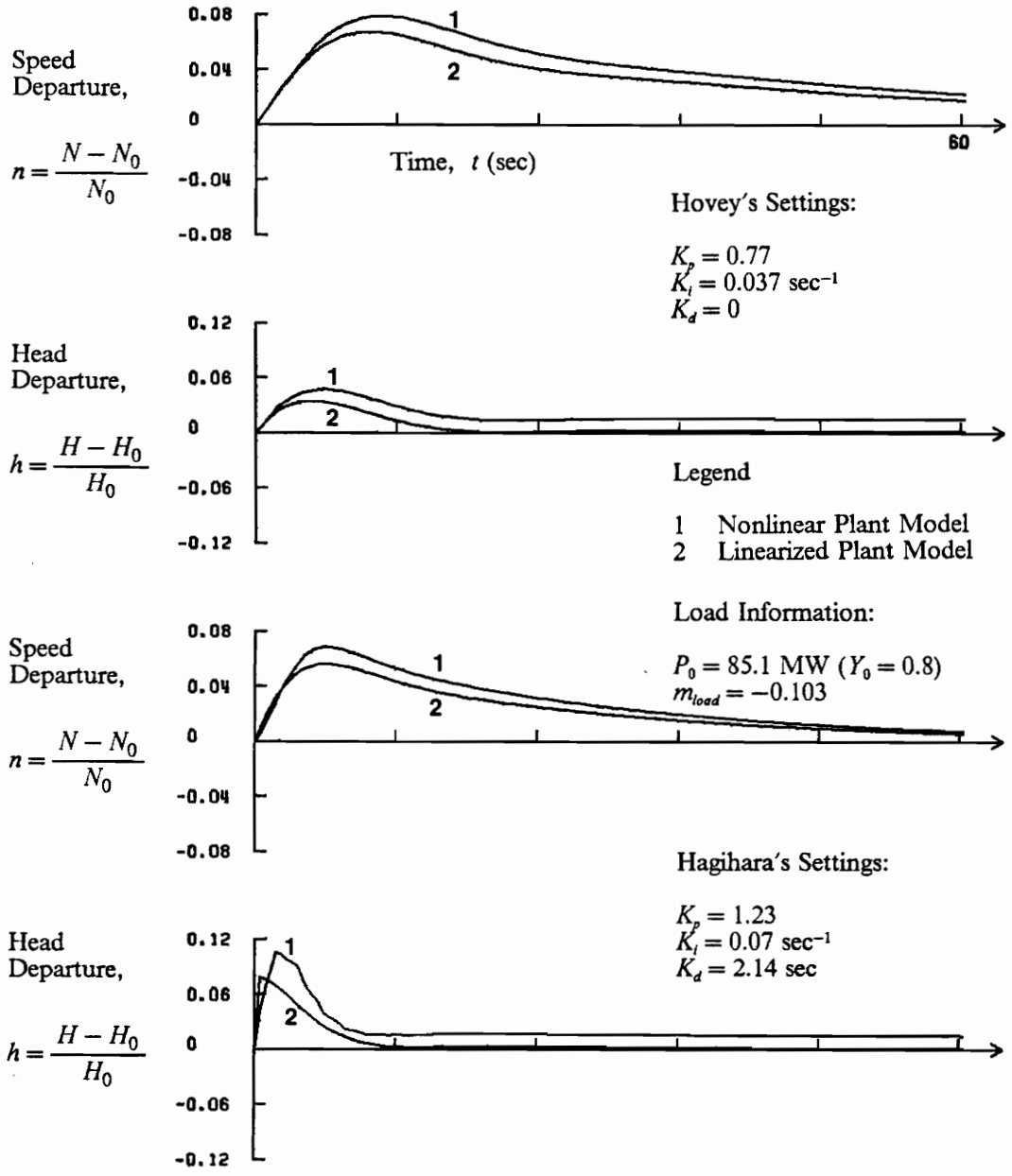

Figure 69. Response of "Long Penstock" Plant Model.

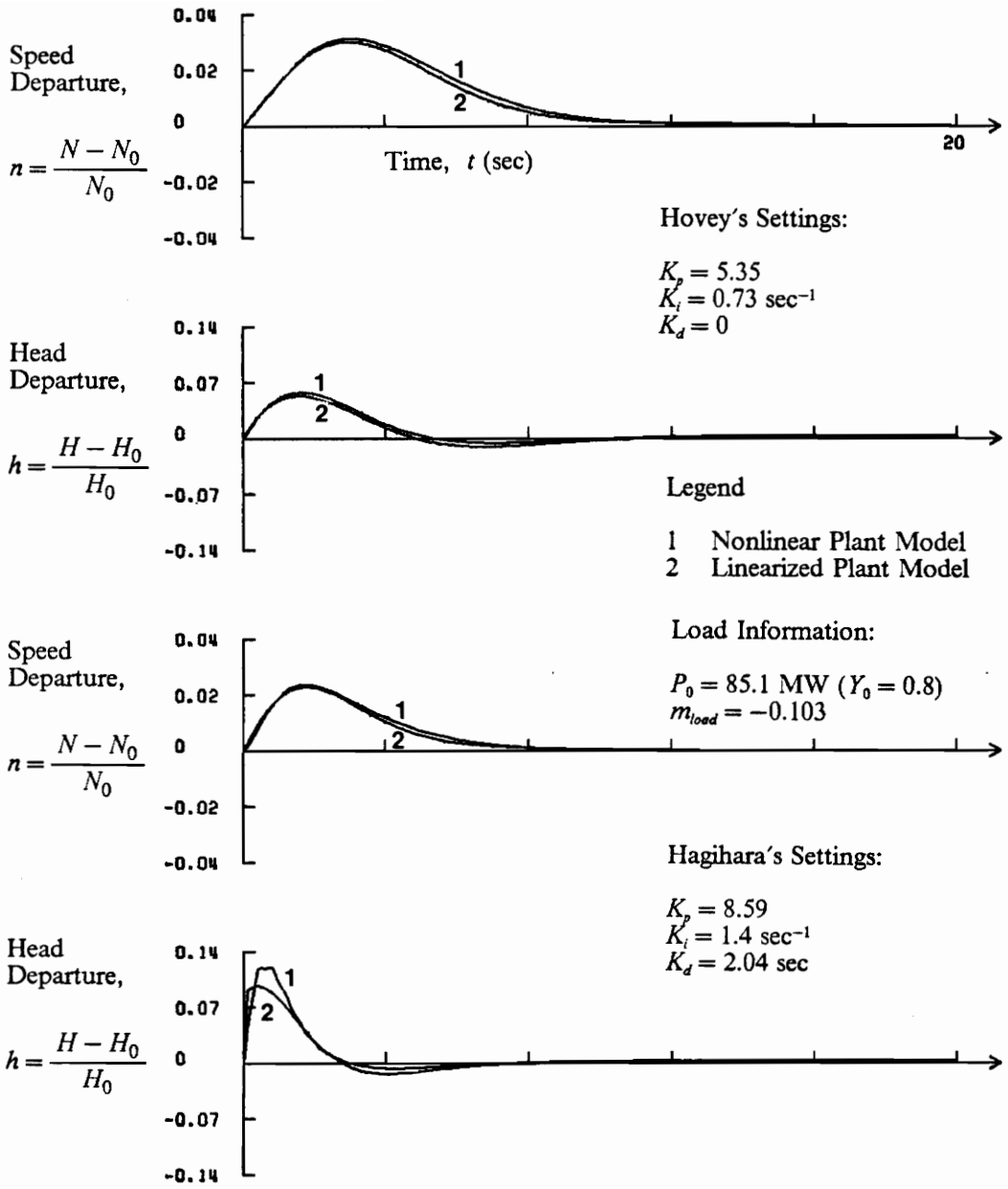

Figure 70. Response of "Short Penstock" Plant Model.

apparent in for the "long penstock" plant simulations are not present for the "short penstock" simulations. The settling times for the "short penstock" plant simulations are approximately 30 percent faster than that of the representative plant simulations. Using the converse reasoning as in the "long penstock" model, since (T_m/T_w) was less than that of the original plant, the water inertia was a less dominant factor in plant response. This allowed the control settings to be livened up in order respond to the load change more quickly.

Summary of Analysis

The proposed analysis has been applied to a representative hydroelectric plant. Specific observations applying to the representative plant were made during the analysis. The most important of these observations are highlighted as a summary.

- Ratios of (T_m/T_w) and (T_c/T_w) locate the representative plant between the "heavy plant" and "light plant" designations. During the anticipated load change, movement of (T_c/T_w) was toward the area in which waterhammer dynamics could be important. It was concluded that both linear and nonlinear models should be studied during the analysis.
- Plant model simulations and plots of linear model stability limits revealed that the theoretical linear model does not satisfactorily represent the plant response. The linearized plant model was the preferred linear model.
- Stability limit plots revealed that waterhammer dynamics come into play for increasing values of derivative gain.
- The optimization process led to the determination of governor settings which could result in at least 39 percent better performance than that resulting from settings currently suggested in the literature although the gate speed limit was shown to limit the control capability.

- The wicket gate speed constraint and the study of zones of satisfactory operation led to governor settings using a reduced value of derivative gain. This set results in 7 percent better performance than that resulting from settings suggested by Hagihara [27] and 51 percent better performance than that resulting from settings suggested by Hovey [13]. In addition to improving plant performance, the settings suggested in this work require only half the gate speed as compared to that required by Hagihara's settings.
- The plant response was shown to be dependent on the initial operating condition and on the magnitude of the load change. Unfortunately linear plant model validity could not be generalized for all operating conditions.
- Based on plant model simulation comparisons, the linearized plant model was shown to be a satisfactory model for load departures from the initial anticipated condition of less than approximately 10 percent.
- For the situation of plant connection to a large electrical system, wicket gate speeds were determined which insure that penstock pressure constraints will not be violated.
- The behaviors of three additional plant models were studied by varying the penstock dimensions of the representative plant model. It was demonstrated that as (T_e/T_w) is increased, the liklihood of waterhammer problems increases, particularly with lively control settings. It was also demonstrated that as the penstock length increases, steady-state errors in plant values may preclude the use of a linear plant model.

These observations were made concerning the analysis as applied specifically to the representative plant. It now remains to make conclusions concerning the analysis in general terms and to discuss the work as a whole.

Chapter 7

Discussion and Recommendations

An integrated plan for the improvement of hydroelectric plant performance has been presented and applied to a representative plant. The plan began with the characterization of the plant from physical information. One or more mathematical models for each plant component were developed. Procedures developed in this work guide in the formulation of an appropriate plant model. Plant models were assembled for plant performance simulation and determination of regions of stable operation. Optimum governor settings were determined which improved plant performance over settings currently recommended in the literature. A unique aspect of this work is that the suggested control settings were studied for satisfactory operation over a broad range of plant operations. Another unique aspect is that a gate speed limit was incorporated in the performance optimization process, which has been overlooked in current linear optimization approaches.

The major objectives of the plan are evaluated in this chapter to draw specific conclusions concerning each aspect of the work. Following evaluation of the objectives, recommendations are made for the future use and extension of this work.

Evaluation of Objectives

Provide Component Models.

Mathematical models for each of the hydroelectric plant components have been provided. An analytical representation and a unique performance characteristic analysis of the hydraulic turbine's hill diagram was developed in this work. This analytical representation is a valuable tool for linear plant model simulation and stability studies. The compatability of each component model with the other components serves to unify the techniques for hydroelectric plant modeling. Although individual models for plant components exist in many references, no one work considers the interrelation of all the candidate component models when assembling a plant model.

Characterize Plant Behavior.

The determination of the three plant parameters T_m , T_w , and T_c from physical plant information was demonstrated. It was desired to characterize the plant response based solely on these three characterizing parameters. Unfortunately, it was shown that the control settings and the magnitude of the load change also affect the nature of the plant response. It was also desired to be able to predict from the three plant parameters whether a linear plant model would be satisfactory or if a nonlinear plant model would be required for simulation. While this ability was not achieved, a qualitative map of (T_m/T_w) versus (T_c/T_w) was developed in order to show which components should dominate plant response.

A rationale was developed and compared to existing literature in order to characterize the ratio of (T_m/T_w). A plant with $(T_m/T_w) > 6$ was categorized as a "heavy plant" in which turbine inertia dominates plant response. A plant with $(T_m/T_w) < 2$ was categorized as a "light plant" in which

water inertia dominates plant response. A frequency analysis was performed on a linear and transcendental penstock model to show that as (T_e/T_w) increases, the likelihood of waterhammer increases. Quantifying the effects of waterhammer depended on the motion of the wicket gate, which could not be determined without knowledge of the control settings. For demonstration purposes, it was shown that the response of a particular plant model with $(T_e/T_w) = 1.6$ suffered from waterhammer and this problem was amplified as the control settings were made more lively. The response of several plant models with $(T_e/T_w) = 0.35$ were shown to not suffer from waterhammer, although the validity of the rigid water column model also depended on steady-state errors in head, flow, and gate position. Based on knowledge of the anticipated operating conditions, the estimation of these errors provided further insight into the choice of a linear or nonlinear model.

Provide Plant Models.

One nonlinear plant model and four linear models were formulated from the plant components. The sixth order linear model which incorporated generator and connected electrical system models was used to demonstrate that the isolated load model is a better model for use in determining optimum control settings. The transcendental plant model was used to give further insight into the potential for waterhammer by way of a plant model stability limit study. A general conclusion from that study revealed that as K_d is increased, the likelihood for waterhammer increases. The theoretical linear model (on which Hovey and Hagihara based their suggested governor settings) was formulated for comparison to the linearized model. The third order linearized plant model which incorporated the results of the hill diagram performance analysis was used for comparison to the nonlinear plant model.

Study Linear and Nonlinear Simulations.

Comparison of simulations using the nonlinear model, the linearized model, and the theoretical linear model of a representative plant revealed that the theoretical linear model is not a satisfactory model for the plant. The analysis of the turbine's hill diagram presented in this work provides an improvement in representing turbine performance over the theoretical performance model.

Most literature concerning hydroelectric plant modeling and simulation utilizes the rigid water column model for the penstock without considering the validity of this model. In the past, this model has usually been valid because wicket gate speeds were usually slow due to the exclusive use of P-I control. Linear and nonlinear simulation comparisons have shown that a new importance must be placed on adequate penstock fluid dyamics modeling because of increased wicket gate speed required by P-I-D control but limited by gate actuator saturation.

It was demonstrated that increasing the control settings, particularly increasing the derivative gain, K_d , required faster turbine wicket gate speed. This requirement was amplified by increasing the load change. A method for estimating the maximum gate speed using Gordon's curves was presented in this work. For control settings which require a gate speed greater than the maximum available, the nonlinear model must be used for plant simulation.

Determine Optimum Settings.

A representative plant model was established to demonstrate the optimization process and to investigate the improvement of plant performance over that using settings currently suggested in the literature. The optimization process resulted in the determination of a family of optimum control settings for fixed values of K_d. For settings with higher K_d, the gate speed required to achieve the desired response exceeded the representative plant's capabilities. The nonlinear plant model proved

to be valuable in enforcing the gate speed limit during the optimization process. Gate speed limitations tend to limit the selection of suggested settings to low values of K_d.

Determine Zones of Satisfactory Operation.

The study of plant operation at conditions different from the anticipated conditions was valuable in the final selection of control settings. Simulations for various candidate P-I-D control settings were investigated for a wide range of plant operation. For the representative plant model, it was demonstrated that settings corresponding to high values of K_d resulted in a small region of satisfactory operation. The suggested settings were then selected in order to achieve improved plant performance but still maintain a reasonable operating region.

Establish Best Control Settings.

The control settings suggested by Hovey and Hagihara depend only on the parameters T_m and T_w and rely on the theoretical linear model as a basis. In general, Hovey's suggested P-I control settings result in sluggish plant response which can be improved easily by implementation of P-I-D control. Use of Hagihara's suggested P-I-D settings did improve on that performance, but his settings were suggested without regard to limitations of wicket gate speed limits. In fact, Hagihara's suggested settings would require a gate speed greater than that available for the representative plant model.

The control settings which were selected using the analysis of this work result in performance which is greatly improved over that of Hovey and about 7 percent over that of Hagihara (for the representative plant model studied). The added benefit of the settings suggested by this plan of analysis is that gate speed limitations and unanticipated operation have been accomodated. The gate speed required by the suggested settings is approximately one third of the speed required by

Hagihara's settings. The primary objective, which was to determine settings that result in improved plant performance, has been achieved. In addition, the analysis developed in this work represents an integrated plan for hydroelectric plant modeling and simulation.

Recommendations for Future Work

It is recommended that this work be extended in three areas. Specific recommendations are discussed for the areas of 1) applying the plan of analysis for study of an operational plant, 2) using aspects of the analysis as a design tool, and 3) extending the analysis.

The analysis was applied to a representative plant model in order to demonstrate the steps in the analysis in this work. The linearized plant model was shown to satisfactorily simulate the response of the Grand Coulee Plant [36], but the literature did not contain sufficient information of any single plant to use as a basis for study and comparison. It is recommended that this plan of analysis be applied to an operational plant. First, the analysis should be applied in order to determine control settings that lead to improved plant performance. Second, the response predicted by models in this work should be compared to actual plant response, particularly speed, head, and gate position. There is a need in the literature for the combination of sufficient plant information (which is listed in Fig. 35 of this work) to define a plant model and associated transient field data in order to help verify plant models.

The plan of analysis presented in this work has relied on the fact that the initial operating condition and the load change is known. Since it is reasonable to expect the plant to operate at different conditions and to respond to different load changes, it is recommended that the optimization process be performed at various initial load conditions. Optimum settings should be determined which allow for satisfactory response to load changes for each initial load condition. In this manner, a table of initial load dependent settings (K_p, K_i, $K_d = f(P_0)$) could be organized. This table of settings could be implemented into a computer-based control system.

The first steps of the analysis involved formulating a plant model from physical plant information. It has been common practice [20] to incorporate the theoretical linear model into multi-plant models of large electrical systems. It is recommended that the modeling techniques provided in this work be utilized to incorporate a more appropriate linearized model into multi-plant simulation models.

It is recommended that this analysis be utilized during the conceptual phase of the design of a new plant. For example, the penstock models have been formulated so that several penstock models could be combined with intermediate surge tanks. For very long water supply systems, one or more surge tanks may be installed in the system to minimize the effects of waterhammer in the penstock. A water supply model more complicated than the one used in this work could be formulated from several penstock and reservoir models. The analysis presented in this work provides a facility for studying the impact that various water supply configurations would have on the plant performance and suggested control settings.

At the end of the analysis, a method was developed to determine the maximum gate speed that would allow a plant connected to a fixed-speed grid to respond to a load change as quickly as possible while also satisfying system head constraints. Wylie [8] presented a general open-loop flow control scheme (referred to as valve stroking) which has been designed to achieve a new steady flow in a pipe quickly as possible while also satisfying specified head constraints. This scheme has shown to be particularly useful for long pipelines in which waterhammer is likely to occur. Given the initial and new desired flow, the valve scheduling scheme involves the computation of valve positions at discrete times. During the transient, the valve (or gate, for the hydroelectric plant) is positioned according to the prescribed schedule. This scheme was investigated for the representative plant and there was no advantage (in terms of time required to achieve the new steady operation) over simply moving the gate at a constant speed. It is recommended that use of the open-loop scheduling scheme be investigated for use with plants with $(T_c/T_w) > 0.5$. A plant in this range is more likely to experience waterhammer problems than the representative plant model studied in this work.

References

1. U. S. Department of Energy, Energy Information Administration, Office of Coal, Nuclear, Electric, and Alternate Fuels, *Inventory of Power Plants in the United States, 1981 Annual,* Sept. 1982, Document DOE/EIA-0095(81).

2. Li, K. W., and A. P. Priddy, *Power Plant System Design,* Wiley, 1985.

3. Virginia Electric and Power Company, "Bath County Pumped Storage Project," Pamphlet PA-175/4-8410M, P. O. Box 26666, Richmond, VA 23261, 1984.

4. Fostiak, R. J., and W. L. Thompson, "Electrical Features of the Bath County Pumped-Storage Project," *IEEE Transactions on Power Apparatus and Systems,* Vol. PAS-101, No. 9, September 1982, pp. 3166-3172.

5. Streeter, V. L., *Fluid Mechanics,* 6th ed., McGraw-Hill, 1975.

6. Brebbia, C. A., and A. Ferrante, *Computational Hydraulics,* Butterworths, 1983.

7. Watters, Gary Z., *Analysis and Control of Unsteady Flow in Pipelines,* Butterworths, 1984.

8. Wylie, E. B., and V. L. Streeter, *Fluid Transients,* FEB Press, P. O. Box 2431, Ann Arbor, MI 48106, Corrected Edition, 1983.

9. Chaudhry, M. H., *Applied Hydraulic Transients,* Van Nostrand Reinhold Co., 1979.

10. Takahashi, Y., M. J. Rabins, and D. M. Auslander, *Control and Dynamic Systems,* Addison-Wesley, 1972.

11. Goodson, R. E., and R. G. Leonard, "A Survey of Modeling Techniques for Fluid Line Transients," *Transactions ASME, Journal of Basic Engineering,* Paper 71-WA-FE-9, pp. 1-9.

12. Wozniak, L., and G. H. Fett, "Conduit Representation in Closed Loop Simulation of Hydroelectric Systems," *Transactions ASME, Journal of Basic Engineering,* September 1972, pp. 599-605.

13. Hovey, L. M., "Optimum Adjustment of Governors in Hydro Generating Stations," *Engineering Journal* (Engineering Institute of Canada), Vol. 43, Nov. 1960, Montreal, Quebec, pp. 64-71.

14. Hovey, L. M., "Optimum Adjustment of Hydro Governors on Manitoba Hydro System," *IEEE Transactions on Power Apparatus and Systems,* Vol. PAS-87, No. 3, Dec. 1962, pp. 581-587.

15. Goldwag, E., "On the Influence of Water Turbine Characteristic on Stability and Response," *Transactions ASME, Journal of Basic Engineering,* December 1971, pp. 481-494.

16. Thorne, D. H., and E. F. Hill, "Extensions of Stability Boundaries of a Hydraulic Turbine Generating Unit," *IEEE Transactions on Power Apparatus and Systems,* Vol. PAS-94, No. 4, July/August 1975, pp. 1401-1409.

17. Thorne, D. H., and E. F. Hill, "Field Testing and Simulation of Hydraulic Turbine Governor Performance," *IEEE Transactions on Power Apparatus and Systems,* Vol. PAS-93, No. 4, July/August 1974, pp. 1183-1191.

18. Phi, D. T., E. J. Bourque, D. H. Thorne, and E. F. Hill, "Analysis and Application of the Stability Limits of a Hydro-Generating Unit," *IEEE Transactions on Power Apparatus and Systems,* Vol. PAS-100, No. 7, July 1981, pp. 3203-3212.

19. Perkins, F. E., et al., *Hydropower Plant Transients,* Report 71, Parts II and III, Department of Civil Engineering, Hydrodynamics Lab, Massachusetts Institute of Technology, Sept., 1964.

20. IEEE Power System Engineering Committee, "Dynamic Models for Steam and Hydro Turbines in Power System Studies," *IEEE Transactions on Power Apparatus and Systems,* Vol. PAS-92, No. 6, 1973, pp. 1904-1915.

21. Gurney, J. H., "Control and Protection Design of the Revelstoke Hydroelectric Project," *IEEE Transactions on Power Apparatus and Systems,* Vol. PAS-104, No. 8, August 1985, pp. 1987-1997.

22. DeMello, F. P., and C. Concordia, "Concepts of Synchronous Machine Stability as Affected by Excitation Control," *IEEE Transactions on Power Apparatus and Systems,* Vol. PAS-88, No. 4, April 1969, pp. 316-329.

23. Marshall, W. K., and W. J. Smolinski, "Dynamic Stability Determination by Synchronizing and Damping Torque," IEEE Paper T 73 007-2, Winter Power Meeting, New York, Feb., 1973.

24. Schleif, F. R., and A. B. Wilbor, "The Coordination of Hydraulic Turbine Governors for Power System Operation," *IEEE Transactions on Power Apparatus and Systems,* Vol. PAS-85, No. 7, July 1966, pp. 750-758.

25. Paynter, H. M., *A Palimpsest on the Electronic Analog Art,* George A. Philbrick Researches, Inc., Boston, MA, p. 228, 1955.

26. Dhaliwal, N. S., and H. E. Wichert, "Analysis of P. I. D. Governors in Multimachine System," *IEEE Transactions on Power Apparatus and Systems,* Vol. PAS-97, No. 2, March/April 1978, pp. 456-463.

27. Hagihara, S., H. Yokota, K. Goda, and K. Isobe, "Stability of a Hydraulic Turbine Generating Unit Controlled by a P. I. D. Governor," *IEEE Transactions on Power Apparatus and Systems,* Vol. PAS-98, No. 6, Nov./Dec. 1979, pp. 2294-2298.

28. Ramamurthi, V., K. Ramachandram, and P. S. Kodandaramaswamy, "Transient Performance and Control of Hydraulic Turbine-Generator Units," *IEEE Transactions on Power Apparatus and Systems,* Vol. PAS-100, No. 1, January 1981, pp. 288-294.

29. Xiao, Tianduo, and Dong Xinglin, "Elastic Water-Hammer Effects on Governing Stabilities of Hydroelectric Plants," *Scientia Sinica (Series A),* Vol. XXV, No. 9, September 1982, pp. 993-1008.

30. Murty, M. S. R., and M. V. Hariharan, "Analysis and Improvement of the Stability of a Hydro-Turbine Generating Unit with Long Penstock," *IEEE Transactions on Power Apparatus and Systems,* Vol. PAS-103, No. 2, February 1984, pp. 360-367.

31. Swiecicki, I., "Regulation of a Hydraulic Turbine Calculated by Step-By-Step Method," *ASME Transactions,* Vol. 83, No. 3, Sept. 1961, pp. 445-455.

32. Wozniak, L., and G. H. Fett, "Optimal Gate Closure Schedule for Hydroelectric Turbine System," *Transactions ASME, Journal of Fluids Engineering,* March 1973, pp. 47-52.

33. Van De Vegte, J., *Feedback Control Systems,* Prentice-Hall, 1986.

34. Wylie, C. R., *Advanced Engineering Mathematics,* 4th ed., McGraw-Hill, 1975.

35. Selby, S. M., editor, *Standard Mathematical Tables,* 21st ed., The Chemical Rubber Co., 18901 Cranwood Parkway, Cleveland, Ohio 44128, pp. 103-104, 1973.

36. Schleif, F. R., and C. G. Bates, "Governing Characteristics for 820,000 Horsepower Units for Grand Coulee Third Powerplant," *IEEE Transactions on Power Apparatus and Systems,* Vol. PAS-90, No. 2, March/April 1971, pp. 882-890.

37. Carnahan, B., H. A. Luther, and J. O. Wilkes, *Applied Numerical Methods,* Wiley, 1969.

Appendix A

Coefficients for Matrix Representation of Linearized Plant Model with Equivalent System Load

The block diagram which describes the linearized hydroelectric plant conneceted to an equivalent dynamic electrical system was presented in Fig. 27. The linear system is sixth order and the block diagram may be manipulated so that the system may be expressed in matrix form as given by:

$$[\dot{x}] = [A]\,[x] + [B]\,[u]$$

where $[x]$ = the 6 x 1 column of states

$[A]$ = the 6 x 6 system matrix

$[u]$ = the 2 x 1 disturbance column, col (p_{sys}, p_{des})

$[B]$ = the 6 x 2 disturbance matrix

The coefficients of the system matrix $[A]$ are given by:

$$a_{11} = \frac{\left[\left(\frac{\partial m}{\partial n}\right) - K_p\left\{\left(\frac{\partial m}{\partial y}\right) - \left(\frac{\partial m}{\partial h}\right)\left(\frac{\partial q}{\partial y}\right) / \left(\frac{\partial q}{\partial h}\right)\right\} - \left(\frac{\partial m}{\partial h}\right)\left(\frac{\partial q}{\partial n}\right) / \left(\frac{\partial q}{\partial h}\right)\right]}{\left[T_m + K_d\left\{\left(\frac{\partial m}{\partial y}\right) - \left(\frac{\partial m}{\partial h}\right)\left(\frac{\partial q}{\partial y}\right) / \left(\frac{\partial q}{\partial h}\right)\right\}\right]}$$

$$a_{12} = \frac{\left\{\left(\frac{\partial m}{\partial y}\right) - \left(\frac{\partial m}{\partial h}\right)\left(\frac{\partial q}{\partial y}\right) / \left(\frac{\partial q}{\partial h}\right)\right\}}{\left[T_m + K_d\left\{\left(\frac{\partial m}{\partial y}\right) - \left(\frac{\partial m}{\partial h}\right)\left(\frac{\partial q}{\partial y}\right) / \left(\frac{\partial q}{\partial h}\right)\right\}\right]}$$

$$a_{13} = \frac{\left(\frac{\partial m}{\partial h}\right) / \left(\frac{\partial q}{\partial h}\right)}{\left[T_m + K_d\left\{\left(\frac{\partial m}{\partial y}\right) - \left(\frac{\partial m}{\partial h}\right)\left(\frac{\partial q}{\partial y}\right) / \left(\frac{\partial q}{\partial h}\right)\right\}\right]}$$

$$a_{14} = \frac{1}{\left[T_m + K_d\left\{\left(\frac{\partial m}{\partial y}\right) - \left(\frac{\partial m}{\partial h}\right)\left(\frac{\partial q}{\partial y}\right) / \left(\frac{\partial q}{\partial h}\right)\right\}\right]}$$

$$a_{15} = 0$$

$$a_{16} = 0$$

$$a_{21} = -K_i$$

$$a_{22} = 0$$

$$a_{23} = 0$$

$$a_{24} = 0$$

$$a_{25} = 0$$

$$a_{26} = 0$$

$$a_{31} = \frac{\left[\left(\frac{\partial q}{\partial h}\right) - \left(\frac{\partial q}{\partial y}\right)(K_p + K_d\, a_{11})\right]}{T_w \left(\frac{\partial q}{\partial h}\right)}$$

$$a_{32} = \frac{\left(\frac{\partial q}{\partial y}\right)[1 - K_d\, a_{12}]}{T_w \left(\frac{\partial q}{\partial h}\right)}$$

$$a_{33} = -\frac{\left[1 + \left(\frac{\partial q}{\partial y}\right) K_d\, a_{12}\right]}{T_w \left(\frac{\partial q}{\partial h}\right)}$$

$$a_{34} = -\frac{\left(\frac{\partial q}{\partial y}\right) K_d\, a_{14}}{\left[T_w \left(\frac{\partial q}{\partial h}\right)\right]}$$

$$a_{35} = 0$$

$$a_{36} = 0$$

$$a_{41} = a_{11}\, D_a + K_a$$

$$a_{42} = a_{12}\, D_a$$

$$a_{43} = a_{13}\, D_a$$

$$a_{44} = a_{14}\, D_a$$

$$a_{45} = \frac{-D_a}{T_{s2}}$$

$$a_{46} = \frac{D_a\, D_{s2}}{T_{s2}} - K_a$$

$$a_{51} = 0$$

$$a_{52} = 0$$

$$a_{53} = 0$$

$$a_{54} = \frac{B}{T_{s1}}$$

$$a_{55} = -\frac{D_{s1}}{T_{s1}}$$

$$a_{56} = 0$$

$$a_{61} = 0$$

$$a_{62} = 0$$

$$a_{63} = 0$$

$$a_{64} = 0$$

$$a_{65} = \frac{1}{T_{s2}}$$

$$a_{66} = -\frac{D_{s2}}{T_{s2}}$$

The coefficients of the disturbance matrix $[B]$ are given by:

$$b_{11} = 0$$

$$b_{12} = \frac{\left\{\left(\frac{\partial m}{\partial y}\right) - \left(\frac{\partial m}{\partial h}\right)\left(\frac{\partial q}{\partial y}\right) / \left(\frac{\partial q}{\partial h}\right)\right\}}{\left[T_m + K_d\left\{\left(\frac{\partial m}{\partial y}\right) - \left(\frac{\partial m}{\partial h}\right)\left(\frac{\partial q}{\partial y}\right) / \left(\frac{\partial q}{\partial h}\right)\right\}\right]}$$

$$b_{21} = 0$$

$$b_{22} = 0$$

$$b_{31} = 0$$

$$b_{32} = \frac{\left(\frac{\partial q}{\partial y}\right)\left[(1 - K_d b_{12}\right]}{T_w \left(\frac{\partial q}{\partial h}\right)}$$

$$b_{41} = 0$$

$$b_{42} = D_a b_{12}$$

$$b_{51} = -\frac{1}{T_{s1}}$$

$$b_{52} = 0$$

$$b_{61} = 0$$

$$b_{62} = 0$$

Vita

The author was born in Portsmouth, Virginia on March 25, 1953 and graduated from Woodrow Wilson High School, Portsmouth, Virginia in June 1971. He entered Virginia Polytechnic Institute and State University in September 1971 and earned a Bachelor of Science degree in Mechanical Engineering in June of 1975. In September 1975, the author entered the Graduate School at Virginia Polytechnic Institute and State University and earned a Master of Science degree in Mechanical Engineering in August, 1976.

Upon completion of his Master's degree requirements, he was employed as a thermal systems engineer by the Procter and Gamble Company in Cincinnati, Ohio. The author participated in on-site startup of a new synthetic detergent facility in Brockville, Ontario, Canada from April 1979 to December 1979.

The author enrolled as a Ph.D. candidate and became an Instructor of Mechanical Engineering in March 1980. He is a licensed Professional Engineer in the Commonwealth of Virginia.

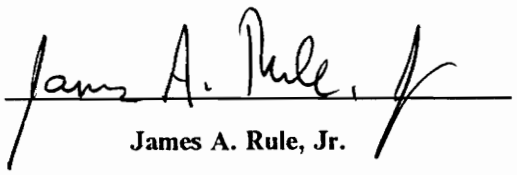

James A. Rule, Jr.